DISSERTATION

POLYCAPROLACTONE NANOWIRE SURFACES AS INTERFACES FOR CARDIOVASCULAR APPLICATIONS

Submitted by

Victoria Leszczak

Department of Mechanical Engineering

In partial fulfillment of the requirements

For the Degree of Doctor of Philosophy

Colorado State University

Fort Collins, Colorado

Summer 2014

Doctoral Committee:

Advisor: Ketul C. Popat

Melissa Reynolds
Prasad Dasi
John Williams

ABSTRACT

POLYCAPROLACTONE NANOWIRE SURFACES AS INTERFACES FOR CARDIOVASCULAR APPLICATIONS

Cardiovascular disease is the leading killer of people worldwide. Current treatments include organ transplants, surgery, metabolic products and mechanical/synthetic implants. Of these, mechanical and synthetic implants are the most promising. However, rejection of cardiovascular implants continues to be a problem, eliciting a need for understanding the mechanisms behind tissue-material interaction. Recently, bioartificial implants, consisting of synthetic tissue engineering scaffolds and cells, have shown great promise for cardiovascular repair. An ideal cardiovascular implant surface must be capable of adhering cells and providing appropriate physiological responses while the native tissue integrates with the scaffold. However, the success of these implants is not only dependent on tissue integration but also hemocompatibility (interaction of material with blood components), a property that depends on the surface of the material. A thorough understanding of the interaction of cardiovascular cells and whole blood and its components with the material surface is essential in order to have a successful application which promotes healing as well as native tissue integration and regeneration. The purpose of this research is to study polymeric nanowire surfaces as potential interfaces for cardiovascular applications by investigating cellular response as well as hemocompatibility.

ACKNOWLEDGEMENTS

Research reported in this dissertation was supported by the National Institute of Arthritis and Musculoskeletal and Skin Diseases of the National Institutes of Health under Award Number 5-R21-AR057341-02. The content is solely the responsibility of the authors and does not necessarily represent the official views of the National Institutes of Health.

The author would like to thank Dr. Ketul Popat for the support and mentorship over the past 4 years. The author would also like to thank the staff at Garth Englund Blood Center and Hartshorn Health center for their assistance with drawing blood.

DEDICATION

This work is dedicated to my incredible family, who has supported my dreams and goals throughout my life, supplying me with constant love and inspiration: Teresa Leszczak, Jan Leszczak and Kristina Leszczak, I thank you.

TABLE OF CONTENTS

LIST OF TABLES

LIST OF FIGURES

CHAPTER 1

CHAPTER 2

CHAPTER 3

CHAPTER 4

surfaces. After 14 days in culture, VE-cadherin expression is significantly higher on cPCL and cNW surfaces compared to PCL and NW surfaces. There is no significant increase in vWF or VE-cadherin expression from day 7 to 14 on any of the surfaces. Experiments were replicated with western blots with at least three different cell populations (nmin = 9).

CHAPTER 5

Figure 5.4. (A) Elongation (*E*) approximations of cells on different surfaces after 1 and 7 days of culture. Experiments were replicated on at least three different samples with at least three different cell populations (n_{min} = 9). Statistical significance was calculated using a one-way ANOVA with Tukey's *post hoc* test. Results indicate that colNW surfaces exhibit a more elongated morphology after 1 and 7 days of culture compared to PCL surfaces at the same time points (*, #, $p < 0.05$). SMCs also become significantly more elongated on cNW surfaces after 7 days of culture compared to those in culture for 1 day on cNW surfaces (¢, $p < 0.05$). Error bars represent the standard error; (B) The image shows how *E* approximations were calculated (outer diameter/inner diameter); A histogram of *E* approximations of cells on different surfaces after (C) 1 day in culture and (D) 7 days in culture.

Figure 5.5. Cell viability measured using the MTT assay for SMCs on different surfaces. Experiments were replicated on at least three different samples with at least three different cell populations (n_{min} = 9). Statistical significance was calculated using a one-way ANOVA with Tukey's *post hoc* test. Results indicate after 1 day in culture that SMCs on the cNW surfaces have significantly lower MTT reduction than the PCL, NW and cPCL surfaces, whereas, there is no significant difference between the PCL, NW and cPCL surfaces. After 7 days in culture, SMCs have a significantly higher MTT reduction on cPCL than the PCL, NW and cNW surfaces. Further, there were significant differences between PCL, NW and cNW surfaces (PCL > NW > cNW). Error bars represent the standard error.

CHAPTER 6

coated with a 10 nm layer of gold and imaged at 5-7 kV. Images show a lower degree of platelet/leukocyte interaction and cellular aggregation on NW surfaces.

Figure 6.7. (a). Representative fluorescence microscope images of platelets immunostained for P-Selectin and leukocytes immunostained for CD45 on different surfaces after 2 hours of incubation in whole blood plasma. The images indicate a considerable reduction in P- Selectin (TR-conjugated) and CD45 (FITC-conjugated) expression on nanostructured surfaces. (b). Western blot analysis of the expression of P-Selectin and CD-45 on different surfaces after 2 hours of incubation in whole blood plasma. Experiments were replicated with western blots with at least three different cell populations ($n_{min} = 9$). Results reveal a significantly elevated amount of P-Selectin and CD-45 expression on cPCL surfaces compared to PCL, NW and cNW surfaces. P-Selectin expression was significantly elevated on PCL surfaces compared to NW and cNW surfaces.

Figure 6.8. Platelet release reaction measured by the amount of PF-4 released from α-granules within the platelets on surfaces after 2 hours of incubation in whole blood plasma. The results indicate a significant increase in PF-4 expression on cPCL surfaces compared to NW and cNW surfaces and a significant decrease in PF-4 expression on NW surfaces compared to PCL and cPCL surfaces.

Figure 6.9. Contact activation measured by the amount of kallikrein on different surfaces after 2 hours of incubation in whole plasma. The results indicate no significant difference in contact activation on the surfaces.

Figure 7.3. Representative SEM images of SMC and EC co-cultures after 7 days of culture on different surfaces. Note: the surfaces were coated with a 10 nm layer of gold and imaged at 7 keV. Experiments were replicated on at least three different samples with at least three different cell populations ($n_{min} = 9$).

Figure 7.4. Western blot analysis of the expression of (A) α-tubulin, (B) VE-cadherin, (C) MYH and (D) SMemb on different surfaces after 7 and 14 days in culture. Experiments were replicated with western blots with at least three different cell populations ($n_{min} = 9$). (B) After 7 days in culture PCL and NW surfaces express significantly higher amounts of VE-cadherin compared to cPCL and cNW surfaces. After 14 days in culture VE-cadherin expression is significantly higher on NW and cNW surfaces compared to PCL and cPCL surfaces. (C) After 7 days in culture MYH expression is significantly higher on cNW surfaces compared to PCL, NW and cPCL surfaces, while PCL surfaces express significantly less MYH than NW, cPCL and cNW surfaces. After 14 days in culture, MYH expression significantly decreases on NW, cPCL and cNW surfaces. (D) After 7 days in culture SMemb expression is significantly higher on NW surfaces compared to PCL, cPCL and cNW surfaces. After 14 days in culture there is a significant decrease in SMemb expression on all surfaces, with no significant difference in expression between all surfaces.

LIST OF KEYWORDS

Polycaprolactone Nanowires

Nanotechnology

Biomaterials

Endothelial Cells

Smooth Muscle Cells

Platelets

Leukocytes

Whole Blood Clotting

Hemocompatiblility

Thrombogenicity

Implantable Biomedical Devices

Cardiovascular Implant Surface

INTRODUCTION

Cardiovascular disease affects 80 million people in the US and is the leading cause of death worldwide. Current treatments for cardiovascular diseases include organ transplants, surgery, metabolic products and mechanical/synthetic implants. Of these, mechanical and synthetic implants have shown great promise in recent years, however, synthetic polymers have been recognized as better candidates for cardiovascular repair due to the thrombogenic nature of metallic cardiovascular implants. In particular, polymers such as polyurethane, poly(L-lactic acid), polyglycolic acid and polycaprolactone have proven to be of tremendous use due to their biocompatibility and controlled mechanical properties. These polymers have been used to develop cardiovascular devices such as vascular grafts, artificial hearts, and heart valves, all of which have been widely used in recent years. These implants have the potential to replace the damaged components of the cardiovascular system, while maintaining the normal tissue function, however, a thorough understanding of the interaction between cells and the biomaterial interface involved is essential in order to have a successful application which promotes healing as well as native tissue integration and regeneration.

An ideal scaffold utilized for cardiovascular engineering should be both physically and chemically biomimetic. A cardiovascular scaffold must be capable of adhering cells, providing a physiochemical biomimetic environment throughout the degradation process and promoting desirable physiological responses while the native tissue integrates with the scaffold. However, the success of these implants is not only dependent on tissue integration but also hemocompatibility (interaction of material with blood components), a property that depends on the surface of the material. Therefore, in order to create a successful scaffold and induce

transplant tolerance, it is critical to understand the interaction of cells and blood components with the material surface.

This Ph.D. document addresses the hypothesis that polymeric nanowire surfaces will provide an advantageous interface for cardiovascular cell functionality and hemocompatibility; leading to enhanced cardiovascular biomaterial implant tolerance. The results of this work identify enhanced endothelial cell and smooth muscle cell interaction and improved hemocompatibility of polycaprolactone nanowire surfaces. This research presents promising results with respect to the use of polycaprolactone nanowire surfaces as interfaces for the cardiovascular applications.

HYPOTHESIS AND SPECIFIC AIMS

Fundamental Hypothesis

Polymeric nanowire surfaces will provide an advantageous interface for cardiovascular cell functionality and hemocompatibility; leading to enhanced cardiovascular biomaterial implant tolerance.

Specific Aims

Hypothesis (1): Nanowire polymeric surfaces can be engineered from polycaprolactone to be highly reproducible as interfaces for cardiovascular implantable devices using a nanotemplating technique.

Specific Aim 1: Fabricate and characterize highly reproducible polycaprolactone nanowire surfaces for cardiovascular applications. This research is discussed in **Chapter 2**.

(a) Fabricate well-controlled, highly reproducible polymeric nanowires using a solvent free nanotemplating technique. Fabricate well-controlled, highly reproducible polymeric nanofibers using the electrospinning technique.

(b) Characterize the surface of polycaprolactone nanowires and nanofibers surfaces using contact angle and SEM.

(c) Immobilize type 1 collagen unto the surface of polycaprolactone nanowires.

(d) Characterize the surface characteristics of collagen immobilized polycaprolactone nanowire surfaces using contact angle SEM, and XPS.

Hypothesis (2): The orientation of nanostructured polymeric surfaces can modulate protein adsorption, platelet adhesion and activation and whole blood clotting on cardiovascular implant interfaces.

Specific Aim 2: Determine the effect of nanostructured polymeric surfaces on the behavior of protein adsorption, platelet adhesion and activation and whole blood clotting. This research is discussed in **Chapter 3**.

(a) Investigate the effect of nanostructured polymeric surfaces on the adsorption of key blood proteins (fibrinogen, albumin and immunoglobulin-G).

(b) Investigate the effect of nanostructured polymeric surfaces on platelet adhesion and activation.

(c) Investigate the effect of nanostructured polymeric surfaces on the blood clotting kinetics by measuring the free hemoglobin concentration.

Hypothesis (3): Polycaprolactone nanowire surfaces will provide a favorable interface for the growth and maintenance of endothelial cell functionality.

Specific Aim 3: Determine endothelial cell functionality on polycaprolactone nanowire surfaces. This research is discussed in **Chapter 4**.

(a) Investigate the effect of polycaprolactone nanowire surfaces on the functionality (adhesion, proliferation, viability, and morphology) of endothelial cells.

(b) Investigate the effect of polycaprolactone nanowire surfaces on the endogenous protein expression of human microvascular endothelial cells.

Hypothesis (4): Polycaprolactone nanowire surfaces will provide a favorable interface for the growth and maintenance of smooth muscle cell functionality.

Specific Aim 4: Determine smooth muscle cell functionality on polycaprolactone nanowire surfaces on. This research is discussed in **Chapter 5**.

(a) Investigate the effect of polycaprolactone nanowire surfaces on the functionality (adhesion, proliferation, viability, and morphology) of smooth muscle cells.

(b) Investigate the effect of polycaprolactone nanowire surfaces on the endogenous protein expression of human aortic smooth muscle cells.

Hypothesis (5): Polycaprolactone nanowire surfaces will provide a favorable cardiovascular implant interface for blood and its components.

Specific Aim 5: Determine the effect of polycaprolactone nanowire surfaces on whole blood and its components by investigation of cytotoxicity, platelet/leukocyte interactions, activation of complement and contact, thrombin generation and hemolysis. This research is discussed in **Chapter 6**.

(a) Investigate toxicity of polycaprolactone nanowire surfaces through the use of whole blood plasma.

(b) Investigate fibrinogen binding on polycaprolactone nanowire surfaces through the use of whole blood plasma.

(c) Investigate the effect of polycaprolactone nanowire surfaces on platelet/leukocyte adhesion, aggregation and complex formation on polycaprolactone surfaces through the use of whole blood plasma.

(d) Investigate the activation of complement and contact on polycaprolactone nanowire surfaces through the use of whole blood plasma.

(e) Investigate thrombin generation and hemolysis on polycaprolactone nanowire surfaces.

Hypothesis (6): Polycaprolactone nanowire surfaces will provide a favorable interface for the growth and maintenance of co-cultures of endothelial cells and smooth muscle cells and increase cellular functionality.

Specific Aim 6: Determine the functionality of co-cultures of endothelial cells and smooth muscle cells on polycaprolactone nanowire surfaces. This preliminary research is discussed in **Chapter 7**.

(a) Investigate the effect of polycaprolactone nanowire surfaces on the adhesion and morphology of co-cultures of human microvascular endothelial cells and human aortic smooth muscle cells.

(b) Investigate the effect of polycaprolactone nanowire surfaces on the endogenous protein expression of both human microvascular endothelial cells and human aortic smooth muscle cells.

CHAPTER 1

LITERATURE REVIEW

1.1. Introduction

Cardiovascular disease affects 80 million people in the US and is the leading cause of death worldwide. Current treatments for cardiovascular disease include organ transplants, surgery, metabolic products and mechanical/synthetic implants [1]. Of these, mechanical and synthetic implants have shown great promise in recent years, however, synthetic polymers have been recognized as better candidates for cardiovascular repair due to the thrombogenic nature of metallic cardiovascular implants [2]. In particular, polymers such as polyurethane [3], poly(L-lactic acid) [4], polyglycolic acid [5] and polycaprolactone [6] have proven to be of tremendous use due to their biocompatibility and controlled mechanical properties. The thermal and tensile properties of degradable polymers used in medical applications have been previously characterized [7], and a summary of these properties are listed in **Table 1.1.** [8]. These polymers have been used to develop cardiovascular devices such as vascular grafts [9], artificial hearts [10], and heart valves [11], all of which have been widely used in recent years [12]. Implants have the potential to replace the damaged components of the cardiovascular system, while maintaining normal tissue function. However, these implants have significant limitations even after decades of research devoted to developing blood-contacting devices [13, 14]. The greatest shortcoming is the lack of complete biocompatibility, leading to poor tissue/biomaterial integration and further biomaterial rejection [15]. Hence, an unmet need exists to develop novel cardiovascular implant surfaces capable of promoting healing as well as native tissue integration and regeneration.

A well-documented, complex cascade of highly interconnected events are initiated in response to blood and tissue interacting with the surface of a biomaterial [16, 17]. The successful integration of long-term implantable devices is highly dependent on the initial events of tissue/biomaterial interaction, promoting wound healing response (extracellular matrix production and vascularization) or rejection of the biomaterial surface with creation of a fibrous capsule (**Figure 1.1.**). The cells needed for the regeneration of healthy tissue are hindered through an unfavorable immune reaction, thus compromising the wound healing process and

Table 1.1. Properties of Polymers. Reproduced with permission from Elsevier © [8].

Polymer	Polymer repeat structure	Melting Point (°C)	Glass Transition (°C)	Processing Method	Approx. Deg time (months)	Area of application and references	Products with regulatory approval
Poly (lactide)	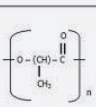	173 - 178	60 - 65	Extrusion. Inj. Moulding. Compression. moulding Solvent Casting.	6 to 12	Orthopedic surgery Oral and Maxillofacial surgery	
Poly (glycolide)	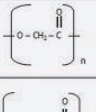	225 - 230	35 - 40	Extrusion. Inj. Moulding. Compression moulding. Solvent Casting.	>24	Orthopedic surgery General surgery Sutures	
Polycaprolactone		-65 - 60	-65 - 60	Extrusion. Inj. Moulding. Compression moulding. Solvent Casting. Electrospinning	>24	Drug Delivery Sutures	
Poly (D,L-lactide-co-glycolide) Poly (D,L-lactide-co-glycolide) 85/15 Poly (D,L-lactide-co-glycolide) 82/18 Poly (L-lactide-co-glycolide) 1090	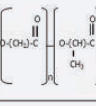	Amorphous	50 - 55	Extrusion. Inj. moulding. Compression moulding. Solvent Casting.	5 to 6	Suture Drug Delivery Oral and maxillofacial surgery General surgery Suture, periodontal surgery, general surgery	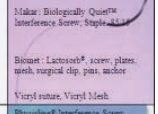
Poly (L-lactide-co-D,L-lactide) 98/2 Poly (L-lactide-co-D,L-lactide) 50/50 Poly (L-lactide-co-D,L-lactide) 70/30 Poly (D-lactide-co-D,L-lactide-coL-lactide		Amorphous	55 - 60	Extrusion. Inj. moulding. Compression moulding. Solvent Casting.	12 to 16 12	Orthopaedic surgery Oral and maxillofacial surgery BD Biosciences – not got clinical approval	
Polydioxanone	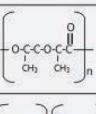	58 - 63	-65 - 60	Extrusion. Inj. moulding. Compression moulding. Solvent Casting.	>24	Orthopaedic surgery General surgery Sutures	Ethipin Orthosorb. Suture mesh foils Bone cement plug
Poly (D-L-lactide-co-caprolactone) 65/35	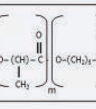	Amorphous		Dip coating from chloroform	24*	Nerve Regeneration	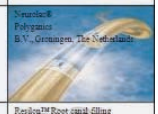
A polycaprolactone-based composite containing dimethacylate monomers		60				Oral surgery Miner 2000 Shipper 6	
Polycaprolactone based polyurethane		amorphous				Tissue reinforcement. Torn tendon replacement patch. Interpositional spacer in osteoarthritis	
Lactide co caprolactone	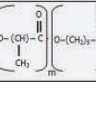				Klopp 2008	To prevent adhesion	

the wound healing process and long term success of implantable biomedical devices [18, 19]. There are an assortment of biochemical and topographical cues present naturally within human tissues that have favorable interactions with whole blood components and cells of the cardiovascular system [20, 21]. By mimicking these cues on scaffold surfaces promising cellular responses have been elicited via biomolecular recognition [22-25], which can easily be regulated with changes to the design parameters of the material surface [26]. An in depth understanding of the reactions that both nanoscaled topographical cues and biochemical cues elicit in cellular functionality is critical in determining the long term success of a cardiovascular implant device.

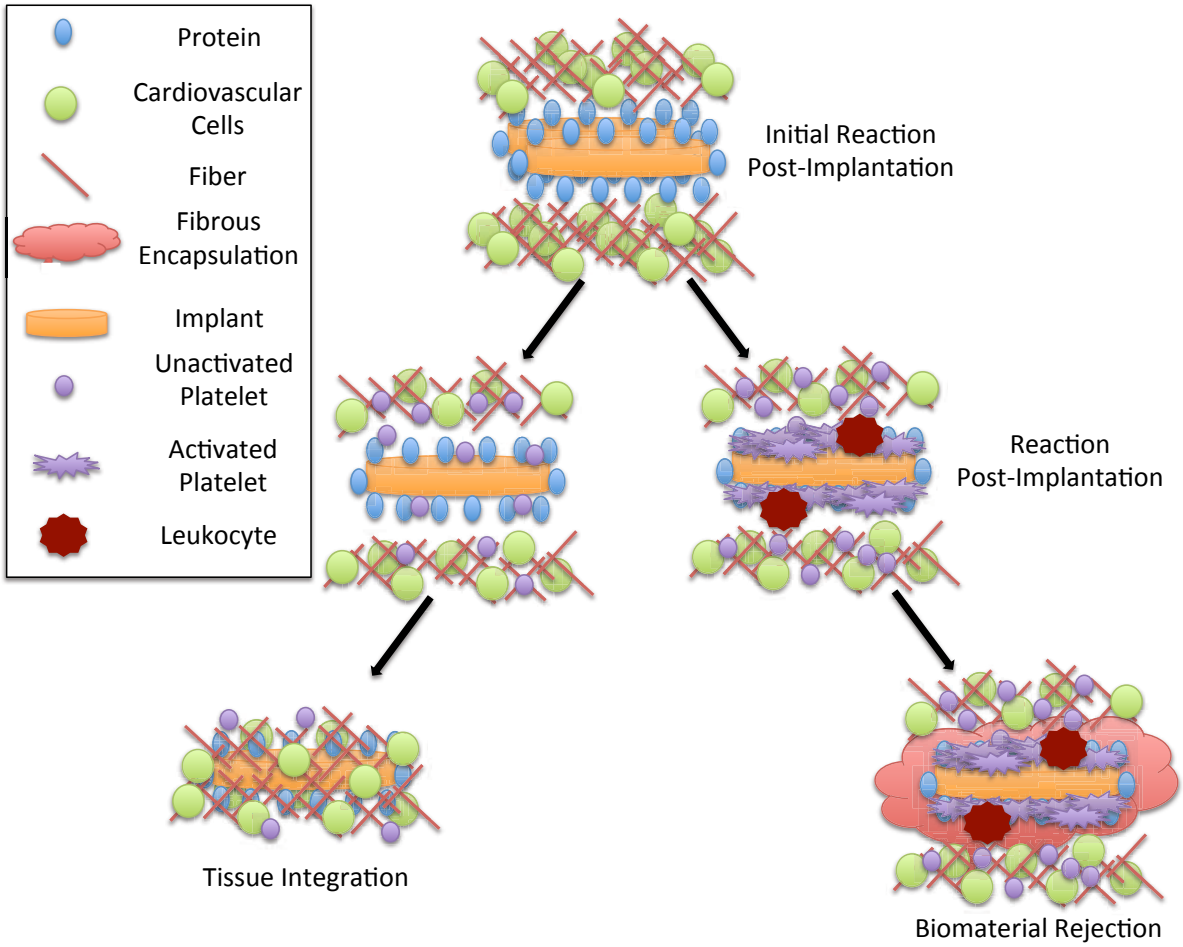

Figure 1.1. Two fates of a cardiovascular implant, either leading to tissue/biomaterial integration or biomaterial rejection via fibrous encapsulation.

1.2. Physiological Response to Implanted Biomaterials

When blood comes in contact with a material surface, an intricate series of highly interconnected events such as platelet and leukocyte adhesion/activation and stimulation of complement and coagulation cascades are initiated, ultimately controlled by properties of the surface (**Figure 1.2**) [27]. Key blood serum proteins, such as fibrinogen, immunoglobulin G and albumin can adsorb and undergo conformational changes on the surface, thus intermediating these events. Proteins can adsorb on the surface in varying quantities, densities, conformations, and orientations, depending on the chemical and physical characteristics of the surface [28]. The layer of adsorbed proteins influences the adhesion and activation of platelets and leukocytes. Platelets are anuclear specialized blood cells released from megakaracytes in bone marrow. The central role of platelets is to terminate haemorrhage following tissue trauma, initiated through the activation of platelets and resulting in the release of a multitude of bioactive factors, such as PF-4 and P-selectin, from platelet granules [29-31]. Platelets are further activated when red blood cells are lysed in response to contacting an unfavorable surface, releasing adenosine diphosphate (ADP), promoting platelet aggregation on the material surface [32]. In turn leukocytes are recruited and infiltrate unto the surface, facilitating the formation of platelet/leukocyte complexes (heterotypic aggregates) [33]. Leukocytes are involved in defending the body against disease and foreign materials and are produced by hematopoietic stem cells. There are five different types of leukocytes (neutrophils, basophils, eosinophils, lymphocytes, monocytes), each serving a specific function. Heterotypic aggregates form when activated platelets undergo degranulation, after which they adhere to circulating leukocytes via P-selectin [34]. This further stimulates two pathways, better known as the intrinsic pathway (contact activation) and the extrinsic pathway (tissue factor), which may lead to thrombosis and/or a fibrous capsule. Both

pathways involve zymogens activating, eventually converging on a common pathway, leading to clot development via formation of thrombin from prothrombin and fibrin from fibrinogen [35]. Thus, in order to fully evaluate the physiological response to the surface of a biomaterial, all of these events must be investigated and understood.

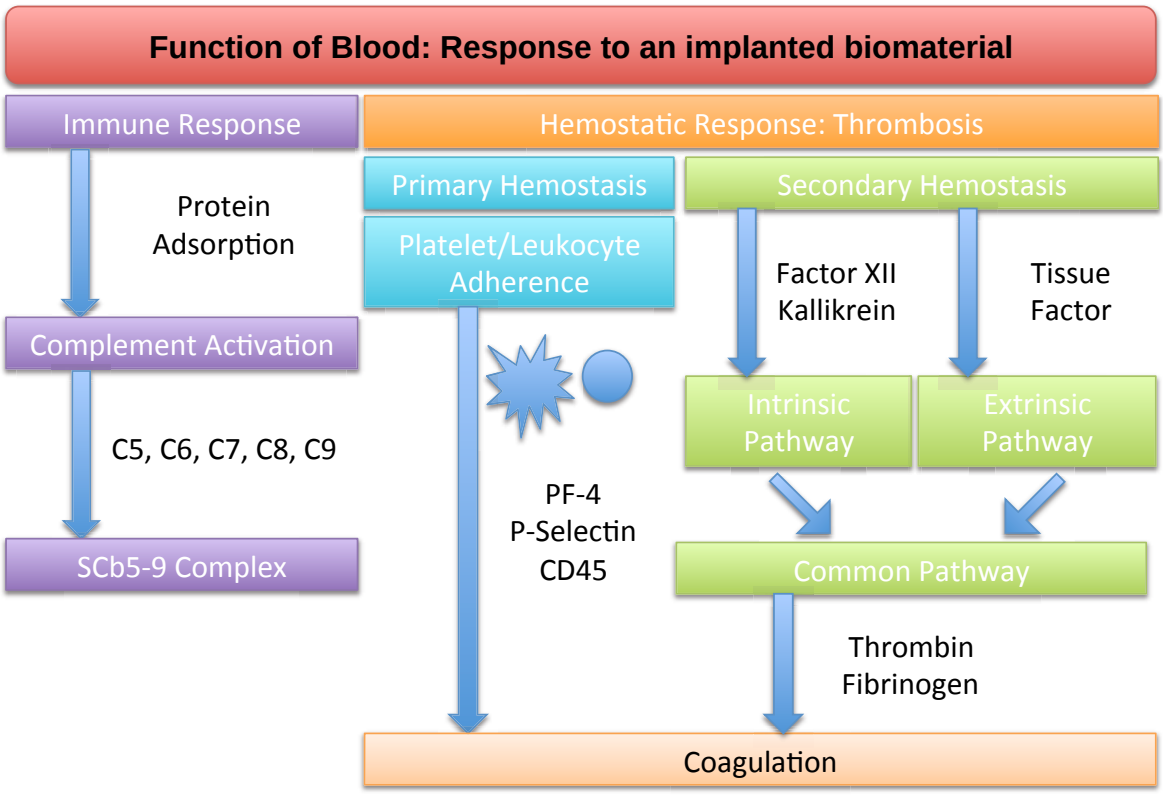

Figure 1.2. Representative schematic of blood response to an implanted biomaterial.

1.3. Structure of cardiovascular tissue.

Cardiovascular tissue, whether looking at arteries or veins, is composed of three main layers of cells (endothelial cells, smooth muscle cells, fibroblasts) (**Figure 1.3.**). The tunica intima is

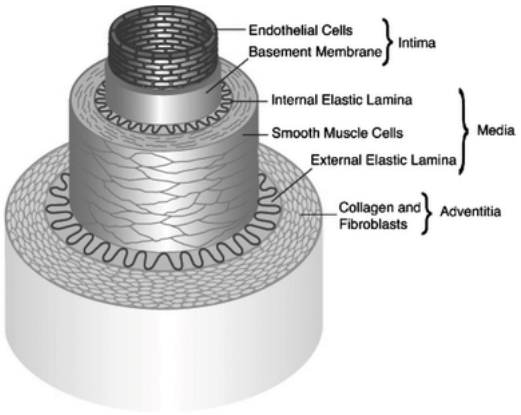

Figure 1.3. Composition of cardiovascular tissue. Reproduced with permission from Springer © [36].

composed of endothelial cells. This layer is in constant exposure to blood and is similar in both arteries and veins. The tunica media is composed of smooth muscle cells and this layer varies in arteries and veins. An increase in smooth muscle is present in arteries to provide extra strength and elasticity in response to surges of blood from the heart. The tunica externa/adventitia is connective tissue composed of fibroblasts. Further collagen is the most abundant protein in the ECM of cardiovascular tissue.

1.4. Endothelial cell-material interface.

The endothelium is a selectively permeable barrier, separating blood from the underlying cellular layers (**Figure 1.3.**). Damage of the endothelial cell (EC) layer exposes the underlying subendothelial extracellular matrix, promoting thrombus formation, inflammation and smooth muscle cell proliferation, thus demonstrating the importance of re-establishing or maintaining the integrity of the EC layer. Previous research has shown that stents seeded with ECs before being implanted can inhibit thrombosis and neointimal hyperplasia [37, 38], however ECs are not able

to maintain adherence when exposed to physiological blood flow. Ensuring their robust adherence capable of withstanding the physiological forces caused by blood flow is vital. Any interruption of contact between terminally differentiated ECs and blood flow is expected to produce an undesirable response that would interfere with proper tissue integration. Non-adherent surfaces prevent ECs from attaching to the endovascular surface, which in turn impedes the development of a protective endothelium. An unmet need therefore exists, to engineer cardiovascular implant surfaces that encourage the development of endothelium.

One major obstacle to overcome is adhering the anchorage-dependent ECs. The level of growth is correlated to the characteristics of the surface and how well the surface mimics cardiovascular ECM. Consequently, in order to create a successful cardiovascular scaffold surface, it is necessary to mimic the interaction between the ECs surface receptors with the extracellular matrix molecules. This interaction is extremely important in regulating adhesion, survival, proliferation, migration and differentiation. Once ECs establish adhesive contacts with surfaces via integrin-mediated interactions, signaling pathways are activated that initiate and direct a diverse amount of cellular activities such as survival, cell-cycle progression, vascularization for oxygenation and nutrient delivery and gene expression [39]. Therefore, the functionality of ECs is dependent on the success of their adherence to the surface. Understanding how to anchor ECs and the nature of the cell surface receptor-ECM interactions will provide a foundation for developing functional biomaterials designed to promote EC adhesion and growth. Further, maintaining normal physiological functions of endothelial cells *in vitro* is a requirement for the successful endothelialization of biomaterials. Therefore studies have been focused on improving endothelial cell attachment and functionality on a variety of polymer surfaces, via surface coatings or the introduction of nanotopography. For example, collagen-

coated poly(L-lactic acid)-co-poly(epsilon-caprolactone) nanofibers have shown increased spreading, viability, attachment and differentiation of ECs [40] and the surface topography of nano/micro-fiber scaffolds fabricated from a blend of starch and polycaprolactone have been shown to elicit and guide the 3D distribution of ECs [23].

1.5. Endothelial-smooth muscle cell interaction.

The communication between cells is essential for the normal maintenance of tissue and a number of pathophysiological responses [41]. In particular, cardiovascular tissue requires interactions between the endothelium with the underlying smooth muscle cells (SMCs), which is vital for cardiovascular health and is considered to be important in the functions of blood vessels [42, 43]. Maintenance of arterial structure relies on this interaction. ECs and SMCs act as a linked system for the communication of signals from receptors confined on the endothelium surface to the arterial wall and vice versa. It has been shown that bidirectional electrical signals flow in response to kinins between ECs and SMCs [44]. ECs and SMCs in the vascular wall can also communicate through the release of signals into the surrounding medium, or via direct cell-cell contact through junctions formed between the cells [45]. For example, during vasculogenesis, growth factors released from ECs promote migration of undifferentiated mesenchymal cells towards ECs and upon contact with ECs the mesenchymal cells differentiate into SMCs [46].

Further, ECs produce both growth inhibitors and stimulators of SMCs. In order to prevent thrombosis, restenosis and ultimate failure of the implant, an intact endothelium at the vessel-biomaterial interface is fundamental, in turn also preventing over-proliferation of the smooth muscle cells. In particular nitric oxide (NO), released by ECs, is responsible for inhibiting the

proliferation of SMCs via the extracellular signal-regulated kinase (ERK) pathway [47]. Studies have also shown that the rate of proliferation of SMCs is directly dependent on the state of endothelium [48]. When the endothelium is proliferating, the rate of proliferation of SMCs is accelerated. However, when the endothelium is in a confluent state, the normal growth rate of SMCs is completely inhibited. For examples, ECs cultured with synthetic state SMCs separated by a porous membrane demonstrated increased EC adhesion molecule expression, suggesting that synthetic SMCs activate the endothelium [49]. Therefore a specific ratio of ECs to SMCs and maintenance of a differentiated cellular state is vital to healthy cardiovascular tissues.

1.6. Smooth muscle cell-surface interaction.

The vascular SMCs main function is contraction and adjustment of blood vessel diameter, blood pressure, and blood flow distribution [50]. SMCs have the capacity for contraction, migration, proliferation, synthesis of extracellular matrix (ECM) components and the secretion of growth factors and cytokines [51]. This allows SMCs to regulate lumen diameter both transiently and chronically [52]. SMCs are key players in the development of vascular disease due to their plasticity or ability to change phenotype and behavior according to varying environmental conditions [53]. SMCs exhibit two well-known phenotypes; contractile and synthetic [54]. Contractile SMCs are elongated and spindle shaped, whereas synthetic SMCs are less elongated and have an epithelioid morphology. Synthetic SMCs contain organelles involved in protein synthesis, whereas in contractile SMCs, these organelles are replaced with contractile filaments. Further, synthetic and contractile SMCs exhibit different proliferation rates. Synthetic SMCs proliferate at higher rates compared to contractile SMCs. Contractile SMCs in adult blood vessels proliferate at an exceptionally low rate, demonstrate low synthetic activity, and express a

high level expression of contractile myofilament proteins such as α-smooth muscle actin (α-SMA), calponin, and myosin [55, 56]. The increased growth potential of smooth muscle cells causes them to be the most significant in vascular diseases such as atherogenesis and intimal hyperplasia. Recent studies show that smooth muscle cells express calcium channels, ICAM-1 and VCAM-1 suggesting that they may contribute to inflammatory reaction as well as the progression of vascular disease [57].

SMCs continue to react unfavorably when in contact with biomaterials, switching to a synthetic phenotype. Recently, research has been aimed at developing material surfaces that induce the contractile state of SMCs, thus reducing proliferation, preventing complications such as restenosis. SMCs cultured on nanopatterned poly(methyl methacrylate) (PMMA) andpoly(dimethylsiloxane) (PDMS) surfaces have exhibited a more elongated phenotype and a reduction in proliferation [58]. Further, a decrease in VSMC proliferation and increased expression of smooth muscle α-actin was seen on nanotubular titanium oxide [59]. These results suggest a correlation between nanotopography and smooth muscle cell proliferation and differentiation.

1.7. Nanostructured surfaces for cardiovascular tissue engineering applications.

Cells are naturally sensitive to their environment. The extracellular matrix (ECM) of all tissues is a multifaceted cellular environment consisting of proteins, proteoglycans, and other soluble molecules that are constantly interacting with surrounding cells (**Figure 1.4.**). These elements that constitute the ECM of macroscale human tissues are on the micrometer and nanometer scale [20]. The ECM offers mechanical support, biochemical cues and biomechanical cues that are important for cell functionality. However, the structure of the ECM varies within each tissue and

exhibits a variety of forms at different stages of development [60]. Developing and tailoring a favorable environment that mimics the complex, nanoscaled organization of native ECM is the most crucial aspect of tissue engineering and one, which remains to be the most difficult.

The motivation to use nanostructured surfaces as interfaces for cardiovascular devices is driven by previous studies that have shown that nanoscale materials affect cell behavior such as morphology, functionality and cell-cell interactions [61-63]. Nanotopography provides a valuable technique for guiding cell growth and differentiation, providing more durable features than surface chemistry alone and is capable of being modified in size and shape to match the chosen application. It is of utmost importance to mimic the *in vivo* environment of cells when designing scaffolds for tissue engineering. Furthermore, studies have shown that nanoscale surfaces improve fibroblast cell adhesion [64], neuronal cell differentiation [39], and osteoblast phenotypic activity [65, 66]. Therefore, nanotopography may result in improved cellular adhesion and therefore, enhanced matrix deposition and an increase in cardiovascular cell differentiation markers.

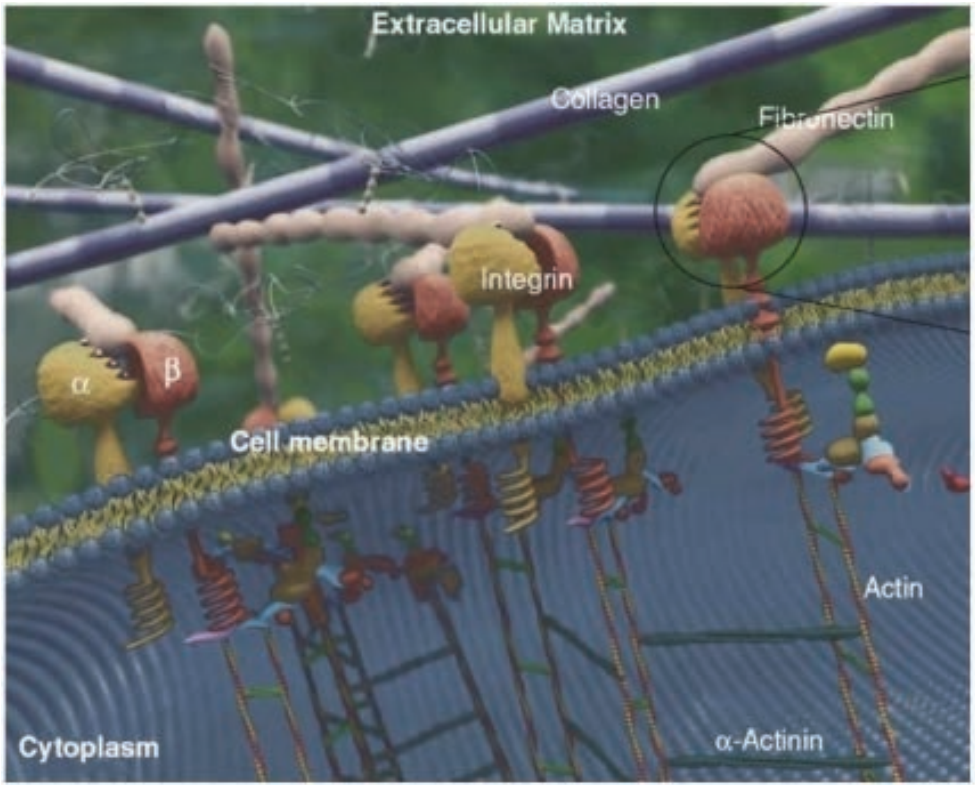

Figure 1.4. Cellular interaction with components of the extracellular matrix. Reproduced with permission from Springer © [67].

1.8. Current polymers used for cardiovascular applications.

Current materials used for cardiovascular stents are either bare metal, such as stainless steel, tantalum and cobalt chromium alloys, or coated metal stents. Pure polymer stents are currently not FDA approved, however polymers are commonly used for coating stents. Polymers used for coating stents can be organized as biostable polymers, biodegradable polymers, copolymers, and biological polymers [68]. A polymer coating allows for drug elution, which has been shown to prevent thrombosis [69]. Three drugs; heparin, sirolimus, and paclitaxel, have been investigated vigorously for treating and/or preventing restenosis. Current drug eluting stent products include CYPHER(®) a sirolimus-eluting Coronary Stent, Taxus(®), Liberte(®),

XIENCE V(™) / Promus(®) and Endeavor Resolute(®) [70]. The CYPHER® stent is composed of three polymer layers. A parylene layer is directly applied to the stent surface, followed by a polyethylene-*co*-vinyl acetate and poly-*n*-butyl methacrylate mixture containing the sirolimus drug. A top layer of only polyethylene-*co*-vinyl acetate and poly-*n*-butyl methacrylate is applied in order to control the elution rate or sirolimus. The Taxus® device has a single copolymer, poly(styrene-*b*-isobutylene-*b*-styrene), mixed with the paclitaxel drug. Further phosphorylcholine coatings are used for the delivery of the Zotarolimus drug from the Endeavor® stent. However, phosphorylcholine-based coatings have also been used as coatings without drug delivery capabilities [71]. Materials commonly used for vascular grafts include artificial grafts, autologous tissue, allografts and xenografts. Common artificial vascular graft materials include expanded poly-tetrafluoroethylene (ePTFE; Gore-Tex), poly-tetrafluoroethylene (Teflon; E.I. du Pont de Nemours and Company) or polyethylene terephthalate (Dacron).

1.9. Current FDA approved polycaprolactone devices.

Polycaprolactone (PCL) is used in a number of FDA approved devices such as sutures, barrier adhesion, wound dressings, contraceptive devices, tissue scaffolds, fixation devices, and in dentistry. Neurolac® is an FDA approved nerve guide conduit device and is a co-polymer of poly(dl-lactide-ε-caprolactone) and PCL [72]. PolyRemedy's PolyFIT™ antimicrobial dressings, composed of polyethylene glycol, ethylene vinyl alcohol and PCL, were recently FDA approved for wound care [73]. The OsteoPlug™ is also composed of a bioresorbable PCL scaffold for burr-hole skull defects. A block copolymer of PCL with glycolide is being sold as a monofilament suture under the trade name MONOCRYL® by Ethicon. In dentistry, a PCL

composite known as Resilon is used as a component of night guards and also in root canal fillings. PCL is also FDA approved in Capronor®, a commercial contraceptive product that is able to deliver levonorgestrel *in vivo* for over a year [74].

1.10. Polycaprolactone for cardiovascular tissue engineering applications.

Although PCL is not currently FDA approved for use in cardiovascular tissue engineering applications, it has a vast amount of benefits. The solubility of PCL in various solvents, its low melting point (~60 ℃), and its rare miscibility with a vast amount of other polymers has stimulated extensive research into its potential application in the biomedical field [75-77]. PCL has emerged as a promising implant polymer due to the fact that it is a bioresorbable polyester with exceptional mechanical strength as well as a tunable degradation rate and glass transition temperature of about 60 °C. PCL biodegrades within several months to several years depending on factors such as the molecular weight, the degree of crystallinity of the polymer, and the conditions of degradation [78-81]. It is derived by chemical synthesis from crude oil and can be prepared by ring opening polymerization of ε-caprolactone using a catalyst. It has good water, oil, solvent and chlorine resistance but can be degraded by hydrolysis of its ester linkages in physiological conditions (such as in the human body) and its degradation products are easily bioresorbed or removed naturally in metabolic pathways such as the citric acid cycle. Degradation of PCL was studied in vivo in rats [82]. Results reveal that PCL with a molecular weight of 66000 remained intact after 2 yrs of implantation while its molecular weight dropped to 15000. PCL with a molecular weight of 3000 was radioactively tagged and results reveal that the material did not accumulate in the body tissue and could be completely excreted.

Extensive in vitro and in vivo biocompatibility and efficacy studies have been performed with PCL, resulting in US Food and Drug Administration approval of a number of medical devices. Recently, PCL has been investigated for tissue engineering and drug delivery applications. It is regarded as a soft and hard tissue compatible bioresorbable material and has been considered as a potential substrate for wide applications, such as drug delivery systems, tissue-engineered skin, axonal regeneration [83] and scaffolds for supporting fibroblasts and osteoblasts growth. PCL is a versatile polymer, capable of being transformed into a variety of topographies and structures. These include nanospheres [84, 85] nanowires [86, 87], nanofibers [88, 89], biodegradable thermoresponsive physical hydrogel nanofibers [90] and ultra-thin membranes [91] (**Figure 1.5**).

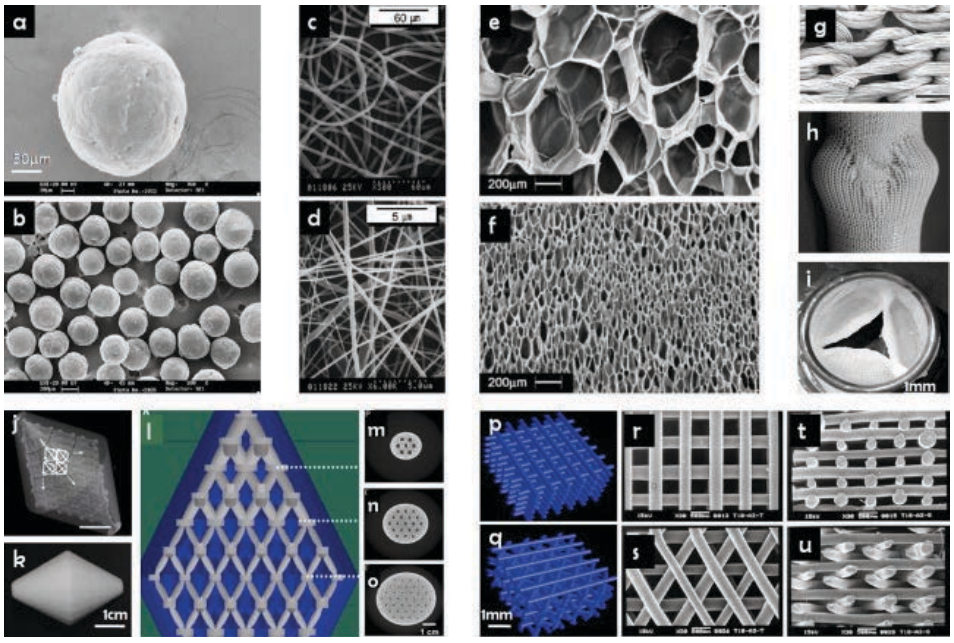

Figure 1.5. Nanostructured topographies from PCL: Nanospheres (a,b). Nanofibres (c,d). Foams (e,f). Knitted textiles (g,h,i). Selective laser sintered scaffold (j-o). Fused deposition modeled scaffolds (p–u). Reproduced with permission from Elsevier © [8].

1.11. Type 1 Collagen.

Collagen, the main protein in the ECM of blood vessels as well as other tissues in the body, has been used extensively to promote cell adhesion [92], specifically for fibroblasts [93], human keratinocytes [94], epithelial cells [95], and endothelial cells [96, 97]. Cell adhesion to collagen is controlled by two integrins: α1β1 and α2β1 [98]. Fibrillar collagen (collagen type I) binds these cellular integrins while exhibiting a triple helical structure, essential to its biological and mechanical properties [99]. Integrin α1β1 binds to collagen via MIDAS motif and is the only collagen receptor capable of activating Shc mediated growth pathways, indicating a distinctive role in cell proliferation on collagen [100]. Integrin α2β1 preferentially binds to a triple helical collagen containing the GFOGER motif [101] and regulates the level of matrix metalloproteinase-1[102]. Thus, collagen has been incorporated onto biomaterial surfaces to promote adhesion via integrin-mediated pathways. For example, collagen has been incorporated into nanofiber matrices and has enhanced rat tibia tissue regenerative processes [103], increased human fibroblast activity [104] enhanced proliferation and differentiation of neural precursor cells [105], improved bioactivity for bone engineering [106, 107] and increased endothelial cell organization and cell survival [108] and increased viability of both smooth muscle cells and endothelial cells [109]. Collagen has also been immobilized [110-112] or conjugated onto a variety of surfaces [40, 113, 114] enabling it to be used in a vast amount of applications. However, not much is known about the hemocompatibility of collagen immobilized surfaces [115, 116].

1.12. Experimental Approach.

Studies have demonstrated that biomimetic surfaces elicit favorable cellular interactions [22-24], which can be controlled by altering surface properties [21, 25, 117, 118]. Recent technologies have facilitated the fabrication of nanostructures on biomaterial surfaces, such as nanofibers [119, 120], nanowires [121, 122], nanorods [123], nanoparticles [122] and nanotubes [124, 125]. Topographies at the nanoscale level have stimulated various changes in cell adhesion [126], motility [127], alignment [128], and gene expression [129, 130]. In particular nanoscale architectures have improved proliferation of endothelial cells and smooth muscle cells [131], augmented differentiation of mesenchymal stem cells into the osteoblast phenotype [132, 133], and controlled growth patterns of neurons [134]. Promoting the functionality of cells further stimulates tissue-biomaterial integration, which can inhibit the rejection of the biomaterial [135, 136]. All of these studies suggest that there is a correlation between nanoscale surface features and cellular functionality.

In this work, we present a novel solvent-free template synthesis technique for fabricating controlled arrays of high aspect ratio, substrate-bound nanowires from PCL, a biocompatible and biodegradable polymer. Template synthesis is a simple procedure, which provides a controlled approach for developing nanoscale polymer constructs for tissue engineering applications in solvent free conditions, which eliminates issues of toxicity. Previous research has shown that PCL nanowires enhance the growth of neurons and promote mesenchymal stem cell differentiation but nothing is known about how whole blood and its components, endothelial cells and smooth muscle cells will interact with this nanotopography [87, 137]. Further, collagen type 1 will be immobilized to the PCL nanowire surfaces.

The development of nanostructured platforms based on novel PCL nanowire surfaces immobilized with collagen will provide key insights into cell-material interactions for the development of improved interfaces for cardiovascular implants. It is envisioned that the incorporation of mechanical and biochemical signals on scaffolds will further facilitate the growth and maintenance of differentiated cell states, and provide long-term cell viability and functionality. It is anticipated that these nanowire surfaces will be able to provide a template for growth and maintenance of human microvascular endothelial cells and human aortic smooth muscle cells. We believe that molecular and cellular assessment of *in vitro* responses to scaffold topography will contribute to the improvement of cardiovascular tissue engineering surfaces. These nanostructured surfaces, which are not able to allow cellular in-growth due to their size, may instead, provide a biomimetic template for ECM deposition, acting as a framework that facilitates synthesis of new cardiovascular tissue. In addition to creating more robust nanostructured scaffold material, we hope to better understand the role of both mechanical and biochemical signals on cell differentiation and vascularization.

REFERENCES

[1] Nugent HM, Edelman ER. Tissue Engineering Therapy for Cardiovascular Disease. Circulation Research. 2003;92:1068-78.

[2] van der Giessen WJ, Lincoff AM, Schwartz RS, van Beusekom HMM, Serruys PW, Holmes DR, et al. Marked Inflammatory Sequelae to Implantation of Biodegradable and Nonbiodegradable Polymers in Porcine Coronary Arteries. Circulation. 1996;94:1690-7.

[3] Ajili SH, Ebrahimi NG, Soleimani M. Polyurethane/polycaprolactane blend with shape memory effect as a proposed material for cardiovascular implants. Acta Biomaterialia. 2009;5:1519-30.

[4] Kim HI, Ishihara K, Lee S, Seo J-H, Kim HY, Suh D, et al. Tissue response to poly(l-lactic acid)-based blend with phospholipid polymer for biodegradable cardiovascular stents. Biomaterials. 2011;32:2241-7.

[5] Shinoka T, Ma PX, Shum-Tim D, Breuer CK, Cusick RA, Zund G, et al. Tissue-engineered heart valves. Autologous valve leaflet replacement study in a lamb model. Circulation. 1996;94:II164-8.

[6] Andukuri A, Kushwaha M, Tambralli A, Anderson JM, Dean DR, Berry JL, et al. A hybrid biomimetic nanomatrix composed of electrospun polycaprolactone and bioactive peptide amphiphiles for cardiovascular implants. Acta Biomaterialia. 2011;7:225-33.

[7] Engelberg I, Kohn J. Physico-mechanical properties of degradable polymers used in medical applications: A comparative study. Biomaterials. 1991;12:292-304.

[8] Woodruff MA, Hutmacher DW. The return of a forgotten polymer—Polycaprolactone in the 21st century. Progress in Polymer Science. 2010;35:1217-56.

[9] Motlagh D, Allen J, Hoshi R, Yang J, Lui K, Ameer G. Hemocompatibility evaluation of poly(diol citrate) in vitro for vascular tissue engineering. Journal of Biomedical Materials Research Part A. 2007;82A:907-16.

[10] Belanger MC, Marois Y, Roy R, Mehri Y, Wagner E, Zhang Z, et al. Selection of a polyurethane membrane for the manufacture of ventricles for a totally implantable artificial heart: Blood compatibility and biocompatibility studies. Artificial Organs. 2000;24:879-88.

[11] Maegdefessel L, Linde T, Krapiec F, Hamilton K, Steinseifer U, van Ryn J, et al. In vitro comparison of dabigatran, unfractionated heparin, and low-molecular-weight heparin in preventing thrombus formation on mechanical heart valves. Thrombosis Research. 2010;126:e196-e200.

[12] Motlagh D, Yang J, Lui KY, Webb AR, Ameer GA. Hernocompatibility evaluation of poly(glycerol-sebacate) in vitro for vascular tissue engineering. Biomaterials. 2006;27:4315-24.

[13] Rose EA, Gelijns AC, Moskowitz AJ, Heitjan DF, Stevenson LW, Dembitsky W, et al. Long-term use of a left ventricular assist device for end-stage heart failure. The New England journal of medicine. 2001;345:1435-43.

[14] Ratner BD. The blood compatibility catastrophe. Journal of Biomedical Materials Research. 1993;27:283-7.

[15] Anderson JM, Rodriguez A, Chang DT. Foreign body reaction to biomaterials. Seminars in immunology. 2008;20:86-100.

[16] Courtney JM, Lamba NMK, Sundaram S, Forbes CD. Biomaterials for blood-contacting applications. Biomaterials. 1994;15:737-44.

[17] Courtney JM, Lamba NMK, Gaylor JDS, Ryan CJ, Lowe GDO. Blood-Contacting Biomaterials: Bioengineering Viewpoints. Artificial Organs. 1995;19:852-6.

[18] Kawabe N, Yoshinao M. The Repair of Full-Thickness Articular Cartilage Defects: Immune Responses to Reparative Tissue Formed by Allogeneic Growth Plate Chondrocyte Implants. Clinical Orthopaedics and Related Research. 1991;268:279-93.

[19] Polikov VS, Tresco PA, Reichert WM. Response of brain tissue to chronically implanted neural electrodes. Journal of Neuroscience Methods. 2005;148:1-18.

[20] Lord MS, Foss M, Besenbacher F. Influence of nanoscale surface topography on protein adsorption and cellular response. Nano Today. 2010;5:66-78.

[21] Norman J, Desai T. Methods for Fabrication of Nanoscale Topography for Tissue Engineering Scaffolds. Ann Biomed Eng. 2006;34:89-101.

[22] Abidian MR, Corey JM, Kipke DR, Martin DC. Conducting-Polymer Nanotubes Improve Electrical Properties, Mechanical Adhesion, Neural Attachment, and Neurite Outgrowth of Neural Electrodes. Small. 2010;6:421-9.

[23] Santos MI, Tuzlakoglu K, Fuchs S, Gomes ME, Peters K, Unger RE, et al. Endothelial cell colonization and angiogenic potential of combined nano- and micro-fibrous scaffolds for bone tissue engineering. Biomaterials. 2008;29:4306-13.

[24] Cheng ZA, Zouani OF, Glinel K, Jonas AM, Durrieu M-C. Bioactive Chemical Nanopatterns Impact Human Mesenchymal Stem Cell Fate. Nano Letters. 2013;13:3923-9.

[25] Bettinger CJ, Langer R, Borenstein JT. Engineering Substrate Topography at the Micro- and Nanoscale to Control Cell Function. Angewandte Chemie International Edition. 2009;48:5406-15.

[26] Feng Y, Zhao H, Zhang L, Guo J. Surface modification of biomaterials by photochemical immobilization and photograft polymerization to improve hemocompatibility. Front Chem Eng China. 2010;4:372-81.

[27] Gorbet MB, Sefton MV. Biomaterial-associated thrombosis: roles of coagulation factors, complement, platelets and leukocytes. Biomaterials. 2004;25:5681-703.

[28] Roach P, Farrar D, Perry CC. Interpretation of Protein Adsorption: Surface-Induced Conformational Changes. Journal of the American Chemical Society. 2005;127:8168-73.

[29] Ruggeri ZM, Mendolicchio GL. Adhesion mechanisms in platelet function. Circulation research. 2007;100:1673-85.

[30] Gay LJ, Felding-Habermann B. Contribution of platelets to tumour metastasis. Nature reviews Cancer. 2011;11:123-34.

[31] Semple JW, Italiano JE, Freedman J. Platelets and the immune continuum. Nature Reviews Immunology. 2011;11:264-74.

[32] Alkhamis TM, Beissinger RL, Chediak JR. Red blood cell effect on platelet adhesion and aggregation in low-stress shear flow. Myth or fact? ASAIO transactions / American Society for Artificial Internal Organs. 1988;34:868-73.

[33] Eming SA, Krieg T, Davidson JM. Inflammation in wound repair: molecular and cellular mechanisms. The Journal of investigative dermatology. 2007;127:514-25.

[34] Freedman JE, Loscalzo J. Platelet–Monocyte Aggregates: Bridging Thrombosis and Inflammation. Circulation. 2002;105:2130-2.

[35] Wang X, Wang E, Kavanagh JJ, Freedman RS. Ovarian cancer, the coagulation pathway, and inflammation. Journal of translational medicine. 2005;3:25.

[36] Sarkar S, Schmitz-Rixen T, Hamilton G, Seifalian A. Achieving the ideal properties for vascular bypass grafts using a tissue engineered approach: a review. Med Bio Eng Comput. 2007;45:327-36.

[37] Dichek DA, Neville RF, Zwiebel JA, Freeman SM, Leon MB, Anderson WF. Seeding of intravascular stents with genetically engineered endothelial cells. Circulation. 1989;80:1347-53.

[38] Shirota T, Yasui H, Shimokawa H, Matsuda T. Fabrication of endothelial progenitor cell (EPC)-seeded intravascular stent devices and in vitro endothelialization on hybrid vascular tissue. Biomaterials. 2003;24:2295-302.

[39] Seidlits SK, Lee JY, Schmidt CE. Nanostructured scaffolds for neural applications. Nanomedicine. 2008;3:183-99.

[40] He W, Ma Z, Yong T, Teo WE, Ramakrishna S. Fabrication of collagen-coated biodegradable polymer nanofiber mesh and its potential for endothelial cells growth. Biomaterials. 2005;26:7606-15.

[41] Rossello RA, Kohn DH. Cell communication and tissue engineering. Commun Integr Biol. 2010;3:53-6.

[42] Jones PA. Construction of an artificial blood vessel wall from cultured endothelial and smooth muscle cells. Proceedings of the National Academy of Sciences of the United States of America. 1979;76:1882-6.

[43] Vernon SM, Campos MJ, Haystead T, Thompson MM, DiCorleto PE, Owens GK. Endothelial cell-conditioned medium downregulates smooth muscle contractile protein expression. The American journal of physiology. 1997;272:C582-91.

[44] Bidirectional electrical communication between smooth muscle and endothelial cells in the pig coronary artery1994.

[45] Fillinger MF, Sampson LN, Cronenwett JL, Powell RJ, Wagner RJ. Coculture of Endothelial Cells and Smooth Muscle Cells in Bilayer and Conditioned Media Models. Journal of Surgical Research. 1997;67:169-78.

[46] Hirschi KK, Rohovsky SA, D'Amore PA. PDGF, TGF-beta, and heterotypic cell-cell interactions mediate endothelial cell-induced recruitment of 10T1/2 cells and their differentiation to a smooth muscle fate. The Journal of cell biology. 1998;141:805-14.

[47] Förstermann U. Nitric oxide and oxidative stress in vascular disease. Pflugers Arch - Eur J Physiol. 2010;459:923-39.

[48] Zuckerbraun BS, Stoyanovsky DA, Sengupta R, Shapiro RA, Ozanich BA, Rao J, et al. Nitric oxide-induced inhibition of smooth muscle cell proliferation involves S-nitrosation and inactivation of RhoA. Am J Physiol Cell Physiol. 2007;292:C824-31. Epub 2006 Aug 16.

[49] Chiu JJ, Chen LJ, Lee CI, Lee PL, Lee DY, Tsai MC, et al. Mechanisms of induction of endothelial cell E-selectin expression by smooth muscle cells and its inhibition by shear stress. Blood. 2007;110:519-28.

[50] Owens GK, Kumar MS, Wamhoff BR. Molecular regulation of vascular smooth muscle cell differentiation in development and disease. Physiological reviews. 2004;84:767-801.

[51] Alexander MR, Owens GK. Epigenetic control of smooth muscle cell differentiation and phenotypic switching in vascular development and disease. Annual review of physiology. 2012;74:13-40.

[52] Halayko AJ, Solway J. Molecular mechanisms of phenotypic plasticity in smooth muscle cells. 1985) 2001.90:358-68.

[53] Owens GK. Molecular control of vascular smooth muscle cell differentiation and phenotypic plasticity. Novartis Foundation symposium. 2007;283:174-91; discussion 91-3, 238-41.

[54] Rensen SS, Doevendans PA, van Eys GJ. Regulation and characteristics of vascular smooth muscle cell phenotypic diversity. Netherlands heart journal : monthly journal of the Netherlands Society of Cardiology and the Netherlands Heart Foundation. 2007;15:100-8.

[55] Owens GK. Regulation of differentiation of vascular smooth muscle cells. Physiological reviews. 1995;75:487-517.

[56] Sakamoto N, Kiuchi T, Sato M. Development of an Endothelial–Smooth Muscle Cell Coculture Model Using Phenotype-Controlled Smooth Muscle Cells. Ann Biomed Eng. 2011;39:2750-8.

[57] Gollasch M, Haase H, Ried C, Lindschau C, Morano I, Luft FC, et al. L-type calcium channel expression depends on the differentiated state of vascular smooth muscle cells. The FASEB Journal. 1998;12:593-601.

[58] Yim EKF, Reano RM, Pang SW, Yee AF, Chen CS, Leong KW. Nanopattern-induced changes in morphology and motility of smooth muscle cells. Biomaterials. 2005;26:5405-13.

[59] Peng L, Eltgroth ML, LaTempa TJ, Grimes CA, Desai TA. The effect of TiO2 nanotubes on endothelial function and smooth muscle proliferation. Biomaterials. 2009;30:1268-72.

[60] Gullberg D, Ekblom P. Extracellular matrix and its receptors during development. Int J Dev Biol. 1995;39:845-54.

[61] Cao H, McHugh K, Chew SY, Anderson JM. The topographical effect of electrospun nanofibrous scaffolds on the in vivo and in vitro foreign body reaction. Journal of Biomedical Materials Research Part A. 2010;93A:1151-9.

[62] Bechara S, Wadman L, Popat KC. Electroconductive polymeric nanowire templates facilitates in vitro C17.2 neural stem cell line adhesion, proliferation and differentiation. Acta Biomaterialia. 2011;7:2892-901.

[63] McMurray RJ, Gadegaard N, Tsimbouri PM, Burgess KV, McNamara LE, Tare R, et al. Nanoscale surfaces for the long-term maintenance of mesenchymal stem cell phenotype and multipotency. Nat Mater. 2011;10:637-44.

[64] Park K, Ju YM, Son JS, Ahn KD, Han DK. Surface modification of biodegradable electrospun nanofiber scaffolds and their interaction with fibroblasts. J Biomater Sci Polym Ed. 2007;18:369-82.

[65] Werner C, Maitz MF, Sperling C. Current strategies towards hemocompatible coatings. Journal of Materials Chemistry. 2007;17:3376-84.

[66] Bechara SL, Judson A, Popat KC. Template synthesized poly(epsilon-caprolactone) nanowire surfaces for neural tissue engineering. Biomaterials. 2010;31:3492-501.

[67] Tirrell M, Kokkoli E, Biesalski M. The role of surface science in bioengineered materials. Surface Science. 2002;500:61-83.

[68] Huang Y, Venkatraman SS, Boey FYC, Lahti EM, Umashankar PR, Mohanty M, et al. In vitro and in vivo performance of a dual drug-eluting stent (DDES). Biomaterials. 2010;31:4382-91.

[69] Kivela A, Hartikainen J. Restenosis related to percutaneous coronary intervention has been solved? Annals of medicine. 2006;38:173-87.

[70] Parker T, Dave V, Falotico R. Polymers for drug eluting stents. Current pharmaceutical design. 2010;16:3978-88.

[71] Garcia-Touchard A, Burke SE, Toner JL, Cromack K, Schwartz RS. Zotarolimus-eluting stents reduce experimental coronary artery neointimal hyperplasia after 4 weeks. European heart journal. 2006;27:988-93.

[72] Kehoe S, Zhang XF, Boyd D. FDA approved guidance conduits and wraps for peripheral nerve injury: A review of materials and efficacy. Injury. 2012;43:553-72.

[73] Meneses P, Elaine Papineau A, Cooper DM. WOUND CLOSURE RATES IN THREE SUBJECTS USING CUSTOMIZED WOUND DRESSINGS.

[74] Darney PD, Monroe SE, Klaisle CM, Alvarado A. Clinical evaluation of the Capronor contraceptive implant: preliminary report. American journal of obstetrics and gynecology. 1989;160:1292-5.

[75] Chandra R, Rustgi R. Biodegradable polymers. Progress in Polymer Science. 1998;23:1273-335.

[76] Okada M. Chemical syntheses of biodegradable polymers. Progress in Polymer Science. 2002;27:87-133.

[77] Nair LS, Laurencin CT. Biodegradable polymers as biomaterials. Progress in Polymer Science. 2007;32:762-98.

[78] Gross RA, Kalra B. Biodegradable polymers for the environment. Science (New York, NY). 2002;297:803-7.

[79] Sinha VR, Bansal K, Kaushik R, Kumria R, Trehan A. Poly-epsilon-caprolactone microspheres and nanospheres: an overview. International journal of pharmaceutics. 2004;278:1-23.

[80] Lam CXF, Teoh SH, Hutmacher DW. Comparison of the degradation of polycaprolactone and polycaprolactone–(β-tricalcium phosphate) scaffolds in alkaline medium. Polymer International. 2007;56:718-28.

[81] Joshi P, Madras G. Degradation of polycaprolactone in supercritical fluids. Polymer Degradation and Stability. 2008;93:1901-8.

[82] Sun H, Mei L, Song C, Cui X, Wang P. The in vivo degradation, absorption and excretion of PCL-based implant. Biomaterials. 2006;27:1735-40.

[83] Schnell E, Klinkhammer K, Balzer S, Brook G, Klee D, Dalton P, et al. Guidance of glial cell migration and axonal growth on electrospun nanofibers of poly-ε-caprolactone and a collagen/poly-ε-caprolactone blend. Biomaterials. 2007;28:3012-25.

[84] Poletto FS, Silveira RP, Fiel LA, Donida B, Rizzi M, Guterres SS, et al. Size-control of poly(epsilon-caprolactone) nanospheres by the interface effect of ethanol on the primary emulsion droplets. Journal of nanoscience and nanotechnology. 2009;9:4933-41.

[85] Singh S, Singh AN, Verma A, Dubey VK. Biodegradable polycaprolactone (PCL) nanosphere encapsulating superoxide dismutase and catalase enzymes. Applied biochemistry and biotechnology. 2013;171:1545-58.

[86] Leszczak V, Smith BS, Popat KC. Hemocompatibility of polymeric nanostructured surfaces. Journal of biomaterials science Polymer edition. 2013;24:1529-48.

[87] Bechara SL, Judson A, Popat KC. Template synthesized poly(ε-caprolactone) nanowire surfaces for neural tissue engineering. Biomaterials. 2010;31:3492-501.

[88] Song T, Zhang Y, Zhou T, Lim CT, Ramakrishna S, Liu B. Encapsulation of self-assembled FePt magnetic nanoparticles in PCL nanofibers by coaxial electrospinning. Chemical Physics Letters. 2005;415:317-22.

[89] Alves da Silva ML, Martins A, Costa-Pinto AR, Costa P, Faria S, Gomes M, et al. Cartilage Tissue Engineering Using Electrospun PCL Nanofiber Meshes and MSCs. Biomacromolecules. 2010;11:3228-36.

[90] Loh XJ, Peh P, Liao S, Sng C, Li J. Controlled drug release from biodegradable thermoresponsive physical hydrogel nanofibers. Journal of Controlled Release. 2010;143:175-82.

[91] Chen F, Lee CN, Teoh SH. Nanofibrous modification on ultra-thin poly(e-caprolactone) membrane via electrospinning. Materials Science and Engineering: C. 2007;27:325-32.

[92] Glowacki J, Mizuno S. Collagen scaffolds for tissue engineering. Biopolymers. 2008;89:338-44.

[93] Chevallay B, Abdul-Malak N, Herbage D. Mouse fibroblasts in long-term culture within collagen three-dimensional scaffolds: Influence of crosslinking with diphenylphosphorylazide on matrix reorganization, growth, and biosynthetic and proteolytic activities. Journal of Biomedical Materials Research. 2000;49:448-59.

[94] Ruberti JW, Zieske JD. Prelude to corneal tissue engineering – Gaining control of collagen organization. Progress in Retinal and Eye Research. 2008;27:549-77.

[95] Duan X, Sheardown H. Dendrimer crosslinked collagen as a corneal tissue engineering scaffold: Mechanical properties and corneal epithelial cell interactions. Biomaterials. 2006;27:4608-17.

[96] Kim JH, Kim SH, Kim HK, Akaike T, Kim SC. Adhesion and growth of endothelial cell on amphiphilic PU/PS IPN surface: Effect of amphiphilic balance and immobilized collagen. Journal of Biomedical Materials Research. 2002;62:613-21.

[97] Orwin EJ, Hubel A. In vitro culture characteristics of corneal epithelial, endothelial, and keratocyte cells in a native collagen matrix. Tissue Eng. 2000;6:307-19.

[98] Tuckwell D, Humphries M. Integrin–collagen binding. Seminars in Cell & Developmental Biology. 1996;7:649-57.

[99] Arnoult O. A NOVEL BENIGN SOLUTION FOR COLLAGEN PROCESSING: Case Western Reserve University; 2010.

[100] Pozzi A, Wary KK, Giancotti FG, Gardner HA. Integrin alpha1beta1 mediates a unique collagen-dependent proliferation pathway in vivo. J Cell Biol. 1998;142:587-94.

[101] Emsley J, Knight CG, Farndale RW, Barnes MJ, Liddington RC. Structural Basis of Collagen Recognition by Integrin α2β1. Cell. 2000;101:47-56.

[102] Riikonen T, Westermarck J, Koivisto L, Broberg A, Kahari VM, Heino J. Integrin alpha 2 beta 1 is a positive regulator of collagenase (MMP-1) and collagen alpha 1(I) gene expression. J Biol Chem. 1995;270:13548-52.

[103] Phipps MC, Clem WC, Grunda JM, Clines GA, Bellis SL. Increasing the pore sizes of bone-mimetic electrospun scaffolds comprised of polycaprolactone, collagen I and hydroxyapatite to enhance cell infiltration. Biomaterials. 2012;33:524-34.

[104] Liu S-J, Kau Y-C, Chou C-Y, Chen J-K, Wu R-C, Yeh W-L. Electrospun PLGA/collagen nanofibrous membrane as early-stage wound dressing. Journal of Membrane Science. 2010;355:53-9.

[105] O'Connor SM, Stenger DA, Shaffer KM, Maric D, Barker JL, Ma W. Primary neural precursor cell expansion, differentiation and cytosolic Ca2+ response in three-dimensional collagen gel. Journal of Neuroscience Methods. 2000;102:187-95.

[106] He F, Li J, Ye J. Improvement of cell response of the poly(lactic-co-glycolic acid)/calcium phosphate cement composite scaffold with unidirectional pore structure by the surface immobilization of collagen via plasma treatment. Colloids and Surfaces B: Biointerfaces. 2013;103:209-16.

[107] Kalaskar DM, Demoustier-Champagne S, Dupont-Gillain CC. Interaction of preosteoblasts with surface-immobilized collagen-based nanotubes. Colloids and Surfaces B: Biointerfaces. 2013;111:134-41.

[108] Huang NF, Okogbaa J, Lee JC, Jha A, Zaitseva TS, Paukshto MV, et al. The modulation of endothelial cell morphology, function, and survival using anisotropic nanofibrillar collagen scaffolds. Biomaterials. 2013;34:4038-47.

[109] Chen ZG, Wang PW, Wei B, Mo XM, Cui FZ. Electrospun collagen–chitosan nanofiber: A biomimetic extracellular matrix for endothelial cell and smooth muscle cell. Acta Biomaterialia. 2010;6:372-82.

[110] Krithica N, Natarajan V, Madhan B, Sehgal PK, Mandal AB. Type I Collagen Immobilized Poly(caprolactone) Nanofibers: Characterization of Surface Modification and Growth of Fibroblasts. Advanced Engineering Materials. 2012;14:B149-B54.

[111] Baek J-Y, Xing Z-C, Kwak G, Yoon K-B, Park S-Y, Park LS, et al. Fabrication and characterization of collagen-immobilized porous PHBV/HA nanocomposite scaffolds for bone tissue engineering. J Nanomaterials. 2012;2012:1-.

[112] Farhadi M, Mirzadeh H, Solouk A, Asghari A, Jalessi M, Ghanbari H, et al. Collagen-immobilized patch for repairing small tympanic membrane perforations: In vitro and in vivo assays. Journal of Biomedical Materials Research Part A. 2012;100A:549-53.

[113] Hong Y, Gao C, Xie Y, Gong Y, Shen J. Collagen-coated polylactide microspheres as chondrocyte microcarriers. Biomaterials. 2005;26:6305-13.

[114] Hong Y, Gong Y, Gao C, Shen J. Collagen-coated polylactide microcarriers/chitosan hydrogel composite: Injectable scaffold for cartilage regeneration. Journal of Biomedical Materials Research Part A. 2008;85A:628-37.

[115] Liu T-Y, Lin W-C, Huang L-Y, Chen S-Y, Yang M-C. Hemocompatibility and anaphylatoxin formation of protein-immobilizing polyacrylonitrile hemodialysis membrane. Biomaterials. 2005;26:1437-44.

[116] Solouk A, Cousins BG, Mirzadeh H, Seifalian AM. Application of plasma surface modification techniques to improve hemocompatibility of vascular grafts: A review. Biotechnology and Applied Biochemistry. 2011;58:311-27.

[117] Chung BG, Kang L, Khademhosseini A. Micro- and nanoscale technologies for tissue engineering and drug discovery applications. Expert Opinion on Drug Discovery. 2007;2:1653-68.

[118] Wheeldon I, Farhadi A, Bick AG, Jabbari E, Khademhosseini A. Nanoscale tissue engineering: spatial control over cell-materials interactions. Nanotechnology. 2011;22:212001.

[119] Li D, Xia Y. Electrospinning of Nanofibers: Reinventing the Wheel? Advanced Materials. 2004;16:1151-70.

[120] Huang Z-M, Zhang YZ, Kotaki M, Ramakrishna S. A review on polymer nanofibers by electrospinning and their applications in nanocomposites. Composites Science and Technology. 2003;63:2223-53.

[121] Leszczak V, Smith BS, Popat KC. Hemocompatibility of polymeric nanostructured surfaces. Journal of Biomaterials Science, Polymer Edition. 2013;24:1529-48.

[122] Veiseh O, Gunn JW, Zhang M. Design and fabrication of magnetic nanoparticles for targeted drug delivery and imaging. Advanced Drug Delivery Reviews. 2010;62:284-304.

[123] Vayssieres L. Growth of Arrayed Nanorods and Nanowires of ZnO from Aqueous Solutions. Advanced Materials. 2003;15:464-6.

[124] Wepasnick KA, Smith BA, Schrote KE, Wilson HK, Diegelmann SR, Fairbrother DH. Surface and structural characterization of multi-walled carbon nanotubes following different oxidative treatments. Carbon. 2011;49:24-36.

[125] Smith BS. Titania nanotube arrays: Interfaces for implantable devices. 2012.

[126] Thompson MT, Berg MC, Tobias IS, Rubner MF, Van Vliet KJ. Tuning compliance of nanoscale polyelectrolyte multilayers to modulate cell adhesion. Biomaterials. 2005;26:6836-45.

[127] Łopacińska JM, Grădinaru C, Wierzbicki R, Køber C, Schmidt MS, Madsen MT, et al. Cell motility, morphology, viability and proliferation in response to nanotopography on silicon black. Nanoscale. 2012;4:3739-45.

[128] Fraser SA, Ting Y-H, Mallon KS, Wendt AE, Murphy CJ, Nealey PF. Sub-micron and nanoscale feature depth modulates alignment of stromal fibroblasts and corneal epithelial cells in serum-rich and serum-free media. Journal of Biomedical Materials Research Part A. 2008;86A:725-35.

[129] Curtis A, Wilkinson C. New depths in cell behaviour: reactions of cells to nanotopography. Biochemical Society symposium. 1999;65:15-26.

[130] Park J, Bauer S, Schmuki P, von der Mark K. Narrow Window in Nanoscale Dependent Activation of Endothelial Cell Growth and Differentiation on TiO2 Nanotube Surfaces. Nano Letters. 2009;9:3157-64.

[131] Mo XM, Xu CY, Kotaki M, Ramakrishna S. Electrospun P(LLA-CL) nanofiber: a biomimetic extracellular matrix for smooth muscle cell and endothelial cell proliferation. Biomaterials. 2004;25:1883-90.

[132] Khang D, Choi J, Im Y-M, Kim Y-J, Jang J-H, Kang SS, et al. Role of subnano-, nano- and submicron-surface features on osteoblast differentiation of bone marrow mesenchymal stem cells. Biomaterials. 2012;33:5997-6007.

[133] Brammer KS, Choi C, Frandsen CJ, Oh S, Jin S. Hydrophobic nanopillars initiate mesenchymal stem cell aggregation and osteo-differentiation. Acta Biomaterialia. 2011;7:683-90.

[134] Baranes K, Chejanovsky N, Alon N, Sharoni A, Shefi O. Topographic cues of nano-scale height direct neuronal growth pattern. Biotechnology and Bioengineering. 2012;109:1791-7.

[135] Kirkpatrick CJ, Krump-Konvalinkova V, Unger RE, Bittinger F, Otto M, Peters K. Tissue response and biomaterial integration: the efficacy of in vitro methods. Biomolecular Engineering. 2002;19:211-7.

[136] Schaffner P, Meyer J, Dard M, Nies B, Verrier S, Kessler H, et al. Induced tissue integration of bone implants by coating with bone selective RGD-peptides in vitro and in vivo studies. Journal of Materials Science: Materials in Medicine. 1999;10:837-9.

[137] Porter JR, Henson A, Popat KC. Biodegradable poly(ε-caprolactone) nanowires for bone tissue engineering applications. Biomaterials. 2009;30:780-8.

CHAPTER 2

FABRICATION OF POLYCAPROLACTONE NANOSTRUCTURED SURFACES

2.1. Introduction

Current treatments for cardiovascular disease include organ transplants, surgery, metabolic products and mechanical/synthetic implants [1]. Of these, mechanical and synthetic implants have shown great promise in recent years, however, synthetic polymers have been recognized as better candidates for cardiovascular repair due to the thrombogenic nature of metallic cardiovascular implants [2]. In particular, polymers such as polyurethane [3], poly(L-lactic acid) [4], polyglycolic acid [5] and polycaprolactone (PCL) [6], have proven to be of tremendous use due to their biocompatibility and controlled mechanical properties. These polymers have been used to develop cardiovascular devices such as vascular grafts [7], artificial hearts [8], and heart valves [9], all of which have been widely used in recent years [10]. Implants have the potential to replace the damaged components of the cardiovascular system, while maintaining normal tissue function. However, these implants have significant limitations even after decades of research devoted to developing blood-contacting devices [11, 12]. The greatest shortcoming is the lack of complete biocompatibility, leading to poor tissue/biomaterial integration and further biomaterial rejection [13].

PCL has emerged as a promising implant polymer due to the fact that it is a bioresorbable polyester with exceptional mechanical strength as well as a tunable degradation rate and glass transition temperature of about 60 °C. Extensive *in vitro* and *in vivo* biocompatibility and efficacy studies have been performed with PCL, resulting in US Food and Drug Administration approval of a number of medical devices. PCL is a versatile polymer, capable of being

transformed into a variety of topographies and structures. These include nanospheres [14, 15] nanowires [16, 17], nanofibers [18, 19], biodegradable thermoresponsive physical hydrogel nanofibers [20] and ultra-thin membranes [21]. In this work, we explore responses to two different nanotopographies, nanofiber and nanowire. PCL nanofibers were fabricated with an electrospinning technique and a novel solvent-free template synthesis technique was used to fabricating controlled arrays of high aspect ratio, substrate-bound nanowires. These two nanotopographies were chosen because they have similar sized features that are aligned differently; NWs are aligned perpendicular to the surface while NFs are aligned parallel to the surface. It is hypothesized that this alteration in the alignment of nanostructures on the surface will result in a very different response to blood components, thus altering the hemocompatibility.

2.2. Materials and Methods

2.2.1. PCL nanofiber fabrication

PCL nanofiber (notation: NF) surfaces were fabricated by an electrospinning technique (**Figure 3.1.**). The electrospinning apparatus consisted of a syringe pump, a glass syringe, teflon fluidic tubing, a 20-gauge blunt-tip catheter, and a male luer lock adapter. A high-voltage power source was connected to the catheter tip with a standard alligator clamp. The collector consisted of an aluminum foil fastened onto a 0.5” thick copper plate with electrical tape and positioned horizontally below the catheter. Polymer solution was prepared by dissolving oleic acid sodium salt (OLA) in methanol. PCL pellets (MW = 80000) were dissolved in chloroform and the polymer solution was mixed with OLA in methanol on a magnetic stir plate to produce a homogeneous mixture with a 4:1 chloroform:methanol volume ratio. The final solution was 12% solid w/w and the PCL:OLA ratio of the solid weight was 97:3 [22]. The volumetric flow rate

was 10ml/hr, applied voltage was 20 kV, and tip-to-collector was distance 9cm. Finally, OLA was leached out by placing nanostructured surfaces in methanol for 1h.

All the surfaces that were used for biological studies were approximately 1cm in diameter. The surfaces were sterilized in 70% ethanol for 30mins, followed by washing (2×) with PBS. They were air dried and further sterilized by uv exposure for 30mins before using for biological studies.

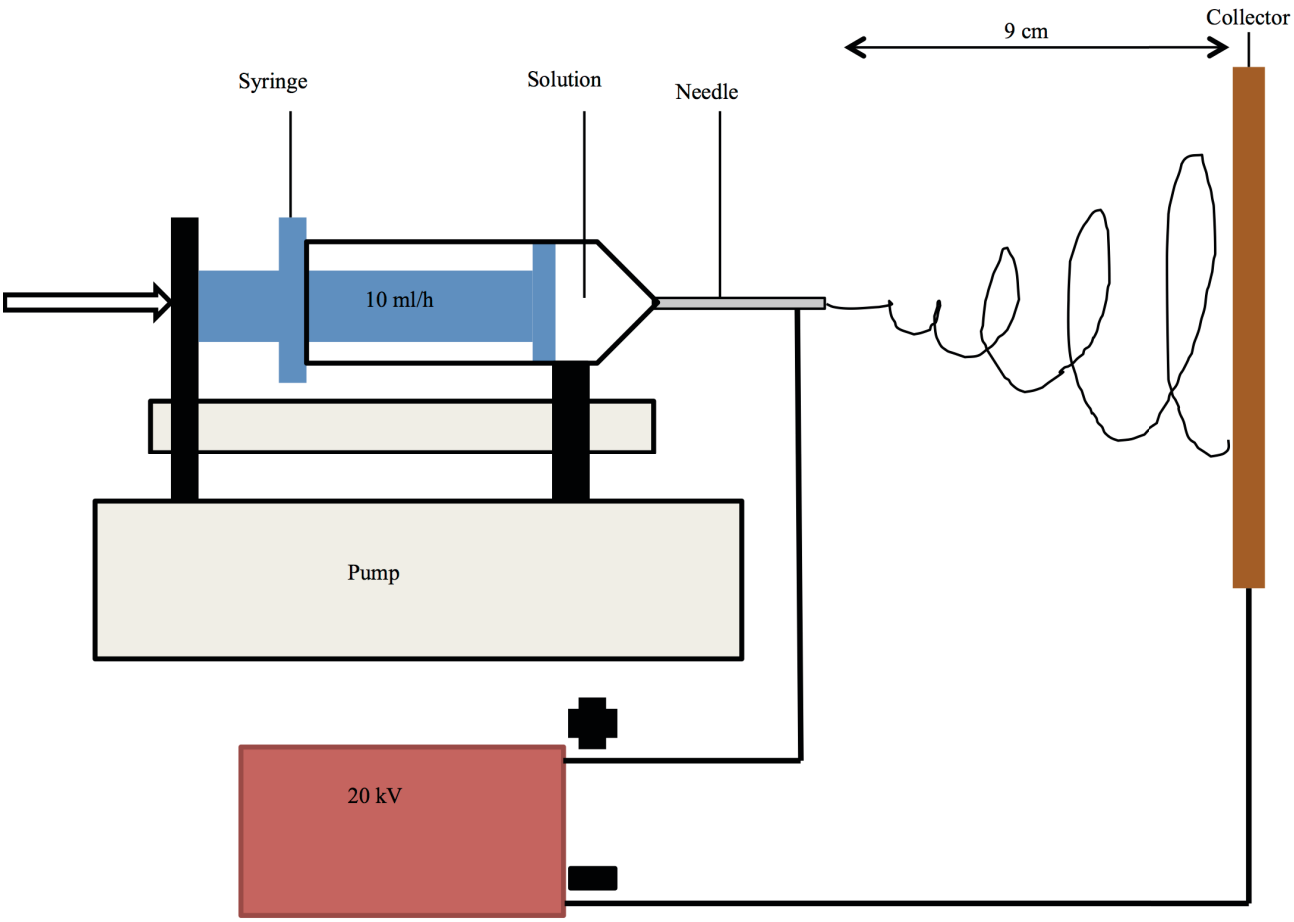

Figure 2.1. Schematic of how PCL nanofiber surfaces were fabricated.

2.2.2. Fabrication of PCL nanowire surfaces

Control (smooth PCL) surfaces were fabricated by sintering PCL pellets (MW = 80000, Sigma) on a glass plate in a 10 mm Teflon washer. The resulting discs were then air-cooled before using a biopsy punch to ensure a common diameter between all surfaces (10 mm).

PCL nanowire surfaces were fabricated using a solvent free nanotemplating technique with 20 nm diameter nanoporous aluminum oxide membranes [23] (**Figure 2.2.**). Previously fabricated PCL discs were placed on the membrane surface and placed in an oven at 115 °C for 3-5 min, thus allowing the nanowires to gravimetrically extrude through the membrane. The aluminum oxide membranes were then dissolved in 1 M NaOH for 75 min and surfaces were then washed in DI water (3x), dried and stored in a desiccator until their use was required.

Prior to any further use, all surfaces were sterilized in 70 % ethanol for 30 min, followed by washing with PBS (2x). Surfaces were then air dried and further sterilized by UV exposure for 30 min.

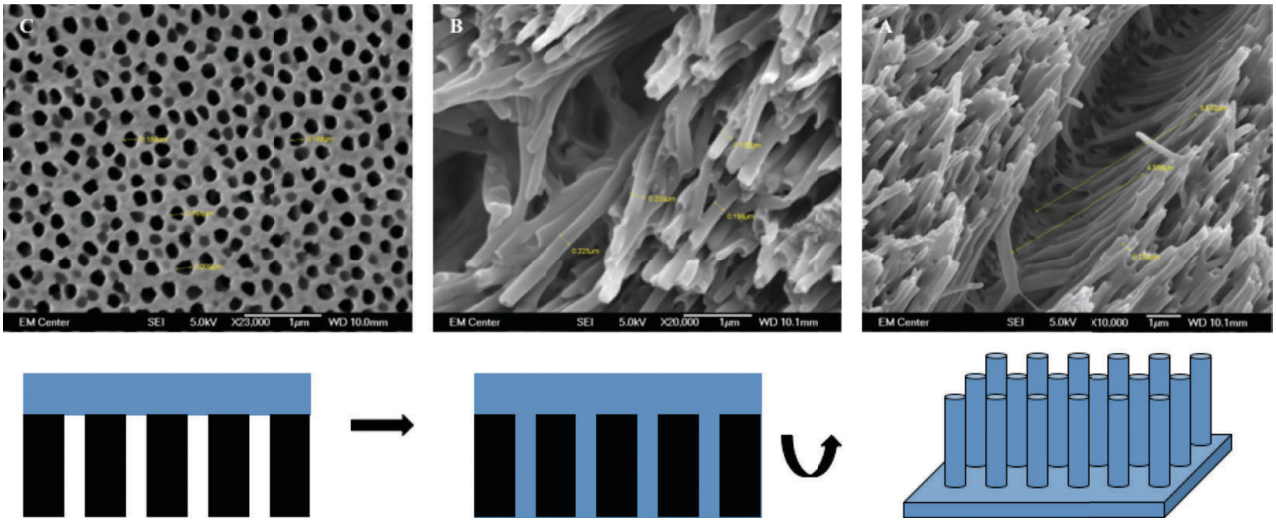

Figure 2.2. Schematic of how PCL nanowires were made via nanotemplating technique. PCL is extruded through an alumina membrane (top left), alumina is dissolved producing nanowire surfaces.

2.2.3. Immobilization of Collagen on PCL and NW surfaces

Surfaces fabricated as described in section 2.3 were immobilized with collagen in three steps:

1. The surfaces were aminolyzed by incubating in 1,6-hexanediamine/2-propanol (6 % w/v) for 10 min at 37 ºC followed by rinsing with DI water (3x) to remove free 1,6-hexanediamine.
2. The surfaces were then incubated in a gluteraldehyde (1 % w/v) solution at 2-4 ℃ for 24 hrs and then rinsed with DI water (3x) to remove free gluteraldehyde.
3. Surfaces were then incubated in collagen (1 % w/v) for 24 hrs at 2-4 ℃. Following the incubation, surfaces were rinsed with 0.1 M acetic acid solution, followed by DI water (3x) to remove excess, ungrafted collagen.

Note: Notation for different surfaces in the rest of this dissertation is as follows - Control (PCL), Control+Collagen (cPCL), Nanowire (NW), Nanowire+Collagen (cNW), Nanofiber (NF).

2.2.4. Characterization of PCL nanowire and nanofiber surfaces

The surface architecture of the nanostructured surfaces was characterized using scanning electron microscope (SEM, JEOL JSM-6300). The surfaces were coated with a 10 nm layer of gold and imaged at 5-7 kV. Nanowire and nanofiber diameters and heights were computed using the image analysis system built into the SEM.

Surface hydrophilicity was characterized by measuring the contact angle of DI water (**Figure 2.3.**). A droplet of DI water, approximately 100 μL in volume, was formed on the tip of the syringe and the machine stage was moved upward so that the droplet contacted and detached

onto the surface. The water droplet image on the surface was captured within 5 secs after the contact by a camera leveled with the surface. Images were then analyzed with the accompanying software to measure the contact angles. Each experiment was performed on three different locations on each surface, and on at least three different surfaces (nmin = 9) [24].

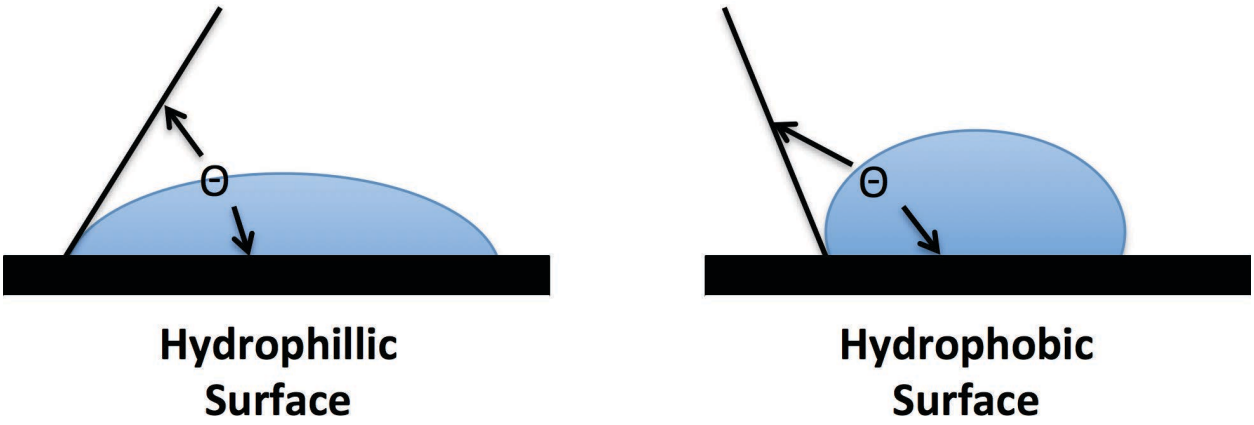

Figure 2.3. Schematic of how contact angle measurements are taken.

2.2.5. Characterization of cPCL and cNW surfaces

The surface architecture of the different surfaces throughout each step in the immobilization process was characterized using scanning electron microscopy (SEM). Prior to imaging, the surfaces were coated with a 10 nm layer of gold and imaged at 5-7 kV. Surface morphology was investigated to ensure a stable architecture throughout the collagen immobilization process.

Surface wettability was characterized by measuring the water contact angle using a goniometer (FTA1000 B Class) (**Figure 2.3.**). A 1 μL droplet of DI water was formed on the tip of the syringe and the stage was moved upward so that the droplet contacted and detached onto the surface. The water droplet image on the surface was captured within 5 secs after the contact

by a camera leveled with the surface. Images were then analyzed with the accompanying Fta32 software to measure the contact angles. Images were also captured every 30 secs for 5 mins after contact of droplet with the surface by a camera leveled with the surface. Images were then analyzed with accompanying software (DROPimage advanced software) to measure contact angles. Each experiment was performed on three different locations on each surface and on at least three different surfaces after each step in the collagen immobilization on PCL and NW surfaces (n_{min} = 9) [24]. From contact angle values, surface energies were calculated using the equation (1):

Equation (1): $E_s = E_{lv} \cos \theta$

where E_{lv} = 72.8 mJ/m^2 at 20 ºC for pure water and θ is the static contact angle [25]. Here E_s is the surface energy of the contacting surface and E_{lv} is the surface energy between the water and air under ambient conditions.

In order to verify the presence of amine groups on PCL surfaces after aminolysis (Step 1), ninhydrin staining was used [26]. Aminolyzed PCL and NW surfaces were first incubated in 1.0 M ninhydrin/ethanol solution for 1 min. Surfaces were then placed in glass petri dishes with a cover and incubated at 37 ºC for 15 min in order to allow color to develop. The surfaces were then photographed using a digital camera. Further, a fluorescamine method was used to quantify the density of -NH_2 groups on the surfaces after aminolysis [27]. Aminolyzed PCL and NW surfaces were dissolved in 2 ml 1,4-dioxane. Once the surfaces were dissolved, 2 ml fluorescamine/acetone solution (1mg/ml) was added, followed by 2 ml of 2-propanol. 300 µl of this solution was then placed in duplicate into the wells of a white 96-well plate. Fluorescence intensity was measured (excitation wavelength 395 nm, maximum emission wavelength 480 nm)

using a microplate reader. A calibration curve was obtained with known concentrations of 1,6-hexanediamine in the same solution to determine the density of $–NH_2$ groups on the surfaces.

Surface composition after each step of collagen immobilization was determined using X-ray photoelectron spectroscopy (XPS). Survey and high-resolution C1s and N1s scans were taken after each step in the immobilization process in order to determine the overall compositional changes. The thickness of immobilized collagen on cPCL and cNW surfaces was determined from the attenuation of C1s peaks from the survey scans. The thickness was acquired by using the standard uniform overlayer model, which is given by equation (2):

Equation (2):
$$I = I_0\left(\frac{t}{E_{\mathrm{L}}\sin\theta} - 1\right)$$

where I_0 is the intensity of C1s peaks before surface modification, I is the intensity of C1s peaks after immobilization with collagen, t is the thickness of the film, E_{L} is the electron attenuation length for carbon peak and θ is the angle at which the X-ray hits the surface. The electron attenuation lengths (E_{L}) for the carbon peak need to be calculated to obtain the film thickness from this equation. E_{L} was calculated using equation (3):

Equation (3):
$$E_{\mathrm{L}} = \frac{49}{E^2\rho} + 0.11\frac{\sqrt{E}}{\rho}$$

where E is the electron energy (X-ray core energy – core binding energy for carbon) = 1486 − 285 = 1201 eV) and ρ is the density of collagen (3.54 g/cm^3).

2.3. Results and Discussion

2.3.1. Characterization Results of PCL nanowire and nanofiber surfaces

In order to characterize the nanoarchitecture of the NW and NF surfaces, SEM imaging was used (**Figure 2.4.**). Using the image analysis system built into the SEM system, the height

and the diameter of the nanowires were computed to be 4.5 ± 0.5μm and 150 ± 50 nm respectively, while the diameter of the nanofibers was computed to be 297.9 ± 206.7 nm. The images show that the NW surfaces have a uniform architecture with occasional interruption in the uniformity by the presence of random microchannels formed due to surface charge effects. Previous studies have shown that similar NW and NF surfaces enhance cellular functionality [22, 28, 29].

The hydrophilic nature of the nanostructured surfaces was characterized by contact angle measurements of DI water using a sessile drop measuring technique. The contact angle is defined as the angle between the surface and the tangent line at the point of contact of the DI water droplet with the surface [24]. Higher surface energy is associated with hydrophilic surfaces, whereas lower surface energy is associated with hydrophobic surfaces. Further, it is well known that increased surface energy improves the interaction between the surface and the biological environment such as increased cell spreading on the surface [30]. The results indicate that the NW surfaces (71.9 ± 3.3º) are more hydrophilic compared to the NF surfaces (98.2º± 6.4º) and PCL surfaces surfaces (84.7 ± 1.5º) (**Figure 2.5.**).

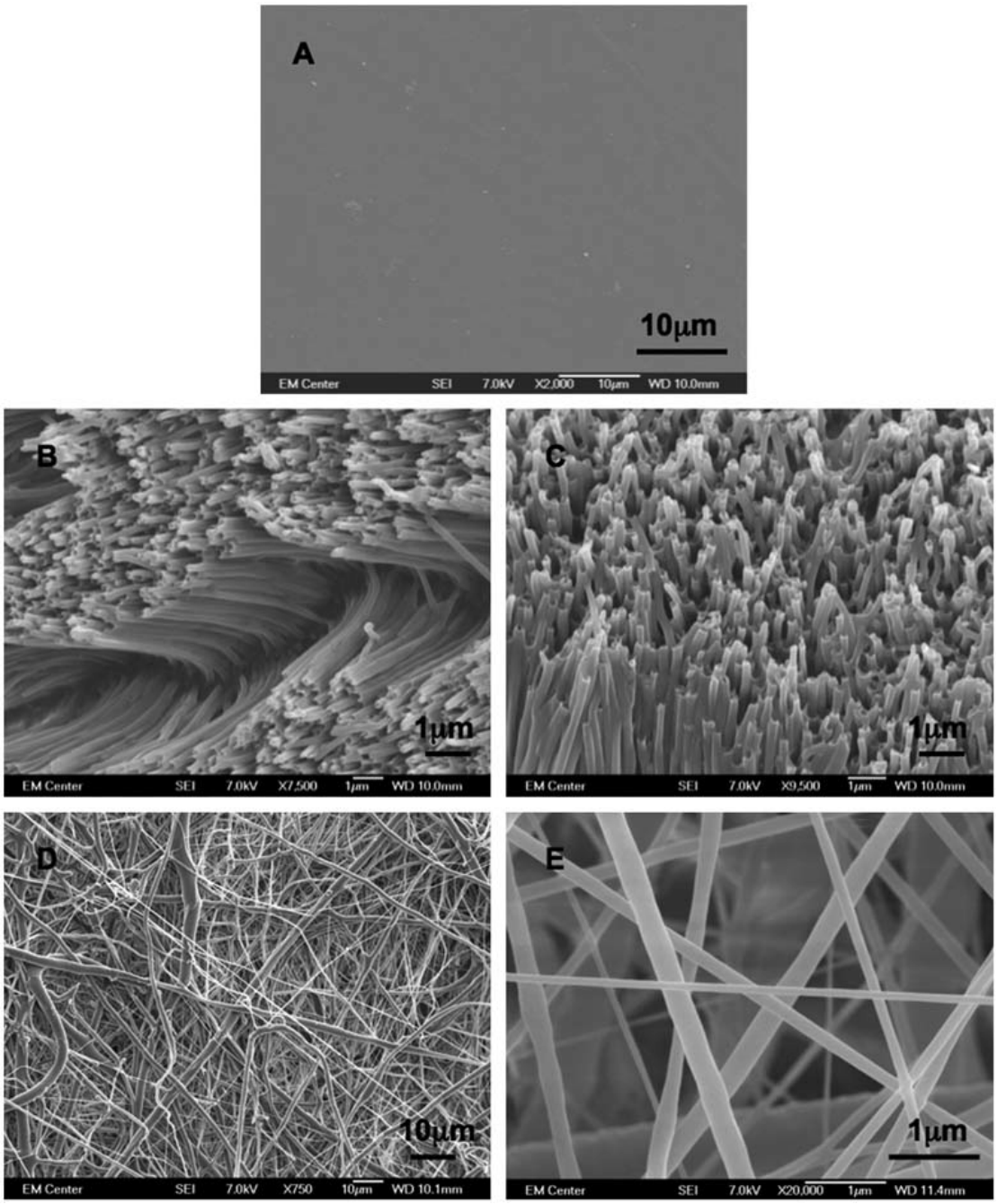

Figure 2.4. Representative SEM images of (A) PCL, (B and C) NW and (D and E) NF surfaces.

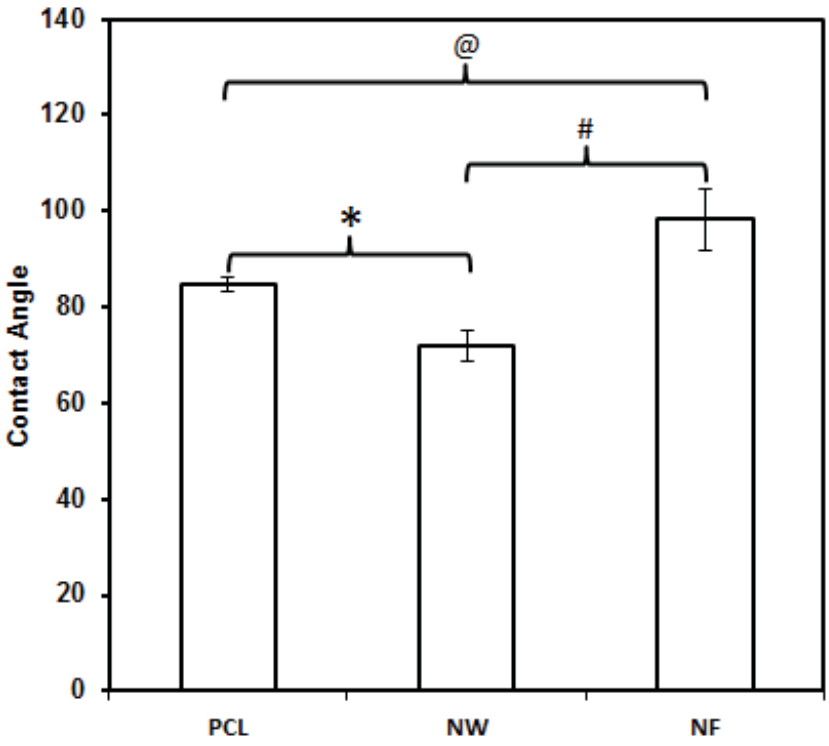

Figure 2.5. Contact angle measurements of PCL, NW and NF surfaces indicating hydrophillic/ hydrophobic nature of the surfaces. Significantly different contact angle measurements were seen on all three surfaces (@, #, *→ $p < 0.05$).

Total surface energy can be defined as the surface area times the specific surface energy. Due to the fact that all three surfaces are fabricated from PCL, the specific surface energy is constant. Thus the total surface energy is solely dependent on the surface area. The nano-architecture on NW contributes to a higher surface area compared to the PCL surface. The surface of the NF surfaces is PCL fibers that do not cover as much area as the PCL surfaces do. Therefore the total surface energy from high to low should be NW, PCL followed by NF. This is consistent with contact angle measurements because a high surface energy corresponds to a

lower contact angle. Therefore, by simply changing the topography, the surface energy can be altered, thus altering the biological response.

2.3.2 Characterization Results of cPCL and cNW surfaces

The surface architecture of PCL and NW surfaces was characterized using SEM after each step of collagen immobilization (**Figure 2.6.**). The unmodified PCL and NW surfaces have been previously characterized in section 2.3.2. [16]. After each step of modification, the SEM images indicate no significant changes as compared to unmodified surfaces. Further, it is evident that the NW surfaces maintain their nanoarchitecture throughout the immobilization process.

Surface wettability was characterized after each step of collagen immobilization by measuring the water contact angle. The results indicate that the surfaces are significantly more hydrophilic after -NH_2 modification and collagen immobilization for both PCL and NW surfaces as compared to unmodified surfaces (**Figure 2.7.(a)**). Further, the NW surfaces before and after -NH_2 modification and collagen immobilization were significantly hydrophilic compared to PCL surfaces before and after NH_2 modification and collagen immobilization. Surface energies were then calculated from the contact angle measurements using equation (1) (**Figure 2.7.(b)**). Results indicate that both PCL and NW surfaces show increase in surface energy after each step of collagen immobilization process, however NW surfaces have a higher surface energy due to the fact that they have more surface area than PCL. Studies have shown enhanced cell adhesion on surfaces with high energies [30, 31]. Furthermore, it has been suggested that nano- and submicron surface patterns with high surface energy can affect the endothelial cell adhesion while retaining bulk material chemistry [32]. Therefore it is hypothesized that a high surface

energy will promote the adherence of anchorage dependent endothelial cells while enhancing matrix production.

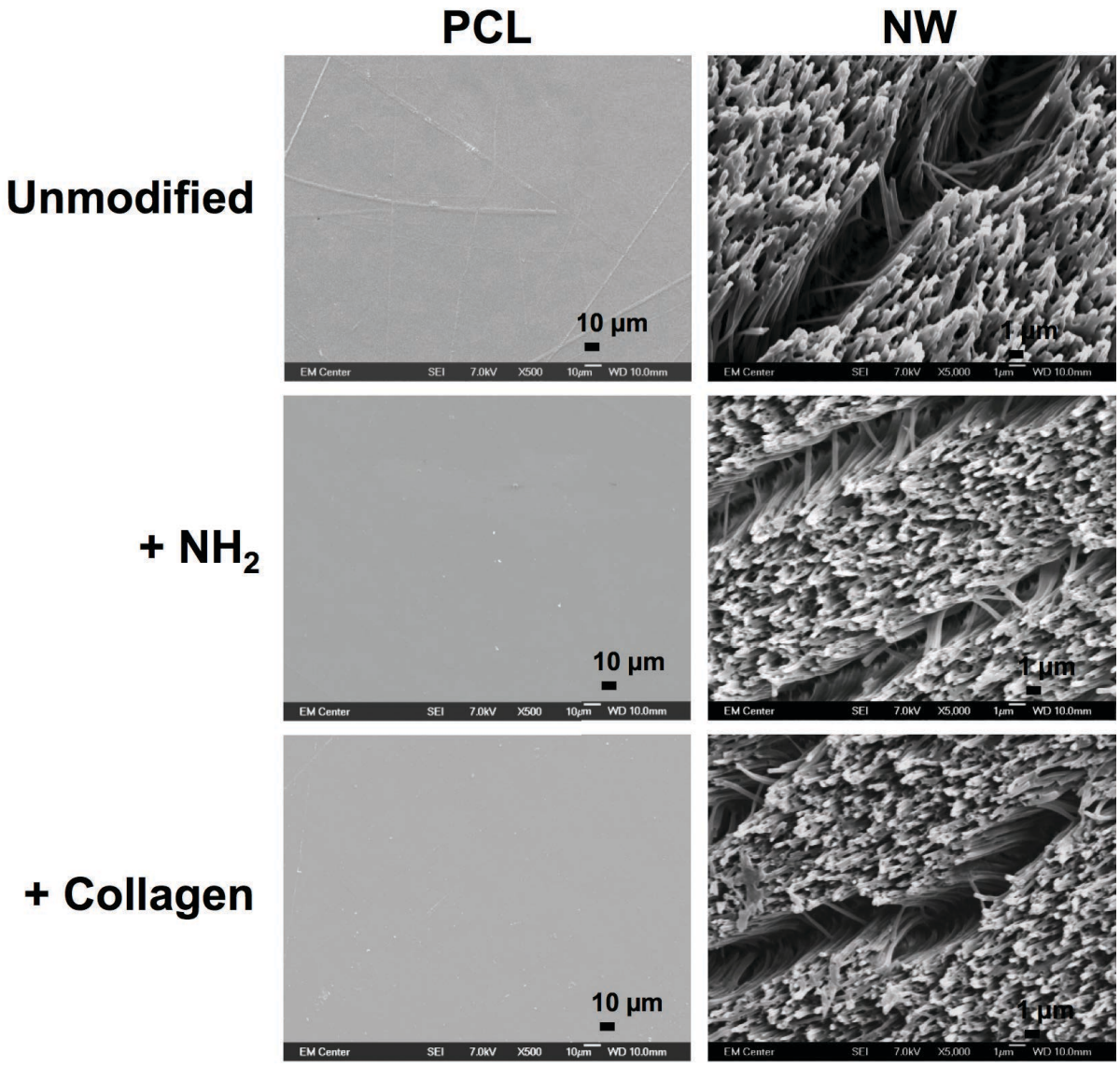

Figure 2.6. Representative scanning electron microscopy images of PCL and NW surfaces after each step of immobilization process (unmodified, + NH_2, + Collagen).

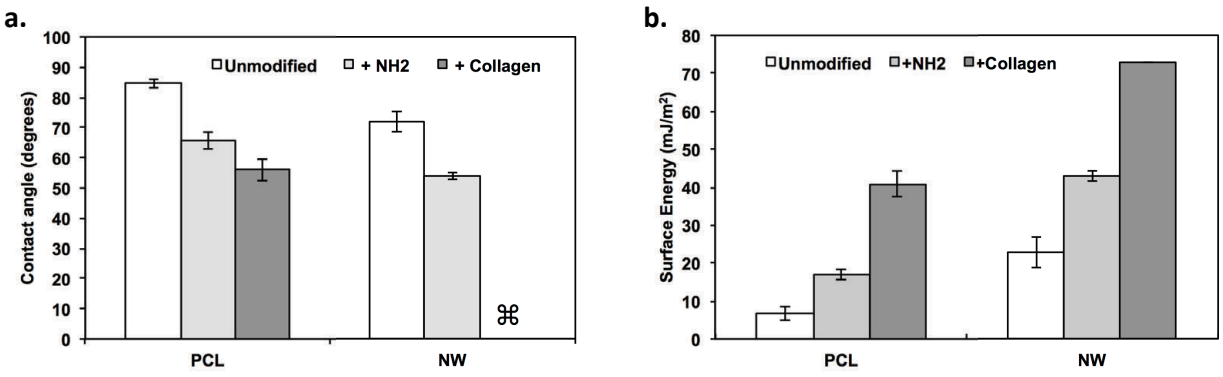

Figure 2.7. (a.) Contact angle measurements on PCL and NW surfaces after each step of immobilization process (unmodified, + NH_2, + Collagen). Experiments were performed on at least three different samples at three different locations (n_{min} = 9). Unmodified, + NH_2 and + Collagen surfaces (for both PCL and NW) were all statistically different ($p < 0.05$). Error bars represent standard deviation. (b.) Surface energies calculated from contact angle measurements for PCL and NW surfaces after each step of immobilization process (unmodified, + NH_2, + Collagen). Unmodified, + NH_2 and + Collagen surfaces (for both PCL and NW) were all statistically different ($p < 0.05$). Error bars represent standard deviation.

Water contact angles were also determined over a course of 5 mins. Contact angle is defined as the angle between the liquid/solid interface [33]. The results indicate significantly different contact angles between all four surfaces that were evaluated (**Figure 2.8.**). PCL surfaces have the highest contact angle, followed by NW and cPCL surfaces with cNW surfaces having the lowest contact angle. Further, the contact angles on all the surfaces decreased after 5 mins of contact with water droplet. However, the contact angle on cNW surfaces dropped within few seconds of contact with water droplet, indicating that the surface is extremely hydrophilic. Contact angles are dependent on surface area as well as specific surface properties such as polarity. The lower surface areas on PCL and cPCL surfaces attribute to the higher contact

angles compared to those on NW and cNW surfaces. Further collagen coating the surfaces decreases contact angle due to an increase in polar groups immobilized to the surface.

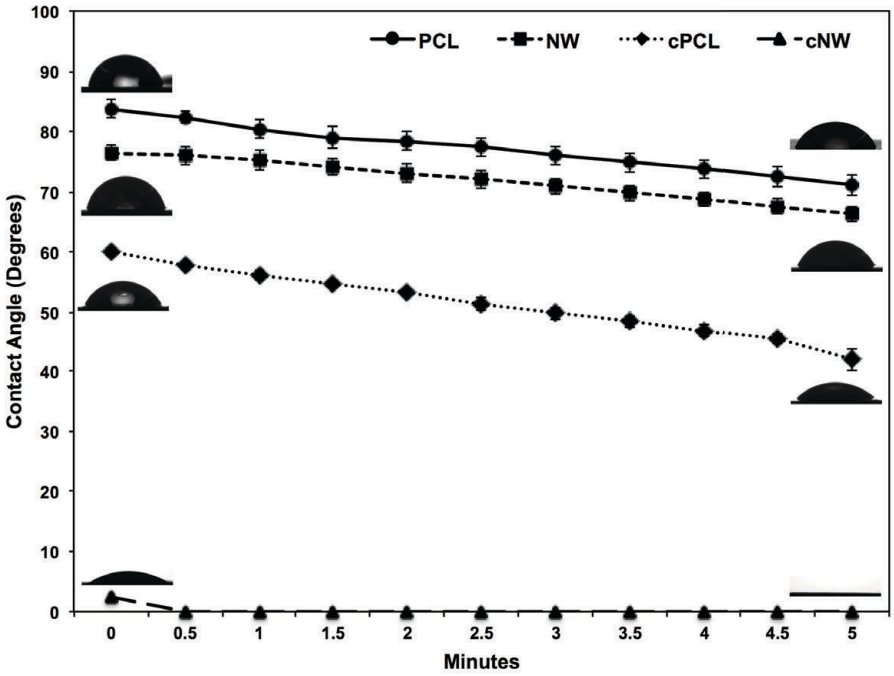

Figure 2.8. Contact angle measurements of PCL, NW, colPCL and colNW surfaces taken every 30 secs for 5 mins. Results indicate significant differences in contact angles on all surfaces (PCL>NW>colPCL>colNW) ($p<0.05$). Experiments were replicated with at least three different cell populations on at least three different samples ($n_{min} = 9$). Error bars represent standard error.

In order to verify the presence of amine groups on PCL surfaces after aminolysis (Step 1), ninhydrin staining was used. Results indicate that $-NH_2$ groups are evenly distributed on both PCL and NW surfaces that were aminolyzed as indicated by the uniform purple color on surfaces (**Figure 2.8**). No purple color was observed on unmodified PCL and NW surfaces indication no $-NH_2$ groups were present on the surfaces. Further, a fluorescamine method was used to quantify

the density of -NH_2 groups on the surfaces after aminolysis. The results indicate significantly higher -NH_2 density on NW surfaces as compared to PCL surfaces after aminolysis (**Figure 2.9.**). The increase in -NH_2 density can be explained due to the increased surface area of NW surfaces. The increase in surface area provides –NH_2 groups with more reactive sites to adhere to.

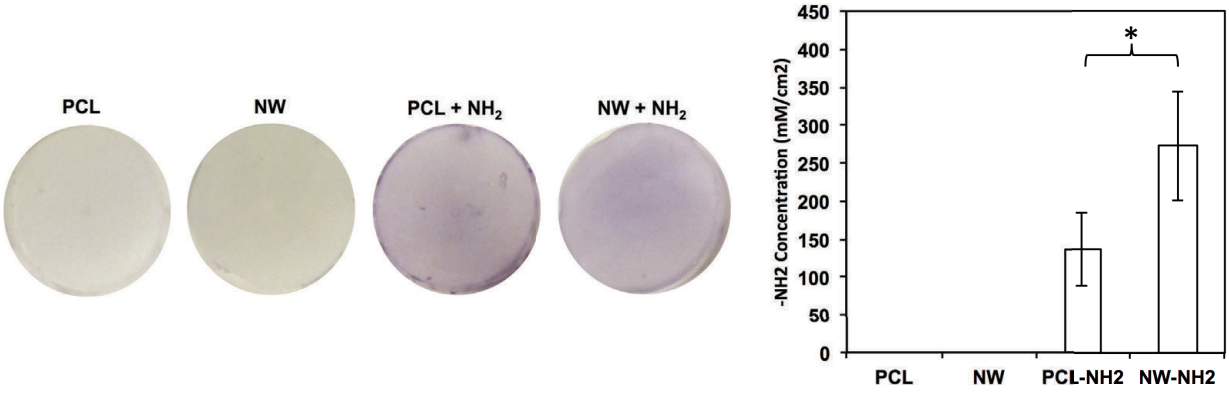

Figure 2.9. Representative images of PCL and NW surfaces before and after aminolysis stained with ninhydrin. The graph shows quantification of NH_2 groups on PCL and NW surfaces before and after aminolysis measured using fluorescamine method. Experiments were performed on at least nine different samples (n_{min} = 9). Unmodified PCL and NW surfaces did not show presence of NH_2 groups on the surface as compared to the surfaces that were aminolyzed. Error bars represent standard deviation.

Surface composition after each step of collagen immobilization was determined using XPS. Survey and high-resolution C1s and N1s scans were taken after each step in the immobilization process in order to determine the overall compositional changes. The survey and high-resolution N1s scans indicate increasing amounts of nitrogen on both PCL and NW surfaces after aminolysis and collagen immobilization (**Figure 2.10. and 2.11.(a)**). Similarly, the high-

resolution C1s scans indicate increasing amounts of carbon on both PCL and NW surfaces after aminolysis and collagen immobilization. (**Figure 2.11.(b)**). Further, the thickness of immobilized collagen on cPCL and cNW surfaces was determined from the attenuation of C1s peaks from the survey scans. The thickness was acquired by using the standard uniform overlayer model, which is given by equation (2). The thickness of collagen layer was approximately 1.56 nm on NW surfaces as compared to 1.65 nm on PCL surfaces, indicating similar film thickness on both surfaces.

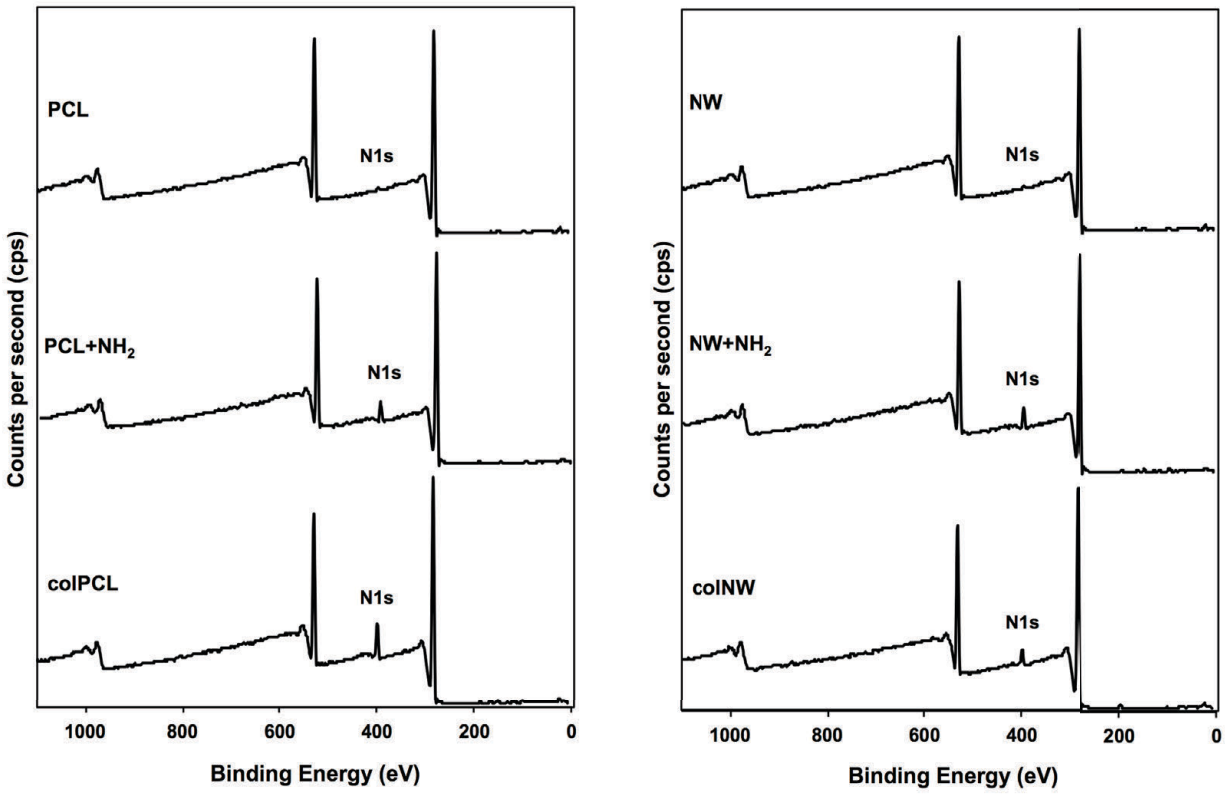

Figure 2.10. Survey XPS scans of PCL, NW, colPCL and colNW surfaces. Results show an increase in the N1s peak throughout the collagen immobilization process.

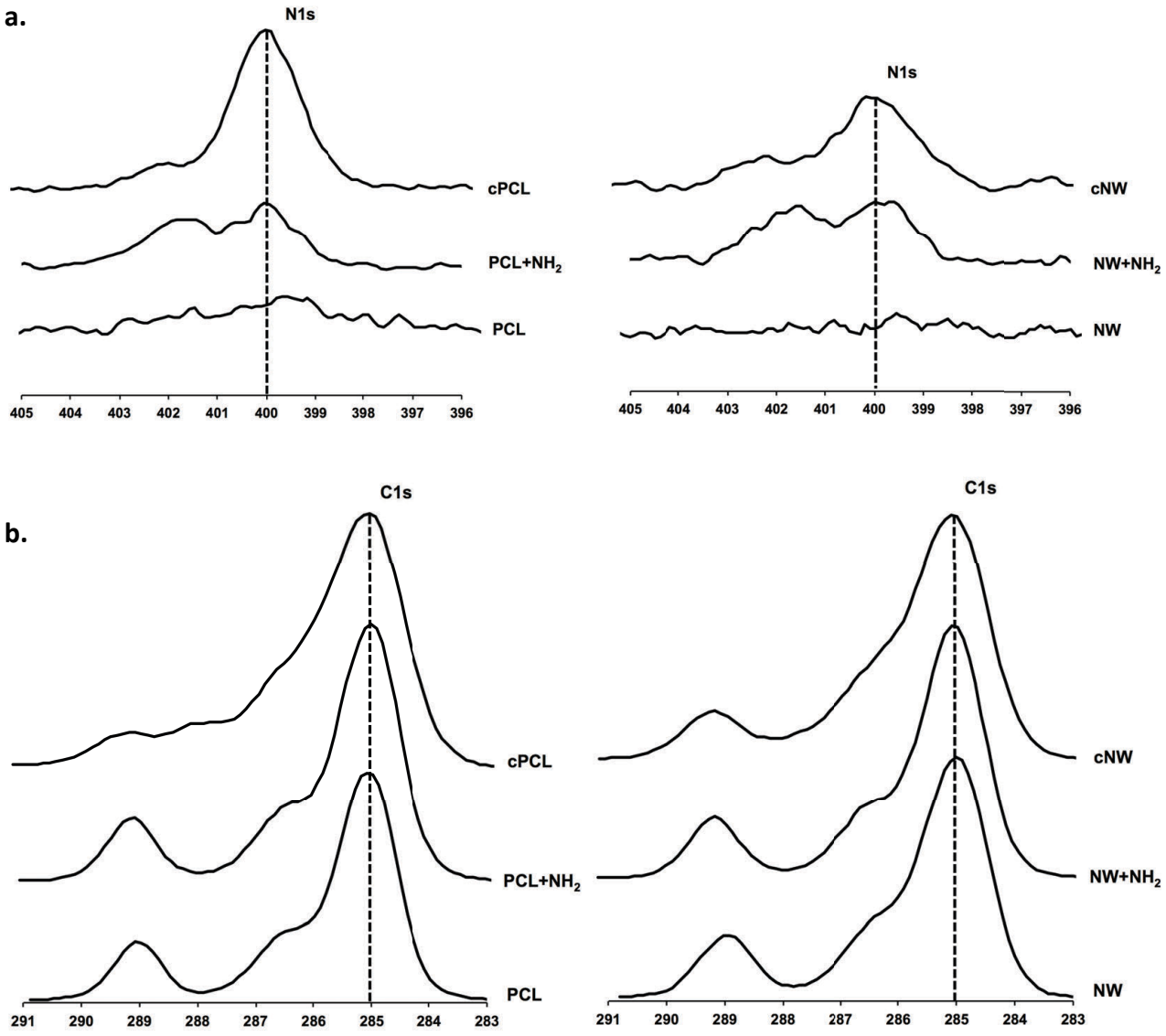

Figure 2.11. Representative high-resolution (a) N1s and (b) C1s XPS scans on PCL and NW surfaces after each step of immobilization process.

2.4. Conclusions

The surface properties of implantable cardiovascular devices are critical for long-term success. This research has investigated the characteristics of similar sized features that are aligned differently; NWs are aligned perpendicular to the surface while NFs are aligned parallel

to the surface. Further characteristics of collagen immobilized surfaces were also elucidated. These characteristics were evaluated using SEM, contact angle and XPS.

Polycaprolactone NFs were fabricated with an electrospinning technique and a novel solvent-free template synthesis technique was used to fabricating controlled arrays of high aspect ratio, substrate-bound NWs. Surfaces were immobilized with collagen utilizing an aminolysis method. The resulting SEM images show the production of either horizontally oriented, uniform NFs or vertically oriented, high aspect ratio and uniform NWs. Immobilizing collagen to the surfaces did not significantly alter the surface topography. Further, results identify a highly hydrophobic NF surface, while NW surfaces exhibit a more hydrophilic surface. The immobilization of collagen on the surfaces further decreases the contact angle. The simple fabrication, physiologically relevant architecture, low contact angle large surface area identify nanowire surface as promising interfaces for implantable biomedical devices. Further studies are now targeted towards understanding the effects of altered extrusion temperatures and membrane pore size on structural and mechanical NW characteristics.

REFERENCES

[1] Nugent HM, Edelman ER. Tissue Engineering Therapy for Cardiovascular Disease. Circulation Research. 2003;92:1068-78.

[2] van der Giessen WJ, Lincoff AM, Schwartz RS, van Beusekom HMM, Serruys PW, Holmes DR, et al. Marked Inflammatory Sequelae to Implantation of Biodegradable and Nonbiodegradable Polymers in Porcine Coronary Arteries. Circulation. 1996;94:1690-7.

[3] Ajili SH, Ebrahimi NG, Soleimani M. Polyurethane/polycaprolactane blend with shape memory effect as a proposed material for cardiovascular implants. Acta Biomaterialia. 2009;5:1519-30.

[4] Kim HI, Ishihara K, Lee S, Seo J-H, Kim HY, Suh D, et al. Tissue response to poly(l-lactic acid)-based blend with phospholipid polymer for biodegradable cardiovascular stents. Biomaterials. 2011;32:2241-7.

[5] Shinoka T, Ma PX, Shum-Tim D, Breuer CK, Cusick RA, Zund G, et al. Tissue-engineered heart valves. Autologous valve leaflet replacement study in a lamb model. Circulation. 1996;94:II164-8.

[6] Andukuri A, Kushwaha M, Tambralli A, Anderson JM, Dean DR, Berry JL, et al. A hybrid biomimetic nanomatrix composed of electrospun polycaprolactone and bioactive peptide amphiphiles for cardiovascular implants. Acta Biomaterialia. 2011;7:225-33.

[7] Motlagh D, Allen J, Hoshi R, Yang J, Lui K, Ameer G. Hemocompatibility evaluation of poly(diol citrate) in vitro for vascular tissue engineering. Journal of Biomedical Materials Research Part A. 2007;82A:907-16.

[8] Belanger MC, Marois Y, Roy R, Mehri Y, Wagner E, Zhang Z, et al. Selection of a polyurethane membrane for the manufacture of ventricles for a totally implantable artificial heart: Blood compatibility and biocompatibility studies. Artificial Organs. 2000;24:879-88.

[9] Maegdefessel L, Linde T, Krapiec F, Hamilton K, Steinseifer U, van Ryn J, et al. In vitro comparison of dabigatran, unfractionated heparin, and low-molecular-weight heparin in preventing thrombus formation on mechanical heart valves. Thrombosis Research. 2010;126:e196-e200.

[10] Motlagh D, Yang J, Lui KY, Webb AR, Ameer GA. Hernocompatibility evaluation of poly(glycerol-sebacate) in vitro for vascular tissue engineering. Biomaterials. 2006;27:4315-24.

[11] Rose EA, Gelijns AC, Moskowitz AJ, Heitjan DF, Stevenson LW, Dembitsky W, et al. Long-term use of a left ventricular assist device for end-stage heart failure. The New England journal of medicine. 2001;345:1435-43.

[12] Ratner BD. The blood compatibility catastrophe. Journal of Biomedical Materials Research. 1993;27:283-7.

[13] Anderson JM, Rodriguez A, Chang DT. Foreign body reaction to biomaterials. Seminars in immunology. 2008;20:86-100.

[14] Poletto FS, Silveira RP, Fiel LA, Donida B, Rizzi M, Guterres SS, et al. Size-control of poly(epsilon-caprolactone) nanospheres by the interface effect of ethanol on the primary emulsion droplets. Journal of nanoscience and nanotechnology. 2009;9:4933-41.

[15] Singh S, Singh AN, Verma A, Dubey VK. Biodegradable polycaprolactone (PCL) nanosphere encapsulating superoxide dismutase and catalase enzymes. Applied biochemistry and biotechnology. 2013;171:1545-58.

[16] Leszczak V, Smith BS, Popat KC. Hemocompatibility of polymeric nanostructured surfaces. Journal of biomaterials science Polymer edition. 2013;24:1529-48.

[17] Bechara SL, Judson A, Popat KC. Template synthesized poly(ε-caprolactone) nanowire surfaces for neural tissue engineering. Biomaterials. 2010;31:3492-501.

[18] Song T, Zhang Y, Zhou T, Lim CT, Ramakrishna S, Liu B. Encapsulation of self-assembled FePt magnetic nanoparticles in PCL nanofibers by coaxial electrospinning. Chemical Physics Letters. 2005;415:317-22.

[19] Alves da Silva ML, Martins A, Costa-Pinto AR, Costa P, Faria S, Gomes M, et al. Cartilage Tissue Engineering Using Electrospun PCL Nanofiber Meshes and MSCs. Biomacromolecules. 2010;11:3228-36.

[20] Loh XJ, Peh P, Liao S, Sng C, Li J. Controlled drug release from biodegradable thermoresponsive physical hydrogel nanofibers. Journal of Controlled Release. 2010;143:175-82.

[21] Chen F, Lee CN, Teoh SH. Nanofibrous modification on ultra-thin poly(e-caprolactone) membrane via electrospinning. Materials Science and Engineering: C. 2007;27:325-32.

[22] Ruckh TT, Kumar K, Kipper MJ, Popat KC. Osteogenic differentiation of bone marrow stromal cells on poly(epsilon-caprolactone) nanofiber scaffolds. Acta Biomaterialia. 2010;6:2949-59.

[23] Popat KC, Porter JR, Henson A. Biodegradable poly(epsilon-caprolactone) nanowires for bone tissue engineering applications. Biomaterials. 2009;30:780-8.

[24] Popat KC, Johnson RW, Desai TA. Characterization of vapor deposited poly (ethylene glycol) films on silicon surfaces for surface modification of microfluidic systems. Journal of Vacuum Science & Technology B. 2003;21:645-54.

[25] Liu X, Lim JY, Donahue HJ, Dhurjati R, Mastro AM, Vogler EA. Influence of substratum surface chemistry/energy and topography on the human fetal osteoblastic cell line hFOB 1.19:

Phenotypic and genotypic responses observed in vitro. Biomaterials. 2007;28:4535-50. Epub 2007 Jul 20.

[26] Zhang H, Lin C-Y, Hollister SJ. The interaction between bone marrow stromal cells and RGD-modified three-dimensional porous polycaprolactone scaffolds. Biomaterials. 2009;30:4063-9.

[27] Zhu Y, Ong WF. Epithelium regeneration on collagen (IV) grafted polycaprolactone for esophageal tissue engineering. Materials Science and Engineering: C. 2009;29:1046-50.

[28] Bechara SL, Judson A, Popat KC. Template synthesized poly(@?-caprolactone) nanowire surfaces for neural tissue engineering. Biomaterials. 2010;31:10-.

[29] Porter JR, Henson A, Popat KC. Biodegradable poly(ε-caprolactone) nanowires for bone tissue engineering applications. Biomaterials. 2009;30:780-8.

[30] Zhao G, Schwartz Z, Wieland M, Rupp F, Geis-Gerstorfer J, Cochran DL, et al. High surface energy enhances cell response to titanium substrate microstructure. Journal of Biomedical Materials Research Part A. 2005;74A:49-58.

[31] Wan Y, Yang J, Yang J, Bei J, Wang S. Cell adhesion on gaseous plasma modified poly-(l-lactide) surface under shear stress field. Biomaterials. 2003;24:3757-64.

[32] Joseph C, Dongwoo K, Thomas JW. Nanometer polymer surface features: the influence on surface energy, protein adsorption and endothelial cell adhesion. Nanotechnology. 2008;19:505103.

[33] Cassie A. Contact angles. Discussions of the Faraday Society. 1948;3:11-6.

CHAPTER 3

HEMOCOMPATIBILITY OF POLYMERIC NANOSTRUCTURED SURFACES

3.1. Introduction

Cardiovascular disease is the leading cause of death worldwide killing 17.3 million people a year [1]. Current treatments for cardiovascular diseases include organ transplants, surgery, metabolic products and mechanical/synthetic implants [2]. Of these, mechanical and synthetic implants have shown great promise in recent years. Metals, natural polymers and synthetic polymers have been used in these mechanical and synthetic cardiovascular implants [3,4]. However, synthetic polymers have been recognized as better candidates for cardiovascular repair due to the thrombogenic nature of metals and limit in processability of natural poly- mers [5,6]. In particular, synthetic polymers such as polyurethane [7], poly(L-lactic acid) [8], polyglycolic acid [9] and polycaprolactone (PCL) [10] have proven to be of tremendous use due to their biocompatibility and controlled mechanical properties. These polymers have been used to develop cardiovascular devices such as vascular grafts [11], artificial hearts [12], and heart valves [13], all of which have been widely used in recent years [14]. These implants have the potential to replace the damaged components of the cardiovascular system, while maintaining the normal tissue function. Tissue integration is important property when inducing transplant tolerance, however, the hemocompatibility of the biomaterial surface also plays an important role in the ultimate success of the implant. Therefore, in order to induce transplant tolerance, it is critical to understand the interaction of blood components with the material surfaces [15,16]. Hemocompatibility is an essential property of biomaterials and can be measured by the interaction between the material and the

various blood components, such as blood plasma proteins, erythrocytes, platelets and leukocytes [17]. Lack of hemocompatibility can lead to either rejection and/or loss of function [18] initially through the activation of the blood coagulation cascade followed by initiation of immune responses [19]. Blood reactions occur as a result of the physical and chemical properties of implant surface, therefore tolerance can potentially be achieved by altering the biomaterial surface properties [20].

When a biomaterial is implanted inside the body, proteins are adsorbed on the material surface [21], followed by platelet adhesion and activation, eventually leading to the formation of thrombus [22]. Previous work has investigated various surface modifications strategies to alter the hemocompatibility of biomaterial surfaces [23–25]. Inorganic and organic coatings [26], polymer surface chemical modification [27], and chemically patterned surfaces [28] have been used to alter hemocompatibility. These surfaces have proven to produce favorable hemocompatible response through inertness, chemical and mechanical stability, and low protein adsorption [19,28]. Unfortunately, these surfaces are not stable when exposed to the shear stresses of blood flow [29], thus it is important to have a robust surface that can withstand physiological forces. The hierarchy of the natural tissue extracellular matrix (ECM), from nano to macro scale, has inspired fabrication of surfaces with different topographies. In recent years, nanostructured surfaces have emerged as a potential solution to improve material integration with the tissue. Studies have shown that surfaces that mimic the ECM nanotopography can promote tissue integration and regeneration [30]. Thus, polymers with tunable properties have been extensively researched. Polymeric nanostructured surfaces have shown to affect cellular growth and functionality [31–33]. In particular, these surfaces have demonstrated improved fibroblast cell adhesion [34], neuronal cell differentiation [35], and

osteoblast phenotypic activity [19,36]. However, it is unclear how these polymeric nanostructured surfaces interact with the blood and its components. An understanding of blood/nanomaterial interaction is essential to understand how transplant tolerance is induced using nanostructured surfaces.

In this study, we have investigated the hemocompatibility of two different nanostructured surfaces: nanowires (NWs) and nanofibers (NFs). These two nanotopographies were chosen because they have similar sized features that are aligned differently; NWs are aligned perpendicular to the surface while NFs are aligned parallel to the surface. It is hypothesized that this alteration in the alignment of nanostructures on the surface will result in a very different response to blood components, thus altering the hemocompatibility. PCL was chosen as the material since it is a bioresorbable polyester with exceptional mechanical strength and low degradation rate [37]. PCL scaffolds have been used extensively in many tissue engineering applications, specifically for vascular tissue [38,39], bone and cartilage [40,41], nerve [42,43], dental [44] and skin [45]. The low degradation rate of PCL is favorable for long-term implants [46,47]. Further, degradation products of PCL in the body can be removed naturally by the metabolic pathways [3,37,48] eliminating the possibility of foreign body reactions. PCL can also be processed into unique nanostructured surfaces such as NWs [49], thin film NWs [50], nano-fibrous networks [51] and NFs [52–54]. These nanostructured features are capable of being tuned. For example, electrospinning has shown promising results with its ability to fabricate surfaces that mimic the ECM hierarchy. By changing electrospinning parameters such as voltage, working distance and polymer concentration, the surface properties can be easily tuned to match the natural ECM hierarchy [55].

To evaluate interactions at the blood-nanomaterial interface, it is necessary to understand the events that occur during the introduction of a foreign object inside the body. Driven by a need for understanding potential biomedical and clinical uses of PCL nanostructured surfaces, this work specifically looks at the earliest stages of blood-material interaction by considering the *in vitro* adsorption of key blood serum proteins, adhesion and activation of platelets and clotting kinetics of whole blood. In this study blood serum protein adsorption on nanostructured surfaces was investigated using a colorimetric assay and X-ray photoelectron spectroscopy (XPS). Fluorescence microscopy and scanning electron microscope (SEM) were used to determine the adhesion and activation of platelets. A simple hemolysis assay was used to investigate the whole blood clotting kinetics. It was found surfaces fabricated from the same material PCL with altered nanotopography orientation, induce different hemocompatible response.

3.2. Materials and methods

3.2.1. Fabrication and characterization of PCL NW and NF surfaces

Surfaces were fabricated and characterized as described in detail in section 2.2.1 and 2.2.2. The nanowire surface architecture was examined for uniformity and repeatability using SEM imaging.

3.2.2. Protein adsorption on PCL NW and NF surfaces

In order to understand how key blood serum proteins interact with the nanostructured sur- faces; albumin (ALB), fibrinogen (FIB) and immunoglobulin-G (IgG) (Sigma) adsorption was investigated on PCL, NW and NF surfaces. Sterilized surfaces were incubated in a 24-

well plate with 100 μg/ml solution of ALB, FIB and IgG in PBS on a horizontal shaker plate (100 rpm) at 37 °C and 5% CO_2. After 2hrs of incubation, the protein solution was aspirated followed by 3 rinses with PBS to remove any non-adherent proteins. The protein adsorption was measured using a commercially available micro-BCA assay (Pierce Biotechnology) and the adsorbed protein on nanostructured surfaces was visualized by SEM imaging.

In order to measure the protein adsorption using micro-BCA assay, all the surfaces were transferred to a fresh 24-well plate and incubated with 1% sodium dodecyl sulfate (SDS) solution (SDS, Sigma) in PBS on a horizontal shaker plate (100 rpm) for 1hr. Following incubation, the excess SDS solution with solubilized proteins was collected from each well. The SDS incubation was repeated 2 more times and the resulting SDS solution with solubi- lized proteins was pooled. The concentration of the total adsorbed protein in the pooled SDS solution was then measured colorimetrically using a micro-BCA assay with a plate reader.

XPS (XPS, ESCASystems X-ray Photoelectron Spectrometer 5800) was used to determine the surface composition of adsorbed proteins on nanostructured surfaces. High-resolution spectra were collected for C1s peak with a pass energy of 10 eV. Peak fit analysis was performed using Multipack and XPSPeak 4.1 (Freeware) software.

Further, the protein adsorbed nanostructured surfaces were air dried and coated with a 10 nm layer of gold and imaged at 5–7 kV.

3.2.3. Platelet isolation from whole blood

Whole blood from healthy individuals, acquired through venopuncture, was drawn into standard 6 ml vacuum tubes coated with the anti-coagulant, ethylenediaminetetra acetic acid (EDTA). The first tube was discarded to account for the skin plug and locally activated platelets resulting from the needle insertion. The blood vials were centrifuged at 150 g for 15 min to separate the plasma from the red blood cells (erythrocytes). The plasma was then pooled into fresh tubes, and used within 2 h.

3.2.4. Platelet adhesion and viability on PCL NW and NF surfaces

Sterilized PCL, NW and NF surfaces were incubated in a 24-well plate with 1,000 µl of pooled plasma at room temperature on a horizontal shaker plate (100 rpm) for 2 h. The effects of the surface nanoarchitecture on platelets adhesion and viability were investigated and compared to that on the control surface.

Platelet adhesion was characterized by staining the cells with calcein-AM (Invitrogen) live stain. Prior to staining, the un-adhered platelets were removed by aspirating the plasma from the surfaces followed by rinsing with PBS. The surfaces were incubated with 2 µM calcein- AM solution in PBS for 30 min on a horizontal shaker plate (100 rpm) at room temperature. The surfaces were then rinsed with PBS and imaged with a fluorescence microscope using appropriate filters. Further, the fluorescence microscopy images were analyzed using ImageJ software to calculate the number of adhered platelets on surfaces.

Platelet viability was characterized using a commercially available MTT assay kit. Through the use of bicinchoninic acid (BCA), this assay detects the cuprous ion (Cu^{+1}), which forms when Cu^{+2} is reduced by protein. The chelation of two molecules of BCA with

one cuprous ion forms a purple reaction product that exhibits a strong absorbance at 562 nm. The production of Cu^{+1} is directly proportional to the concentration of the protein and the incubation time in BCA. Thus, protein concentration can be calculated using a standardized protein curve. Prior to measuring the MTT activity, the un-adhered platelets were removed by aspirating the plasma from the surfaces followed by rinsing with PBS. The nanostructured surfaces were incubated with 10% MTT solution in hepes-tyrode buffer for 4hrs on a horizontal shaker plate (100 rpm) at room temperature. The resulting formazan crystals were dissolved by adding MTT solvent in the amounts equal to the hepes-tyrode buffer. The absorbance of the solution was measured using a plate reader.

3.2.5. Platelet activation on PCL NW and NF surfaces

Sterilized PCL, NW and NF surfaces were incubated in a 24-well plate with 1,000 μl of pooled plasma at room temperature on a horizontal shaker plate (100 rpm) for 2 h. Un-adhered platelets were removed by aspirating the plasma from the surfaces followed by rinsing with PBS. Platelet activation on nanostructured surfaces was visualized using SEM imaging. The platelets were fixed by incubating the surfaces in a solution of primary fixative (3% glutaraldehyde (Sigma), 1.1 M sodium cacodylate (Polysciences), and 0.1 M sucrose (Sigma) for 45 min. This was followed by incubation in a solution of secondary fixative (primary fixative without gluteralde- hyde) for 2 h. This was followed by a dehydration step where the surfaces were incubated in consecutive solutions of ethanol (35, 50, 70, 95, and 100%) for 10 min. Further dehydration of the platelets was accomplished by incubating the surfaces in hexamethyldisilazane (HMDS, Sigma) for 10 min. The surfaces were coated with a 10 nm layer of gold and imaged at 5–7 kV. The SEM images were then used to determine the percentage of

the adhered platelets that were unactivated, or had a short-dendritic or a long-dendritic morphology. The following scheme was used to determine the morphology of the platelets:

- Unactivated: Platelets that are normal and with compact central body.
- Short-dendritic: Platelets with smaller dendrites and partially activated.
- Long-dendritic: Platelets with many long dendrites and completely activated.

3.2.6. Whole blood clotting on PCL NW and NF surfaces

Sterilized PCL, NW and NF surfaces were transferred to a 24-well plate to evaluate whole blood clotting kinetics. Whole human blood from healthy individuals was drawn, and 5 μl of the blood was immediately dropped on the surfaces. The blood was allowed to clot for up to 60 min, and the free hemoglobin concentration was measured at 15 min intervals. In order to measure the free hemoglobin concentration, the surfaces were transferred into a different 24-well plate with 500 μl of DI water. The surfaces were gently agitated for 30 s and left in the DI water for 5 min to release free hemoglobin from red blood cells that were not trapped in the thrombus. The absorbance of the DI water with free hemoglobin was measured at a wavelength of 540 nm using a plate reader. The value of absorbance is directly proportional to the concentration of free hemoglobin in DI water. Further, the surfaces were air dried, coated with a 10 nm layer of gold and imaged with SEM at 5–7 kV.

3.2.7. Statistical analysis

Each experiment was reconfirmed on three different surfaces of each PCL, NW and NF with at least three different platelet populations (n_{min} = 9). The protein adsorption results were confirmed on three different surfaces of each PCL, NW and NF with at least two

repetitions (n_{min} = 6). All the quantitative results were analyzed using t-test. Statistical significance was considered at $p < 0.05$.

3.3. Results and discussion

Current treatments for cardiovascular disease include organ transplants, surgery, metabolic products and mechanical/synthetic implants. However, rejection of cardiovascular implants continues to be a problem, eliciting a need for understanding the mechanisms behind tissue– material interaction. Recently, there has been an increased interest in exploring nanostructured surface topographies as interfaces for implantable devices. Several studies have reported favor- able cellular response on such nanostructured topographies, however few studies report the hemocompatibility of these surfaces. In this work, we have evaluated the hemocompatibility of NW and NF surfaces fabricated by nano-templating method and electrospinning respectively.

3.3.1. Fabrication and characterization of PCL NW and NF surfaces

In order to characterize the nanoarchitecture of the NW and NF surfaces, SEM imaging was used (**Figure 3.1.**). Using the image analysis system built into the SEM system, the height and the diameter of the NWs (Figure 1(B) and (C)) were computed to be 4.5 ± 0.5 μm and 150 ± 50 nm respectively, while the diameter of the NFs was computed to be 290 ± 200 nm (Figure 1(D) and (E)). The images show that the NW surfaces have a uniform architecture with occasional interruption in the uniformity by the presence of random microchannels formed due to surface charge effects. Previous studies have shown that similar NW and NF surfaces enhance cellular functionality [57,59,60].

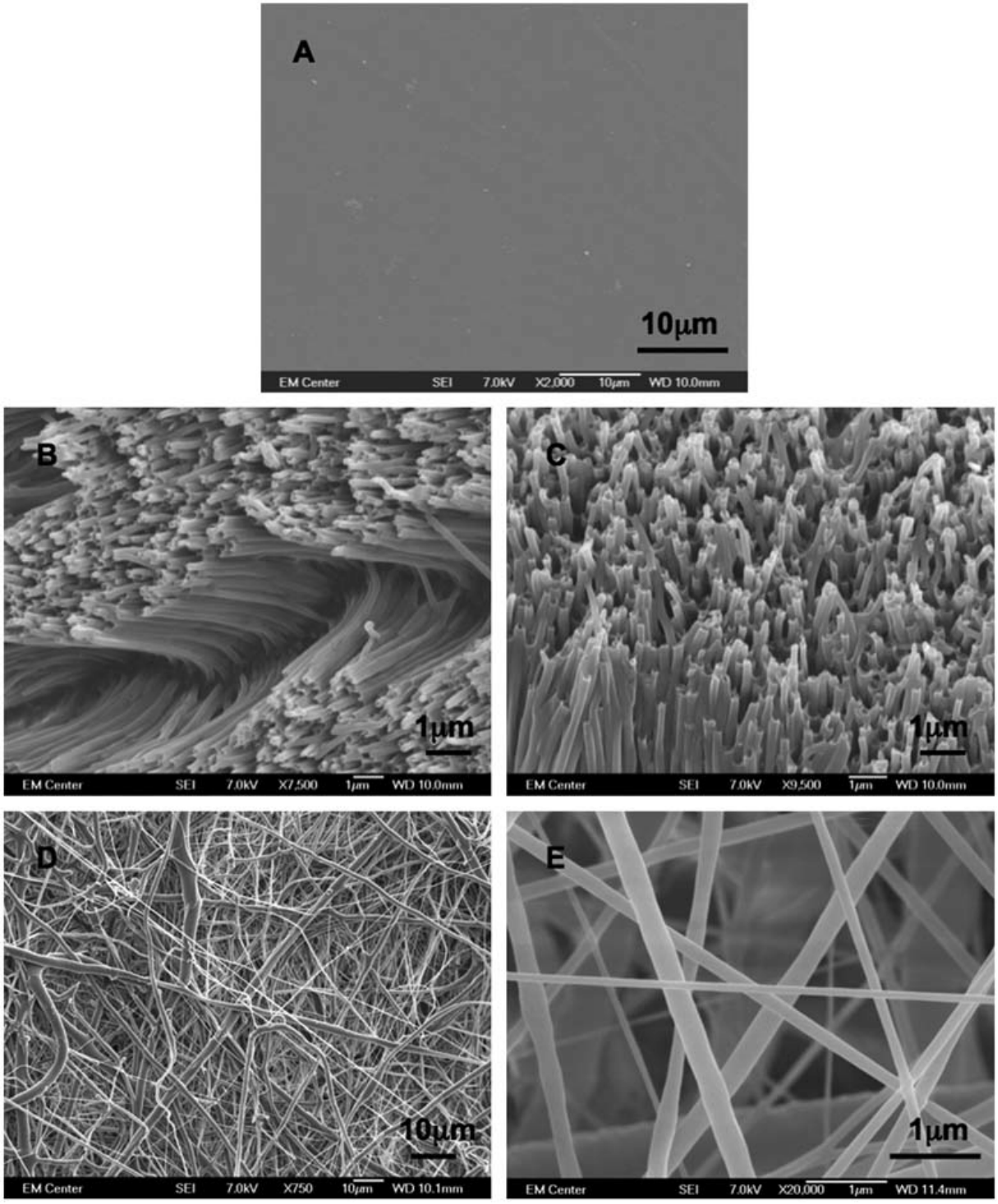

Figure 3.1. Representative SEM images of (A) PCL, (B and C) NW and (D and E) NF surfaces.

3.3.2. Protein adsorption on PCL NW and NF surfaces

When a biomaterial is implanted, proteins from the blood and surrounding tissue are adsorbed onto the surface within seconds to minutes. Protein adsorption is an active process where the surface characteristics presented dictate the differing quantities, densities, conformations and orientations of which proteins adsorb [62]. Further biological processes, such as activation of coagulation and inflammation cascades are impacted by the early adsorption of blood serum proteins. Therefore, the effect of protein adsorption on nanostructured surfaces is an important indicator of blood compatibility.

In this study, adsorption of key blood serum proteins, ALB, FIB and IgG was assessed on nanostructured surfaces. ALB is the main protein in blood plasma that functions mainly to regulate and maintain colloidal osmotic pressure of blood. It is a globular protein and may be distorted upon interaction with the surface.[62] FIB is a plasma glycoprotein that plays a key role in the inflammatory response by assisting in clot formation. It forms a Y shaped structure with two identical halves (F_{ab}) linked by a globular domain in the center (F_c).[62] IgG is the main antibody isotype found in the blood that functions to control infection of body tissues. It also exhibits a Y shaped formation, similar to that of FIB, however it is not as elongated as FIB. The amount of protein adhered on the surfaces were determined using two different methods: a micro-BCA assay and XPS surface analysis. The micro-BCA assay was used to measure the total protein adsorption (bulk plus surface), whereas XPS was used to measure the surface protein adsorption. The adsorbed proteins on the nanostructured surfaces were further visualized using SEM.

In order to evaluate the total protein adsorption, the proteins adsorbed on the surfaces were desorbed using an anionic detergent, SDS and their amounts were evaluated using

micro-BCA assay. The results indicate no significant differences in ALB adsorption on all the surfaces (**Figure 3.2.**). However, FIB and IgG adsorbed significantly more on NW, followed by PCL surfaces and NF surfaces.

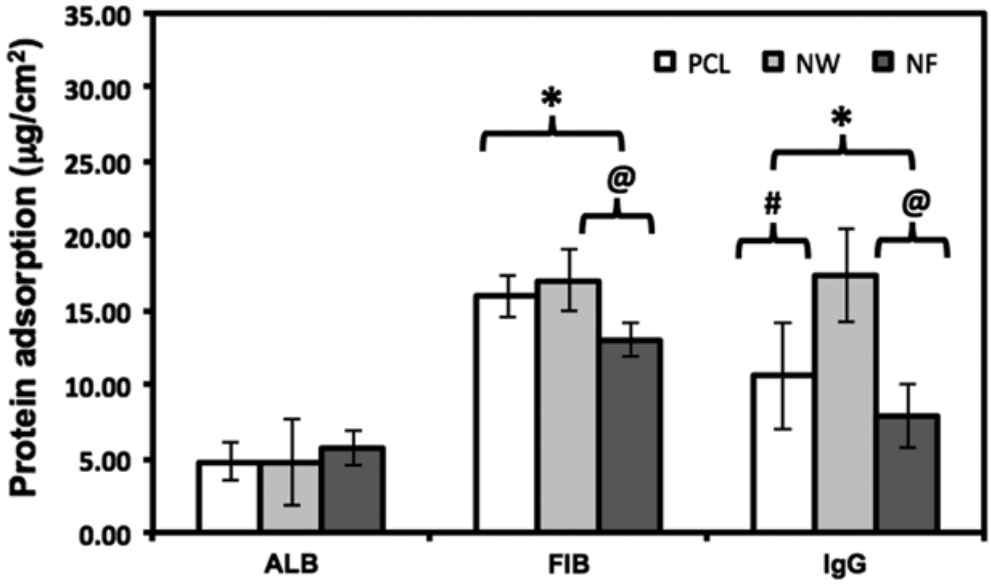

Figure 3.2. Overall blood serum protein adsorption on PCL, NW and NF surfaces determined by micro- BCA assay. Note: No significant differences in ALB adsorption on PCL, NW and NF surfaces. Significant differences in FIB adsorption on PCL and NF surfaces, and NW and NF surfaces ($p < 0.05$). Significant differences in IgG adsorption on all surfaces ($p < 0.05$).

In order to evaluate the surface protein adsorption, high-resolution C1s scans were taken using XPS. The high resolution C1s peak consists of three sub-peaks: C–C, C–N and N–C=O. A precise way to characterize proteins adsorbed on the surface is to determine the contribution of N–C=O (amide) peak (the N–C=O peaks is at a shift 1.8 eV from the C–C peak) in the overall C1s peak. (**Figure 3.3.** and **Table 3.1.**). The results indicate that all the three surfaces had similar contribution of N–C=O peak for ALB adsorption, indicating

similar amounts of ALB adsorbed on all the surfaces. However, NF surfaces had higher contribution of N–C=O peak for both FIB and IgG adsorption, indicating higher FIB and IgG adsorption compared to that on NW and PCL surfaces.

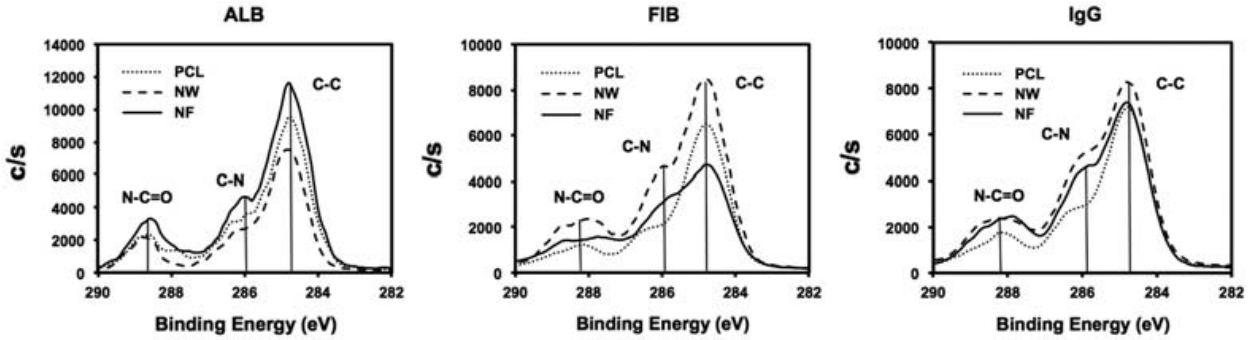

Figure 3.3. High resolution C1s scans for surfaces adsorbed blood serum proteins on PCL, NW and NF surfaces showing C–C, C–N and N–C=O for ALB, FIB and IgG.

Table 3.1. Adsorption of key blood serum proteins ALB, FIB and IgG were investigated on PCL, NW and NF surfaces. The contribution of C–C, C–N and N–C=O peaks in the overall C1s peak are given as percentages.

		C–C	C–N	N–C=O
ALB	PCL	53.7	32.5	13.8
	NW	57	27.3	15.7
	NF	56	28.7	15.3
FIB	PCL	70.5	18.4	11.1
	NW	60.2	20.5	19.3
	NF	53	18.5	28.5
IgG	PCL	67	18.2	14.8
	NW	54.6	27.3	18.1
	NF	56.3	22.2	21.5

The results obtained from XPS are in contrast with that from micro-BCA assay. This can be explained based on variations in the surface nanotopography as well as the structure of the protein and how it is adsorbed on different nanostructured surfaces. It is evident from SEM images (Figure 1) that nanostructured surfaces at a nanoscale level can be considered to have a three-dimensional structure. In case of NW surfaces, this three-dimensional structure can be visualized due to the presence of gaps between the individual NWs as well as the microchannels that are formed due to the surface tension interaction during the membrane dissolution process. The proteins will not only adsorb on the surface of NWs, but also may penetrate through the three-dimensional structure and adsorb into the gaps and the microchannels. In case of NF surfaces, the three-dimensional structure can be visualized as an interconnected porous network formed by continuous NFs that are present through the bulk of the substrate. The proteins will not only adsorb on the surface of NF, but also may infiltrate into the interconnected porous network and adsorb on the fibers beneath the surface. In case of PCL surfaces, the lack of any surface nanoarchitecture limits the proteins adsorption to the surface.

The results indicate that total as well as surface ALB adsorption was similar on all three nanostructured surfaces. ALB is a globular protein that is typically more hydrophobic than hydrophilic.[63] This may prevent the protein molecules from infiltrating into the three-dimensional structure of the nanostructured surfaces. Thus, all the ALB adsorbed on the surface similar to that of the PCL surface. This resulted in similar trends in total and surface ALB adsorption on nanostructured surfaces. In contrast, FIB and IgG adsorption was different on different surfaces. Further, the results indicate that NW surfaces had higher total FIB and IgG adsorption compared to NF and PCL surfaces. In contrast, NW surface

had lower surface FIB and IgG adsorption compared to NF and PCL surfaces. This can be explained based on the structure of FIB and IgG as well as the ability of the surfaces to allow protein infiltration. Both FIB and IgG have a planar Y shape structure, with FIB being more elongated then IgG. Studies have shown that FIB [62] and F_C portion of IgG [64–66] is more attracted to hydrophobic surfaces. Due to the Y shape structure of both FIB and IgG as well their tendency to be less attracted towards hydrophilic surfaces, the protein molecules will adsorb less on the NW surfaces. However, the protein molecules may still penetrate through the three-dimensional structure and adsorb into the gaps and the microchannels, resulting in higher total protein adsorption on NW surfaces due to the availability of higher surface area for protein molecules to interact. In contrast, NF surfaces are more hydrophobic then NW surfaces, resulting in higher surface FIB and IgG adsorption. However, due to the interconnected porous network formed by continuous NFs and the Y shape of both FIB and IgG, the protein molecules may not be able to infiltrate that easily into the three-dimensional structure, resulting in lower total FIB and IgG adsorption on NF surfaces as compared to NW surfaces. In case of PCL surfaces, the lack of nanotopography resulted in all the protein adsorbed on the surface and total protein adsorption is equal to the surface protein adsorption.

Adsorbed proteins on the nanostructured surfaces were also visualized using SEM (**Figure 3.4.**). As expected, all the proteins that were adsorbed on PCL surfaces crystalized, whereas, the proteins adsorption was uniform on both NW and NF surfaces. This may be due to the fact that both surfaces have significantly higher surface area as compared to PCL surfaces.

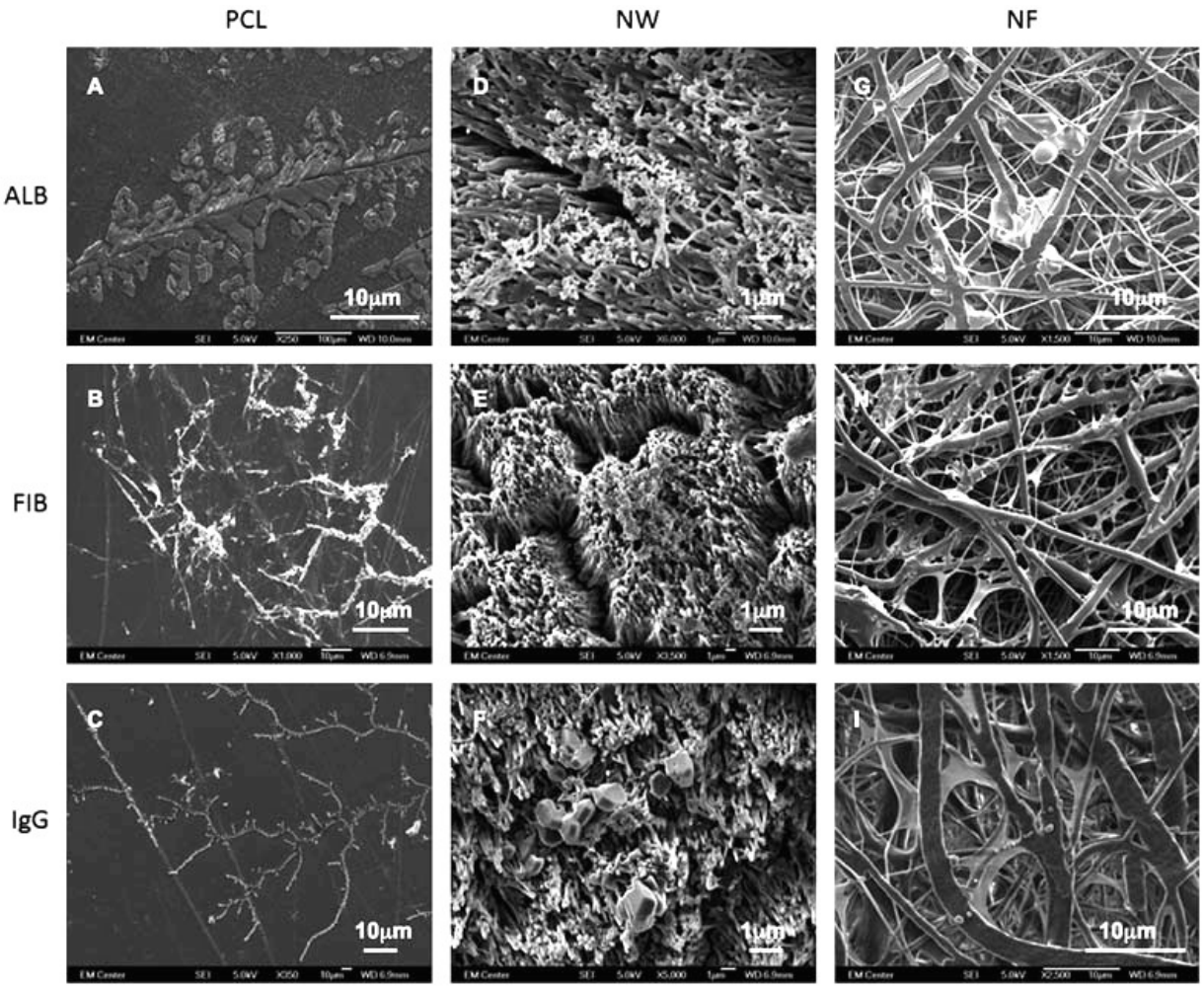

Figure 3.4. Representative SEM images of ALB (A, D and G), FIB (B, E and H) and IgG (C, F and I) adsorbed on PCL (A–C), NW (D–F) and NF (G–I) surfaces.

3.3.3. Platelet adhesion and viability on PCL NW and NF surfaces

Platelet adhesion on a surface triggers the coagulation of blood and therefore is an important indicator of thrombogenecity. In this study, platelets were isolated from whole human blood and their adhesion on nanostructured surfaces was investigated after 2 h of contact time. The platelets were stained with calcein-AM and the surfaces were examined under a fluorescence microscope to evaluate the platelet adhesion. The results indicate

significantly higher platelet adhesion on NF surfaces followed by PCL surfaces and NW surfaces (**Figure 3.5.**). Further, high-magnification images reveal that platelets are clustering and probably infiltrating in the NF surfaces (Figure 6(G)–(I)). In contrast, the platelets on PCL and NW surfaces do not form clusters (Figure 6 PCL: A, B and C; NW: D, E and F).

Further, low magnification (10x) fluorescence microscopy images were analyzed using ImageJ software to determine the number of platelets adhered on different surfaces. The results indicate significantly higher platelet adhesion on NF surfaces followed by PCL surfaces and NW surfaces (**Figure 3.6.**). Platelet adhesion results were consistent with the protein adsorption results. The NF surfaces had higher surface FIB adsorption compared to PCL and NW surfaces resulting in higher platelet adhesion. This is consistent with recent work demonstrating higher platelet adhesion and activation on NF surfaces [67].

Platelet viability was evaluated using an MTT assay. The MTT assay determines the amount of mitochondrial activity in the live cells via dehydrogenase activity. This assay measures the absorbance of formazan, which is reduced by MTT in living cells. Therefore, the amount of adhered platelets directly corresponds to the absorbance values of formazan. The results indicate significantly higher platelet viability on NF surfaces as compared to PCL and NW surfaces, indicating higher number of platelets present on NF surfaces (**Figure 3.7.**). These results also validate the results obtained from fluorescence microscopy.

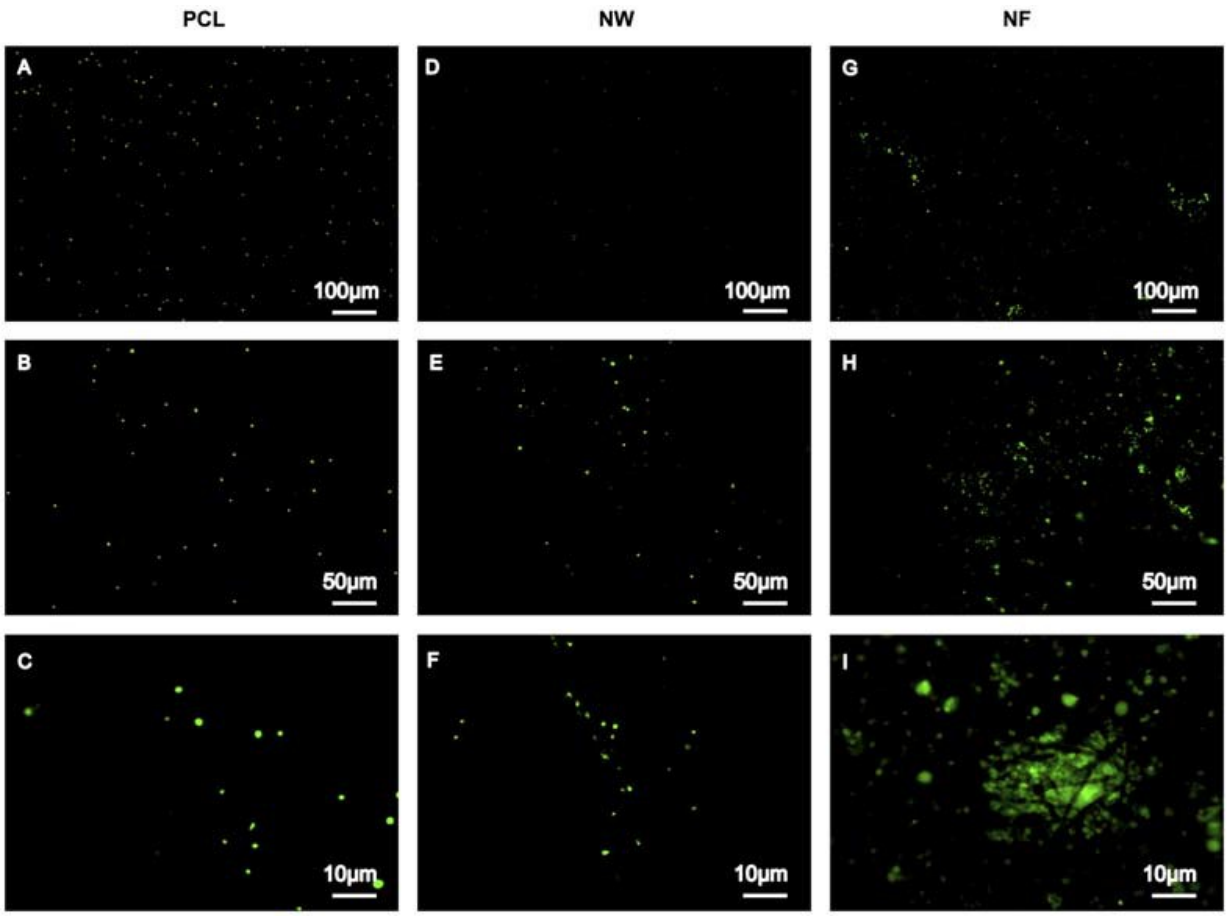

Figure 3.5. Representative fluorescence microscopy images of adhered platelets stained with calcein-AM on PCL (A–C), NW (D–F) and NF (G–I) surfaces.

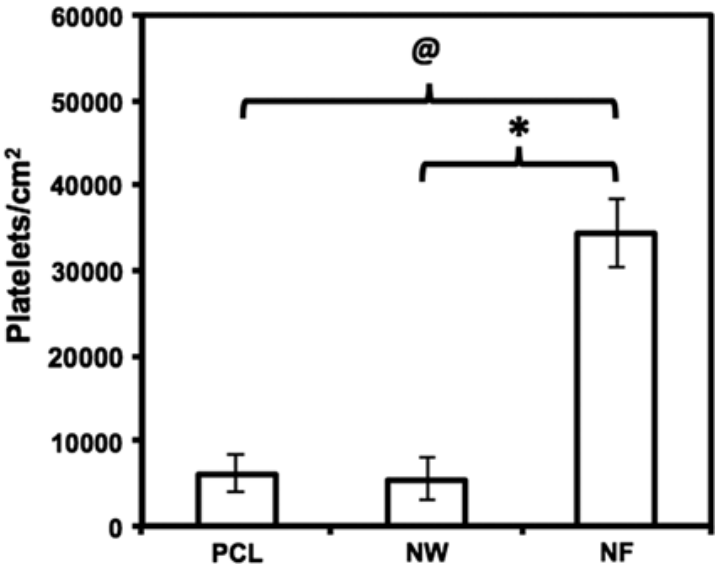

Figure 3.6. Number of adhered platelets on PCL, NW and NF surfaces calculated using fluorescence microscopy images and ImageJ software. Significant differences in number of platelets adhered on PCL and NF surfaces (@ → $p < 0.05$), and NW and NF surfaces (*→ $p < 0.05$).

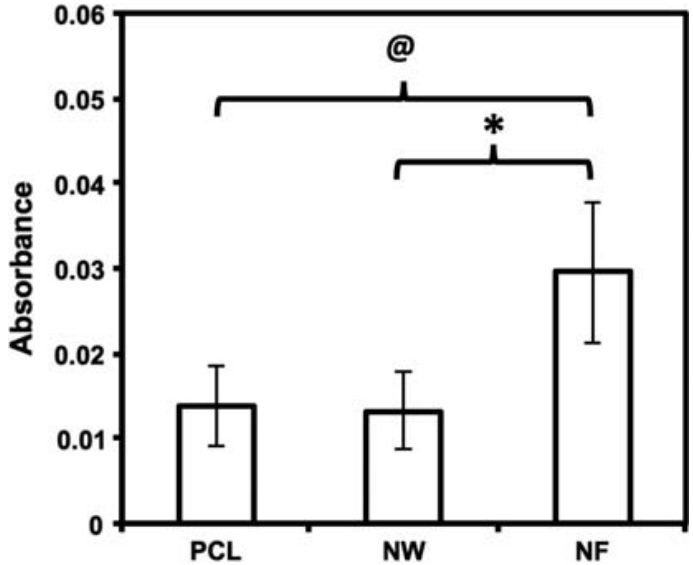

Figure 3.7. MTT assay results indicating viability of adhered platelets on PCL, NW and NF surfaces. Significant differences in viability of platelets adhered on PCL and NF surfaces (@ → $p < 0.05$), and NW and NF surfaces (*→ $p < 0.05$).

3.3.4. Platelet activation on PCL NW and NF surfaces

Once plasma proteins adsorb on a biomaterial surface, a series of biochemical events that cause platelet adhesion and activation is initiated. Activated platelets trigger the activation of plasma coagulation factors which lead to the generation of a fibrin clot.[68] Platelet activation after 2 h of contact time with nanostructured surfaces was investigated with SEM imaging. The nanostructured surfaces were coated with a 10 nm layer of gold and imaged at 5–7 kV. The SEM images at low magnifications indicate significantly higher number of platelets on NF surfaces followed by PCL surfaces and NW surfaces (**Figure 3.8.**). These results are in conjunction with fluorescence microscopy images as well as MTT assay.

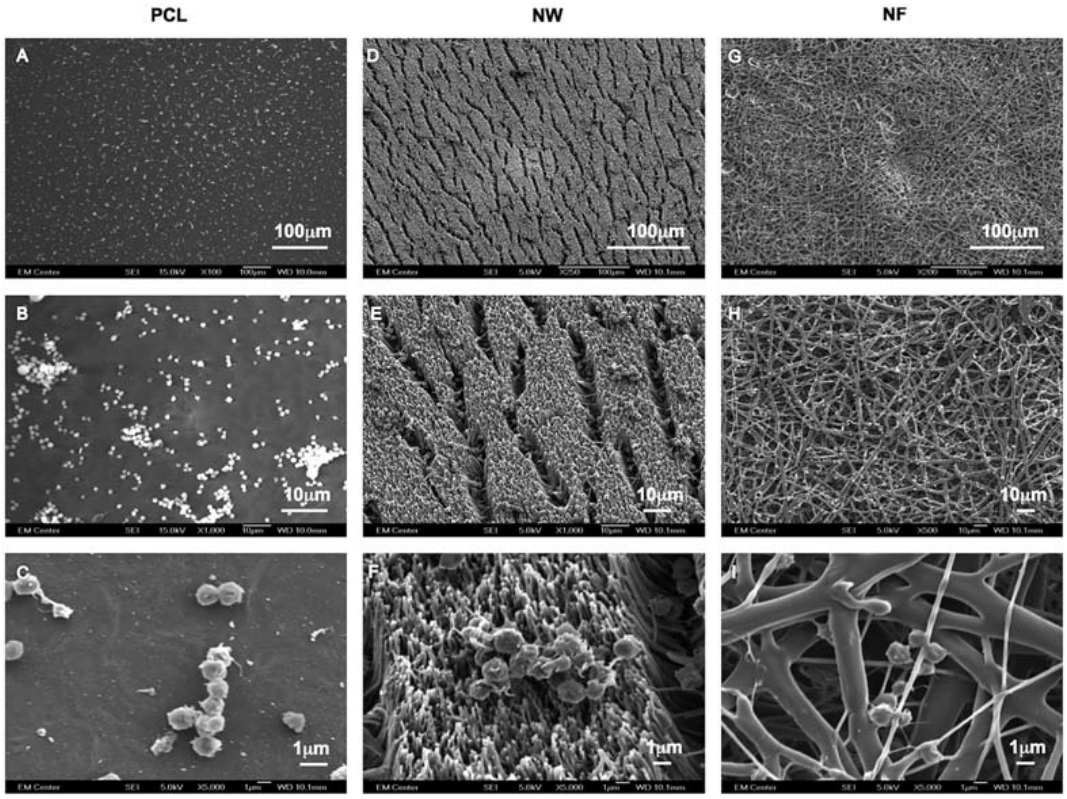

Figure 3.8. Representative SEM images of adhered platelets on PCL (A–C), NW (D–F) and NF (G–I) surfaces.

High magnification SEM images reveal significant morphological differences in platelets adhered on the different surfaces. The SEM images were used to determine the percentage of adhered platelets that were unactivated or had a dendritic (short-dendritic or long-dendritic) morphology (**Figure 3.9.**). The results show NF surfaces with a higher percentage of platelets with long-dendritic morphology (~50%) indicating complete activation, followed by platelets with short-dendritic morphology (~30%), and fewer platelets with unactivated morphology (~20%). In contrast, PCL surfaces has higher percentage of platelets with short-dendritic morphology (~56%), followed by platelets with unactivated morphology (~23%), and fewer platelets that are completely activated (~21%). NW surfaces have a higher percentage of platelets with a n unactivated morphology (~55%), followed by platelets with short-dendritic morphology (~27%), and fewer platelets exhibiting long-dendritic morphology (~17%). It is important to note that PCL and NW surfaces can potentially activate platelets as the clotting cascade progresses despite the fact that they do not support significant platelet adhesion. Furthermore, these results indicate the importance of surface topography in influencing the platelet activation on the material surface.

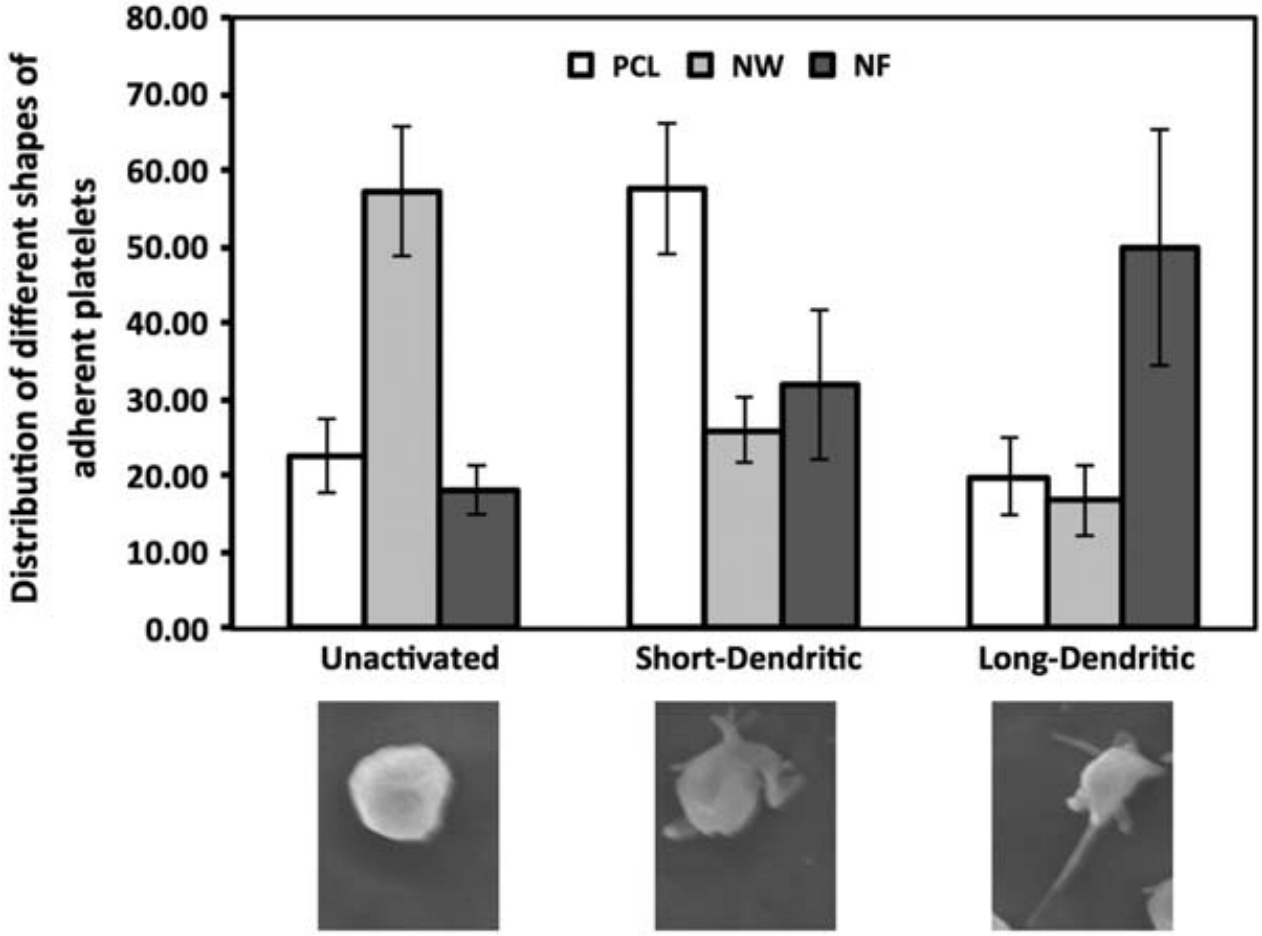

Figure 3.9. Distribution of different shapes of adhered platelets on PCL, NW and NF surfaces. Representative morphology of platelets shown below the graph.

3.3.5. Whole blood clotting on PCL NW and NF surfaces

Following platelet adhesion and activation, the next step in the cascade of blood coagulation is the formation of a fibrin matrix. The kinetics of whole blood clotting is important in determining the success of a long-term blood contacting material. If a clot forms abruptly tissue integration will be inhibited. The results indicated that blood clotted on all surfaces within 1hr of exposure, however the rate of clotting was different for different surfaces (**Figure 3.10.**). After 30 min of clotting, there were significant differences in the

amount of free hemoglobin in the blood that was in contact with NW surfaces indicating least clotting on the surface, followed by NF and PCL surfaces. Further, increased amounts of free hemoglobin were in the blood that was in contact with NW surfaces compared to both PCL and NF surfaces throughout the entire clotting process. These results are consistent with platelet activation studies as well as surface FIB adsorption.

The blood clotting cascade is initiated by the enzyme thrombin, which converts FIB into fibrin, eventually forming a clot network. The fibrin network after 60 min of clotting time on PCL, NW and NF surfaces was examined using SEM imaging. Visual inspections show the fibrin matrix formation to be altered on all three surfaces (**Figure 3.11.**). Due to the hydrophobic nature of PCL surfaces, the blood drop did not spread when it contact with the surface, resulting in well-defined blood-PCL interface (Figure 12(A)–(C)). In contrast, due to the hydrophilic nature of the NW surface, the blood drop spread on the surface and infiltrated the nanoarchitecture, resulting in a 'gradient-like' blood-NW interface (Figure 12(D)–(F)). However, due to the porous nature of NF surfaces, the blooddrop completely infiltrated in the surface without any trace of blood-NF interface (Figure 12(G)–(I)).

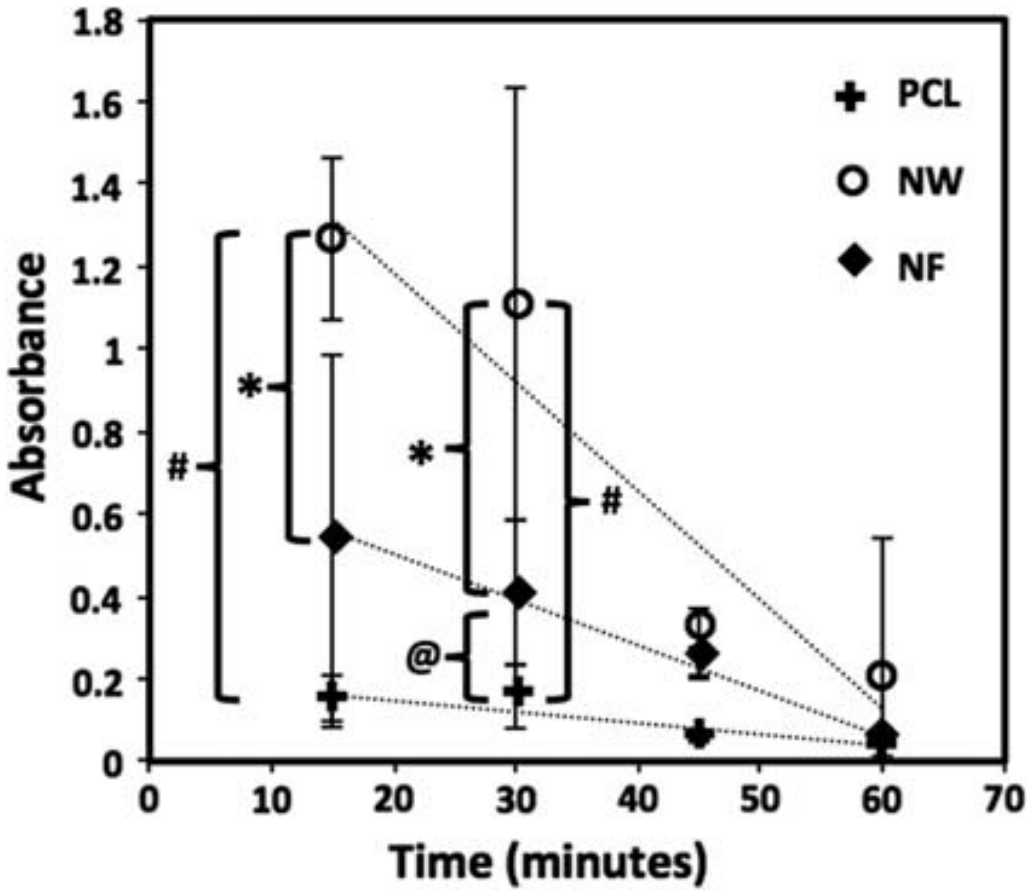

Figure 3.10. Free hemoglobin concentration determined in terms of its absorbance on PCL, NW and NF surfaces for 60 min of clotting time. Significant differences in free hemogloblin concentrations after 15 min on NW and NF surfaces, and NW and PCL surfaces (*, # → p<0.05). Significant differences in few hemogblobin concentrations after 30 mins on all surfaces (*, # and@→p<0.05).

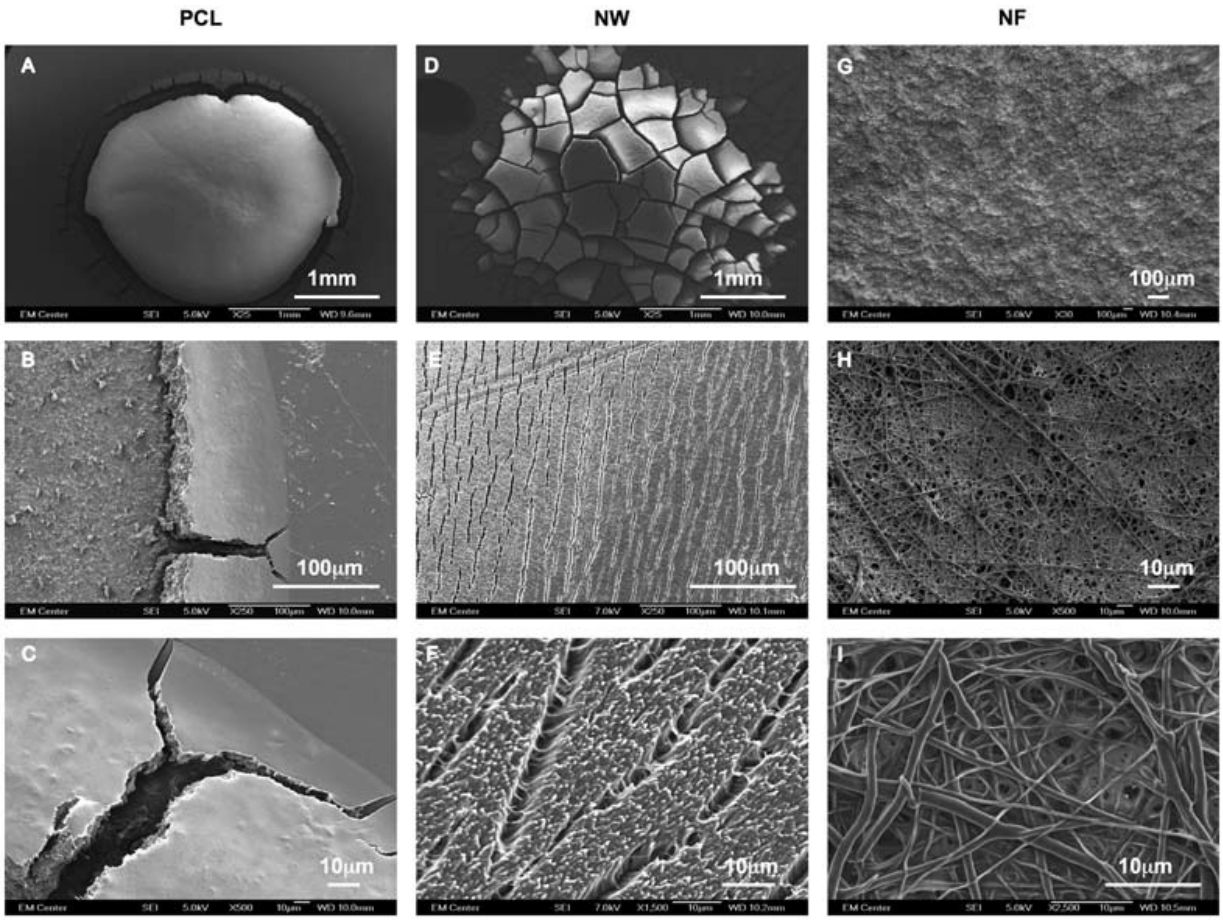

Figure 3.11. Representative SEM images of whole blood clotted on PCL (A–C), NW (D–F) and NF (G–I) surfaces.

3.4. Conclusion

Recently, there has been an increased interest in exploring nanostructured surface topographies as interfaces for implantable devices. Several studies have reported favorable cellular response on different nanostructured topographies, however few studies report the hemocompatibility of these surfaces. In this work, we have evaluated the hemocompatibility of NW and NF surfaces fabricated by nano-templating method and electrospinning respectively. The results indicate no significant differences in ALB adsorption on all surfaces. However, NW

surfaces had higher total FIB and IgG adsorption compared to NF and PCL surfaces. In contrast, NW surfaces had lower surface FIB and IgG adsorption compared to NF and PCL surfaces. This can be explained based on the structure of FIB and IgG as well as the ability of the surfaces to allow protein infiltration. Platelet adhesion and viability studies show a large amount of adhesion and clustering of platelets on the NF surfaces as compared to PCL and NW surfaces. Platelet activation studies reveal that NW surfaces have the highest percentage of unactivated platelets, whereas NF surfaces have the highest percentage of fully activated platelets. Whole blood clotting results indicate that NW surfaces maintain an increased amount of free hemoglobin during the clotting process compared to PCL and NF surface, indicating less clotting and slower rate of clotting on their surfaces. The results presented here indicate that the surface nanoarchitecture and how it is presented to the biological environment can modulate the hemocompatibility. Further studies are now directed towards evaluating the effects of altered lengths and diameters of nanofeatures on hemocompatibility and specific components of the innate immune response.

REFERENCES

[1] Smith SC, Jr. Our time: a call to save preventable death from cardiovascular disease (heart disease and stroke). J. Am. College Cardiol. 2012;60:2343–2348.

[2] Nugent HM, Edelman ER. Tissue engineering therapy for cardiovascular disease. Circulat. Res. 2003;92:1068–1078.

[3] Seyednejad H, Gawlitta D, Kuiper RV, de Bruin A, van Nostrum CF, Vermonden T, Dhert WJ, Hennink WE. *In vivo* biocompatibility and biodegradation of 3D-printed porous scaffolds based on a hydroxyl-functionalized poly(ε-caprolactone). Biomaterials. 2012;33:4309–4318.

[4] Heublein B, Rohde R, Kaese V, Niemeyer M, Hartung W, Haverich A. Biocorrosion of magnesium alloys: a new principle in cardiovascular implant technology? Heart. 2003;89:651–656.

[5] van der Giessen WJ, Lincoff AM, Schwartz RS, van Beusekom HMM, Serruys PW, Holmes DR, et al. Marked inflammatory sequelae to implantation of biodegradable and nonbiodegradable polymers in porcine coronary arteries. Circulation. 1996;94:1690–1697.

[6] Zhang Y, Ouyang H, Lim CT, Ramakrishna S, Huang Z-M. Electrospinning of gelatin fibers and gelatin/ PCL composite fibrous scaffolds. J. Biomed. Mater. Res., Part B: Appl. Biomater. 2005;72B:156–165.

[7] Ajili SH, Ebrahimi NG, Soleimani M. Polyurethane/polycaprolactane blend with shape memory effect as a proposed material for cardiovascular implants. Acta Biomater. 2009;5:1519–1530.

[8] Kim HI, Ishihara K, Lee S, Seo J-H, Kim HY, Suh D, Kim MU, Konno T, Takai M, Seo JS. Tis- sue response to poly(l-lactic acid)-based blend with phospholipid polymer for biodegradable cardio- vascular stents. Biomaterials. 2011;32:2241–2247.

[9] Shinoka T, Ma PX, Shum-Tim D, Breuer CK, Cusick RA, Zund G, Langer R, Vacanti JP, Mayer JE, Jr. Tissue-engineered heart valves. Autologous valve leaflet replacement study in a lamb model. Circu- lation. 1996;94:II164–II168.

[10] Andukuri A, Kushwaha M, Tambralli A, Anderson JM, Dean DR, Berry JL, Sohn YD, Yoon YS, Brott BC, Jun HW. A hybrid biomimetic nanomatrix composed of electrospun polycaprolactone and bioactive peptide amphiphiles for cardiovascular implants. Acta Biomater. 2011;7:225–233.

[11] Motlagh D, Allen J, Hoshi R, Yang J, Lui K, Ameer G. Hemocompatibility evaluation of poly(diol citrate) *in vitro* for vascular tissue engineering. J. Biomed. Mater. Res. Part A. 2007;82A:907–916.

[12] Belanger MC, Marois Y, Roy R, Mehri Y, Wagner E, Zhang Z, et al. Selection of a polyurethane membrane for the manufacture of ventricles for a totally implantable artificial heart: blood compatibility and biocompatibility studies. Artif. Org. 2000;24:879–888.

[13] Maegdefessel L, Linde T, Krapiec F, Hamilton K, Steinseifer U, van Ryn J, Raaz U, Buerke M, Wer- dan K, Schlitt A. In vitro comparison of dabigatran, unfractionated heparin, and low-molecular- weight heparin in preventing thrombus formation on mechanical heart valves. Thrombos. Res. 2010;126:e196–e200.

[14] Motlagh D, Yang J, Lui KY, Webb AR, Ameer GA. Hernocompatibility evaluation of poly(glycerol- sebacate) *in vitro* for vascular tissue engineering. Biomaterials. 2006;27:4315–4324.

[15] Baker DW, Liu X, Weng H, Luo C, Tang L. Fibroblast/fibrocyte: surface interaction dictates tissue reactions to micropillar implants. Biomacromolecules. 2011;12:997–1005.

[16] Muthusubramaniam L, Lowe R, Fissell W, Li L, Marchant R, Desai TA, Roy S. Hemocompatibili- ty of silicon-based substrates for biomedical implant applications. Ann. Biomed. Eng. 2011;39: 1296–1305.

[17] Huang N, Yang P, Leng YX, Chen JY, Sun H, Wang J, Wang GJ, Ding PD, Xi TF, Leng Y. Hemo- compatibility of titanium oxide films. Biomaterials. 2003;24:2177–2187.

[18] Feng Y, Zhao H, Zhang L, Guo J. Surface modification of biomaterials by photochemical immobilization and photograft polymerization to improve hemocompatibility. Front. Chem. Eng. China. 2010;4:372–381.

[19] Werner C, Maitz MF, Sperling C. Current strategies towards hemocompatible coatings. J. Mater. Chem. 2007;17:3376–3384.

[20] Ziats NP, Miller KM, Anderson JM. *In vitro* and *in vivo* interactions of cells with biomaterials. Biomaterials. 1988;9:5–13.

[21] Anderson JM, McNally AK. Biocompatibility of implants: lymphocyte/macrophage interactions. Semin. Immunopathol. 2011;33:221–233.

[22] André P, Delaney SM, LaRocca T, Vincent D, DeGuzman F, Jurek M, Koller B, Phillips DR, Con- ley PB. P2Y12 regulates platelet adhesion/activation, thrombus growth, and thrombus stability in injured arteries. J. Clin. Investigat. 2003;112:398–406.

[23] Cerda-Cristerna BI, Flores H, Pozos-Guillén A, Pérez E, Sevrin C, Grandfils C. Hemocompatibility assessment of poly(2-dimethylamino ethylmethacrylate) (PDMAEMA)-based polymers. J. Control Release. 2011;153:269–277.

[24] Major TC, Brant DO, Burney CP, Amoako KA, Annich GM, Meyerhoff ME, Handa H, Bartlett RH. The hemocompatibility of a nitric oxide generating polymer that catalyzes S-nitrosothiol decomposition in an extracorporeal circulation model. Biomaterials. 2011;32:5957–5969.

[25] Cerda-Cristerna BI, Flores H, Pozos-Guillen A, Perez E, Sevrin C, Grandfils C. Hemocompatibility assessment of poly(2-dimethylamino ethylmethacrylate) (PDMAEMA)-based polymers. J. Control Release. 2011;153:269–277.

[26] de Jonge L, Leeuwenburgh S, Wolke J, Jansen J. Organic–inorganic surface modifications for titanium implant surfaces. Pharmaceut. Res. 2008;25:2357–2369.

[27] Ishihara K, Oshida H, Endo Y, Ueda T, Watanabe A, Nakabayashi N. Hemocompatibility of human whole blood on polymers with a phospholipid polar group and its mechanism. J. Biomed. Mater. Res. 1992;26:1543–1552.

[28] Ekblad T, Liedberg B. Protein adsorption and surface patterning. Curr. Opin. Colloid Interf. Sci. 2010;15:499–509.

[29] Faria M, Brogueira P, de Pinho MN. Sub-micron tailoring of bi-soft segment asymmetric polyure- thane membrane surfaces with enhanced hemocompatibility properties. Colloids Surf. B:Biointerf. 2011;86:21–27.

[30] Kim HN, Jiao A, Hwang NS, Kim MS, Kang DH, Kim D-H, Suh KY. Nanotopography-guided tis- sue engineering and regenerative medicine. Adv. Drug Deliv. Rev. 2012.

[31] Cao H, McHugh K, Chew SY, Anderson JM. The topographical effect of electrospun nanofibrous scaffolds on the *in vivo* and *in vitro* foreign body reaction. J. Biomed. Mater. Res. Part A. 2010;93A:1151–1159.

[32] Bechara S, Wadman L, Popat KC. Electroconductive polymeric nanowire templates facilitates *in vitro* C17.2 neural stem cell line adhesion, proliferation and differentiation. Acta Biomater. 2011;7:2892–2901.

[33] McMurray RJ, Gadegaard N, Tsimbouri PM, Burgess KV, McNamara LE, Tare R, Murawski K, Kingham E, Oreffo RO, Dalby MJ. Nanoscale surfaces for the long-term maintenance of mesen- chymal stem cell phenotype and multipotency. Nat. Mater. 2011;10:637–644.

[34] Park K, Ju YM, Son JS, Ahn KD, Han DK. Surface modification of biodegradable electrospun nanofi- ber scaffolds and their interaction with fibroblasts. J. Biomater. Sci. Polym. Ed. 2007;18:369–382.

[35] Seidlits SK, Lee JY, Schmidt CE. Nanostructured scaffolds for neural applications. Nanomedicine. 2008;3:183–199.

[36] Bechara SL, Judson A, Popat KC. Template synthesized poly(epsilon-caprolactone) nanowire surfaces for neural tissue engineering. Biomaterials. 2010;31:3492–3501.

[37] Woodruff MA, Hutmacher DW. The return of a forgotten polymer – polycaprolactone in the 21st century. Prog. Polym. Sci. 2010;35:1217–1256.

[38] Liu L, Guo SR, Chang J, Ning CQ, Dong CM, Yan DY. Surface modification of

polycaprolactone membrane via layer-by-layer deposition for promoting blood compatibility. J. Biomed. Mater. Res., Part B: Appl. Biomater. 2008;87B:244–250.

[39] Xiang P, Li M, Zhang CY, Chen DL, Zhou ZH. Cytocompatibility of electrospun nanofiber tubular scaf- folds for small diameter tissue engineering blood vessels. Int. J. Biolog. Macromol. 2011;49:281–288.

[40] Li WJ, Cooper JA, Mauck RL, Tuan RS. Fabrication and characterization of six electrospun poly (alpha-hydroxy ester)-based fibrous scaffolds for tissue engineering applications. Acta Biomater. 2006;2:377–385.

[41] De Santis R, Gloria A, Russo T, D'Amora U, Zeppetelli S, Dionigi C, Sytcheva A, Herrmannsdörfer T, Dediu V, Ambrosio L. A basic approach toward the development of nanocomposite magnetic scaffolds for advanced bone tissue engineering. J. Appl. Polym. Sci. 2011;122:3599–3605.

[42] Sangsanoh P, Waleetorncheepsawat S, Suwantong O, Wutticharoenmongkol P, Weeranantanapan O, Chuenjitbuntaworn B, Cheepsunthorn P, Pavasant P, Supaphol P. In vitro biocompatibility of Schwann cells on surfaces of biocompatible polymeric electrospun fibrous and solution-cast film scaffolds. Bio- macromolecules. 2007;8:1587–1594.

[43] Cooper A, Bhattarai N, Zang MQ. Fabrication and cellular compatibility of aligned chitosan-PCL fibers for nerve tissue regeneration. Carbohyd. Polym. 2011;85:149–156.

[44] Lee W, Oh JH, Park JC, Shin HI, Baek JH, Ryoo HM, Woo KM. Performance of electrospun poly (epsilon-caprolactone) fiber meshes used with mineral trioxide aggregates in a pulp capping proce- dure. Acta Biomater. 2012;8:2986–2995.

[45] Ng KW, Khor HL, Hutmacher DW. In vitro characterization of natural and synthetic dermal matrices cultured with human dermal fibroblasts. Biomaterials. 2004;25:2807–2818.

[46] Lam CX, Hutmacher DW, Schantz JT, Woodruff MA, Teoh SH. Evaluation of polycaprolactone scaffold degradation for 6 months *in vitro* and *in vivo*. J. Biomed. Mater. Res. A. 2009;90: 906–919.

[47] Christopher XFL, Monica MS, Swee-Hin T, Dietmar WH. Dynamics of *in vitro* polymer degradation of polycaprolactone-based scaffolds: accelerated versus simulated physiological conditions. Biomed. Mater. 2008;3:034108.

[48] Sachlos E, Czernuszka JT. Making tissue engineering scaffolds work. Review: the application of solid freeform fabrication technology to the production of tissue engineering scaffolds. Eur. Cell Mater. 2003;5:29–39.

[49] Bechara SL, Judson A, Popat KC. Template synthesized poly(ε-caprolactone) nanowire surfaces for neural tissue engineering. Biomaterials. 2010;31:3492–3501.

[50] Redenti S, Tao S, Yang J, Gu P, Klassen H, Saigal S, Desai T, Young MJ. Retinal tissue engineer- ing using mouse retinal progenitor cells and a novel biodegradable, thin-film poly(e-

caprolactone) nanowire scaffold. J. Ocular. Biol. Dis. Informat. 2008;1:19–29.

[51] He L, Liu B, Xipeng G, Xie G, Liao S, Quan D, Cai D, Lu J, Ramakrishna S. Microstructure and properties of nano-fibrous PCL-b-PLLA scaffolds for cartilage tissue engineering. Eur. Cell Mater. 2009;18:63–74.

[52] Mavis B. Compartmentalization of synthetic body fluid constituents for coating electrospun PCL nanofiber mats with different calcium phosphate phases. J. Biomech. 2011;44:7.

[53] Ye L, Wu X, Mu Q, Chen B, Duan Y, Geng X, Gu Y, Zhang A, Zhang J, Feng ZG. Heparin-con- jugated PCL Scaffolds fabricated by electrospinning and loaded with fibroblast growth factor 2. J. Biomater. Sci. Polym. Ed. 2010;21:21.

[54] Ye L, Wu X, Duan H-Y, Geng X, Chen B, Gu Y-Q, et al. The *in vitro* and *in vivo* biocompatibility evaluation of heparin–poly(ε-caprolactone) conjugate for vascular tissue engineering scaffolds. J. Biomed. Mater. Res. Part A. 2012;100A:3251–3258.

[55] Murugan R, Ramakrishna S. Nano-featured scaffolds for tissue engineering: a review of spinning methodologies. Tissue Eng. 2006;12:435–447.

[56] Popat KC, Porter JR, Henson A. Biodegradable poly(epsilon-caprolactone) nanowires for bone tissue engineering applications. Biomaterials. 2009;30:780–788.

[57] Ruckh TT, Kumar K, Kipper MJ, Popat KC. Osteogenic differentiation of bone marrow stromal cells on poly(epsilon-caprolactone) nanofiber scaffolds. Acta Biomater. 2010;6:2949–2959.

[58] Popat KC, Johnson RW, Desai TA. Characterization of vapor deposited poly (ethylene glycol) films on silicon surfaces for surface modification of microfluidic systems. J. Vacuum Sci. Technol. B. 2003;21:645–654.

[59] Bechara SL, Judson A, Popat KC. Template synthesized poly(e-caprolactone) nanowire surfaces for neural tissue engineering. Biomaterials. 2010;31:3492–3501.

[60] Porter JR, Henson A, Popat KC. Biodegradable poly(ε-caprolactone) nanowires for bone tissue engineering applications. Biomaterials. 2009;30:780–788.

[61] Zhao G, Schwartz Z, Wieland M, Rupp F, Geis-Gerstorfer J, Cochran DL, Boyan BD. High sur- face energy enhances cell response to titanium substrate microstructure. J. Biomed. Mater. Res. Part A. 2005;74A:49–58.

[62] Roach P, Farrar D, Perry CC. Interpretation of protein adsorption: surface-induced conformational changes. J. Am. Chem. Soc. 2005;127:8168–8173.

[63] Xm H, Dc C. Atomic structure and chemistry of human serum albumin. Nature. 1992 Jul 16;358:209–215.

[64] Buijs J, van den Berg PAW, Lichtenbelt JWT, Norde W, Lyklema J. Adsorption dynamics of IgG and Its F(*ab*')2and Fc fragments studied by reflectometry. J. Colloid Interf. Sci. 1996;178: 594–605.

[65] van Erp R, Linders YE, van Sommeren AP, Gribnau TC. Characterization of monoclonal antibodies physically adsorbed onto polystyrene latex particles. J. Immunol. Meth. 1992;152:191–199.

[66] Nagaoka S, Kanno M, Kawakami H, Kubota S. Evaluation of blood compatibility of fluorinated polyimide by immunolabeling assay. J. Artif. Org. 2001;4:107–112.

[67] Wan L-S, Xu Z-K. Polymer surfaces structured with random or aligned electrospun nanofibers to promote the adhesion of blood platelets. J. Biomed. Mater. Res. Part A. 2009;89A:168–175.

[68] Heemskerk JW, Bevers EM, Lindhout T. Platelet activation and blood coagulation. Thromb Haemost. 2002;88:186–193.

CHAPTER 4

ENDOTHELIAL CELL INTERACTION ON COLLAGEN IMMOBILIZED NANOWIRES

4.1. Introduction

In order to create an optimal cardiovascular scaffold design, it is critical to understand the events that occur at the cardiovascular tissue-material interface. In particular human vascular endothelial cells are important to study due to the fact that they form an interface between circulating blood and the rest of the vessel wall. Vascular endothelial cells line the entire interior of the circulatory system and have very distinctive functions such as filtering fluids, hemostasis, hormone trafficking and regulating blood pressure by synthesizing nitric oxide [1, 2]. Furthermore, the success of cardiovascular implants is associated with the development of an endothelium formed by endothelial cells, which is critical with the prevention of intimal hyperplasia, calcification and thrombosis [3]. A thorough understanding of the interaction between vascular endothelial cells and the biomaterial involved is essential in order to have a successful application which promotes healing and regeneration through integration with native tissue. One major obstacle to overcome is adhering the anchorage-dependent and slowly renewing endothelial cells [4]. The level of growth is correlated to the characteristics of the surface and how well they mimic cardiovascular extracellular matrix. Non-adherent surfaces prevent endothelial cells from attaching to the endovascular surface, which in turn impedes the development of a protective endothelium. A need exists to engineer surfaces for cardiovascular applications that encourage the development of endothelium on synthetic surfaces.

Consequently, in order to create a successful cardiovascular scaffold, it is necessary to mimic the interaction between the endothelial cell surface receptors with the extracellular matrix molecules. This interaction is extremely important in regulating cell adhesion, survival, proliferation, migration and differentiation. Once endothelial cells establish adhesive contacts with surfaces via integrin-mediated interactions, signaling pathways are activated that initiate and direct a diverse amount of cellular activities such as survival, cell-cycle progression, vascularization for oxygenation and nutrient delivery and gene expression [5, 6]. Therefore, the functionality of endothelial cells is dependent on the success of their adherence to the surface. Previous studies have shown enhanced endothelial cell proliferation on surfaces with biochemical cues such as growth factors [7] and natural ECM proteins [8], both of which induce cell-material interactions.

Collagen, the main protein in the ECM of blood vessels as well as other tissues in the body, has been used extensively to promote cell adhesion [9], specifically for fibroblasts [10], human keratinocytes [11], epithelial cells [12], and endothelial cells [13, 14]. Cell adhesion to collagen is controlled by two integrins: $\alpha 1\beta 1$ and $\alpha 2\beta 1$ [15]. Fibrillar collagen (collagen type I) binds these cellular integrins while exhibiting a triple helical structure, essential to its biological and mechanical properties [16]. Integrin $\alpha 1\beta 1$ binds to collagen via MIDAS motif and is the only collagen receptor capable of activating Shc mediated growth pathways, indicating a distinctive role in cell proliferation on collagen [17]. Integrin $\alpha 2\beta 1$ preferentially binds to a triple helical collagen containing the GFOGER motif [18] and regulates the level of matrix metalloproteinase-1[19]. Thus, collagen has been incorporated onto biomaterial surfaces to promote adhesion via integrin-mediated pathways. For example, collagen has been incorporated into nanofiber matrices and has enhanced rat tibia tissue regenerative processes [20], increased

human fibroblast activity [21] and increased viability of both smooth muscle cells and endothelial cells [22]. Collagen has also been immobilized [23-25] or conjugated onto a variety of surfaces [26-28] enabling it to be used in a vast amount of applications.

Cardiovascular engineered surfaces must not only promote adhesion through cell receptors but must also mimic the structure of the natural ECM of the tissue, in turn driving gene and protein expression, adhesion, migration, proliferation and differentiation [29]. The motivation to use nanostructured surfaces for cardiovascular tissue engineering is driven by this fact. Previous studies have shown that nanoscale materials affect cell growth and functionality [30-32]. Specifically, nanoscale surfaces improve fibroblast cell adhesion [33], neuronal cell differentiation [6], and osteoblast phenotypic activity [34, 35]. Topographical features that mimic the natural extracellular matrix have also been shown to encourage endothelial cell attachment, proliferation and bioactivity [36]. Nanotopography may result in improved cellular adhesion, ultimately leading to enhanced vascularization. Thus, a polymer that is capable of being tuned with nanoscale features is required. In this work, we have used polycaprolactone (PCL) since it can easily be processed to have nanoscaled features. PCL also has exceptional properties for implantation due to the fact that it is bioresorbable polyester with outstanding mechanical strength as well as a low degradation rate. Further, its degradation products are easily bioresorbed or removed naturally in metabolic pathways such as the citric acid cycle. Thus PCL has therefore received a great deal of attention for use as an implantable biomaterial and its processability needs to be studies further.

In this work, we present the immobilization of collagen unto PCL nanowire surfaces. PCL nanowire surfaces were fabricated by a solvent-free template synthesis technique developed for fabricating controlled arrays of high aspect ratio, substrate-bound nanowires from

PCL. This nanotopography was chosen due to the fact that studies have shown it has favorable hemocompatible properties [37] and transcellular growth capabilities, specifically neurons [38] and mesenchymal stem cells [39]. However, not much is known about how endothelial cells will interact to this surface. It is envisioned that the incorporation of collagen unto such nanoarchitectures will further act as a framework that may facilitate the synthesis of endothelium and promote vascularization. Understanding how to anchor human microvascular endothelial cells and the interaction of these cell surface receptors with ECM components will provide a foundation for developing functional biomaterials designed to promote human microvascular endothelial cell adhesion and growth.

4.2. Materials and methods

4.2.1. Fabrication and characterization of PCL and NW surfaces.

Surfaces were fabricated and characterized as described in detail in section 2.2.1 and 2.2.2. The nanowire surface architecture was examined for uniformity and repeatability using SEM imaging.

4.2.2. Human Microvascular Endothelial Cell (EC) Culture

ECs (Invitrogen) were suspended in MCDB 131 media enhanced with microvascular growth supplement (supplemented with 2 mmol/l glutamine, 100 ug/ml penicillin, and 100 ug/ml streptomycin) and added to 75 cm^2 culture flasks and incubated at 37 ºC under a 5 % CO_2 atmosphere. This study was performed using ECs that were passage 3-6.

ECs were seeded on PCL, NW, cPCL and cNW surfaces in a 48-well plate. Prior to seeding all surfaces were subjected to 30 min UV exposure and conditioned for 5 min in 400 µl

of culture medium. ECs cells were seeded at a density of 2×10^4 cells/well. The surfaces were incubated at 37 °C under a 5 % CO_2 atmosphere in 400 µl of cell rich medium and investigated for adhesion, proliferation and viability after 1 and 7 days culture. Further, cellular differentiation was investigated after 7 and 14 days of culture.

4.2.3. Adhesion and proliferation of ECs on different surfaces

Cell adhesion and proliferation was investigated by staining cells with rhodamine phalloidin (Cytoskeleton) and 4′,6-diamidino-2-phenylindole dihydrochloride (DAPI) (Invitrogen) nucleus stain by fluorescence microscope imaging after 1 and 7 days of culture.

Prior to staining non-adherent cells were removed by aspirating the cell rich medium from the surfaces followed by two gentle rinses with PBS. The surfaces were then transferred to a new 48-well plate and fixed with 3.7% formaldehyde 15 mins at room temperature. This was followed by incubating the surfaces in 1 % Triton-X 100 for 3 mins in order to permeabilize the cells. The surfaces were transferred to a new 48-well plate, then incubated in rhodamine-phalloidin at a concentration of 5 µL/mL for 30 mins. DAPI was added at a concentration of 1 µL/mL after 25 mins. All the surfaces were rinsed with PBS and imaged with a fluorescence microscope (Zeiss). The number of adhered cells on the surfaces was determined using DAPI stained images that were analyzed using ImageJ software.

Cells with evident boundaries adhered onto different surfaces after 1 and 7 days of culture were examined using ImageJ software. The cell shape factor was evaluated by the aspect ratio of cellular width to cellular length. The cellular width was defined as the diameter of the largest circle that would fit entirely within the cell; cellular length was defined by the diameter of the smallest circle that encompassed the entire cell.

The cell viability was characterized using a commercially available methylthiazol tetrazolium (MTT) assay kit (Sigma) after 1 and 7 days of culture. Prior to measuring mitochondrial activity, the non-adherent cells were removed by aspirating the cell rich media from the surfaces followed by two gentle rinses with PBS. Surfaces were transferred to a new 48-well plate and incubated in 400 µl of a 10 % MTT solution in PBS for 4 hrs at 37 ºC and 5 % CO_2. The resulting formazan crystals were dissolved by adding 400 µl of a 10 % SDS solution in 0.01 M HCl in PBS to the previous MTT solution. The surfaces were then incubated at 37 ºC and 5 % CO_2 for 6.5 hrs. The absorbance of the resulting solution was was measured at a wavelength of 690 nm using a plate reader (BMG Labtech). The absorbance is an indirect measurement of viability of cells on different surfaces.

The cell morphology was investigated using SEM imaging to visualize the cellular interaction with the surface nanoarchitecture. The non-adherent cells were removed by aspirating the cell rich media from the surfaces followed by two gentle rinses with PBS. The surfaces were then transferred to a clean petri dish where the cells were fixed and dehydrated. The cells were fixed by incubating the surfaces in a solution of primary fixative (3 % glutaraldehyde (Sigma), 0.1 M sodium cacodylate (Polysciences), and 0.1 M sucrose (Sigma)) for 45 min. They were then incubated in a solution of secondary fixative (primary fixative without gluteraldehyde) for 10 min. Subsequently, the surfaces were dehydrated by incubation in consecutive solutions of increasing ethanol concentrations (35 %, 50 %, 70 %, 95 %, and 100 %) for 10 min each. Further dehydration of the cells was accomplished by incubating the surfaces in hexamethyldisilazane (HMDS, Sigma) for 10 min. They were then air dried and stored in a desiccator until further imaging by SEM. The surfaces were coated with a 10 nm layer of gold and imaged at 5-7 kV.

4.2.4. Differentiation of ECs on different surfaces

After 7 and 14 days of culture, indirect immunofluorescence staining was used to determine cellular expression and differentiation through the presence of membrane specific marker proteins on ECs. The ECs were immunostained for the presence of the endogenous proteins, von Willebrand factor (vWF) and vascular endothelial cadherin (VE-cadherin). Further, a western blot analysis was used to quantify the expression of these proteins on different surfaces.

The non-adherent cells were removed by aspirating the cell rich media from the surfaces followed by two gentle rinses with PBS. The surfaces were then transferred to a new 48-well plate. Adherent cells were fixed in 3.7 % w/v formaldehyde in PBS for 15 min at room temperature and washed three times in PBS. The cell membrane was permeabilized by incubating the surfaces in a 1 % Triton-X solution in PBS at room temperature for 3 mins, followed by gentle rinse with PBS. To block nonspecific binding, the surfaces were incubated in 10 % blocking serum in PBS for 30 mins at room temperature. The surfaces were then incubated in a primary antibody solution (mouse monoclonal, rabbit polyclonal) (dilution 1:50, Santa Cruz Biotechnology) with 2 % blocking serum in PBS for 1 hr at room temperature. The surfaces were then washed three times (5 mins per wash) in PBS, and incubated with an appropriate fluorescently labeled secondary antibody solution (chicken anti-mouse-HRP, goat anti-rabbit-HRP) (dilution 1:100, Santa Cruz Biotechnology) with 2 % blocking serum in PBS for 1 hr at room temperature. The surfaces were washed three times (5 mins per wash) in PBS, and imaged with a fluorescence microscope.

Western blotting was performed to identify endothelial cell–specific proteins, vWF, and VE-cadherin expression in ECs. Briefly, cells on surfaces after 7 and 14 days in culture were

homogenized in RIPA lysis buffer (10.0 mM Tris pH 7.4, 100.0 mM NaCl, 5.0 mM EDTA, 5.0 mM EGTA, 1.0% Deoxycholate, 0.1% SDS, 1.0% Triton X-100) containing protease inhibitor cocktail. The lysate protein content was determined by micro-BCA assay. The lysate was heated to 65 °C for 20 mins in sample buffer (62.5 mM Tris-HCl pH 6.8, 10.0 % glycerol, 5.0 % β-mercaptoethanol, 2.0% SDS, 0.025 % Bromophenol blue) in order to denature the proteins prior to gel loading. 20 μg of total extract protein was electrophoresed through 8 % Tris-SDS gels and transferred to PVDF membranes in 7.5% methanol. Blots were blocked for 1 hr at room temperature. Primary monoclonal antibodies for vWF and VE-cadherin were diluted 1:500 in 3% BSA in PBS-tween solution and incubated overnight at 4 °C. The blots were then washed three times with PBS-tween solution (5 mins per wash) before they were incubated with goat anti-mouse or donkey anti-rabbit horseradish peroxidase (HRP) conjugated secondary antibodies (Santa Cruz Biotechnology) at a dilution of 1:5000 for 1 hr at room temperature. The blots were then washed three times with PBS-tween solution (5 mins per wash) followed by protein detection using chemiluminescence (WestPico Chemiluminescent Substrate; Pierce). The blots were imaged using an Alpha Innotech Fluorchem gel documentation system, and band intensities were analyzed using ImageJ software.

4.2.5. Statistics

Each experiment was confirmed on three different surfaces with at least three different cell populations ($n_{min} = 9$). All the quantitative results were analyzed using ANOVA and statistical significance was considered at $p < 0.05$.

4.3. Results and Discussion

Understanding how to anchor ECs and the interaction of the cell surface receptors with the ECM components will provide a foundation for developing functional biomaterials designed to promote EC adhesion and growth. ECs must be capable of withstanding blood flow and their viability is essential for cardiovascular health. It has been shown that endothelial cells exhibit enhanced adherence to collagen, while maintaining their in vivo phenotype on nanostructured surfaces. Therefore, the interaction of ECs with collagen immobilized PCL nanowire surfaces was investigated in this study.

4.3.1. Characterization of different surfaces

Surfaces were fabricated and characterized as described in detail in section 2.2.1 and 2.2.2. The nanowire surface architecture was examined for uniformity and repeatability using SEM imaging (**Figure 4.1.**).

4.3.2. Adhesion and proliferation of ECs on different surfaces

EC adhesion and proliferation was evaluated after 1 and 7 days of culture by staining adhered cells with rhodamine-phalloidin, a cytoskeleton stain, and DAPI, a nuclei stain and imaging the surfaces using fluorescence microscope (**Figure 4.2.**). At day 1 it is evident that cells adhered unto NW, cPCL and cNW surfaces have an elongated phenotype compared to PCL surfaces. Furthermore, after 7 days of culture there are more cells covering and interacting on both cPCL and cNW surfaces compared to plain PCL and NW surfaces.

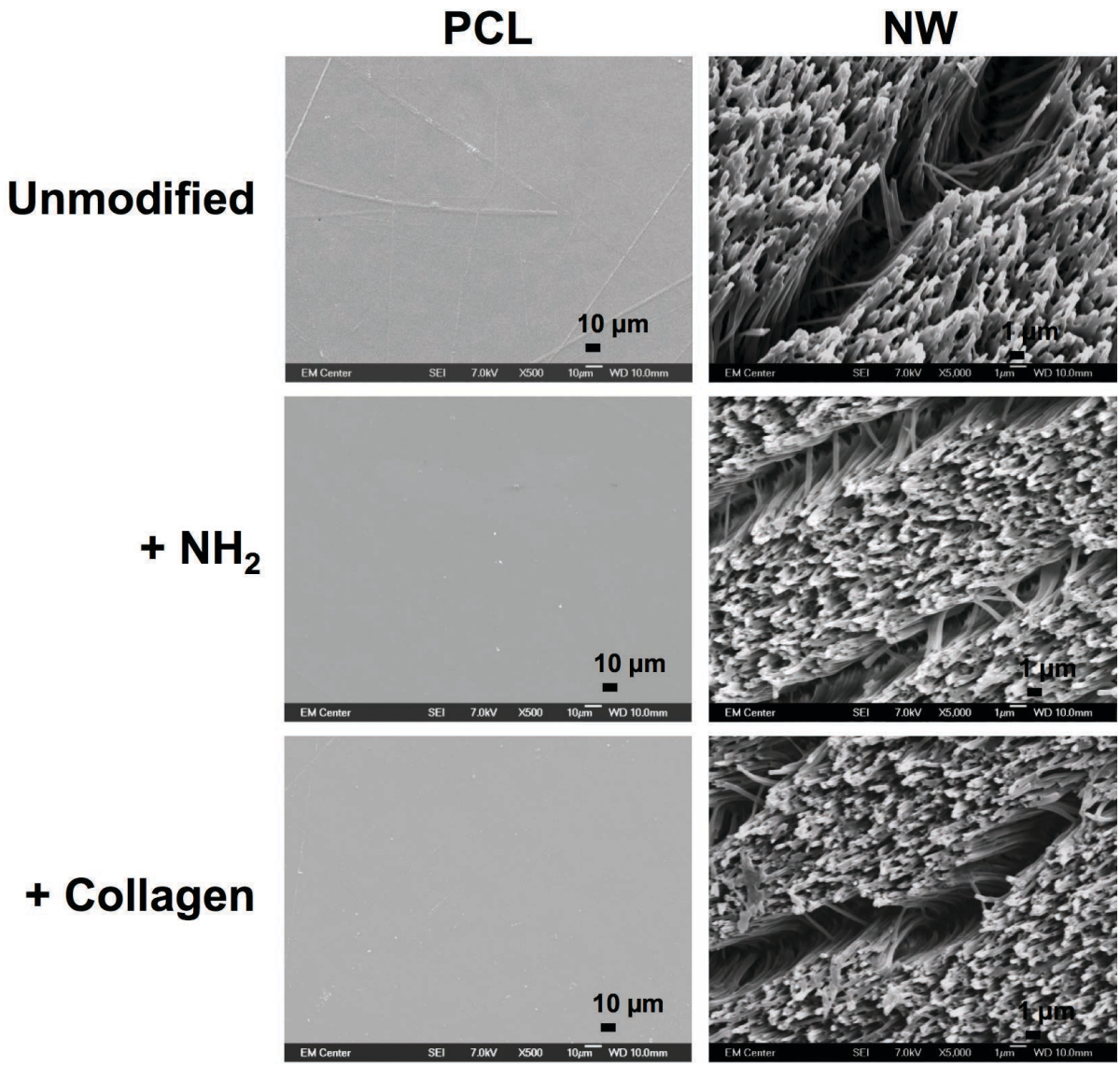

Figure 4.1. Representative scanning electron microscopy images of PCL and NW surfaces after each step of immobilization process (unmodified, + NH_2, + Collagen).

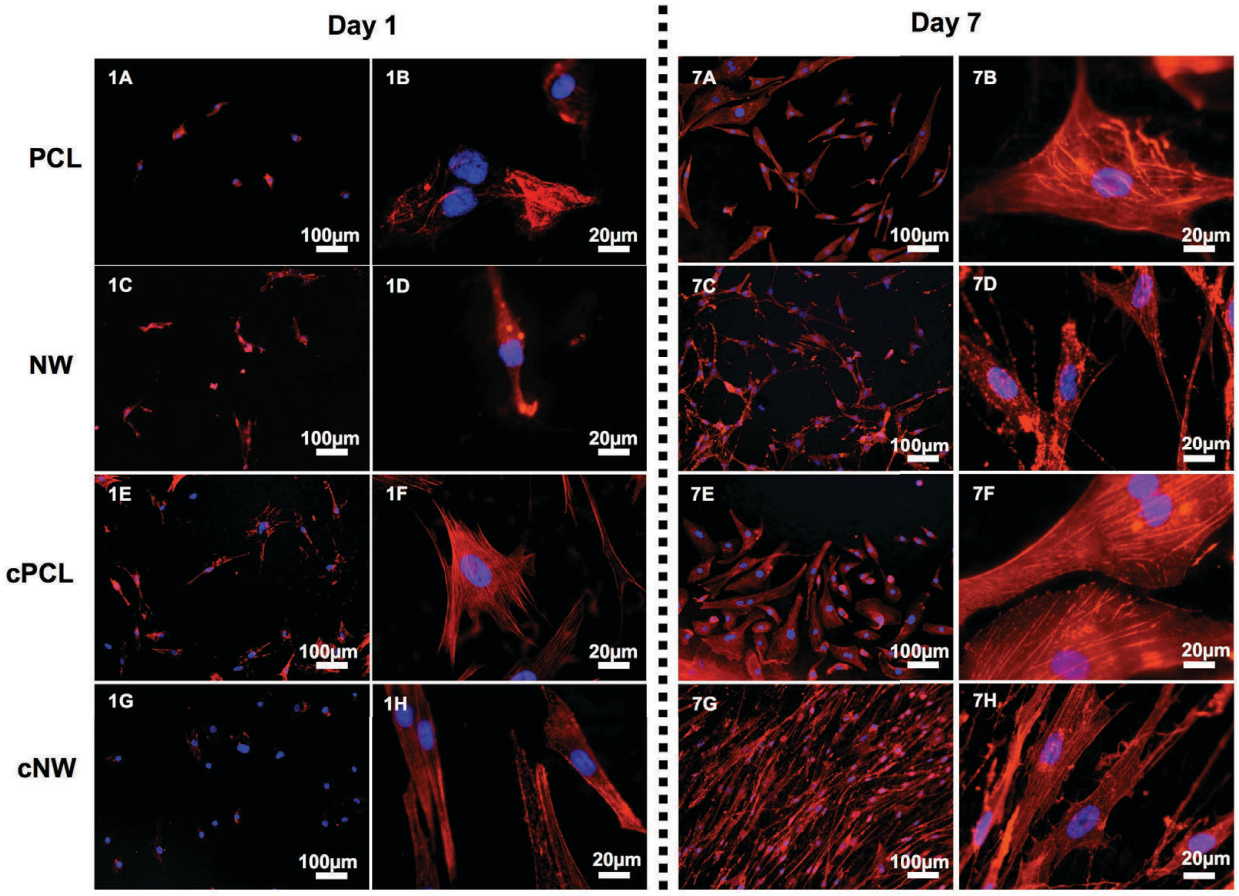

Figure 4.2. Representative fluorescence microscopy images of ECs stained with Rhodamine Phalloidin (red) and DAPI (blue) on PCL, NW, cPCL and cNW surfaces. Experiments were replicated on at least three different samples with at least three different cell populations (n_{min} = 9).

EC adhesion was quantified by counting the number of DAPI stained nuclei on each fluorescent image. The results indicate that the cell adhesion of ECs on day 1 and 7 is significantly higher on NW, cPCL and cNW surfaces compared to PCL surfaces (**Figure 4.3.(a)**). This may be due to the enhanced surface energy of these surfaces compared to PCL. Higher surface energies are known to increase the adhesion of cells. Further, collagen has been known to increase cellular anchorage to substrates via the ß$_1$ integrin family of extracellular

matrix receptors [26, 40]. Cellular adhesion plays a large role in cellular communication and regulation, indicating that collagen immobilized surfaces may serve as an excellent substrate for the anchorage dependent endothelial cells. By introducing nanoarchitecture as well as a cell binding motif it is apparent that more cells are adhering, indicating that mimicking the natural-like hierarchy of tissue and providing ECM components are important in anchoring ECs.

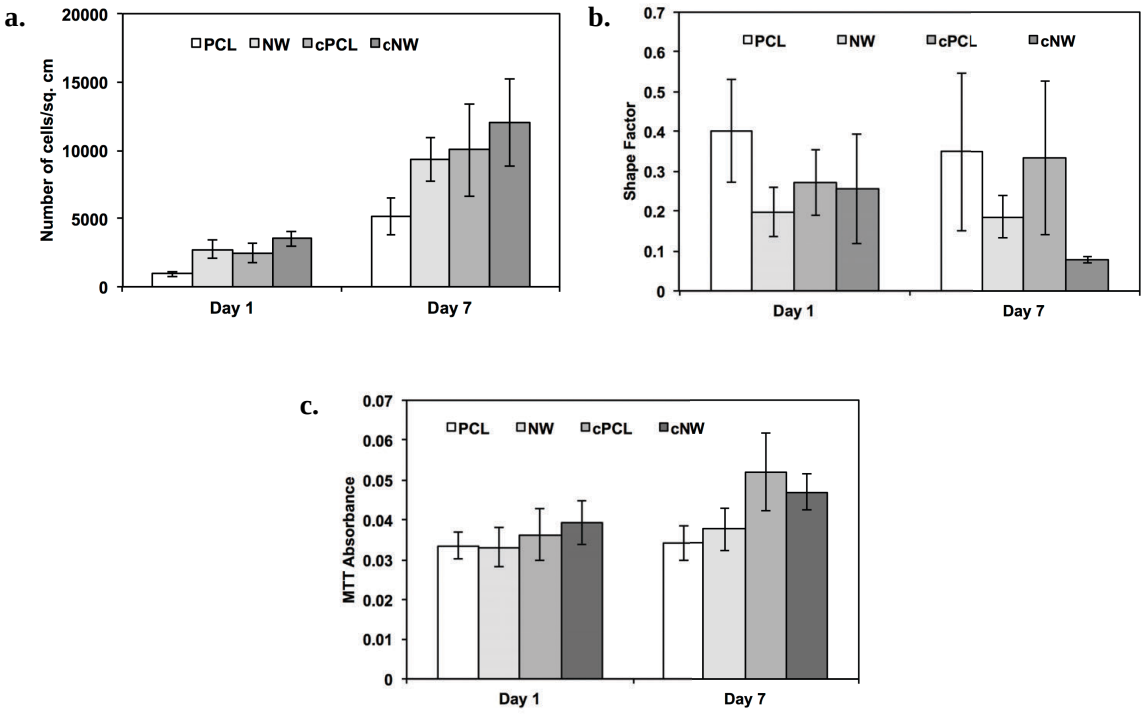

Figure 4.3. (a) Cell counts on different surfaces after 1 and 7 days of culture. Cell nuclei stained with DAPI were quantified using ImageJ software. After 1 and 7 days of culture, there were statistically less number of cells adhered on PCL surfaces as compared to NW, cPCL and cNW ($p < 0.05$). (b) Shape factor approximations of cells on different surfaces after 1 and 7 days of culture. After 1 day of culture, ECs on NW surfaces had a significantly lower shape factor (more elongated body) than those on PCL surfaces ($p < 0.05$). After 7 days of culture, ECs on cNW surfaces had significantly lower shape factor than those on PCL, NW and cPCL surfaces. (c)

Cell viability measured using the MTT assay for ECs on different surfaces. PCL, NW, cPCL and cNW surfaces had a significant increase in EC mitochondrial activity from day 1 to day 7. After 1 day of culture, cell viability was significantly increased on cNW surfaces compared to PCL and NW surfaces ($p < 0.05$). After 7 days of culture, cell viability was significantly increased on cPCL and cNW surfaces compared to both PCL and NW surfaces ($p < 0.05$). Error bars represent standard deviation. Experiments were replicated on at least three different samples with at least three different cell populations ($n_{min} = 9$). Error bars represent standard deviation.

Further, as evident from the fluorescence microscope images (**Figure 4.2.**), the cells exhibit different morphologies on different surfaces. Thus, cell shape factor was evaluated on each surface by determining the aspect ratio of cellular width to cellular length (**Figure 4.3.(b)**). A low cell shape factor indicates an elongated cell body and high cell shape factor indicated a spherical cell body. Cell shape factor calculations show that cells on nanostructured surfaces are more elongated than on surfaces without nanoarchitecture. After 1 day of culture, cells on NW surfaces had a significantly lower shape factor (more elongated body) than cells on PCL surfaces. After 7 days of culture, cells on cNW surfaces had significantly lower shape factors than cells on PCL, NW and cPCL surfaces. The significant elongation of ECs on cNW surfaces may be due to the increased anchorage of these cells. Vascular endothelial cells appear to be aligned with the flow in the immediate vicinity of the vascular wall and have a shape which is more ellipsoidal in regions of high shear and more polygonal in regions of low shear stress [41]. This shape is induced with nanotopography that may be important to maintaining the natural phenotype of ECs and promoting cell viability.

The viability of cells on different surfaces was determined using a commercially available MTT assay. This colorimetric assay measures cellular metabolic activity via NAD(P)H-dependent cellular oxidoreductase enzymes. Cellular enzymes reduce tetrazolium dye into its insoluble formazan form, giving it a purple color. This colored solution can be quantified by measuring absorbance at 690 nm with a spectrophotometer. The results indicate that the cell viability increases on all surfaces after 7 days of culture, however the cell viability was significantly greater on cPCL and cNW surfaces compared to PCL and NW surfaces (**Figure 4.3.(c)**). These results are consistent with cell adhesion results (**Figure 4.3.(a)**). More cells adhering unto surfaces leads to an increase in cell-cell contact and cellular alignment on cPCL and cNW surfaces, ultimately increasing cellular activity and viability.

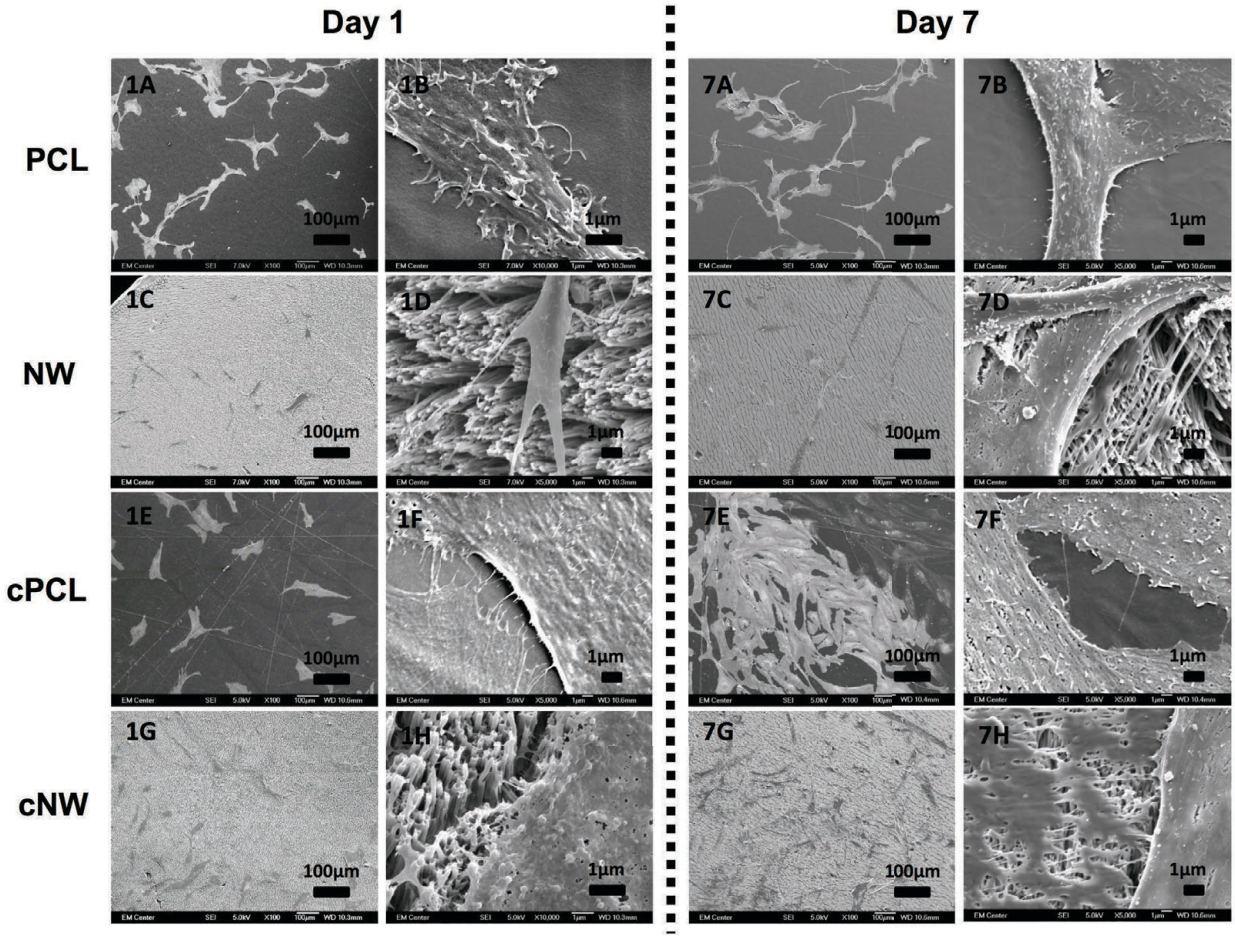

Figure 4.4. Representative SEM images of ECs after 1 and 7 days of culture on different surfaces. Note: the surfaces were coated with a 10 nm layer of gold and imaged at 7 keV. Experiments were replicated on at least three different samples with at least three different cell populations ($n_{min} = 9$).

The cell morphology was investigated using SEM imaging to visualize the cellular interaction with the surface nanoarchitecture. The nanoscale surface topography of materials is known to play a significant role in interactions with biological systems such as proteins and cells [42]. Results indicate that cells interact with NW and cNW by forming filopodia that network with the nanoscale features present (**Figure 4.4.**). It is evident that on day 7, ECs on NW and

cNW surfaces are depositing more extracellular matrix proteins on the surface compared to PCL, and cPCL surfaces, with cNW surfaces depositing the most. The nanoscale topography present on both NW and cNW surfaces contribute to the deposition of more extracellular proteins. It has also been shown that endothelial cells exhibit more of their natural phenotype in vitro on nanostructured surfaces versus in flat culture dishes [43]. Furthermore, ECs on cPCL surfaces form cell-cell junctions as evident from the filopodia extending between cells present both on day 1 and day 7. ECs do not seem to interact as well with PCL surfaces when compared to NW, cPCL and cNW surfaces as evident by the lack of filopodia and ECM deposition. This may be due to the lack of nano-architecture and cell binding motifs.

4.3.3. Differentiation of ECs on different surfaces

Differentiation of cells on surfaces was investigated by detecting vWF and VE-cadherin expression both through immunofluorescence and western blotting techniques. vWF and VE-cadherin are specific to endothelial cells and are expressed only when endothelial cells differentiate into mature phenotype. vWF is a large glycoprotein synthesized by vascular endothelial cells but is also found in plasma and platelets. It plays a role in the coagulation of blood at injury sites. VE-cadherin mediates cell-cell binding critical to tissue structure and morphogenesis. VE-cadherin is the major determinant of endothelial cell contact integrity and regulation of its activity or its presence at cell contacts is an essential step that controls the permeability of the blood vessel wall for cells and substances [44]. Immunofluorescence images indicate no clear differences in vWF expression on different surfaces (**Figure 4.5.(a))**. Clustering of vWF is seen on the collagen immobilized surfaces. vWF is known to bind to collagen which may be why clustering is occurring [45]. Further, immunofluorescence images

indicate an increase in VE-cadherin expression on NW, cPCL and cNW surfaces compared to PCL surfaces (**Figure 4.5.(b)**).

In order to quantify vWF and VE-cadherin protein expression, a western blotting technique was used. Results indicate that after 7 days of culture, vWF expression is statistically higher on NW surfaces (**Figure 4.6.(a)**). However, after 14 days in culture, vWF expression is statistically similar on all surfaces. Further, there is no significant increase in vWF expression from day 7 to day 14 on any of the surfaces. vWF expression is extremely important in endothelial cells. Platelets adhere to vWF, initiating the blood clotting cascade when injury occurs. Thus, endothelial cells must be capable of vWF expression, however an increase in vWF secretion is not desirable.

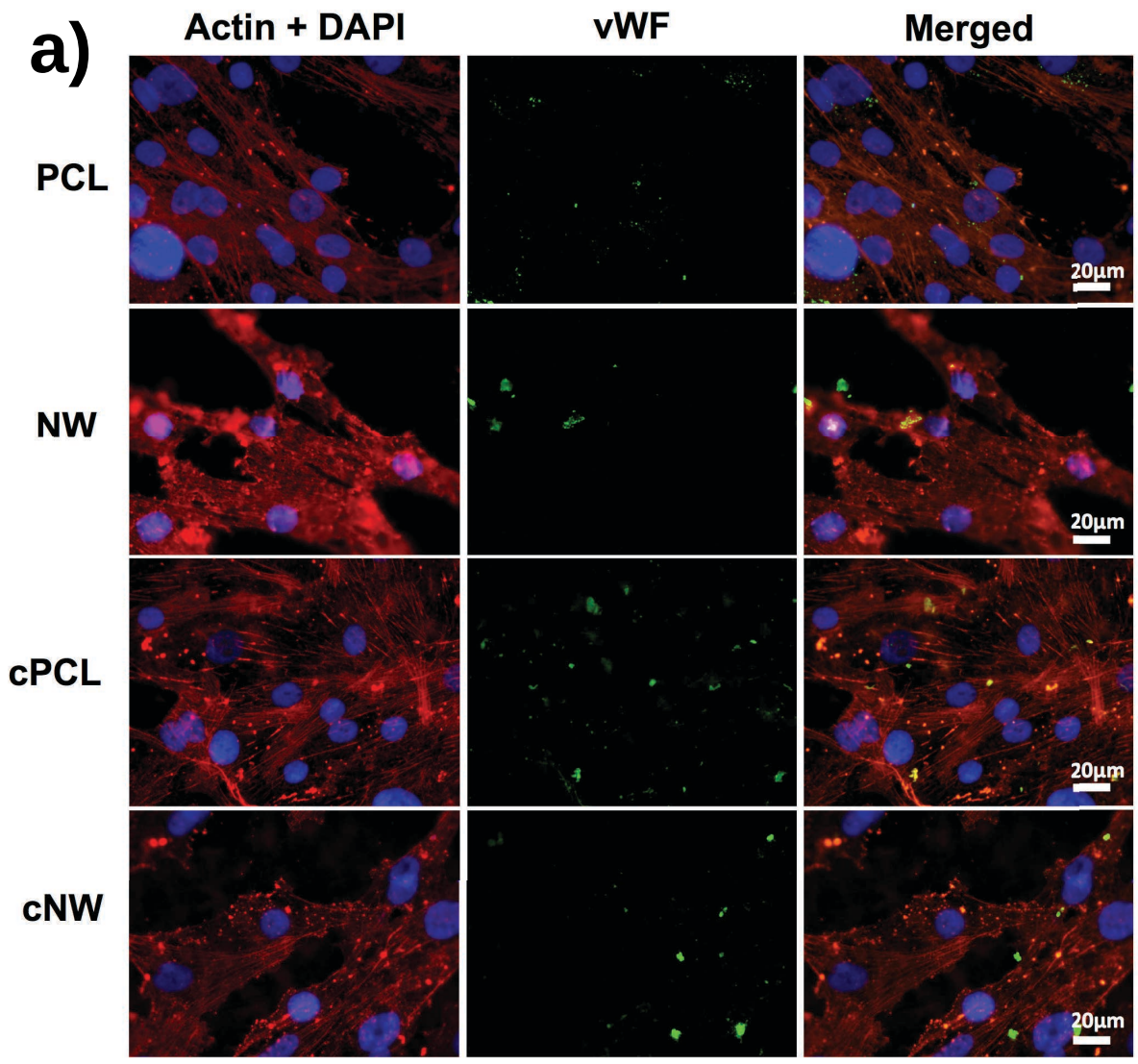
a)
Actin + DAPI
vWF
Merged
PCL
NW
cPCL
cNW
20µm
20µm
20µm
20µm

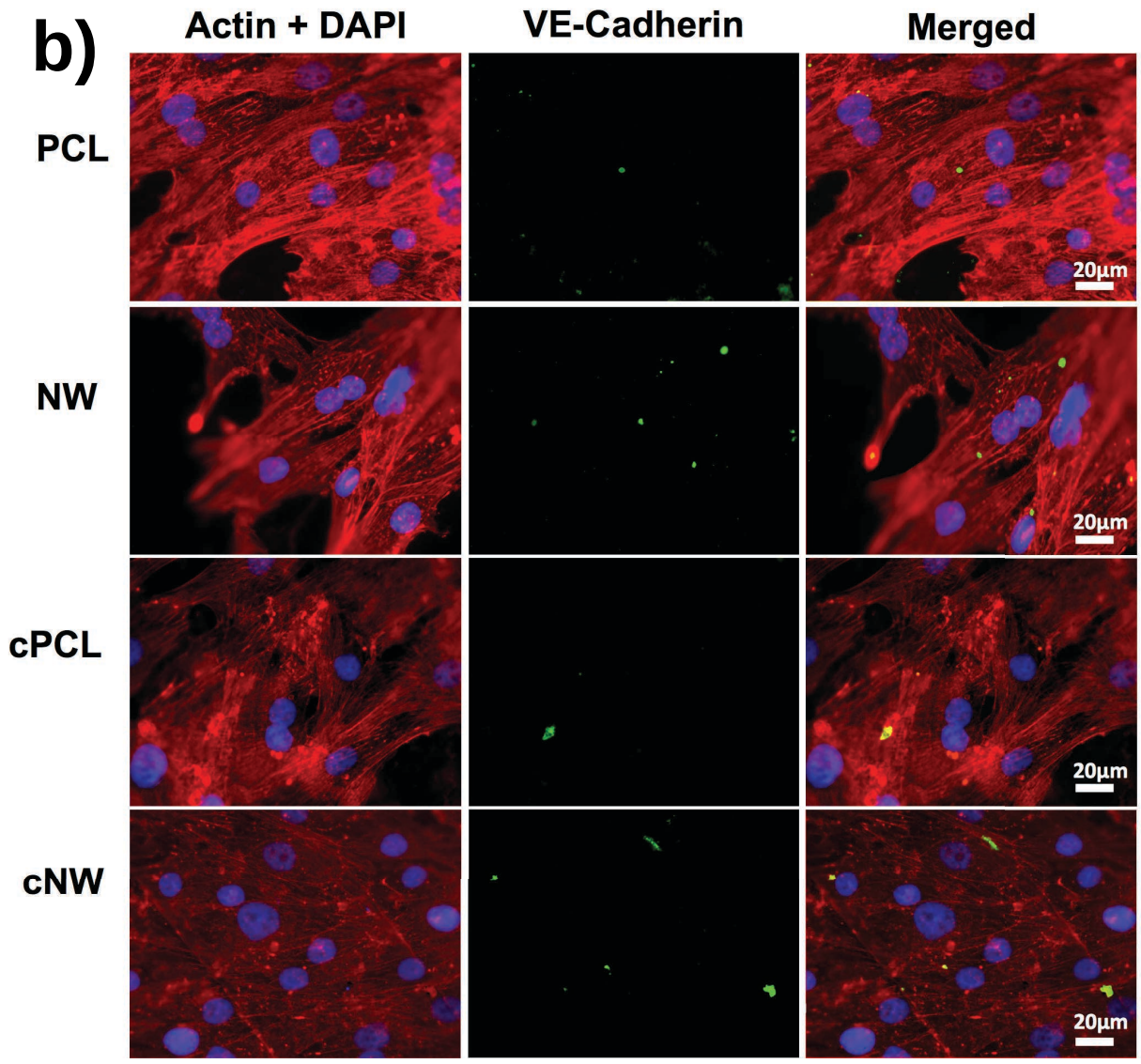

Figure 4.5. Representative fluorescence microscopy images of ECs immunostained with (a) vWF and (b) VE-cadherin. Experiments were replicated on at least three different samples with at least three different cell populations (n_{min} = 9).

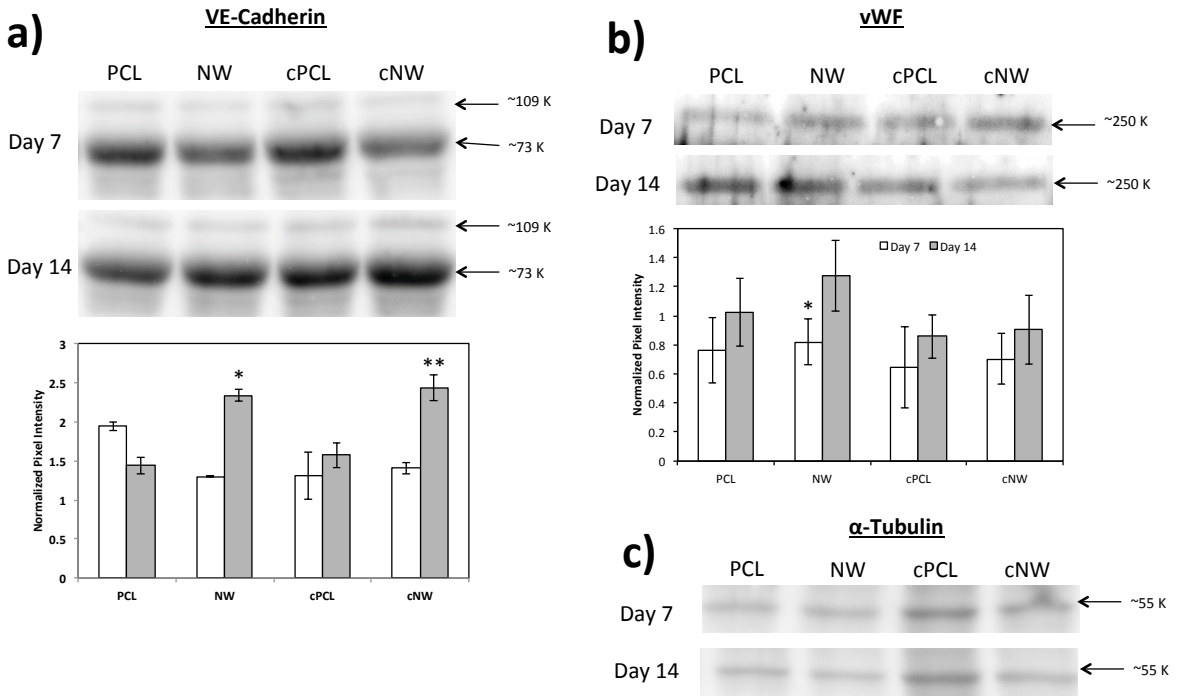

Figure 4.6. Western blot analysis of the expression of (a) vWF and (b) VE-Cadherin on different surfaces after 7 and 14 days in culture normalized to (c) α-tubulin. After 7 days of culture vWF expression is statistically higher on NW surfaces. After 14 days in culture, vWF expression is statistically similar on all surfaces. After 7 in culture, VE-cadherin expression is similar on all surfaces. After 14 days in culture, VE-cadherin expression is significantly higher on nanostructured surfaces (NW and cNW) compared to PCL and cPCL surfaces. There is also a significant increase in VE-cadherin expression from day 7 to 14 on NW and cNW surfaces. Experiments were replicated with western blots with at least three different cell populations

After 7 in culture, VE-cadherin expression is similar on all surfaces (**Figure 4.6.(b)**). However, after 14 days in culture, VE-cadherin expression is significantly higher on nanostructured surfaces (NW and cNW) compared to PCL and cPCL surfaces. There is also a significant increase in VE-cadherin expression from day 7 to 14 on NW and cNW surfaces. VE-

cadherin expression is important in cellular contacts, which will eventually regulate the permeability of the blood vessel, therefore an increase in VE-cadherin expression is necessary for healthy vasculature. Increased expression can be seen on surfaces with nanostructured features (NW and cNW).

4.4. Conclusion

A thorough understanding of the interaction between ECs and the biomaterial surface is essential in order to promote healing and regeneration through integration with native tissue. One major obstacle to overcome is adhesion of the anchorage-dependent and slowly renewing ECs on material surfaces. The level of cell growth is correlated to the characteristics of the material surface and its ability to mimic properties similar to extracellular matrix. Therefore, providing ECs with nanotopography and cell-binding motifs such as collagen may affect the cell adhesion, viability, morphology and differentiation. In this study, ECs exhibited increased adhesion and viability on NW, cPCL and cNW surfaces. ECs have a more elongated body and low shape factor on nanostructured surfaces (NW and cNW) compared to smooth surfaces (PCL and cPCL). The differentiation potential of collagen immobilized nanowire surfaces was also evaluated by immunostaining and western blotting for key endothelial cell markers, vWF and VE-cadherin. The expression of VE-cadherin is increased on nanostructured surfaces after 14 days in cuture, indicating more cell-cell contacts. The expression of vWF is statistically similar on all surfaces after 14 days in culture with no significant increase from 7 to 14 days in culture, indicating that increased perturbation of the endothelial layer on any surface is not occurring. The results presented here indicate that ECs adhesion and differentiation can be modulated by providing surfaces with nanotopography and cell binding motifs such as collagen.

REFERENCES

[1] Palmer RMJ, Bridge L, Foxwell NA, Moncada S. The role of nitric oxide in endothelial cell damage and its inhibition by glucocorticoids. British Journal of Pharmacology. 1992;105:11-2.

[2] Mantovani A, Bussolino F, Dejana E. Cytokine regulation of endothelial cell function. Faseb J. 1992;6:2591-9.

[3] de Mel A, Jell G, Stevens MM, Seifalian AM. Biofunctionalization of Biomaterials for Accelerated in Situ Endothelialization: A Review. Biomacromolecules. 2008;9:2969-79.

[4] Gimbrone MA, Cotran RS, Folkman J. HUMAN VASCULAR ENDOTHELIAL CELLS IN CULTURE: Growth and DNA Synthesis. The Journal of Cell Biology. 1974;60:673-84.

[5] Bidarra SJ, Barrias CC, Fonseca KB, Barbosa MA, Soares RA, Granja PL. Injectable in situ crosslinkable RGD-modified alginate matrix for endothelial cells delivery. Biomaterials. 2011;32:7897-904.

[6] Seidlits SK, Lee JY, Schmidt CE. Nanostructured scaffolds for neural applications. Nanomedicine. 2008;3:183-99.

[7] Shen YH, Shoichet MS, Radisic M. Vascular endothelial growth factor immobilized in collagen scaffold promotes penetration and proliferation of endothelial cells. Acta Biomater. 2008;4:477-89. doi: 10.1016/j.actbio.2007.12.011. Epub 8 Feb 5.

[8] Shin H, Jo S, Mikos AG. Biomimetic materials for tissue engineering. Biomaterials. 2003;24:4353-64.

[9] Glowacki J, Mizuno S. Collagen scaffolds for tissue engineering. Biopolymers. 2008;89:338-44.

[10] Chevallay B, Abdul-Malak N, Herbage D. Mouse fibroblasts in long-term culture within collagen three-dimensional scaffolds: Influence of crosslinking with diphenylphosphorylazide on matrix reorganization, growth, and biosynthetic and proteolytic activities. Journal of Biomedical Materials Research. 2000;49:448-59.

[11] Ruberti JW, Zieske JD. Prelude to corneal tissue engineering – Gaining control of collagen organization. Progress in Retinal and Eye Research. 2008;27:549-77.

[12] Duan X, Sheardown H. Dendrimer crosslinked collagen as a corneal tissue engineering scaffold: Mechanical properties and corneal epithelial cell interactions. Biomaterials. 2006;27:4608-17.

[13] Kim JH, Kim SH, Kim HK, Akaike T, Kim SC. Adhesion and growth of endothelial cell on amphiphilic PU/PS IPN surface: Effect of amphiphilic balance and immobilized collagen. Journal of Biomedical Materials Research. 2002;62:613-21.

[14] Orwin EJ, Hubel A. In vitro culture characteristics of corneal epithelial, endothelial, and keratocyte cells in a native collagen matrix. Tissue Eng. 2000;6:307-19.

[15] Tuckwell D, Humphries M. Integrin–collagen binding. Seminars in Cell & Developmental Biology. 1996;7:649-57.

[16] Arnoult O. A NOVEL BENIGN SOLUTION FOR COLLAGEN PROCESSING: Case Western Reserve University; 2010.

[17] Pozzi A, Wary KK, Giancotti FG, Gardner HA. Integrin alpha1beta1 mediates a unique collagen-dependent proliferation pathway in vivo. J Cell Biol. 1998;142:587-94.

[18] Emsley J, Knight CG, Farndale RW, Barnes MJ, Liddington RC. Structural Basis of Collagen Recognition by Integrin α2β1. Cell. 2000;101:47-56.

[19] Riikonen T, Westermarck J, Koivisto L, Broberg A, Kahari VM, Heino J. Integrin alpha 2 beta 1 is a positive regulator of collagenase (MMP-1) and collagen alpha 1(I) gene expression. J Biol Chem. 1995;270:13548-52.

[20] Phipps MC, Clem WC, Grunda JM, Clines GA, Bellis SL. Increasing the pore sizes of bone-mimetic electrospun scaffolds comprised of polycaprolactone, collagen I and hydroxyapatite to enhance cell infiltration. Biomaterials. 2012;33:524-34.

[21] Liu S-J, Kau Y-C, Chou C-Y, Chen J-K, Wu R-C, Yeh W-L. Electrospun PLGA/collagen nanofibrous membrane as early-stage wound dressing. Journal of Membrane Science. 2010;355:53-9.

[22] Chen ZG, Wang PW, Wei B, Mo XM, Cui FZ. Electrospun collagen–chitosan nanofiber: A biomimetic extracellular matrix for endothelial cell and smooth muscle cell. Acta Biomaterialia. 2010;6:372-82.

[23] Krithica N, Natarajan V, Madhan B, Sehgal PK, Mandal AB. Type I Collagen Immobilized Poly(caprolactone) Nanofibers: Characterization of Surface Modification and Growth of Fibroblasts. Advanced Engineering Materials. 2012;14:B149-B54.

[24] Baek J-Y, Xing Z-C, Kwak G, Yoon K-B, Park S-Y, Park LS, et al. Fabrication and characterization of collagen-immobilized porous PHBV/HA nanocomposite scaffolds for bone tissue engineering. J Nanomaterials. 2012;2012:1-.

[25] Farhadi M, Mirzadeh H, Solouk A, Asghari A, Jalessi M, Ghanbari H, et al. Collagen-immobilized patch for repairing small tympanic membrane perforations: In vitro and in vivo assays. Journal of Biomedical Materials Research Part A. 2012;100A:549-53.

[26] He W, Ma Z, Yong T, Teo WE, Ramakrishna S. Fabrication of collagen-coated biodegradable polymer nanofiber mesh and its potential for endothelial cells growth. Biomaterials. 2005;26:7606-15.

[27] Hong Y, Gao C, Xie Y, Gong Y, Shen J. Collagen-coated polylactide microspheres as chondrocyte microcarriers. Biomaterials. 2005;26:6305-13.

[28] Hong Y, Gong Y, Gao C, Shen J. Collagen-coated polylactide microcarriers/chitosan hydrogel composite: Injectable scaffold for cartilage regeneration. Journal of Biomedical Materials Research Part A. 2008;85A:628-37.

[29] Chew SY, Low WC. Scaffold-based approach to direct stem cell neural and cardiovascular differentiation: An analysis of physical and biochemical effects. Journal of Biomedical Materials Research Part A. 2011;97A:355-74.

[30] Cao H, McHugh K, Chew SY, Anderson JM. The topographical effect of electrospun nanofibrous scaffolds on the in vivo and in vitro foreign body reaction. Journal of Biomedical Materials Research Part A. 2010;93A:1151-9.

[31] Bechara S, Wadman L, Popat KC. Electroconductive polymeric nanowire templates facilitates in vitro C17.2 neural stem cell line adhesion, proliferation and differentiation. Acta Biomaterialia. 2011;7:2892-901.

[32] McMurray RJ, Gadegaard N, Tsimbouri PM, Burgess KV, McNamara LE, Tare R, et al. Nanoscale surfaces for the long-term maintenance of mesenchymal stem cell phenotype and multipotency. Nat Mater. 2011;10:637-44.

[33] Park K, Ju YM, Son JS, Ahn KD, Han DK. Surface modification of biodegradable electrospun nanofiber scaffolds and their interaction with fibroblasts. J Biomater Sci Polym Ed. 2007;18:369-82.

[34] Werner C, Maitz MF, Sperling C. Current strategies towards hemocompatible coatings. Journal of Materials Chemistry. 2007;17:3376-84.

[35] Bechara SL, Judson A, Popat KC. Template synthesized poly(epsilon-caprolactone) nanowire surfaces for neural tissue engineering. Biomaterials. 2010;31:3492-501.

[36] Williamson MR, Black R, Kielty C. PCL–PU composite vascular scaffold production for vascular tissue engineering: Attachment, proliferation and bioactivity of human vascular endothelial cells. Biomaterials. 2006;27:3608-16.

[37] Leszczak V, Smith BS, Popat KC. Hemocompatibility of polymeric nanostructured surfaces. Journal of Biomaterials Science, Polymer Edition. 2013:1-20.

[38] Bechara SL, Judson A, Popat KC. Template synthesized poly(ε-caprolactone) nanowire surfaces for neural tissue engineering. Biomaterials. 2010;31:3492-501.

[39] Porter JR, Henson A, Ryan S, Popat KC. Biocompatibility and mesenchymal stem cell response to poly(epsilon-caprolactone) nanowire surfaces for orthopedic tissue engineering. Tissue Eng Part A. 2009;15:2547-59. doi: 10.1089/ten.tea.2008.0476.

[40] Clyman RI, McDonald KA, Kramer RH. Integrin receptors on aortic smooth muscle cells mediate adhesion to fibronectin, laminin, and collagen. Circulation Research. 1990;67:175-86.

[41] Levesque MJ, Nerem RM. The elongation and orientation of cultured endothelial cells in response to shear stress. Journal of biomechanical engineering. 1985;107:341-7.

[42] Lord MS, Foss M, Besenbacher F. Influence of nanoscale surface topography on protein adsorption and cellular response. Nano Today. 2010;5:66-78.

[43] Dalby MJ, Riehle MO, Johnstone H, Affrossman S, Curtis ASG. In vitro reaction of endothelial cells to polymer demixed nanotopography. Biomaterials. 2002;23:2945-54.

[44] Vestweber D. VE-Cadherin: The Major Endothelial Adhesion Molecule Controlling Cellular Junctions and Blood Vessel Formation. Arteriosclerosis, Thrombosis, and Vascular Biology. 2008;28:223-32.

[45] Ruggeri ZM, Mendolicchio GL. Adhesion Mechanisms in Platelet Function. Circulation Research. 2007;100:1673-85.

CHAPTER 5

SMOOTH MUSCLE CELL FUNCTIONALITY ON COLLAGEN IMMOBILIZED NANOWIRES

5.1. Introduction

The vascular smooth muscle cell's (SMC) main function is contraction and adjustment of blood vessel diameter, blood pressure, and blood flow distribution [1]. SMCs have the capacity for contraction, migration, proliferation, synthesis of extracellular matrix (ECM) components and the secretion of growth factors and cytokines [2]. This allows SMCs to regulate lumen diameter both transiently and chronically [3]. SMCs are key players in the development of vascular disease due to their plasticity or ability to change phenotype and behavior according to varying environmental conditions [4]. The standard treatment for vascular disease is coronary angioplasty, which leads to disorder of the endothelial layer. This leaves a highly prothrombotic surface exposed to the blood stream and promotes SMC dedifferentiation followed by proliferation [5, 6]. Restoration of an endothelium represents a crucial process in re-establishing an intact vessel surface, but in order to do this SMC proliferation must be controlled. Enhanced SMC proliferation often leads to restenosis, the reocclusion of the blood vessel. This can be caused by SMC migration, proliferation and neointimal thickening and further limits the success of balloon angioplasty and stent implantation [7].

SMCs exhibit two well-known phenotypes; contractile and synthetic [8]. Contractile SMCs are elongated and spindle shaped, whereas synthetic SMCs are less elongated and have an epithelioid morphology. Synthetic SMCs contain organelles involved in protein synthesis, whereas in contractile SMCs, these organelles are replaced with contractile filaments. Further,

synthetic and contractile SMCs exhibit different proliferation rates. Synthetic SMCs proliferate at higher rates compared to contractile SMCs. Contractile SMCs in adult blood vessels proliferate at an exceptionally low rate, demonstrate low synthetic activity, and express a unique selection of contractile proteins and signaling molecules required for contractile function [9]. SMCs within adult blood vessels are incredibly plastic and can easily change phenotype, a process also known as phenotypic switching. This occurs in response to vascular injury, allowing them to proliferate at high rates [10, 11]. SMC phenotypic switching is characterized by a decrease in the expression of SMC specific differentiation proteins and increased SMC proliferation, migration, and synthesis of ECM components required for repair of vasculature. An unfortunate consequence of SMC plasticity is that environmental cues and signals can promote SMC phenotypic switching and stimulate the development and/or progression of vascular disease [2]. There is evidence that phenotypic switching of SMCs plays a significant role in a repertoire of diseases in humans, such as atherosclerosis, asthma, hypertension, and cancer [4]. A decrease in proliferation, however, is not sufficient to promote SMC differentiation [2].

Biomaterial–cell interactions are fundamental in various biological events and determine the longevity and functionality of implanted devices. It is well known that cardiovascular biomaterial implants, such as stents, perturb the endothelium layer, promoting SMC migration and proliferation, ultimately leading to restenosis and failure of the implant [12]. However, this may be avoidable with the design of a biomaterial surface capable of influencing cellular interactions. Enhancement of cell-biomaterial interactions can be altered by immobilizing surfaces with extracellular matrix (ECM) molecules such as fibronectin, laminin, collagen, or vitronectin [13]. By modifying biomaterial surfaces with these ECM components, cell-binding

sites are introduced which may promote cell functionality. One such ECM molecule is collagen 1. It is the main component in the ECM of blood vessels as well as other tissues in the body, and has been used extensively to promote smooth muscle cell adhesion on biomaterial surfaces [14, 15]. Further, it is also known to promote the contractile phenotype in SMCs [16]. Another popular approach for controlling cell functionality on implant surfaces is the introduction of surface topographies at a nanometer or micrometer scale. Due to the existence of functional nanoscale structures within native tissue, nanostructured surfaces have attracted attention. Nanoscale features can influence cellular responses ranging from initial attachment and migration to differentiation and synthesis of new ECM. Studies have shown that proliferation of the SMCs is significantly reduced on the nanopatterned surfaces, while these surfaces also promote the alignment of cells [17, 18]. Topographical features that mimic the natural extracellular matrix have also been shown to encourage SMC attachment and bioactivity, [19, 20] while limiting proliferation [21].

In this study, we have used polycaprolactone since it has exceptional properties for implantation such as outstanding mechanical strength and a low degradation rate in physiological conditions. It can also easily be processed to have nanoscaled features. Further, its degradation products are easily bioresorbed or removed naturally in metabolic pathways such as the citric acid cycle. Polycaprolactone has therefore received a great deal of attention for use as an implantable biomaterial for many tissue engineering applications including cardiovascular applications [22-24].

In this work, we present the immobilization of collagen I unto polycaprolactone nanowire surfaces. Polycaprolactone nanowire surfaces were fabricated by a solvent-free template synthesis technique developed for fabricating controlled arrays of high aspect ratio, substrate-

bound nanowires from polycaprolactone. This nanotopography was chosen since it has shown promising hemocompatible properties [25] and transcellular growth capabilities, specifically neurons [26] and mesenchymal stem cells [27]. However, not much is known about how SMCs will interact with this surface. It is envisioned that the incorporation of collagen on nanowires may facilitate the adherence and differentiation of SMCs. The objective of this work is to investigate how SMCs interact with nanowire topography to see if these surfaces have potential for cardiovascular implants. Understanding how to anchor smooth muscle cells and the interaction of the cell surface receptors with the ECM components will provide a foundation for developing functional vascular biomaterials that inhibit unwarranted vascular SMC proliferation and preserve a differentiated state of SMCs to manage and avoid vascular disease conditions.

5.2. Materials and Methods

5.2.1. Fabrication of PCL nanowire surfaces

Surfaces were fabricated and characterized as described in detail in section 2.2.1 and 2.2.2. The nanowire surface architecture was examined for uniformity and repeatability using SEM imaging.

5.2.2. Smooth Muscle Cell Culture

Human Aortic SMCs (Life Technologies) were suspended in MCDB 131 media (Life Technologies) enhanced with SMC growth supplement (supplemented with 2 mmol/l glutamine, 100 ug/ml penicillin, and 100 ug/ml streptomycin) and added to 75 cm^2 culture flasks and incubated at standard culture conditions. This study was performed using SMCs that were passage 4.

SMCs were cultured on PCL, NW, cPCL and cNW surfaces in a 48-well plate. Prior to seeding, all surfaces were subjected to 30 min UV exposure and conditioned for 5 min in 400 µl of culture medium. SMCs cells were seeded at a density of 2×10^4 cells/well. The surfaces were incubated in standard culture conditions in 400 µl of cell rich medium and investigated for adhesion, proliferation and viability after 1 and 7 days culture. After 7 days in culture, media changes were done with MCDB 131 media enhanced with with SMC differentiation supplement (supplemented with 2 mmol/l glutamine, 100 ug/ml penicillin, and 100 ug/ml streptomycin). SMC differentiation was investigated after 14 and 21 days of culture.

5.2.3. Adhesion and proliferation of SMCs on different surfaces

Cellular adhesion and proliferation was investigated using 5-Chloromethylfluorescein Diacetate (CMFDA) live cytoplasm stain (Invitrogen), Rhodamine Phalloidin F-actin cytoskeleton stain (Cytoskeleton) and 4′,6-diamidino-2-phenylindole dihydrochloride (DAPI) nucleus stain (Invitrogen) by fluorescence microscope imaging after 1 and 7 days of culture.

Prior to staining nonadherent cells were removed by aspirating the medium from the surfaces followed by two gentle rinses with PBS. The surfaces were then transferred to a new 48-well plate and incubated with 10 µM CMFDA solution in PBS for 30 min at 37 °C and 5 % CO_2 followed by another incubation in PBS for another 30 min at 37 °C and 5 % CO_2. 3.7 % formaldehyde was then added to fix the cells for 15 min at room temperature. This was followed by 2 gentle rinses in PBS prior to incubating the surfaces in 1 % Triton-X 100 for 3 min in order to permeabilize the cells. The surfaces were rinsed in PBS (3x 5 min), and then incubated in 5 µL/mL rhodamine-phalloidin solution for 30 min. After 25 min 1 µL/mL DAPI was added to the rhodamine-phalloidin solution. All the surfaces were rinsed and stored in PBS until imaged using

a Zeiss Axioplan 2 fluorescence microscope. The number of cells adherent on the surfaces was determined from the number of stained nuclei in the DAPI fluorescence images using ImageJ software.

5.2.4. SMC elongation on different surfaces

SMCs adhered onto cPCL and cNW surfaces after 1 and 7 days of culture with evident boundaries were examined using ImageJ software to acquire an approximation for cellular elongation. Cellular elongation was calculated as the aspect ratio of cellular length to cellular width, outputting an elongation [*E*] parameter [28]. Cellular length was defined by the diameter of the smallest circle that encompassed the entire cell, while cellular width was defined as the diameter of the largest circle that would fit entirely within the cell. *E* provides a description for the extent of equimomental elipse lengthening. Thus, *E* is zero for a circle, and one for an ellipse with an axis ratio of 1:2.

5.2.5. Viability of SMCs on different surfaces

The cell viability was characterized using a commercially available Methylthiazol Tetrazolium (MTT) assay kit (Sigma) on days 1 and 7 in culture. Prior to measuring mitochondrial activity, the unadhered SMCs were removed by aspirating the cell rich media from the surfaces followed by two gentle rinses with PBS. Surfaces were transferred to a new 24-well plate and incubated in 10 % MTT solution in PBS for 3.5 hrs at 37 ºC and 5 % CO_2. The subsequent formazan crystals were dissolved by adding a 10 % Triton-X in MTT solvent mixture in equal amounts to the MTT solution in PBS. The absorbance of the solution was measured at a

wavelength of 690 nm using a plate reader (BMG Labtech). The mitochondric activity of the cells on different surfaces correlate to the resulting absorbance values.

5.2.6. Morphology of SMCs on different surfaces

SMC morphology was investigated using SEM imaging to visualize the cellular interaction with the nano-architecture. The un-adhered cells were removed by aspirating media from the surfaces followed by two gentle rinses with PBS. The surfaces were then transferred to a clean petri-dish where the cells were fixed and dehydrated on the surface. The cells were fixed by incubating the surfaces in a solution of primary fixative (3 % glutaraldehyde (Sigma), 0.1 M sodium cacodylate (Polysciences), and 0.1 M sucrose (Sigma)) for 45 min. Surfaces were then incubated in a solution of secondary fixative (primary fixative without gluteraldehyde) for 10 min. Next, the surfaces were dehydrated by incubation in consecutive solutions of increasing ethanol concentrations (35 %, 50 %, 70 %, 95 %, and 100 %) for 10 min each. Further dehydration of the cells was accomplished by incubating the surfaces in hexamethyldisilazane (HMDS, Sigma) for 10 min. Surfaces were then air dried and stored in a desiccator until imaging by SEM. The surfaces were coated with a 10 nm layer of gold and imaged at 5-7 kV.

5.2.7. Differentiation of SMCs on different surfaces

The SMCs on different surfaces were studied for the expression of heavy chain myosin (MYH) and calponin (CAL). MYH expression has never been detected in non-SMCs and is the only marker protein that is also SMC specific during embryogenesis. CAL is a thin filament protein involved in the regulation of actin-myosin interactions in SMCs.

First, western blotting was performed to identify SMC specific proteins, MYH and CAL, and semi-quantify their expression. Briefly, cells on surfaces after 7, 14 and 21 days in culture were homogenized in RIPA lysis buffer (10.0 mM Tris pH 7.4, 100.0 mM NaCl, 5.0 mM EDTA, 5.0 mM EGTA, 1.0% Deoxycholate, 0.1% SDS, 1.0% Triton X-100) containing protease inhibitor cocktail. The lysate protein content was determined by micro-BCA assay. The lysate was heated to 95 ℃ for 20 min in sample buffer (62.5 mM Tris-HCl pH 6.8, 10.0 % glycerol, 5.0 % β-mercaptoethanol, 2.0 % SDS, 0.025 % Bromophenol blue) in order to denature the proteins prior to gel loading. An equivalent amount of total extract protein was electrophoresed through 8 % Tris-SDS gels and transferred to PVDF membranes in 7.5 % methanol. Blots were blocked for 1 hr at room temperature. Primary monoclonal antibodies for MYH and CAL were diluted 1:200 in 3% BSA in PBS-tween solution and incubated overnight at 4 ℃. The blots were then washed with PBS-tween solution (3x 5 min) before they were incubated with goat anti-mouse or donkey anti-rabbit horseradish peroxidase (HRP) conjugated secondary antibodies (Santa Cruz Biotechnology) at a dilution of 1:5000 for 1 hr at room temperature. The blots were then washed with PBS-tween solution (3x 5 min) followed by protein detection using chemiluminescence (WestPico Chemiluminescent Substrate; Pierce). The blots were imaged using an Alpha Innotech Fluorchem gel documentation system, and band intensities were analyzed using ImageJ software.

After 21 days of culture, indirect immunofluorescence staining was used to determine cellular phenotype through the presence of endogenous proteins specific to SMCs when in a mature state. The un-adhered SMCs were removed by aspirating the cell rich media from the surfaces followed by two gentle rinses with PBS. The surfaces were then transferred to a new 48-well plate. Adherent cells were fixed in 3.7 wt% formaldehyde in PBS for 15 min at room

temperature and washed in PBS (3x 5 min). The cell membranes were permeabilized using 1 % Triton-X in PBS at room temperature for 3 min, and washed in PBS (3x 5 min). Subsequently, surfaces were incubated in 10 % BSA in PBS for 30 min at room temperature. A primary antibody (dilution 1:50, Santa Cruz Biotechnology) with 2 % blocking serum in PBS was administered for 1 hr at room temperature.

Surfaces were then washed in PBS (3x 5 min), and incubated with an appropriate secondary fluorescently labeled antibody (dilution 1:100, Santa Cruz Biotechnology, Santa Cruz, CA) with 2 % blocking serum in PBS for 1 hr at room temperature. The surfaces were washed in PBS (3x 5 min) and imaged with a fluorescent microscope. All images were processed using ImageJ Software. Cellular differentiation and expression were determined by increased fluorescence.

5.2.8. Statistics

Each experiment was confirmed on three different substrates with at least three different cell populations ($n_{min} = 9$). All the quantitative results were analyzed using ANOVA and a Tukey's post hoc test. Statistical significance was considered at $p < 0.05$.

5.3. Results and Discussion

Understanding how SMCs respond to biomaterial surfaces as well as how cell surface receptors interact with the ECM components will provide a foundation for developing functional biomaterials designed to promote a contractile SMC phenotype. In general SMC phenotypic switching is characterized by markedly reduced expression of SMC-selective differentiation marker genes and increased SMC proliferation, migration, and synthesis of extra- cellular matrix

components required for vascular repair. This can often lead to restenosis and can progress the development of vascular disease. In this study, we explore the effect that the combination of both surface nanoarchitecture and cell binding motifs on SMC adhesion, viability, proliferation and differentiation.

5.3.1. Characterization of Surfaces

The surface architecture of the different surfaces before and after the collagen immobilization process was characterized using SEM. Results reveal that surface architecture remains consistent before and after collagen immobilization (**Figure 5.1.**).

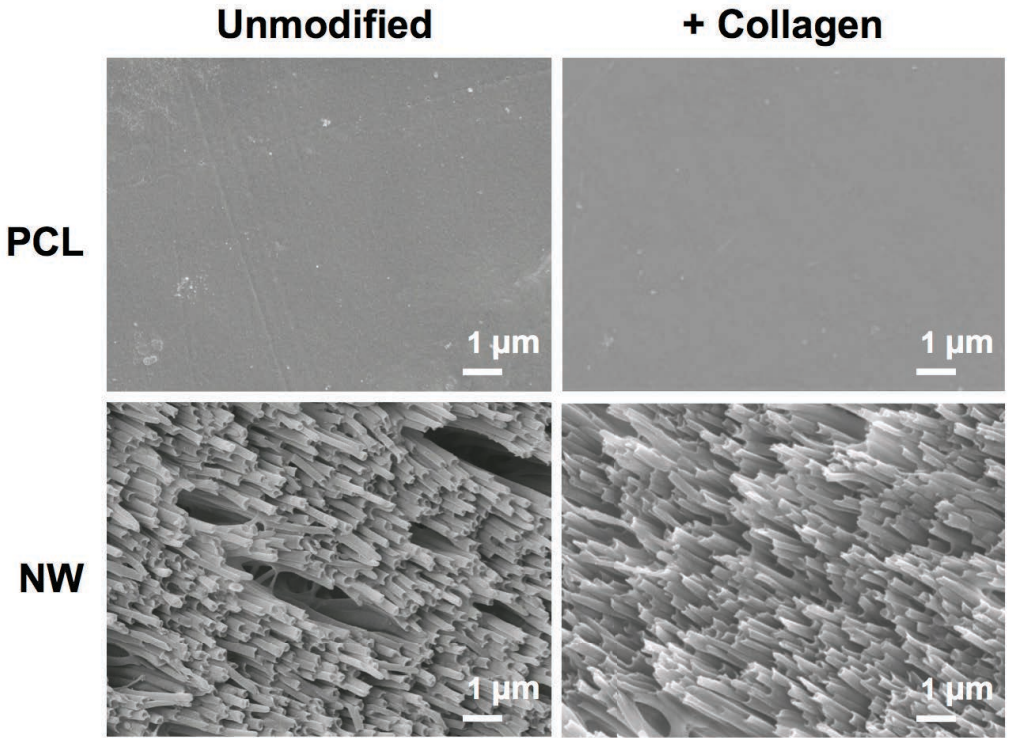

Figure 5.1. Representative SEM images of PCL and NW surfaces before and after collagen immobilization.

5.3.2. Adhesion and Proliferation of SMCs

SMC adhesion and proliferation was evaluated after 1 and 7 days of culture by using 5-Chloromethylfluorescein Diacetate (CMFDA) live stain (Invitrogen), Rhodamine Phalloidin (Cytoskeleton) and 4′,6-diamidino-2-phenylindole dihydrochloride (DAPI) (Invitrogen) nucleus stain, followed by imaging with a fluorescence microscope (**Figure 5.2.**). At day 1, it is evident that cells adhered on NW, cPCL and cNW surfaces have an elongated phenotype compared to PCL surfaces. SMCs on NW, cPCL and cNW also exhibit multiple cellular extensions interacting with the surfaces as well as with surrounding cells. After 7 days of culture there are more cells covering and interacting on both cPCL and cNW surfaces as compared to PCL and NW surfaces. It is important to note that the cells on the nanostructured surfaces (NW and cNW) seem to be aligning and more spindle-shaped compared to the flat surfaces (PCL and cPCL).

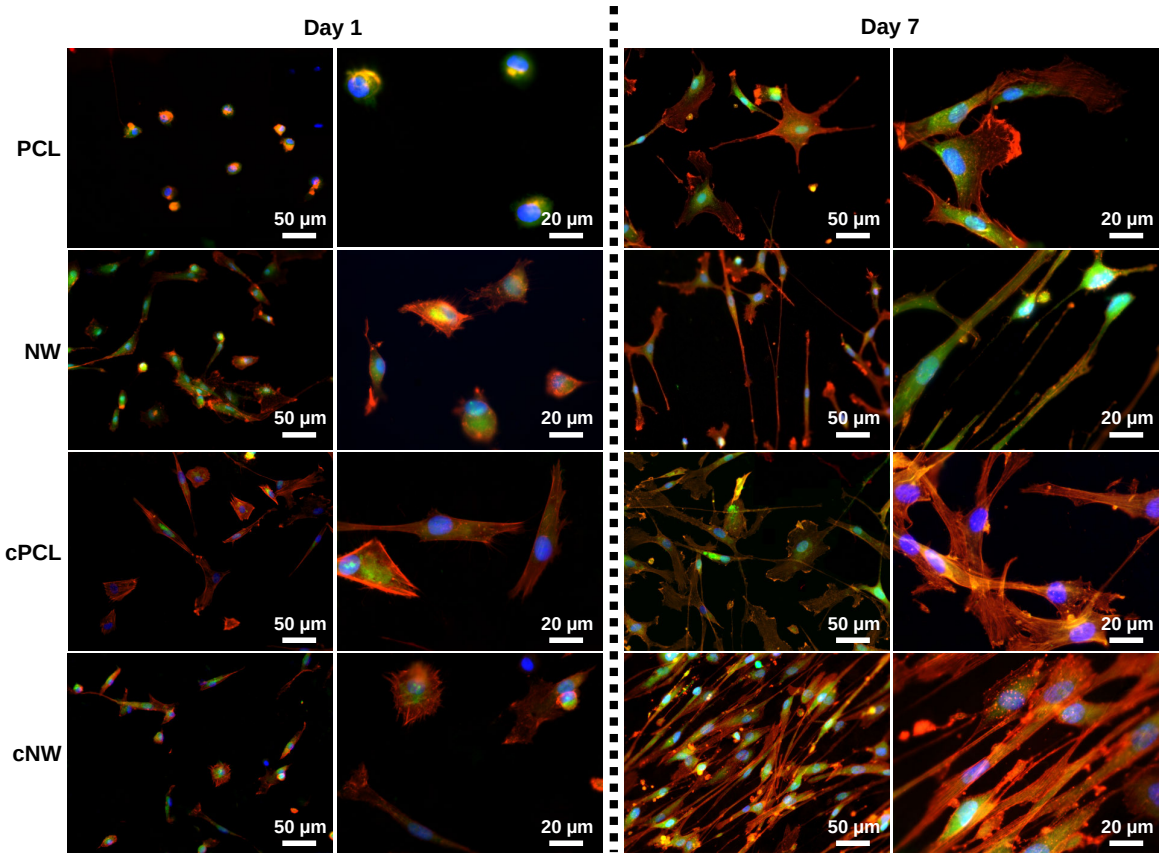

Figure 5.2. Representative fluorescence microscopy images of SMCs stained with CMFDA (green), Rhodamine Phalloidin (red) and DAPI (blue) on PCL, NW, cPCL and cNW surfaces. Experiments were replicated on at least three different samples with at least three different cell populations (n_{min} = 9).

SMC adhesion was quantified by counting the number of DAPI stained nuclei on fluorescence microscopy images using ImageJ software. The results indicate that after 1 day in culture SMC adhesion on PCL surfaces is statistically similar to that on cPCL surfaces, however adhesion on PCL surfaces is significantly lower than that on NW and cNW surfaces (**Figure 5.3.**). After 7 days of culture, NW, cPCL and cNW surfaces exhibit higher cellular adhesion as compared to PCL surfaces. There is also a significant increase in cellular adhesion on cNW

surfaces from day 1 to 7. This may be due to the enhanced energy of these surfaces compared to PCL surface. Higher surface energy is known to promote cell adhesion. Further, collagen immobilized unto these surfaces presents more cell binding motifs for cells to adhere to. In natural tissue cells are surrounded with ECM, therefore cells will interact with a biomaterial in a comparable way if it contains similar binding sites to that of the natural ECM [29]. Collagen has been known to increase cellular anchorage to substrates via the $ß_1$ integrin family of extracellular matrix receptors [30, 31]. Cellular adhesion plays a large role in cellular communication and regulation, indicating that collagen immobilized surfaces may serve as an excellent substrate for the adhesion of SMCs. The nanostructured and collagen immobilized surfaces promote initial cellular adhesion, and hence there are more cells on these surfaces. By introducing nanoarchitecture as well as a cell binding motif it is apparent that more cells are adhering, indicating that mimicking the natural-like hierarchy of tissue and providing ECM components are important in anchoring SMCs.

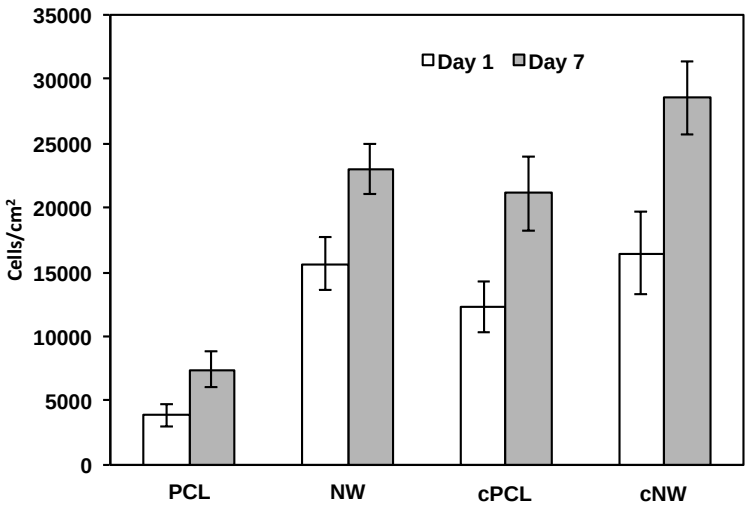

Figure 5.3. Cell counts on different surfaces after 1and 7 days of culture. Cell nuclei stained with DAPI were quantified using ImageJ software. Experiments were replicated on at least three different samples with at least three different cell populations (n_{min} = 9). Statistical significance

was calculated using a one-way ANOVA with Tukey's *post hoc* test. After 1 day in culture, the cellular adhesion of SMCs on PCL surfaces is significantly lower than the adhesion on NW and cNW surfaces, whereas there is no significant difference between cellular adhesion on cPCL, NW and cNW surfaces. After 7 days in culture, the cPCL, NW and cNW surfaces exhibit significantly higher cellular adhesion than PCL surfaces, whereas, there is no significant difference between cellular adhesion on the cPCL, NW and cNW surfaces. Error bars represent the standard error.

5.3.2. SMC elongation on different surfaces

SMCs adhered onto different surfaces after 1 and 7 days of culture with evident boundaries were examined using ImageJ software to acquire an approximation for cellular elongation. Cellular elongation was calculated as the aspect ratio of cellular length to cellular width, outputting an elongation [*E*] parameter. Results indicate that cNW surfaces exhibit a more elongated morphology after 1 and 7 days of culture compared to PCL surfaces at the same time points **Figure 5.4(A).** SMCs also exhibited significantly more elongation on cNW surfaces after 7 days of culture as compared to those after 1 day of culture. Contractile SMCs are more elongated and spindle-shaped cells, whereas synthetic SMCs have a cobblestone morphology also known as epithelioid. Thus a higher *E* value is associated with a contractile phenotype. The large error in average *E* value is attributed to the vast distribution of cellular elongation on the surfaces. Therefore, a histogram of cellular *E* values on the different surfaces was constructed in order to see the distribution of cellular shapes **Figure 5.4.(C, D)**. After 1 day in culture, the histogram indicates that the majority of cells on PCL surfaces have an *E* value between 1 and 2. SMCs on NW and cPCL surfaces have a large distribution of cell shapes with peaks being

between *E* values of 3 and 4. Cells on cNW surfaces, which contain both nanoarchitecture as well as cell binding motifs, have the largest number of elongated cells (*E* values greater than 10). Further, after 7 days of culture NW and cNW surfaces are the only surfaces which adhere SMCs with an *E* value greater than 20.

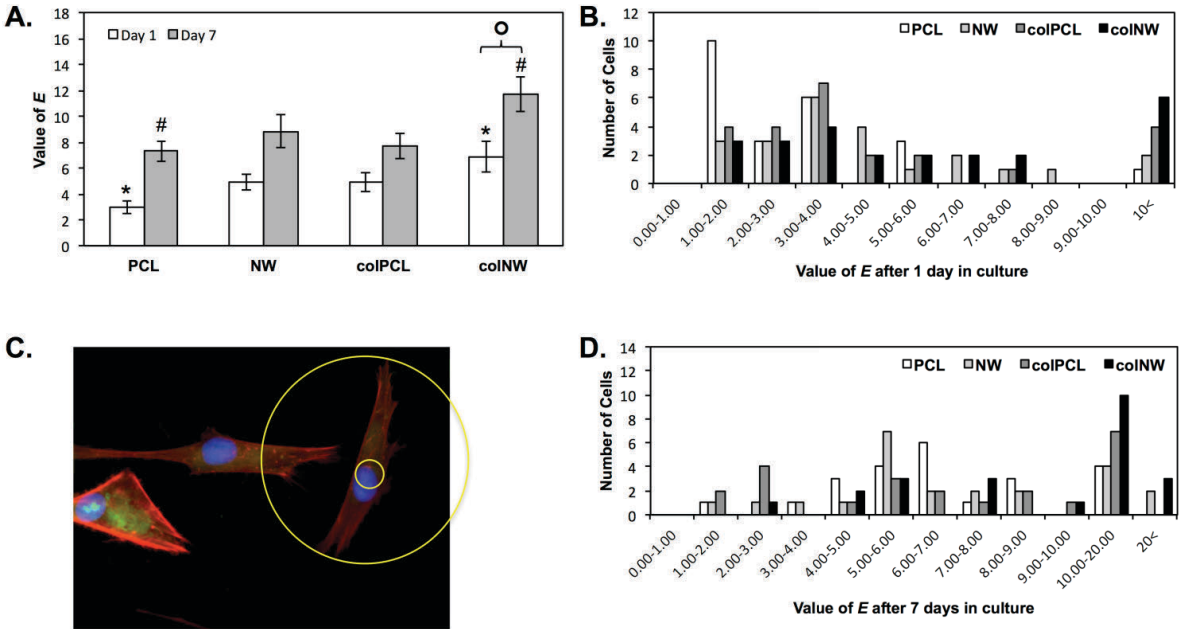

Figure 5.4. (**A**) Elongation (*E*) approximations of cells on different surfaces after 1 and 7 days of culture. Experiments were replicated on at least three different samples with at least three different cell populations (n_{min} = 9). Statistical significance was calculated using a one-way ANOVA with Tukey's *post hoc* test. Results indicate that colNW surfaces exhibit a more elongated morphology after 1 and 7 days of culture compared to PCL surfaces at the same time points (*****, #, $p < 0.05$). SMCs also become significantly more elongated on cNW surfaces after 7 days of culture compared to those in culture for 1 day on cNW surfaces (¢, $p < 0.05$). Error bars represent the standard error; (**B**) The image shows how *E* approximations were calculated (outer diameter/inner diameter); A histogram

of *E* approximations of cells on different surfaces after (**C**) 1 day in culture and (**D**) 7 days in culture.

5.3.3. Viability of SMCs on surfaces

The cell viability was characterized using a commercially available Methylthiazol Tetrazolium (MTT) assay kit (Sigma) after days 1 and 7 in culture. This assay is dependent on NAD(P)H-dependent oxidoreductase enzymes located in the cytosolic compartment of cells, which reduce the tetrazolium dye [32, 33]. Therefore, this assay can be used to measure the loss of viable cells or the cytostatic activity of cells. Results indicate after 1 day in culture SMCs on cNW surfaces have significantly lower MTT reduction rates than PCL, NW and cPCL surfaces (**Figure 5.5.**). After 7 days in culture, SMCs have significantly higher MTT reduction rates on cPCL>(PCL>NW>cNW). Studies have shown that proliferation of smooth muscle cells is significantly reduced on nanopatterned surfaces [21]. Rapidly dividing cells demonstrate high rates of MTT reduction, while differentiated cells exhibit low rates of MTT reduction. This can be seen in the lower values of MTT reduction of SMCs on NW and cNW surfaces compared to both PCL and cPCL surfaces. Despite significantly higher number of cells on cNW surfaces after day 7 of culture as compared to PCL, NW and cPCL surfaces, the cells on cNW surfaces are significantly more elongated than the other surfaces, indicating that they may have differentiated phenotype. Contractile SMCs in adult blood vessels proliferate at an extremely low rate and exhibit low synthetic activity so despite the fact that there are more cells on cNW surfaces; these cells may be in a quiescent state.

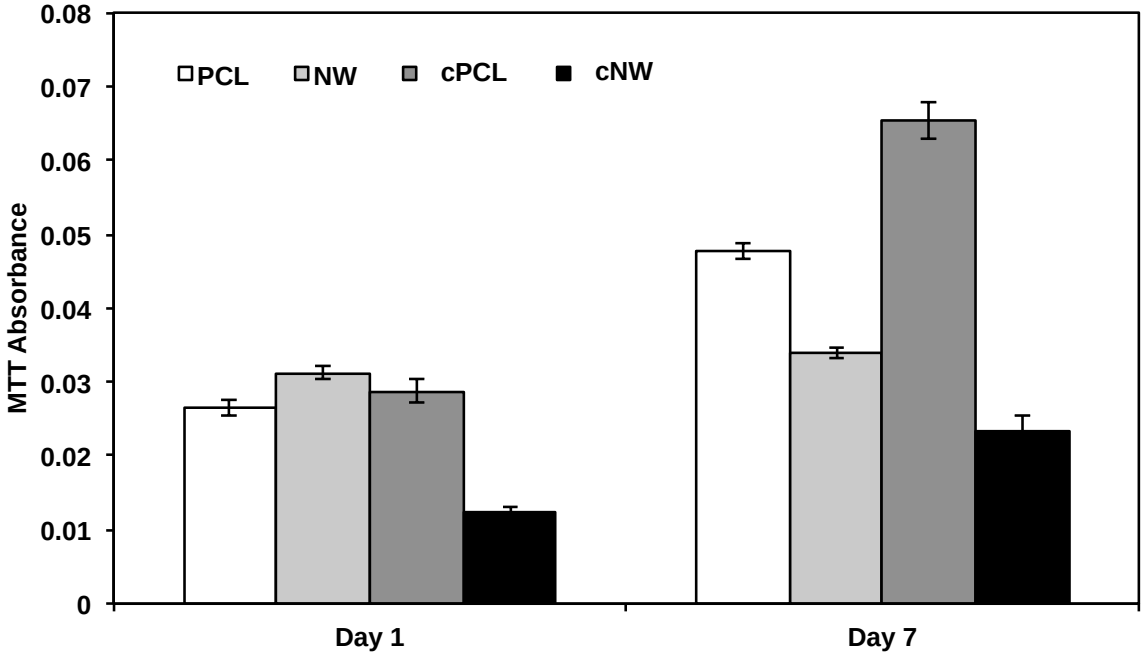

Figure 5.5. Cell viability measured using the MTT assay for SMCs on different surfaces. Experiments were replicated on at least three different samples with at least three different cell populations (n_{min} = 9). Statistical significance was calculated using a one-way ANOVA with Tukey's *post hoc* test. Results indicate after 1 day in culture that SMCs on the cNW surfaces have significantly lower MTT reduction than the PCL, NW and cPCL surfaces, whereas, there is no significant difference between the PCL, NW and cPCL surfaces. After 7 days in culture, SMCs have a significantly higher MTT reduction on cPCL than the PCL, NW and cNW surfaces. Further, there were significant differences between PCL, NW and cNW surfaces (PCL > NW > cNW). Error bars represent the standard error.

5.3.4. SMC Morphology on different surfaces

SMC morphology was investigated using SEM imaging to visualize the cellular interaction with the surface nanoarchitecture. The nanoscale surface topography of materials has

been shown to be significant in interactions with biological systems such as proteins and cells [34]. Results indicate that there is a clear interaction between SMC's filopodia and the nanofeatures present on both NW and cNW surfaces as well as with the collagen immobilized surfaces (cPCL and cNW) (**Figure 5.6**). After 1 day in culture it is evident that there are SMCs present on PCL and cPCL surfaces with a round morphology, as opposed to SMCs adhered on to NW and cNW surfaces. Further, confirming fluorescent imaging results, it is apparent that SMCs on NW and cNW surfaces seem to be more elongated than those on PCL and cPCL surfaces after 1 and 7 days of culture. After 7 days in culture SMCs on PCL and cPCL surfaces are no longer round, but are still not nearly as elongated as SMCs on NW and cNW surfaces. SMCs do not seem to interact as well with PCL surfaces when compared to NW, cPCL and cNW surfaces as evident by the clear lack of filopodia. This may be due to the lack of nano-architecture and cell binding motifs.

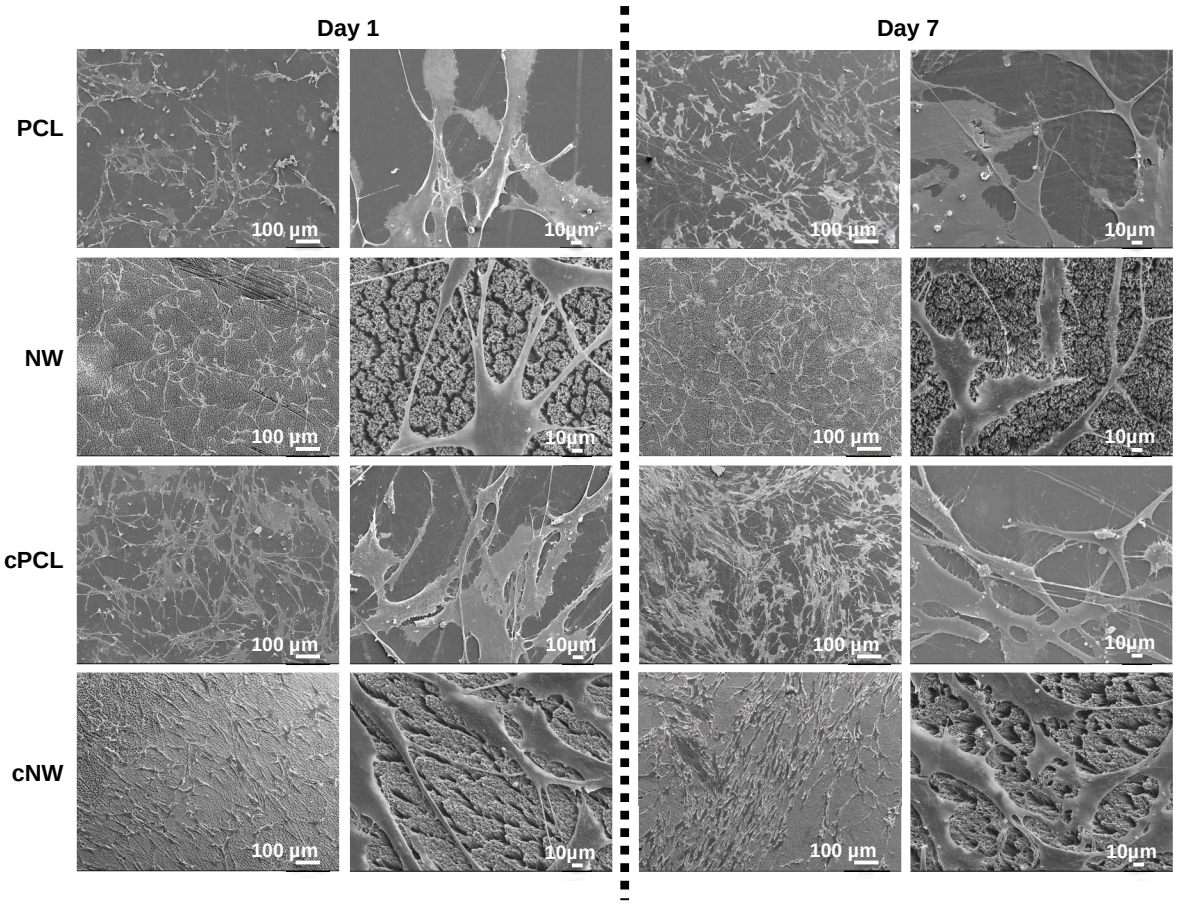

Figure 5.6. Representative SEM images of SMCs after 1 and 7 days of culture on different surfaces. Note: the surfaces were coated with a 10 nm layer of gold and imaged at 7 keV. Experiments were replicated on at least three different samples with at least three different cell populations ($n_{min} = 9$).

5.3.5. Differentiation of SMCs on different surfaces

Expression of SMC contractile proteins is essential to healthy vasculature as cardiovascular diseases are characterized by the transition of SMC phenotype from contractile to synthetic. During differentiation of SMCs, caldesmon, smooth muscle myosin heavy chain, calponin, SM22, α- and ß-tropomyosins, and αl integrin genes are transcriptionally regulated. However, in differentiated SMCs transcription of these genes is upregulated in differentiated

SMCs, and downregulated in dedifferentiated SMCs [35]. Down-regulation of SMC lineage markers has been shown to be associated with calcification [36]. Therefore, differentiation of SMCs on surfaces was investigated by detecting CAL and MYH expression both through blotting techniques after 7, 14 and 21 days in culture and with immunofluorescence after 21 days in culture and western. CAL and MYH are specific to smooth muscle cells and are expressed only when smooth muscles cells differentiate into a mature phenotype. CAL is a calcium binding protein, located in the thin filaments of smooth muscle. It is present at a stoichiometry of 1 mol calponin/7 mol actin [37]. MYH is involved in contraction and is a highly specific marker for the SMC lineage. The expression of MYH has never been found in cells other than SMCs in vivo, and MYH is the only marker protein that is also SMC specific during embryogenesis [38].

A western blotting technique was used to partially quantify the presence of MYH and CAL on the surfaces. The MYH and CAL expressions were normalized to α–tubulin expression. After 7 days in culture, differentiation was investigated without supplying the cells with differentiation media. Results reveal that the cells are beginning to differentiate on all surfaces. CAL (**Figure 5.7.A**) and MYH (**Figure 5.7.B**) expression is significantly higher on NW surfaces compared to PCL, cPCL and cNW surfaces, while cNW surfaces express significantly higher amounts of CAL and MYH compared to PCL and cPCL surfaces. This indicates that cells are significantly more differentiated on nanostructured surfaces at day 7, explaining why MTT results were significantly lower on these surfaces. It is important to note that the bands for day 7 are larger than for days 14 and 21 because more protein lysate was loaded after 7 days in culture, compared to after 14 and 21 days in culture. However, all bands were normalized to α-tubulin expression to account for this. After 14 days in culture (7 days after providing differentiation media), CAL expression is significantly higher on cNW surfaces compared to PCL and NW

surfaces. Both collagen immobilized surfaces (cPCL and cNW) express significantly more MYH than PCL and NW surfaces, while PCL surfaces expressing significantly more MYH than NW surfaces. After 21 days in culture CAL and MYH expression is elevated significantly on cPCL and cNW surfaces compared to PCL and NW surfaces. These results are in agreement with a study that found collagen type I, type IV and laminin promoted the contractile/differentiated phenotype in SMCs [16].

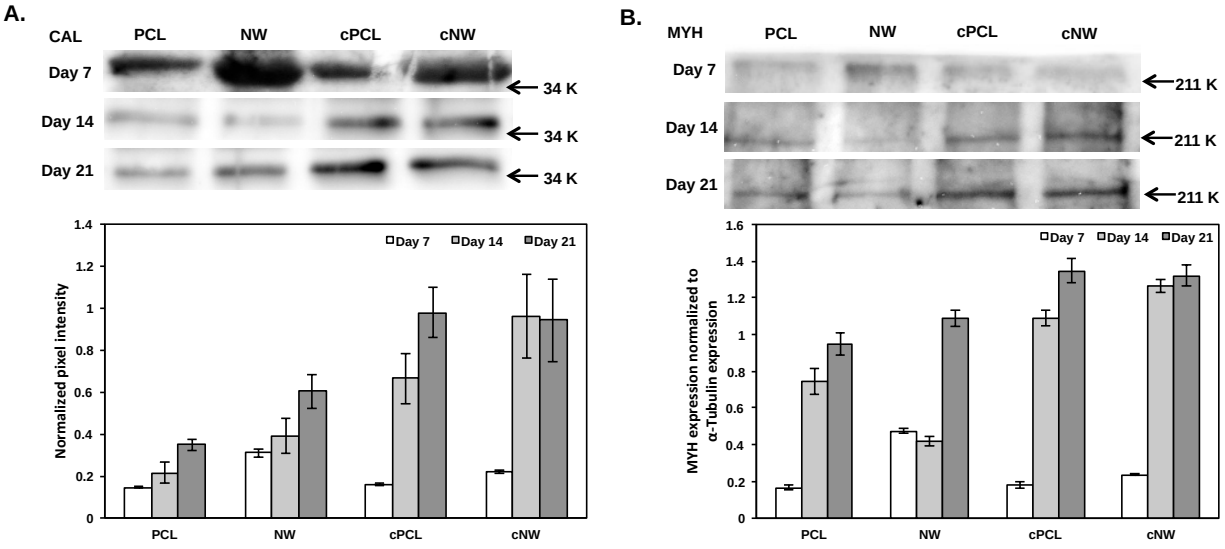

Figure 5.7. Western blot analysis of the expression of (A) CAL and (B) MYH on different surfaces after 7, 14 and 21 days in culture. Experiments were replicated with western blots with at least three different cell populations (n_{min} = 9). After 7 days in culture NW and cNW express significantly more amounts of CAL and MYH compared to PCL and cPCL surfaces, while NW surfaces express CAL and MYH significantly more than cNW. After 14 days in culture, CAL expression is significantly higher on cNW surfaces compared to PCL and NW surfaces. After 14 days in culture, both collagen immobilized surfaces (cPCL and cNW) express significantly more MYH than PCL and NW surfaces, while PCL surfaces expressing significantly more MYH than

NW surfaces. After 21 days in culture CAL and MYH expression is elevated significantly on cPCL and cNW surfaces compared to PCL and NW surfaces.

Immunofluorescence was done after 21 days in culture. Results of immunofluorescence indicate that cells on all surfaces are expressing both CAL (**Figure 5.8.A**) and MYH (**Figure 5.8.B**). It is important to note that even with differentiation media the SMCs are proliferating on all surfaces but more so on PCL surfaces. Further, SMCs on all surfaces exhibit an elongated spindle-shaped morphology.

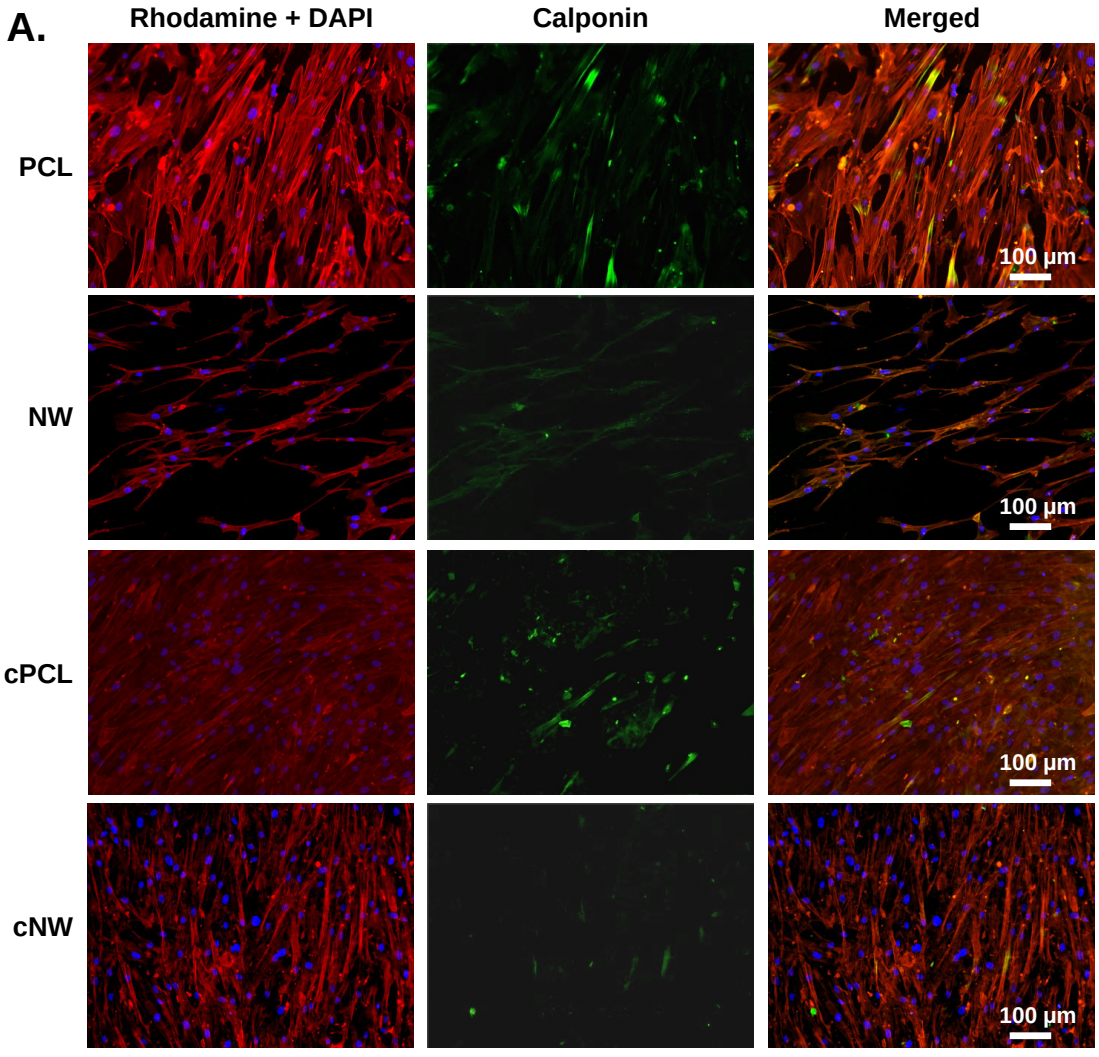

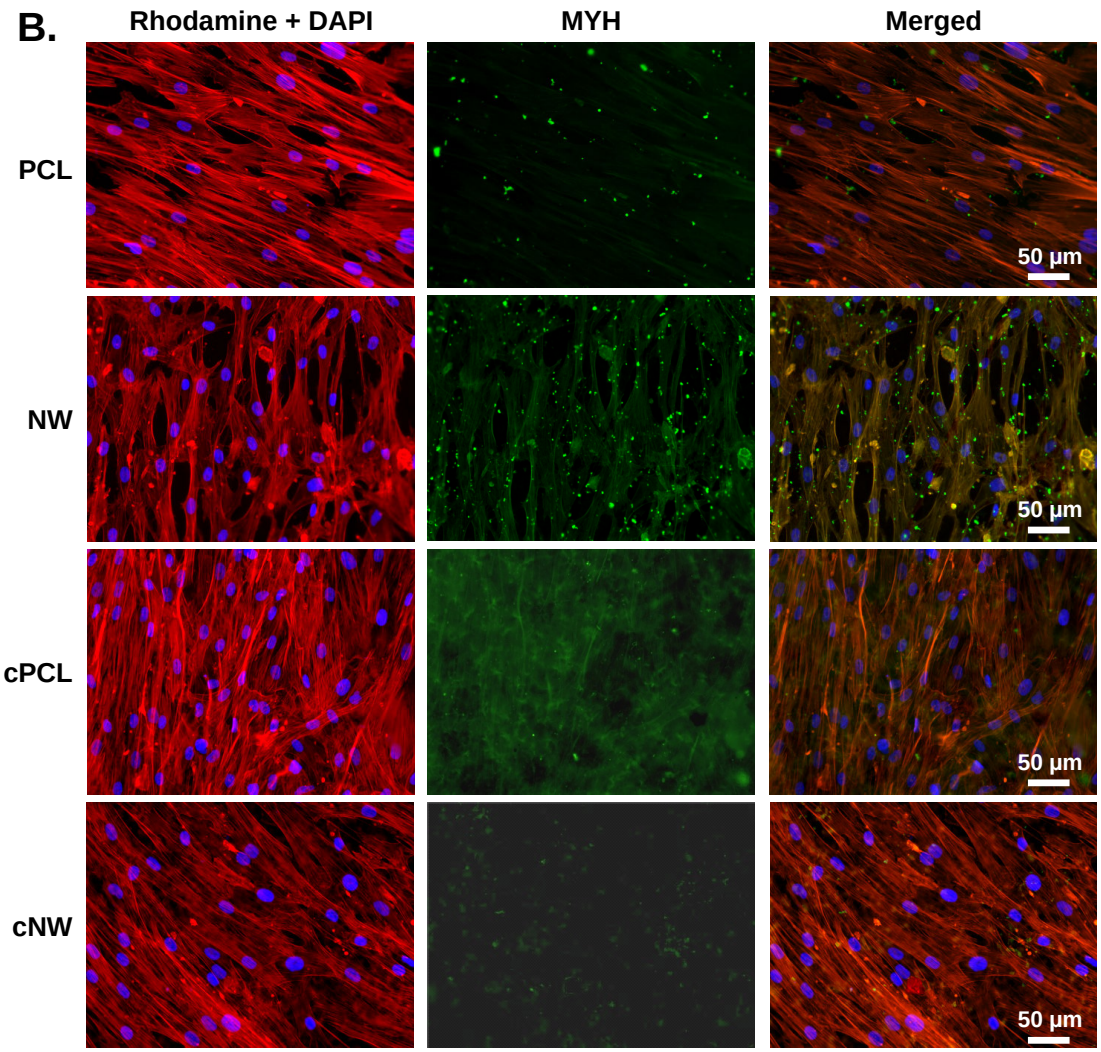

Figure 5.8. Representative fluorescence microscopy images of SMCs immunostained with (A) CAL and (B) MYH. Experiments were replicated on at least three different samples with at least three different cell populations (n_{min} = 9).

5.4. Conclusions

Inhibition of unnecessary vascular SMC proliferation and preservation of a differentiated state in SMCs are important aspects in the management and avoidance of vascular diseases. The level of cell functionality on biomaterial surfaces is also correlated to the characteristics of the surface and its ability to mimic properties similar to that of extracellular matrix. Therefore,

providing SMCs with nanotopography and cell-binding motifs such as collagen may affect the cell adhesion, viability, morphology and differentiation. In this study, SMCs exhibited increased adhesion on NW, cPCL and cNW surfaces, however SMCs on nanostructured surfaces seemed to be more elongated than those on PCL surfaces. SEM results also revealed considerable amounts of filopodia interacting with surfaces and neighboring cells on NW, cPCL and cNW surfaces, but this interaction is lacking on PCL surfaces. The reduction of MTT was higher on flat surfaces (PCL and cPCL), indicating a higher rate of proliferation. This suggests that SMCs on nanostructured surfaces (NW and cNW) may be in a more differentiated state and slowly dividing. This was confirmed by a significant increase in differentiation markers (CAL and MYH) on these surfaces after 7 days in culture without providing cells with differentiation cues. After giving the cells differentiation media, SMCs on all surfaces become spindle shaped. However the expression of endogenous proteins, CAL and MYH, specific to a contractile SMC phenotype is up-regulated on collagen immobilized surfaces (cPCL and cNW). These results suggest that nanotopography affects cell proliferation as well as cell elongation, while collagen immobilized surfaces greatly affect cell differentiation with proper differentiation cues.

REFERENCES

[1] Owens GK, Kumar MS, Wamhoff BR. Molecular regulation of vascular smooth muscle cell differentiation in development and disease. Physiological reviews. 2004;84:767-801.

[2] Alexander MR, Owens GK. Epigenetic control of smooth muscle cell differentiation and phenotypic switching in vascular development and disease. Annual review of physiology. 2012;74:13-40.

[3] Halayko AJ, Solway J. Molecular mechanisms of phenotypic plasticity in smooth muscle cells. 1985) 2001.90:358-68.

[4] Owens GK. Molecular control of vascular smooth muscle cell differentiation and phenotypic plasticity. Novartis Foundation symposium. 2007;283:174-91; discussion 91-3, 238-41.

[5] Johnson JL, van Eys GJ, Angelini GD, George SJ. Injury induces dedifferentiation of smooth muscle cells and increased matrix-degrading metalloproteinase activity in human saphenous vein. Arteriosclerosis, thrombosis, and vascular biology. 2001;21:1146-51.

[6] Doevendans PA, van Eys G. Smooth muscle cells on the move: the battle for actin. Cardiovascular research. 2002;54:499-502.

[7] Hehrlein C, Gollan C, Dönges K, Metz J, Riessen R, Fehsenfeld P, et al. Low-Dose Radioactive Endovascular Stents Prevent Smooth Muscle Cell Proliferation and Neointimal Hyperplasia in Rabbits. Circulation. 1995;92:1570-5.

[8] Rensen SS, Doevendans PA, van Eys GJ. Regulation and characteristics of vascular smooth muscle cell phenotypic diversity. Netherlands heart journal : monthly journal of the Netherlands Society of Cardiology and the Netherlands Heart Foundation. 2007;15:100-8.

[9] Owens GK. Regulation of differentiation of vascular smooth muscle cells. Physiological reviews. 1995;75:487-517.

[10] Chamley-Campbell JH, Campbell GR, Ross R. Phenotype-dependent response of cultured aortic smooth muscle to serum mitogens. The Journal of Cell Biology. 1981;89:379-83.

[11] Bentzon JF, Weile C, Sondergaard CS, Hindkjaer J, Kassem M, Falk E. Smooth muscle cells in atherosclerosis originate from the local vessel wall and not circulating progenitor cells in ApoE knockout mice. Arteriosclerosis, thrombosis, and vascular biology. 2006;26:2696-702.

[12] Costa MA, Simon DI. Molecular basis of restenosis and drug-eluting stents. Circulation. 2005;111:2257-73.

[13] Mao X, Peng H, Ling J, Friis T, Whittaker AK, Crawford R, et al. Enhanced human bone marrow stromal cell affinity for modified poly(l-lactide) surfaces by the upregulation of adhesion molecular genes. Biomaterials. 2009;30:6903-11.

[14] Marcovich R, Seifman B, Beduschi R, Wolf JS. Surface modification to improve in vitro attachment and proliferation of human urinary tract cells. BJU international. 2003;92:636-40.

[15] Bisson I, Kosinski M, Ruault S, Gupta B, Hilborn J, Wurm F, et al. Acrylic acid grafting and collagen immobilization on poly(ethylene terephthalate) surfaces for adherence and growth of human bladder smooth muscle cells. Biomaterials. 2002;23:3149-58.

[16] Glukhova M, Koteliansky V, Fondacci C, Marotte F, Rappaport L. Laminin variants and integrin laminin receptors in developing and adult human smooth muscle. Developmental biology. 1993;157:437-47.

[17] Yim EK, Reano RM, Pang SW, Yee AF, Chen CS, Leong KW. Nanopattern-induced changes in morphology and motility of smooth muscle cells. Biomaterials. 2005;26:5405-13.

[18] Nivison-Smith L, Weiss AS. Alignment of human vascular smooth muscle cells on parallel electrospun synthetic elastin fibers. Journal of Biomedical Materials Research Part A. 2012;100A:155-61.

[19] Choudhary S, Haberstroh KM, Webster TJ. Enhanced functions of vascular cells on nanostructured Ti for improved stent applications. Tissue engineering. 2007;13:1421-30.

[20] Choudhary S, Berhe M, Haberstroh KM, Webster TJ. Increased endothelial and vascular smooth muscle cell adhesion on nanostructured titanium and CoCrMo. International journal of nanomedicine. 2006;1:41-9.

[21] Yim EKF, Reano RM, Pang SW, Yee AF, Chen CS, Leong KW. Nanopattern-induced changes in morphology and motility of smooth muscle cells. Biomaterials. 2005;26:5405-13.

[22] Wulf K, Teske M, Lobler M, Luderer F, Schmitz KP, Sternberg K. Surface functionalization of poly(epsilon-caprolactone) improves its biocompatibility as scaffold material for bioartificial vessel prostheses. Journal of biomedical materials research Part B, Applied biomaterials. 2011;98:89-100.

[23] Williamson MR, Woollard KJ, Griffiths HR, Coombes AG. Gravity spun polycaprolactone fibers for applications in vascular tissue engineering: proliferation and function of human vascular endothelial cells. Tissue engineering. 2006;12:45-51.

[24] Sarkar S, Lee GY, Wong JY, Desai TA. Development and characterization of a porous micro-patterned scaffold for vascular tissue engineering applications. Biomaterials. 2006;27:4775-82.

[25] Leszczak V, Smith BS, Popat KC. Hemocompatibility of polymeric nanostructured surfaces. Journal of Biomaterials Science, Polymer Edition. 2013:1-20.

[26] Bechara SL, Judson A, Popat KC. Template synthesized poly(ε-caprolactone) nanowire surfaces for neural tissue engineering. Biomaterials. 2010;31:3492-501.

[27] Porter JR, Henson A, Ryan S, Popat KC. Biocompatibility and mesenchymal stem cell response to poly(epsilon-caprolactone) nanowire surfaces for orthopedic tissue engineering. Tissue Eng Part A. 2009;15:2547-59. doi: 10.1089/ten.tea.2008.0476.

[28] Andersson A-S, Bäckhed F, von Euler A, Richter-Dahlfors A, Sutherland D, Kasemo B. Nanoscale features influence epithelial cell morphology and cytokine production. Biomaterials. 2003;24:3427-36.

[29] Solouk A, Mirzadeh H, Shokrgozar MA, Solati-Hashjin M, Najarian S, Seifalian AM. The study of collagen immobilization on a novel nanocomposite to enhance cell adhesion and growth. Iranian biomedical journal. 2011;15:6-14.

[30] Clyman RI, McDonald KA, Kramer RH. Integrin receptors on aortic smooth muscle cells mediate adhesion to fibronectin, laminin, and collagen. Circulation Research. 1990;67:175-86.

[31] He W, Ma Z, Yong T, Teo WE, Ramakrishna S. Fabrication of collagen-coated biodegradable polymer nanofiber mesh and its potential for endothelial cells growth. Biomaterials. 2005;26:7606-15.

[32] Berridge MV, Herst PM, Tan AS. Tetrazolium dyes as tools in cell biology: new insights into their cellular reduction. Biotechnology annual review. 2005;11:127-52.

[33] Berridge MV, Tan AS. Characterization of the Cellular Reduction of 3-(4,5-dimethylthiazol-2-yl)-2,5-diphenyltetrazolium bromide (MTT): Subcellular Localization, Substrate Dependence, and Involvement of Mitochondrial Electron Transport in MTT Reduction. Archives of Biochemistry and Biophysics. 1993;303:474-82.

[34] Lord MS, Foss M, Besenbacher F. Influence of nanoscale surface topography on protein adsorption and cellular response. Nano Today. 2010;5:66-78.

[35] Sobue K, Hayashi Ki, Nishida W. Expressional regulation of smooth muscle cell-specific genes in association with phenotypic modulation. Mol Cell Biochem. 1999;190:105-18.

[36] Steitz SA, Speer MY, Curinga G, Yang HY, Haynes P, Aebersold R, et al. Smooth muscle cell phenotypic transition associated with calcification: upregulation of Cbfa1 and downregulation of smooth muscle lineage markers. Circulation research. 2001;89:1147-54.

[37] Winder SJ, Walsh MP. Calponin: thin filament-linked regulation of smooth muscle contraction. Cellular signalling. 1993;5:677-86.

[38] Miano JM, Cserjesi P, Ligon KL, Periasamy M, Olson EN. Smooth muscle myosin heavy chain exclusively marks the smooth muscle lineage during mouse embryogenesis. Circulation research. 1994;75:803-12.

CHAPTER 6

ALTERED HEMOCOMPATIBILITY ON POLYCAPROLACTONE NANOWIRE SURFACES

6.1. Introduction

There are a multitude of polymeric materials such as ultra-high molecular weight polyethylene [1], polyether ether ketone [2], and polycaprolactone [3], currently utilized in several blood-contacting implantable medical devices such as tissue grafts [4-6], coronary and vascular stents [7], and orthopedic implants [8]. Despite how often these devices are used to treat tissue or organ failure, all these materials suffer from undesirable blood-material interactions. The thrombogenic nature of the material surface can cause serious complications in patients such as acute or chronic inflammation, fibrosis, infection and/or thrombosis [9, 10], ultimately leading to implant failure [11]. Further, almost all short and long term implanted medical devices that come in contact with blood require a considerable amount of anticoagulation treatment which comes with a high risk and a high cost to the patient [12]. Current research is focused on understanding the interaction of the blood and its components with material surfaces as well as developing surfaces that have towards favorable interactions with blood and its components [13-15]. The ability to regulate immune reactions on a material surface is vital for the success of any implantable biomedical device and also determines its hemocompatibility. To this day, there is no truly hemocompatible surface [12]. All blood-contacting materials have shown to initiate an immunological response. Thus, improving the material surface compatibility with blood and its components could eliminate the need for intervention post-implantation.

When blood comes in contact with a material surface, an intricate series of highly inter-connected events, such as platelet and leukocyte adhesion/activation and stimulation of complement and coagulation cascades, are initiated and controlled by the surface properties [16]. Key blood serum proteins, such as fibrinogen, adsorb and undergo conformational changes on the surface, thus mediating these events. Proteins can adsorb on the surface in different quantities, densities, conformations, and orientations, depending on the chemical and physical characteristics of the surface [17]. The layer of adsorbed proteins influences the adhesion and activation of platelets and leukocytes. Activated platelets express proteins such as Platelet Factor-4 (PF-4) and P-selectin, which in turn recruits leukocytes on the surface, facilitating the formation of platelet/leukocyte complexes. This further stimulates two pathways, better known as the intrinsic pathway (contact activation) and the extrinsic pathway (tissue factor), which may lead to thrombosis and/or a fibrous capsule. Both pathways involve activation of zymogens, eventually converging on a common pathway leading to clot development via formation of thrombin and fibrin [18]. Further, red blood cells may also get lysed when in contact with the surface, releasing adenosine diphosphate (ADP) which additionally promotes platelet aggregation on the material surface [19]. Thus, it is critical to evaluate and understand these events on material surfaces.

There are a variety of biochemical and topographical cues present naturally within human tissues that have favorable interactions with blood. Biomimetic surfaces have elicited promising cellular responses via biomolecular recognition, which can easily be regulated with changes to design parameters of the material surface [20]. Enhanced cellular response to polymers surfaces modified with ECM components, such as collagen I are well documented. Collagen I is the main component in the ECM of blood vessels as well as other tissues in the body, making it an

attractive molecule to modify the material surface. Studies with biofunctionalized collagen scaffolds have shown enhanced proliferation and differentiation of neural precursor cells [21], improved bioactivity for bone engineering [22, 23] and increased endothelial cell organization and cell survival [24]. However, not much is known about the hemocompatibility of collagen immobilized surfaces [25, 26]. Further, cells in vivo are constantly interacting with their surroundings that are composed of cues at a micrometer and nanometer level [27, 28]. Thus, by mimicking this environment *in vitro,* cell interaction with the surface can be controlled [29-32]. Nanostructured material surfaces have shown to elicit appropriate cellular interactions with the biomaterial surface such as promotion of an osteoblast phenotype [33, 34], adhesion and alignment of smooth cells [35, 36] and enhanced filopodia interactions with the environment [37]. Despite all these studies that suggest a correlation between nanoscale surface features and cell functionality, there is a limited amount of information in literature about the hemocompatibility of nanostructured surfaces [38, 39].

In this study, we have evaluated the ability of collagen-immobilized nanostructured surfaces as interfaces for blood-contacting materials. Nanowire surfaces were fabricated from polycaprolactone using a nanotemplating technique. Polycaprolactone is used in a multitude of FDA approved implants, drug delivery devices, sutures as well as adhesion barriers [40, 41]. Previous studies have shown that polycaprolactone nanowire surfaces have favorable hemocompatible properties and improve cellular functionality [38]. The nanowire surfaces were also immobilized with collagen, a protein abundantly found in the extracellular matrix of all tissues. Studies have shown enhanced cellular response to these surfaces. Thus, in this study, the effect of the collagen immobilization on nanowire surfaces to blood and its components was investigated to better understand their effects on hemocompatibility. Fibrinogen binding from

blood plasma to the surfaces after 2 hours was investigated using an ELISA. The functionality of platelets and leukocytes were investigated on surfaces after 2 hours of contact with whole blood plasma using a cell cytotoxicity assay, fluorescence microscopy and scanning electron microscopy (SEM). PF-4 release from activated platelets, SC5b-9 and thrombin anti-thrombin complexes were quantified using ELISA. Contact activation was characterized via chromogenic analysis to determine the amount of kallikrein deposited on the surfaces. Further, a hemolytic assay was used to determine erythrocyte lysis. This work provides an in depth look at the hemocompatibility of collagen immobilized nanowire surfaces that can lead to further development of these surfaces for blood-contacting implantable devices.

6.2. Materials and Methods

6.2.1. Fabrication of nanostructured surfaces

Surfaces were fabricated and characterized as described in detail in section 2.2.1 and 2.2.2. The nanowire surface architecture was examined for uniformity and repeatability using SEM imaging.

6.2.2. Plasma isolation from whole blood and incubation on different surfaces

Whole blood from a healthy individual was drawn into standard 10 ml ethylenediaminetetraacetic acid (EDTA) coated vacuum tubes using venipuncture by a phlebotomist. To account for the platelet plug and locally activated platelets resulting from the needle insertion, the first tube was discarded. The blood vials were centrifuged at 300 g for 15 min to separate the plasma from the erythrocytes. The plasma was then pooled into fresh tubes and allowed to sit for 15 min prior to being used. The surfaces were incubated with 1 ml of

pooled plasma in a 24-well plate at 37 °C and 5 % CO_2 on a horizontal shaker plate (100 rpm) for 2 hrs.

6.2.3. Cytotoxicity Assay

The material cytotoxicity was characterized using a commercially available lactate dehydrogenase (LDH) cytotoxicity assay kit (Cayman Chemical). The protocol provided by the manufacturer was followed. In brief, the plasma-incubated surfaces were shaken on a horizontal shaker plate (1000 rpm) for 5 min at room temperature. The surface-exposed plasma samples as well as the standards were transferred to a 96 well plate. A reaction solution consisting of 96% v/v assay buffer, 1% v/v NAD+1%, v/v Lactic Acid, 1% v/v INT, and 1% v/v LDH Diaphorase was added in equivalent amounts (1:1) to all standards and samples. This solution was incubated with gentle shaking on horizontal shaker plate (100 rpm) for 30 min at room temperature. After the incubation, the absorbance of the solution was immediately measured at a wavelength of 490 nm to determine the cytotoxic effects of the different surfaces.

6.2.4. Fibrinogen binding from plasma on different surfaces

Fibrinogen binding from plasma on different surfaces was investigated using an enzyme-linked immunoassay (ELISA, GenWay). The protocol provided by the manufacturer was followed. In brief, diluted surface-exposed plasma samples (1:200 in assay diluent) and human fibrinogen antigen standards were transferred into a microassay well plate and incubated for 60 mins at room temperature. The samples were removed and the wells were washed (4x) with the wash buffer and were incubated with enzyme antibody conjugate for 30 min at room temperature without exposure to light. The samples were removed and the wells were washed (4x) with the

wash buffer and were incubated with tetramethyl benzidine buffer (TMB) solution for 10 mins at room temperature in a dark environment. The reaction was stopped with stop solution and the optical density was immediately measured using a spectrophotometer at 450 nm.

6.2.5. Platelet/leukocyte adhesion on different surfaces

Cellular adhesion on different surfaces was investigated by fluorescence microscopy imaging using rhodamine phalloidin cytoskeleton stain and 4'6-diamidino-2-phenylindole-dihydrochloride (DAPI). The un-adhered cells were removed by aspirating the plasma from the surfaces followed by gently rinsing (2x) with PBS. The surfaces were then transferred to a new 24-well plate. Cells that adhered to the surfaces were fixed in 3.7 wt % formaldehyde in PBS for 15 min at room temperature and washed (3x, 5 min each) in PBS. The cell membranes were permeabilized using 1 % Triton-X in PBS at room temperature for 3 min. The surfaces were then transferred to a new 24-well plate and incubated with 500 µl of rhodamine phalloidin solution in PBS for 25 min at room temperature. After 25 min, 0.2 µg/ml DAPI stain was added to each well. Following 5 min incubation, the solution was aspirated, surfaces were rinsed with PBS and then imaged using a fluorescence microscope (Zeiss). Adherent leukocytes on 50x images were counted. All images were processed using ImageJ Software.

6.2.6. Platelet/leukocyte morphology on different surfaces

The platelet-leukocyte morphology and interaction with the surfaces was investigated using SEM imaging. The un-adhered cells were removed by aspirating the plasma from the surfaces followed by gently rinsing (2x) with PBS. The surfaces were then transferred to a glass petri-dish and the platelets and leukocytes that adhered were fixed by incubation in a solution of

primary fixative (6 % gluteraldehyde (Sigma), 0.1 M sodium cacodylate (Polysciences), and 0.1 M sucrose (Sigma)) for 45 min. The surfaces were then transferred to a secondary fixative (primary fixative without gluteraldehyde) for 10 min. The surfaces were then placed in consecutive solutions of ethanol (35 %, 50 %, 70 % and 100 %) for 10 min each. For further dehydration, surfaces were placed into a solution of hexamethyldisilazane (HMDS, Sigma) for 10 min. The surfaces were then air-dried and stored in a desiccator until further imaging by SEM. Prior to imaging, the substrates were coated with a 10 nm layer of gold and imaged at 7 kV.

6.2.7. Platelet/leukocyte detection on different surfaces by immunofluorescence and western blotting

Immunofluorescence staining and a western blotting technique were used to determine the cellular expression of proteins exclusive to platelets and leukocytes. The un-adhered cells were removed by aspirating the plasma from the surfaces followed by gently rinsing (2x) with PBS. The surfaces were then transferred to a new 24-well plate and adherent cells were fixed in 3.7 wt% formaldehyde in PBS for 15 min at room temperature and washed (3x 5 min) in PBS. The cell membranes were permeabilized using 1 % Triton-X in PBS at room temperature for 3 min, followed by washing with PBS (3x, 5mins each). The surfaces were then incubated in a blocking solution (10 % BSA in PBS) for 30 min at room temperature. The surfaces were washed (3x, 5 mins each) in PBS and incubated in primary antibodies specific to platelets and leukocytes, P-Selectin and CD45 respectively (dilution 1:50, Santa Cruz Biotechnology) in a solution of 2 % BSA in PBS for 1 hr at room temperature. The surfaces were placed in new 24-well plates then washed (3x, 5 min each) in PBS, and incubated with fluorescently-labeled

secondary antibodies, donkey anti-goat conjugated with Texas Red (for P-Selectin) and chicken anti-mouse conjugated with FITC (for CD45) (dilution 1:100, Santa Cruz Biotechnology) in a solution of 2 % BSA in PBS for 1 hr at room temperature. The surfaces were washed (3x, 5 mins each) in PBS and imaged with a fluorescence microscope (Zeiss). All images were processed using ImageJ Software.

Western blotting was performed to partially quantify the expression of P-Selectin and CD-45. Briefly, the cells adhered on surfaces after 2 hrs of incubation in whole blood plasma were homogenized in RIPA lysis buffer (10.0 mM Tris pH 7.4, 100.0 mM NaCl, 5.0 mM EDTA, 5.0 mM EGTA, 1.0% Deoxycholate, 0.1% SDS, 1.0% Triton X-100) containing protease inhibitor cocktail. The lysate protein content was determined by micro-BCA assay. The lysate was heated to 95 °C for 10 mins in sample buffer (62.5 mM Tris-HCl pH 6.8, 10.0 % glycerol, 5.0 % β-mercaptoethanol, 2.0% SDS, 0.025 % Bromophenol blue) in order to denature the proteins prior to gel loading. 20 μg of total extract protein was electrophoresed through 8 % Tris-SDS gels and transferred to PVDF membranes in 7.5 % methanol. Blots were blocked for 1 hr at room temperature in 10 % BSA solution. Primary monoclonal antibodies for P-selectin and CD-45 were diluted 1:500 in 3% BSA in PBS-tween solution and incubated overnight at 4 °C. The blots were then washed with PBS-tween solution (3x, 5 mins) before they were incubated with goat anti-mouse or donkey anti-goat horseradish peroxidase (HRP) conjugated secondary antibodies (Santa Cruz Biotechnology) at a dilution of 1:5000 for 1 hr at room temperature. The blots were then washed with PBS-tween solution (3x, 5 mins) followed by protein detection using chemiluminescence (WestPico Chemiluminescent Substrate, Pierce). The blots were imaged using an Alpha Innotech Fluorchem gel documentation system, and band intensities were analyzed using ImageJ software.

6.2.8. PF-4 Expression on different surfaces

PF-4 expression was measuresd using a commercially available enzyme linked immunosorbant assay kit (ELISA, RayBio) to evaluate platelet activation on different surfaces. The protocol provided by the manufacturer was followed. In brief, diluted substrate-exposed plasma samples (1:200 in assay diluent) and PF-4 standards were transferred into a microassay well plate and incubated for 2.5 hrs on a horizontal shaker plate (100 rpm) at room temperature. The wells were washed (4x) with wash buffer, and incubated with biotinylated antibody for 1 hr on a horizontal shaker plate (100 rpm) at room temperature. The wells were then washed (4x) to remove unbound biotinylated antibody. This was followed by incubating the wells with a horseradish peroxidase (HRP)-streptavidin solution (1:25,000 in assay diluent) and incubated for 45 mins on a horizontal shaker plate (100 rpm) at room temperature. Wells were then washed (4x) with the wash buffer. The TMB solution was then immediately added to each well and incubated for 30 mins on a horizontal shaker plate (100 rpm) at room temperature with no exposure to light. The reaction was stopped with a stop solution and the optical density of the resulting solution was measured immediately thereafter at 450 nm to determine the amount of PF-4 released by platelets on each of the substrates.

6.2.9. Contact activation on different surfaces

In order to investigate contact activation on different surfaces, the degree of plasma kallikrein expression (Chromogenix) present on surface-exposed plasma was evaluated with an acid stop method. The protocol provided by the manufacturer was followed. In brief, the surface-exposed plasma samples were diluted 10 fold in Tris Buffer (pH 7.8). 100 µl of each diluted surface-exposed plasma sample was placed in a 96-well plate and incubated at 37 °C and 5

%CO_2 for 3-4 mins. 100 µl of pre-warmed (37 °C) substrate solution was added to all the samples and incubated at 37 °C and 5 %CO_2 for 10 mins. The reaction was stopped by 100 µl of 20 % acetic acid to all samples. Plasma blanks were prepared by adding reagents in reverse order, without incubation. The optical density of samples was measured at 405 nm using a spectrophotometer to determine the degree of contact activation on the different surfaces.

6.2.10. Complement activation on different surfaces

Complement activation was evaluated on different surfaces using an enzyme immunoassay (EIA, Quidel Corporation) to evaluate SC5b-9 complement activation. The protocol provided by the manufacturer was followed. In brief, microassay wells were rehydrated by incubating in a wash solution for 2 mins at room temperature. Wash solution was aspirated and 100 µl of diluted surface-exposed plasma samples (1:10 in assay diluent), standards and controls were transferred into microassay wells and incubated for 60 mins at room temperature. The wells were washed (5x) with wash buffer and incubated in SC5b-9 plus conjugate for 30 mins at room temperature. Wells were then washed (5x) with wash buffer, followed by incubation in TMB solution for 15 mins at room temperature without exposure to light. The reaction was stopped with stop solution and optical density was measured at 450 nm with a spectrophotometer to determine the amount of SC5b-9 complement activation present on the different surfaces.

6.2.11. Thrombin anti-thrombin (TAT) complex formation on different surfaces

Thrombin anti-thrombin (TAT) concentration was measured using a thrombin anti-thrombin human ELISA kit (HaemoScan). The protocol provided by the manufacturer was

followed. In brief a Nunc Maxisorp 96-well microtiter plate was coated with capture antibody in coating buffer overnight at 2-8 °C. The plate was washed (3x) with PBS-Tween wash buffer. 100 µl of surface-exposed diluted plasma samples (1:200) along with standards were placed into the wells and incubated for 1 hr at room temperature. The wells were washed (3x) before 100 µl of detection antibody solution was added and incubated at room temperature for 1 hr. The wells were washed (3x) and 100 µl of substrate solution was added. After 20 mins the reaction was stopped with 50 µl of stop solution and optical density was read at 450 nm with a spectrophotometer.

4.2.12. Thrombin generation on different surfaces

The rate of thrombin generation on different surfaces was calculated using a thrombin generation assay (TGA) (HaemoScan). The protocol supplied by the manufacturer was followed. In brief, all surfaces were incubated in 350 µl diluted TGA plasma for 15 mins. 175 µl of a prepared mixture of TGA reagent A and TGA reagent B was added to each vial. After 1 min, 10 µl of this mixture was placed into a vial containing 490 µl buffer B. Vials were immediately placed back in the water bath after sampling. This was repeated after 2 min, 4 min, and 6 min for each sample and reference material. 150 µl of samples from each surface and standards were placed into a 96-well plate and incubated for 2 min at 37 °C and 5 %CO_2. 50 µl of diluted substrate solution was added to each well and the covered well plate was incubated for 20 min at 37 °C and 5 %CO_2. 50 µl of stop solution was added to each well and optical density was read immediately at 405 nm, using 540 nm as a reference wavelength. Thrombin generation rate was calculated by determining the highest velocity between the two measured time points and correcting for the dilution factor (50x).

6.2.13. Hemolytic activity on different surfaces

Hemolytic activity of different surfaces was investigated using a biomaterial hemolytic assay (HaemoScan). The protocol supplied by the manufacturer was followed. In brief, cleaned surfaces along with reference materials were placed in syringes. One syringe without material was used as a negative control. An erythrocyte suspension (500 µl) was added to each syringe with specimen (test material, reference material or negative control). Air was removed and parafilm was used to close the outlet. Vials were incubated at 37 °C for 24 hrs while subjected to end-over end rotating. The erythrocyte suspension was carefully transferred to a centrifuge tube (1.5 mL) followed by centrifugation at high speed (3600g) for 1 min. 20 µL of supernatant from each sample or standard was placed into a 96-well plate along with 180 µL of assay buffer. The 96-well plate was mixed on a shaker plate before measuring optical density at 415nm.

6.2.14. Statistical Analysis

Each qualitative experiment was performed on at least three different surfaces with at least three different whole blood plasma populations ($n_{min} = 9$). All ELISA and EIA experiments were done on five surfaces. Further, all of the quantitative results were evaluated using one-way analysis of variance (ANOVA) with a Tukey's post-hoc test. Statistical significance was considered at $p < 0.05$.

6.3. Results and Discussion

To this day, there is no truly hemocompatible surface that has appropriately interacts with blood and its components [12]. All blood-contacting materials continue to induce unfavorable responses to whole blood and its components, such as protein adsorption, platelet and leukocyte

adhesion/activation and stimulation of complement and coagulation cascades. These complications can potentially lead to implant failure and can limit the long-term success of blood-contacting devices. Thus, in this study we have evaluated the effect of collagen immobilization to nanowire surfaces on blood and its components to better understand their effects on hemocompatibility. Improving the material surface compatibility with blood and its components could eliminate the need for intervention post-implantation.

6.2.1. Fabrication and characterization of PCL NW and NF surfaces

Surfaces were fabricated and characterized as described in detail in section 2.2.1 and 2.2.2. The nanowire surface architecture was examined for uniformity and repeatability using SEM imaging (**Figure 6.1.**).

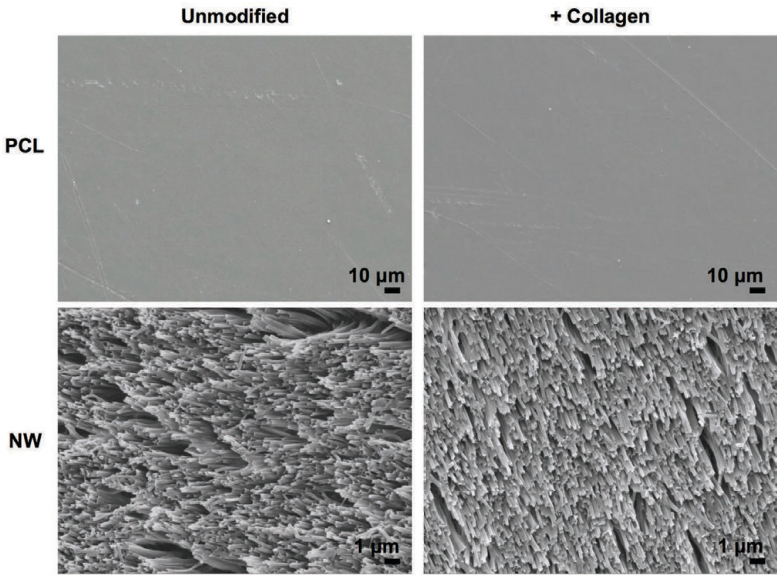

Figure 6.1. Representative SEM images of unmodified and collagen-immobilized PCL and NW surfaces. Results indicate similar nanostructured features before and after collagen immobilization.

6.3.2. Cytotoxicity Assay

The material cytotoxicity was investigated after 2 hours of incubation in whole blood plasma using a commercially available lactate dehydrogenase (LDH) assay kit. LDH is a soluble enzyme located inside the cytoplasm of cells that is released upon loss of membrane integrity due to apoptosis or necrosis. Thus this enzyme acts as a good marker of cell membrane integrity and can be used to evaluate the cytotoxic effects of the surfaces in this study. This assay measures the amount of formazan following a two-step reaction, where first LDH catalyzes NAD+ to NADH and H+ by oxidation and a subsequent reaction by diaphorase converts the tetrazolium salt to a colored formazan. Formazan absorbs strongly at 490-520 nm, therefore the amount of LDH released can be determined using a spectrophotometer. These measurements indicate the level of cytotoxicity. The results indicate all the surfaces demonstrate a comparable cytotoxicity on platelets/leukocytes (**Figure 6.2**). Thus, none of the surfaces progress short-term cytotoxic effects on the components of whole blood plasma. It is well known that polycaprolactone is nontoxic and is also approved by the FDA for use in several implantable devices [42]. The results here indicate that topographical and biomolecular modifications to polycaprolactone does not significantly alter the cytotoxicity of resulting surfaces.

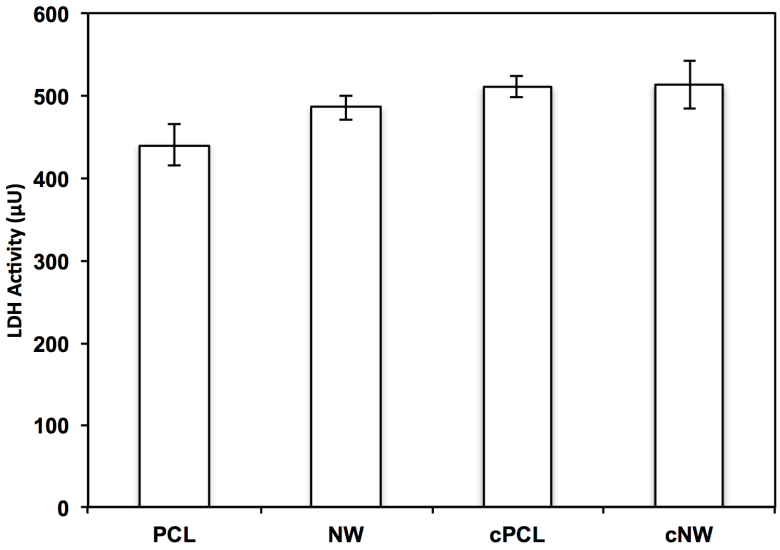

Figure 6.2. Cell cytotoxicity measured using an LDH Assay on different surfaces after 2 hours of incubation in whole blood plasma. The results indicate no significant difference in LDH activity on all the surfaces. Experiments were replicated with at least three different cell populations on at least three different samples ($n_{min} = 9$). Error bars represent standard error.

6.3.3. Fibrinogen binding from plasma on different surfaces

Fibrinogen, produced by the liver, is present in blood plasma at a concentration of 200-400 mg/dL. Fibrinogen has two roles in the blood clotting cascade. It yields monomers that can polymerize into fibrin and is a cofactor in platelet aggregation. Prothrombin initiates the coagulation cascade when it is proteolytically cleaved to form thrombin. Thrombin then acts as a serine protease, which converts fibrinogen into fibrin. Under normal conditions, polymeric fibrin fibers form a thrombus network, also known as a blood clot. This clot can be characterized by the strength of the fibrin network that captures many components of blood. In order to evaluate the pro-coagulant activity, fibrinogen binding from blood plasma on different surfaces was evaluated after 2 hours of incubation using commercially available human fibrinogen antigen

assay. The plasma exposed to different surfaces was assayed to determine the amount of fibrinogen that was not bound on the material surface. The results indicate a significantly higher concentration of fibrinogen in the NW and cNW exposed whole blood plasma compare to that of PCL exposed whole blood plasma (**Figure 6.3.**). This indicates significantly lower amount of fibrinogen binding on NW and cNW surfaces compared to PCL surfaces. Fibrinogen includes both hydrophobic and hydrophilic regions, giving it amphiphilic properties [43]. This allows it to bind on to a plethora of surfaces. However, blood plasma proteins have a higher affinity for binding unto uncharged hydrophobic surfaces as opposed to hydrophilic surfaces [44, 45]. PCL surfaces are significantly more hydrophobic compared to NW and cNW surfaces, thus binding significantly more amount of fibrinogen compared to NW and cNW surfaces. However, the conformation and/or orientation of bound fibrinogen on the material surface plays a major role in determining its biocompatibility as well. It was found that platelet adhesion to biomaterial surfaces increases with increased coverage of fibrinogen only if the bound fibrinogen maintains a conformation so that its functional domain is recognizable by antibody probes [46]. The results from fibrinogen binding indicate that nanostructured surfaces may reduce fibrin clot formation, further promoting material hemocompatibility.

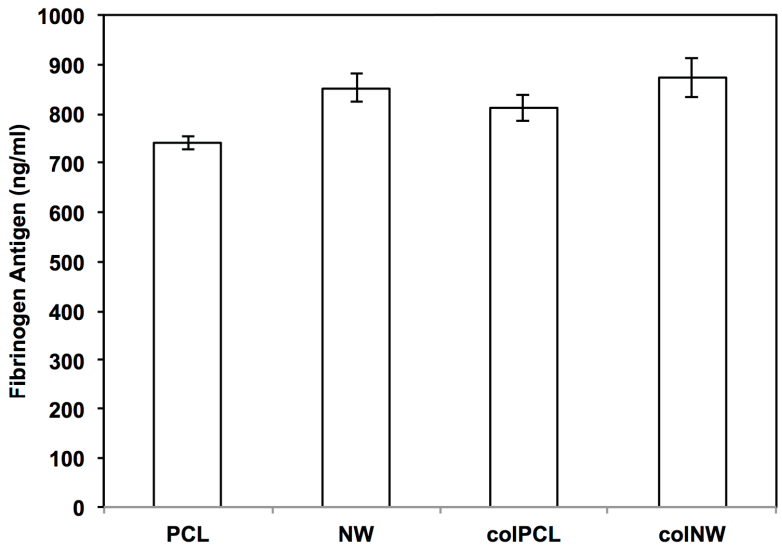

Figure 6.3. Human fibrinogen antigen concentration measured on surfaces after 2 hours of incubation in whole blood plasma. The results indicate a significantly higher concentration of fibrinogen in the NW and cNW exposed whole blood plasma compare to that of PCL exposed whole blood plasma, indicating significantly lower amount of fibrinogen binding on NW and cNW surfaces compared to PCL surfaces. Experiments were replicated with at least three different cell populations on at least three different samples (n_{min} = 9). Error bars represent standard error.

6.3.4. Platelet/leukocyte adhesion on different surfaces

Cellular adhesion on different surfaces was investigated by fluorescence microscope imaging using rhodamine phalloidin cytoskeleton stain and DAPI nucleus stain to identify adherent platelets and leukocytes. Rhodamine phalloidin stained the cytoskeleton of both platelets and leukocytes. However, DAPI stained selectively for leukocytes as platelets are anuclear. The activated platelets can bind to each other as well as interact with leukocytes by

binding to them, producing mixed aggregates. This platelet aggregation can be visualized using fluorescence microscopy. The results indicate lower cell adhesion and minimal platelet aggregation on NW surfaces as compared to PCL, cPCL and cNW surfaces (**Figure 6.4.**). Further, results also indicate higher cell adhesion on PCL surfaces followed by cNW and cPCL surfaces. However, there was minimal platelet aggregation observed on PCL surfaces as compared to cNW and cPCL surfaces. Upon platelet aggregation, micro-platelet membrane particles are released, further promoting plasma coagulation [47]. Thus, the results indicate that NW surfaces may be less likely to promote plasma coagulation due to the lack in platelet aggregation.

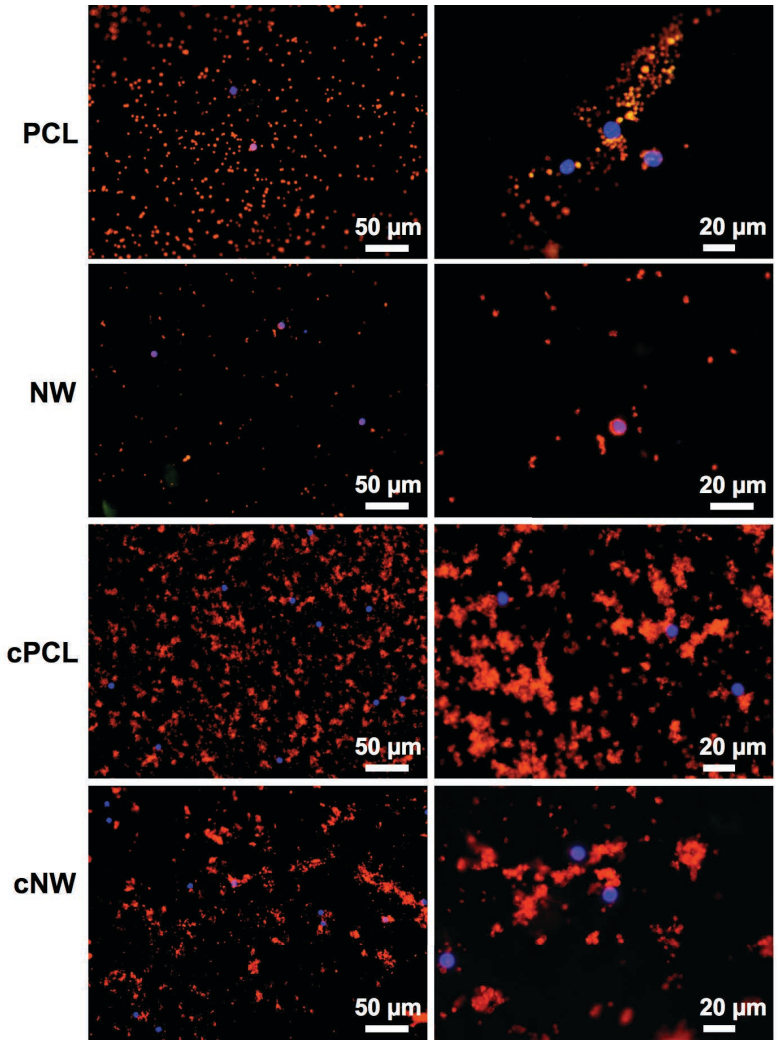

Figure 6.4. Representative fluorescence microscope images of adhered platelets and leukocytes stained with rhodamine-conjugated phalloidin (cytoskeleton) and DAPI (nucleus) on different surfaces after 2 hours of incubation in whole blood plasma. The images indicate a decrease in cell adhesion and platelet aggregation on NW surfaces.

Further, the fluorescence microscopy images were used to calculate the number of adhered leukocytes on different surfaces. The number of platelets could not be calculated due to higher degree of aggregation on the surfaces. The results indicate that there is no significant difference in leukocyte adhesion on the different surfaces (**Figure 6.5.).**

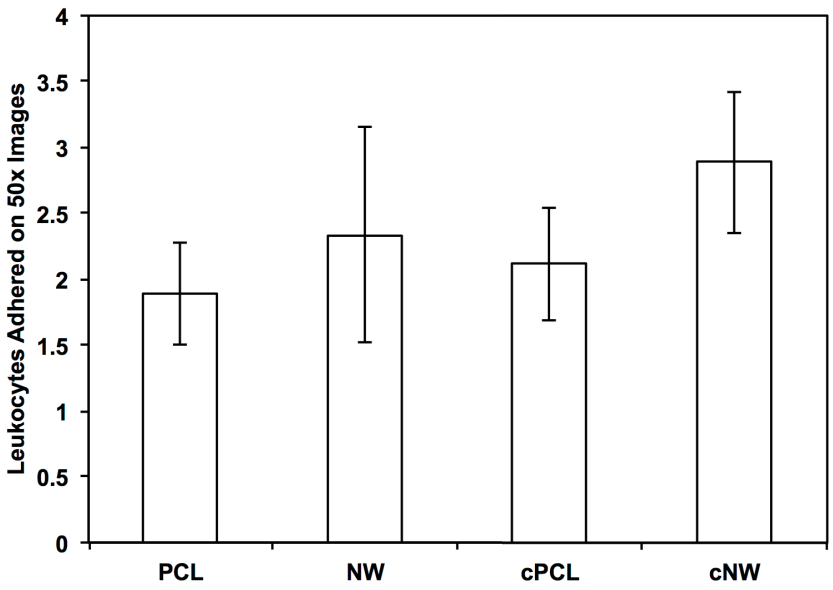

Figure 6.5. Adhered leukocytes after 2 hours of incubation in whole blood plasma on different surfaces. No significant differences in leukocyte adhesion was seen on different surfaces. Experiments were replicated with at least three different cell populations on at least three different samples ($n_{min} = 9$). Error bars represent standard error.

6.3.5. Platelet/leukocyte morphology on different surfaces

Platelet and leukocyte morphology, aggregation and interaction on different surfaces were investigated using SEM imaging. The results indicate a decrease in platelet aggregation on NW surfaces as compared to PCL, cPCL and cNW surfaces (**Figure 6.6.**). High magnification SEM images reveal increased platelet aggregation on cPCL surfaces followed by PCL and cNW surfaces. Further, the SEM images also show no platelet/leukocyte interaction and complex formation on NW followed by minimal platelet/leukocyte interaction and complex formation on cNW surfaces. However, there is increased platelet/leukocyte interaction and complex formation on PCL and cPCL surfaces. Platelet/leukocyte interaction and complex formation appears to

promote activation of platelets as evident by their altered morphology and dendritic extensions on PCL and cPCL surfaces. This platelet/leukocyte interaction is a reliable marker of a prothrombotic state and mixed aggregates are linked to several cardiovascular conditions [48]. Leukocytes may influence coagulation either directly, by producing procoagulant and anticoagulant molecules, or indirectly, by acting on vascular cells such as platelets, endothelial cells, and other leukocytes [49]. Studies have also shown that platelets-leukocyte interaction may also result in increased tissue factor (TF) expression, leading to fibrin deposition [50]. Thus, the results presented here indicate that NW surfaces may be more hemocompatible with lower probability for thrombogenic effects. The results also indicate that cNW surfaces may also reduce thrombogenic effects due to the decrease in platelet/leukocyte interaction and complex formation.

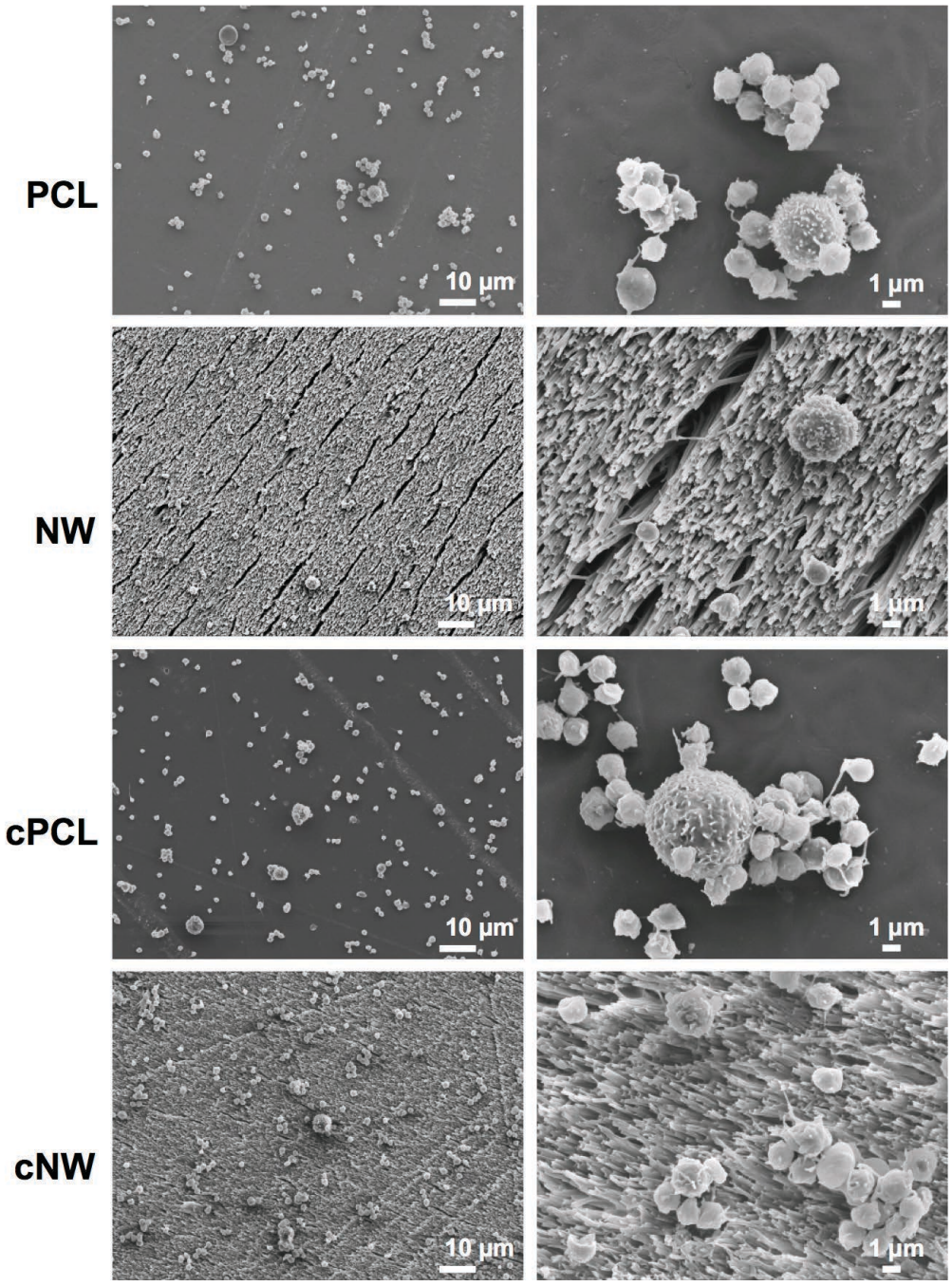

Figure 6.6. Representative SEM images of adhered platelets and leukocytes on different surfaces after 2 hrs of incubation in whole blood plasma. The surfaces were coated with a 10 nm layer of gold and imaged at 5-7 kV. Images show a lower degree of platelet/leukocyte interaction and cellular aggregation on NW surfaces.

6.3.6. Platelet/leukocyte detection on different surfaces by immunofluorescence and western blotting

Platelet/leukocyte interaction and complex formation promotes further activation of platelets and leukocytes, advancing the coagulation cascade. In this study, platelet and leukocyte activation was investigated after 2 hours of incubation in whole blood plasma by immunofluorescence staining and a western blotting technique for specific marker proteins, P-selectin and CD-45, that are known to be expressed in activated platelets and leukocytes respectively. P-selectin expression by platelets plays an essential role in the initial recruitment of leukocytes to the site of inflammation, further promoting fibrin deposition. It then promotes platelet aggregation via platelet-fibrin or platelet-platelet binding. CD-45 is a transmembrane protein present on all human leukocytes and plays a role in signal transduction. CD-45 has found to be not expressed by platelets. The results indicate a decrease in both P-selectin (TR-conjugated) and CD45 (FITC-conjugated) expression on NW and cNW surfaces compared to PCL and cPCL surfaces (**Figure 6.7.(a)**). Further, a western blot technique was used to partially quantify the expression of P-selectin and CD45 on the surfaces. The results confirm the immunofluorescence images indicating a significant increase in P-Selectin and CD-45 expression on cPCL surfaces compared to PCL, NW and cNW surfaces (**Figure 6.7.(b)**). P-Selectin expression was also significantly higher on PCL surfaces compared to NW and cNW surfaces. Leukocytes adhere to the surface of an implanted biomaterial following platelet adhesion and activation in order to defend the body against foreign materials and this recruitment of leukocytes can cause further thrombogenic effects. Upon activation, leukocytes release granules, allowing them to easily adhere to collagen. Thus, increased adhesion and activation of platelets results in increased P-selectin expression on PCL and cPCL surfaces, which further promotes

more leukocyte recruitment resulting in increased CD45 expression. Further, the cPCL surfaces provide signals to leukocytes, which further promotes their adherence.

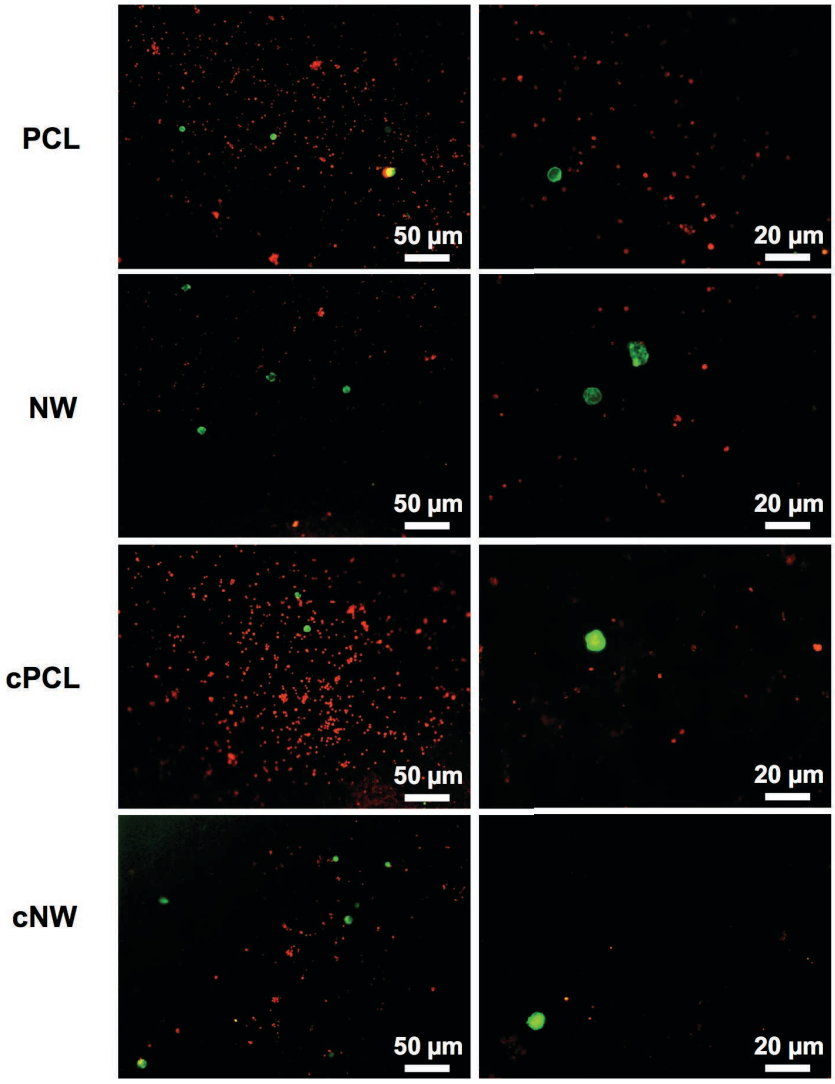

Figure 6.7.(a). Representative fluorescence microscope images of platelets immunostained for P-Selectin and leukocytes immunostained for CD45 on different surfaces after 2 hours of incubation in whole blood plasma. The images indicate a considerable reduction in P- Selectin (TR-conjugated) and CD45 (FITC-conjugated) expression on NW and cNW surfaces compared to PCL and cPCL surfaces.

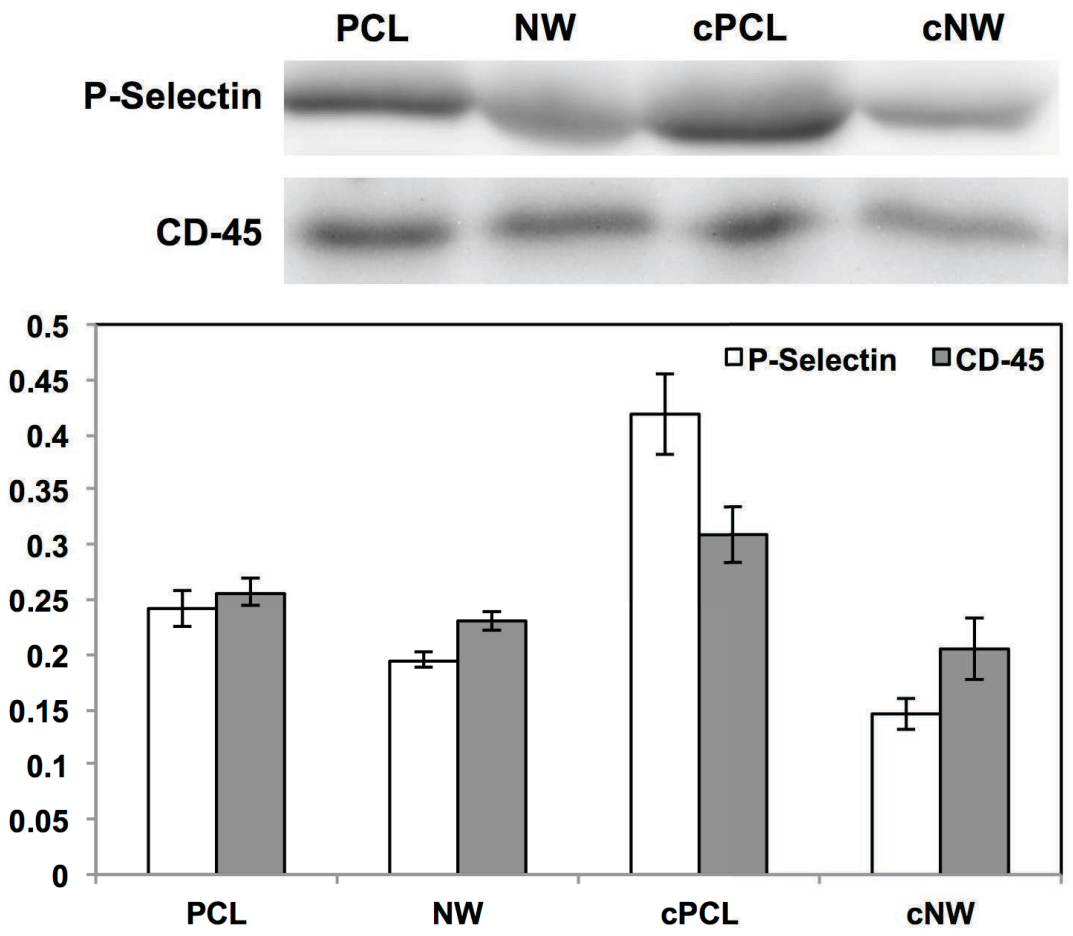

Figure 6.7.(b). Western blot analysis of P-Selectin and CD-45 expression on different surfaces after 2 hours of incubation in whole blood plasma. Results indicate significant increase in P-Selectin and CD-45 expression on cPCL surfaces compared to PCL, NW and cNW surfaces. P-Selectin expression was also significantly higher on PCL surfaces compared to NW and cNW surfaces. Experiments were replicated with at least three different cell populations on at least three different samples ($n_{min} = 9$). Error bars represent standard error.

6.3.7. PF-4 Expression on different surfaces

To further quantify platelet activation, the amount of PF-4 present in surface-exposed plasma samples was investigated. PF-4 is released from alpha-granules in activated platelets

during aggregation in a platelet release reaction. PF-4 is therefore an excellent indicator of platelet activation. A human PF-4 ELISA was used to quantify the amount of PF-4 released by activated platelets after 2 hours of incubation in whole blood plasma. The results indicate a significant increase in PF-4 expression on cPCL surfaces compared to NW and cNW surfaces, and a significant decrease in PF-4 expression on NW surfaces compared to PCL and cPCL surfaces (**Figure 6.8.**). Platelet activation and release of biomolecules such as PF-4 from activated platelets is influenced by the presence and interaction of leukocytes with platelets [10]. Further, the lower release of PF-4 from platelets after being exposed to NW and cNW surfaces may be due to the decrease in platelet/leukocyte interaction and complex formation (**Figure 6.6.**).

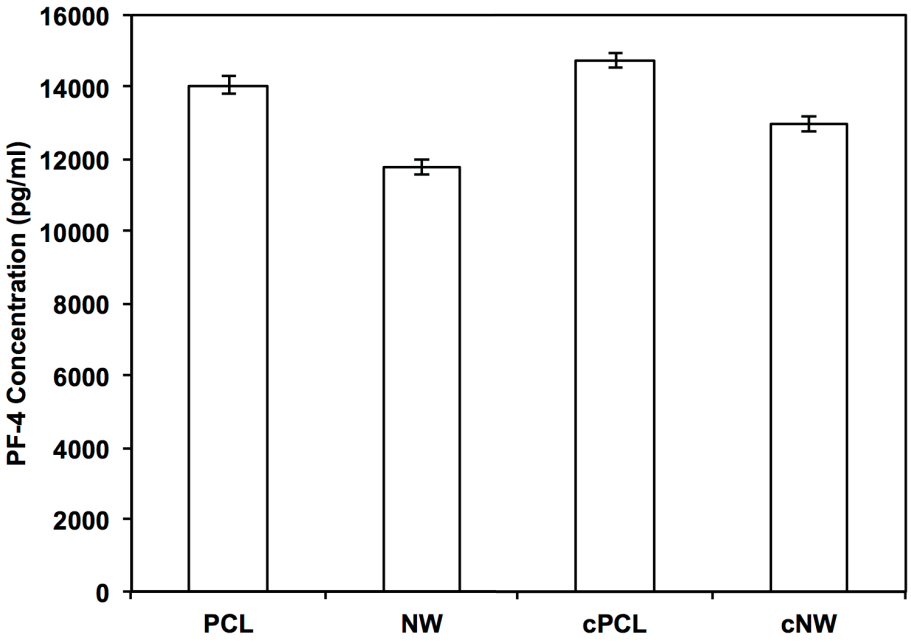

Figure 6.8. Platelet release reaction measured by the amount of PF-4 released from α- granules within the platelets on different surfaces after 2 hours of incubation in whole blood plasma. The results indicate a significant increase in PF-4 expression on cPCL surfaces compared to NW and

cNW surfaces and a significant decrease in PF-4 expression on NW surfaces compared to PCL and cPCL surfaces. Experiments were replicated with at least three different cell populations on at least three different samples ($n_{min} = 9$). Error bars represent standard error.

6.3.8. Contact activation on different surfaces

Contact activation has been considered a significant cause for insufficient hemocompatiblity of blood-contacting biomaterials because it is initiated by blood-biomaterial contact [51]. The proteins involved in the contact activation system such as factors VII, IX, XI, XII, prekallikrein and high molecular weight kininogen, have functions of being profibrinolytic, anti-adhesive, anti-coagulant and pro-inflammatory [52]. The degree of contact activation on the different surfaces after 2 hours of incubation in whole blood plasma was determined by measuring the activity of the kallikrein-a2-macroglobulin complex. Unlike factor XIIa, all kallikrein is released from the surface of the biomaterial. The results indicate no significant difference in contact activation on all the surfaces (**Figure 6.9.**). This may be due to the fact that the surfaces have a similar surface charge due to the fact that all surfaces are made from polycaprolactone.

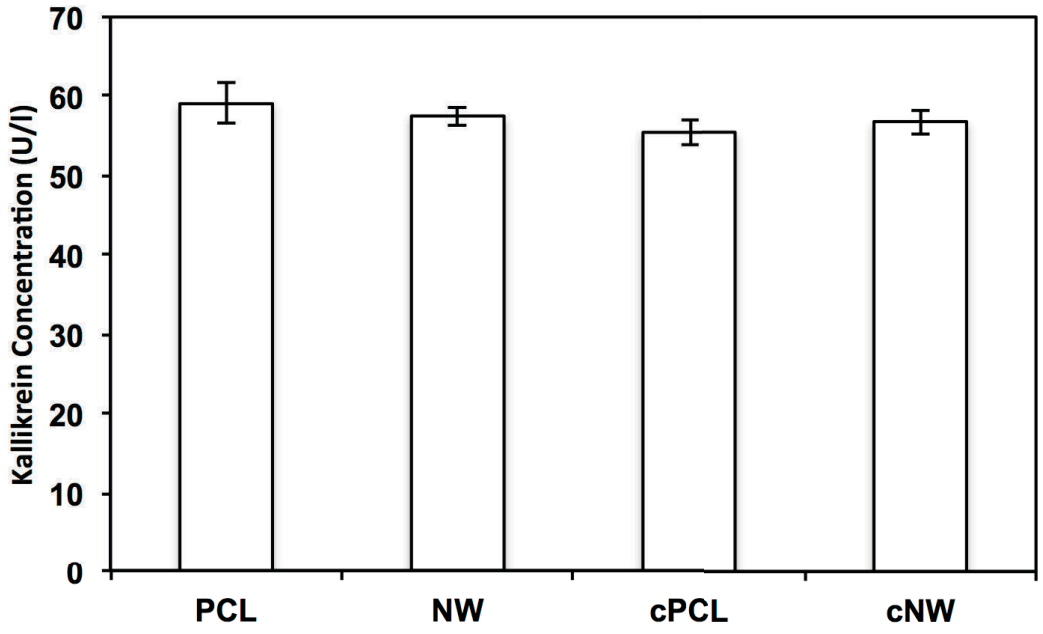

Figure 6.9. Contact activation measured by the amount of kallikrein on different surfaces after 2 hours of incubation in whole plasma. The results indicate no significant difference in contact activation on the surfaces. Experiments were replicated with at least three different cell populations on at least three different samples ($n_{min} = 9$). Error bars represent standard error.

6.3.9. Complement activation on different surfaces

The complement system, consisting of over 20 plasma proteins, such as C3 and C5, plays a significant role in the body's defense mechanisms against infection and “foreign” objects and supports the innate immune system [16, 53]. Complement activation facilitates antibodies and phagocytic cells when clearing pathogens from an organism. The main functions are opsonization, chemotaxis, cell lysis and aggregation of antigen-bearing agents. There are three pathways of complement activation, which converge to form the terminal complement complex (TCC) or SC5b-9 complex [54]. The surface of an implant may activate an inflammatory reaction leading to the formation of the SC5b-9 complex. Therefore quantifying this complex

provides an accurate measurement of the degree of complement activation occurring in response to a material surface. In this study, a quantitative SC5b-9 EIA analysis was performed after surfaces were exposed to whole blood plasma for 2 hours (**Figure 6.10.**). The results indicate no significant difference in SC5b-9 complex formation in response to the different surfaces indicating a similar inflammatory response. This indicates that altering the topography of PCL does not significantly increase the activation of the complement system.

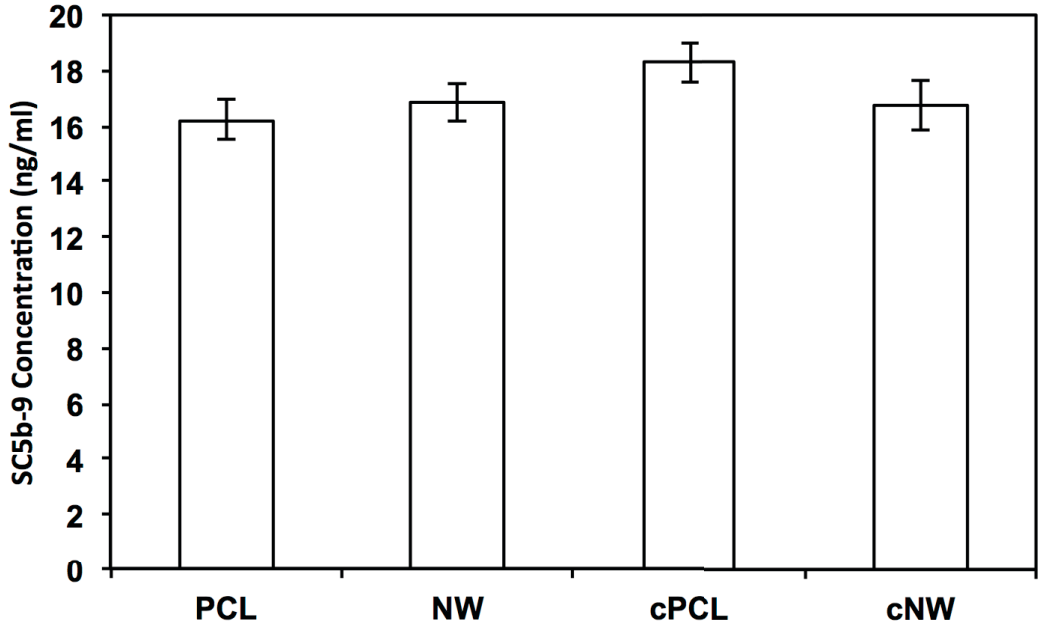

Figure 6.10. Complement activation measured by the amount of SC5b-9 activation on different surfaces after 2 hours of incubation in human plasma. The results indicate no significant difference in the level of complement activation. Experiments were replicated with at least three different cell populations on at least three different samples (n_{min} = 9). Error bars represent standard error.

6.3.10. Thrombin anti-thrombin (TAT) complex formation on different surfaces

Thrombin, one of the key enzymes in the coagulation cascade, is known to promote the activation and aggregation of platelets. Thrombin also has a short half-life, making it difficult to determine its activity. Upon activation of the coagulation cascade, prothrombin is activated into thrombin. The primary inhibitor of thrombin is anti-thrombin and it forms a complex known as the thrombin anti-thrombin (TAT) complex. The TAT complex has been used as a marker for thrombin generation. The ability for the different surfaces to affect intrinsic coagulation cascade turnover for thrombin generation was investigated with a TAT ELISA. The results indicate a significant decrease in TAT concentration on NW surfaces compared to PCL, cPCL and cNW surfaces, and an significant increase in TAT concentration on cPCL surfaces compared to PCL, NW and cNW surfaces (**Figure 6.11.**). These results are in agreement with platelet activation results (**Figure 6.7. and 6.8.**). Thrombin generation ultimately leads to platelet activation, and an increase in platelet activation was observed on cPCL surfaces, while there was a decrease in platelet activation was observed on NW surfaces.

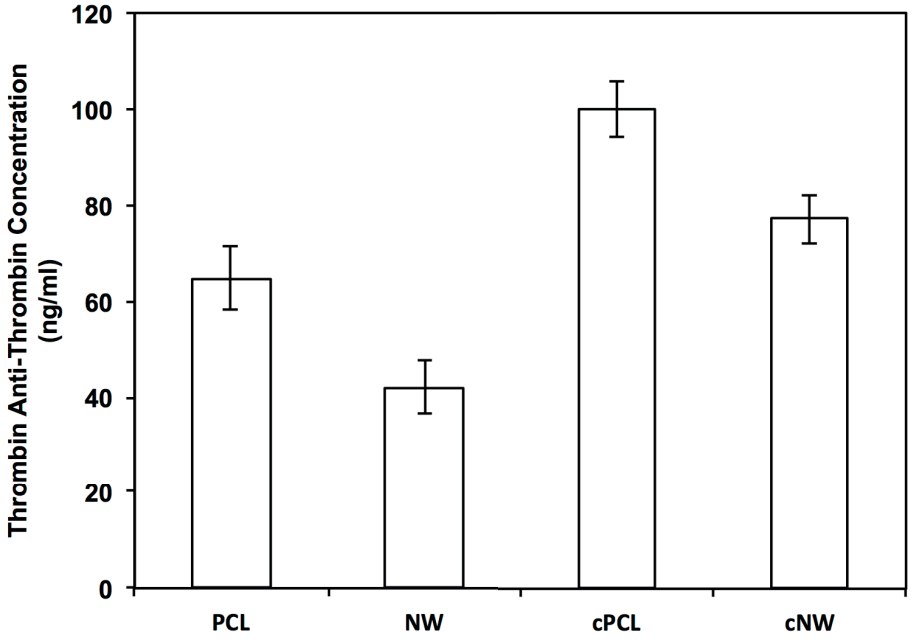

Figure 6.11. TAT concentration determined after 2 hours of incubation of different surfaces in whole blood plasma. Results indicate a significant decrease in TAT concentration on NW surfaces compared to PCL, cPCL and cNW surfaces and an increase in TAT concentration on cPCL surfaces compared to PCL, NW and cNW surfaces. Experiments were replicated with at least three different cell populations on at least three different samples (n_{min} = 9). Error bars represent standard error.

6.3.11. Thrombin generation on different surfaces

Further, the velocity of thrombin generation on different surfaces was calculated using a thrombin generation assay (TGA). Thrombin promotes platelet activation and aggregation and is one of the key enzymes in the coagulation cascade. Thrombin has a short half-life, which makes it difficult to accurately determine its activity. HaemoScan's assay uses a special plasma product

in order to determine thrombin activity and this method is suited to evaluate haemocompatibilty of biomaterials and medical devices.

Results indicate that thrombin generation velocity was greatest on cNW surfaces over a period of 6 mins, followed by cPCL surfaces, with NW surfaces having the lowest thrombin generation velocity (**Figure 6.12.**). It is important to note that this assay was done over the course of 6 mins while the previous assay determined TAT complex formation after 2 hrs. These combined results indicate that the initial generation of thrombin is greatest on cNW surfaces, however, after 2 hrs TAT complex formation is significantly higher on cPCL surfaces.

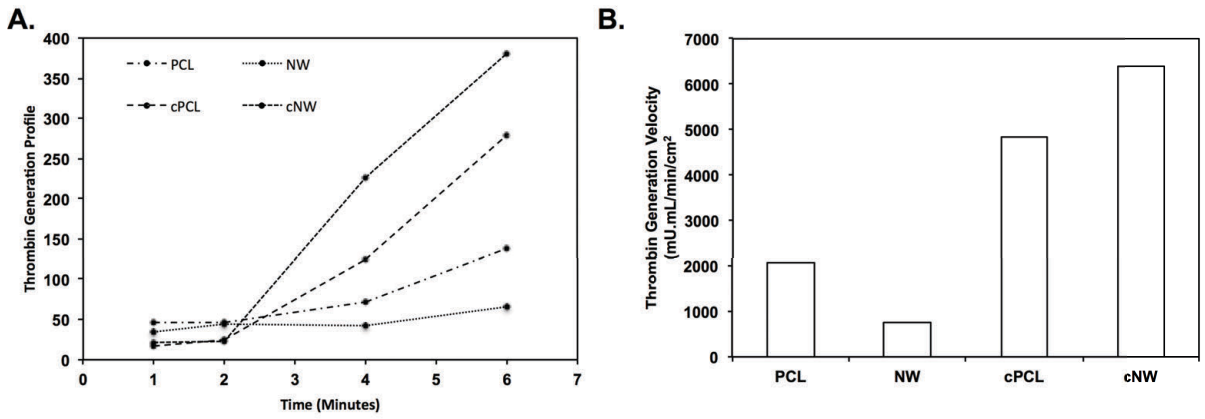

Figure 6.12. **(A)** Thrombin generation profile was measured with a spectrophotometer after 1 min, 2 mins, 4 mins and 6 mins. **(B)** Thrombin generation velocity was calculated as the largest difference between two points and normalized to area of each surface. No statistics were done as this experiment was only performed once.

6.3.12. Hemolysis on different surfaces

Hemolytic activity of different surfaces was investigated using a biomaterial hemolytic assay. Hemolytic activity is required to be tested for any blood contacting medical device. The

assay is centered on erythrocyte lysis, which can be induced by a variety of reasons such as contact, leachables, toxins, metal ions, surface charge or any other cause of erythrocyte lysis. The membranes of red blood cells undergo dynamic stress when exposed to a biomaterial and are considered fragile. The assay measures release of hemoglobin spectrophotometrically. Further, this assay is suited to evaluate the haemocompatibility of biomaterials and medical devices according to the international standard ISO 10993-4:2002. The results indicate a significant increase in the amount of hemoglobin released on PCL surfaces indicating more hemolysis compared to NW, cPCL and cNW surfaces (**Figure 6.13.**). This is undesirable since erythrocytes contain adenosine diphosphate (ADP), which is released when they are lysed resulting in further platelet aggregation [19]. Studies have shown that material surfaces with the high contact angles and high work of adhesion cause more lysis of erythrocytes [55]. PCL surfaces have the highest contact angles compared to cPCL, NW and cNW surfaces, which may be why significantly more erythrocyte lysis is caused by the PCL surfaces.

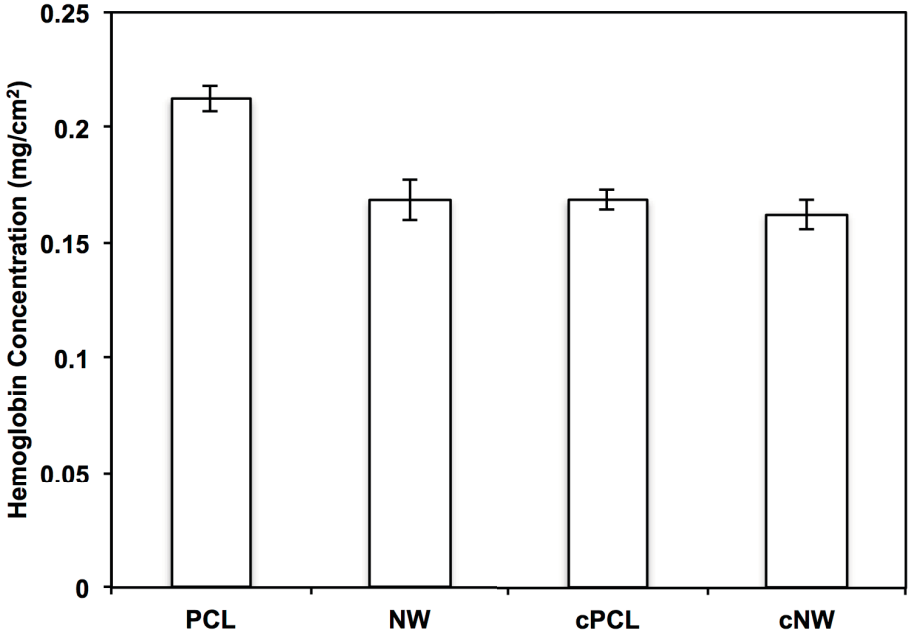

Figure 6.13. Hemoglobin release from an erythrocyte suspension was measured with a spectrophotometer after an incubation period of 24 hrs. Results indicate a significant increase in the amount of hemoglobin released on PCL surfaces compared to NW, cPCL and cNW surfaces. Experiments were replicated with at least three different cell populations on at least three different samples ($n_{min} = 9$). Error bars represent standard error.

6.4. Conclusion

The thrombogenic effects of four different surfaces (PCL, NW, cPCL, cNW) were investigated for their use as interfaces for blood-contacting implants. This study sheds light on the intricate relationship of blood-biomaterial interactions. The clotting cascade consists of many pathways that eventually converge to a common pathway and lead to the formation of a blood clot. It is important to understand how components of the clotting cascade will interact with a biomaterial surface in order to be able to produce a truly biocompatible implant surface. The results presented her indicate a decrease in thrombogenic effects on NW surfaces compared

to PCL, cPCL and cNW surfaces. Proteins found in plasma, such as thrombin and fibrinogen, molecules released from platelets and leukocytes and collagen are known to be potent platelet activators [16]. Findings from this study show that even surfaces coated with collagen did not produce fully activated platelets alone, but did produce more platelet aggregation, which is a very interesting finding. Although there were no significant differences in leukocyte adhesion, there was a decrease in platelet adhesion on NW surfaces. SEM images showed a decrease in platelet/leukocyte complexes on cNW surfaces and no apparent complexes were formed on NW surfaces compared to PCL and cPCL surfaces. The increase in these complexes likely contributed to a higher expression of specific markers for platelet and leukocyte activation on PCL and cPCL surfaces. No significant differences were found in contact and complement activation. Further, thrombin anti-thrombin complexes were significantly reduced on NW surfaces. A significant increase in hemolysis and fibrinogen adsorption was identified on PCL surfaces likely caused by its hydrophobic surface. Further studies are now directed towards utilizing other coatings to further enhance the biocompatibility of NW surfaces.

REFERENCES

[1] Pruitt L, Furmanski J. Polymeric biomaterials for load-bearing medical devices. JOM. 2009;61:14-20.

[2] Kurtz SM, Devine JN. PEEK biomaterials in trauma, orthopedic, and spinal implants. Biomaterials. 2007;28:4845-69.

[3] Low S, Ng Y, Yeo T, Chou N. Use of OsteoplugTM polycaprolactone implants as novel burr-hole covers. Singapore Med J. 2009;50:777-80.

[4] Ze Z, King MW, Guidoin R, Therrien M, Pezolet M, Adnot A, et al. Morphological, physical and chemical evaluation of the Vascugraft® arterial prosthesis: comparison of a novel polyurethane device with other microporous structures. Biomaterials. 1994;15:483-501.

[5] Venkatraman S, Boey F, Lao LL. Implanted cardiovascular polymers: Natural, synthetic and bio-inspired. Progress in Polymer Science. 2008;33:853-74.

[6] Puskas JE, Chen Y. Biomedical Application of Commercial Polymers and Novel Polyisobutylene-Based Thermoplastic Elastomers for Soft Tissue Replacement†. Biomacromolecules. 2004;5:1141-54.

[7] Li G, Liu Y, Lan P, Li Y, Li Y. A prospective bifurcated biomedical stent with seamless woven structure. The Journal of The Textile Institute. 2013;104:1017-23.

[8] Middleton JC, Tipton AJ. Synthetic biodegradable polymers as orthopedic devices. Biomaterials. 2000;21:2335-46.

[9] Anderson JM, Rodriguez A, Chang DT. Foreign body reaction to biomaterials. Seminars in immunology. 2008;20:86-100.

[10] Gorbet MB, Sefton MV. Biomaterial-associated thrombosis: roles of coagulation factors, complement, platelets and leukocytes. Biomaterials. 2004;25:5681-703.

[11] Wise DL, Trantolo DJ, Lewandrowski K-U, Gresser JD, Cattaneo MV, Yaszemski MJ. Biomaterials engineering and devices: human applications: Springer; 2000.

[12] Ratner BD. The catastrophe revisited: Blood compatibility in the 21st Century. Biomaterials. 2007;28:5144-7.

[13] Sin M-C, Sun Y-M, Chang Y. Zwitterionic-Based Stainless Steel with Well-Defined Polysulfobetaine Brushes for General Bioadhesive Control. ACS Applied Materials & Interfaces. 2013;6:861-73.

[14] Hoshi RA, Van Lith R, Jen MC, Allen JB, Lapidos KA, Ameer G. The blood and vascular cell compatibility of heparin-modified ePTFE vascular grafts. Biomaterials. 2013;34:30-41.

[15] Mohan CC, Chennazhi KP, Menon D. In vitro hemocompatibility and vascular endothelial cell functionality on titania nanostructures under static and dynamic conditions for improved coronary stenting applications. Acta Biomaterialia. 2013;9:9568-77.

[16] Gorbet MB, Sefton MV. Biomaterial-associated thrombosis: roles of coagulation factors, complement, platelets and leukocytes. Biomaterials. 2004;25:5681-703.

[17] Roach P, Farrar D, Perry CC. Interpretation of Protein Adsorption: Surface-Induced Conformational Changes. Journal of the American Chemical Society. 2005;127:8168-73.

[18] Wang X, Wang E, Kavanagh JJ, Freedman RS. Ovarian cancer, the coagulation pathway, and inflammation. Journal of translational medicine. 2005;3:25.

[19] Alkhamis TM, Beissinger RL, Chediak JR. Red blood cell effect on platelet adhesion and aggregation in low-stress shear flow. Myth or fact? ASAIO transactions / American Society for Artificial Internal Organs. 1988;34:868-73.

[20] Feng Y, Zhao H, Zhang L, Guo J. Surface modification of biomaterials by photochemical immobilization and photograft polymerization to improve hemocompatibility. Front Chem Eng China. 2010;4:372-81.

[21] O'Connor SM, Stenger DA, Shaffer KM, Maric D, Barker JL, Ma W. Primary neural precursor cell expansion, differentiation and cytosolic Ca2+ response in three-dimensional collagen gel. Journal of Neuroscience Methods. 2000;102:187-95.

[22] He F, Li J, Ye J. Improvement of cell response of the poly(lactic-co-glycolic acid)/calcium phosphate cement composite scaffold with unidirectional pore structure by the surface immobilization of collagen via plasma treatment. Colloids and Surfaces B: Biointerfaces. 2013;103:209-16.

[23] Kalaskar DM, Demoustier-Champagne S, Dupont-Gillain CC. Interaction of preosteoblasts with surface-immobilized collagen-based nanotubes. Colloids and Surfaces B: Biointerfaces. 2013;111:134-41.

[24] Huang NF, Okogbaa J, Lee JC, Jha A, Zaitseva TS, Paukshto MV, et al. The modulation of endothelial cell morphology, function, and survival using anisotropic nanofibrillar collagen scaffolds. Biomaterials. 2013;34:4038-47.

[25] Liu T-Y, Lin W-C, Huang L-Y, Chen S-Y, Yang M-C. Hemocompatibility and anaphylatoxin formation of protein-immobilizing polyacrylonitrile hemodialysis membrane. Biomaterials. 2005;26:1437-44.

[26] Solouk A, Cousins BG, Mirzadeh H, Seifalian AM. Application of plasma surface modification techniques to improve hemocompatibility of vascular grafts: A review. Biotechnology and Applied Biochemistry. 2011;58:311-27.

[27] Lord MS, Foss M, Besenbacher F. Influence of nanoscale surface topography on protein adsorption and cellular response. Nano Today. 2010;5:66-78.

[28] Norman J, Desai T. Methods for Fabrication of Nanoscale Topography for Tissue Engineering Scaffolds. Ann Biomed Eng. 2006;34:89-101.

[29] Abidian MR, Corey JM, Kipke DR, Martin DC. Conducting-Polymer Nanotubes Improve Electrical Properties, Mechanical Adhesion, Neural Attachment, and Neurite Outgrowth of Neural Electrodes. Small. 2010;6:421-9.

[30] Santos MI, Tuzlakoglu K, Fuchs S, Gomes ME, Peters K, Unger RE, et al. Endothelial cell colonization and angiogenic potential of combined nano- and micro-fibrous scaffolds for bone tissue engineering. Biomaterials. 2008;29:4306-13.

[31] Cheng ZA, Zouani OF, Glinel K, Jonas AM, Durrieu M-C. Bioactive Chemical Nanopatterns Impact Human Mesenchymal Stem Cell Fate. Nano Letters. 2013;13:3923-9.

[32] Bettinger CJ, Langer R, Borenstein JT. Engineering Substrate Topography at the Micro- and Nanoscale to Control Cell Function. Angewandte Chemie International Edition. 2009;48:5406-15.

[33] Karlsson M, Palsgard E, Wilshaw PR, Di Silvio L. Initial in vitro interaction of osteoblasts with nano-porous alumina. Biomaterials. 2003;24:3039-46.

[34] Chesnutt BM, Yuan Y, Buddington K, Haggard WO, Bumgardner JD. Composite chitosan/nano-hydroxyapatite scaffolds induce osteocalcin production by osteoblasts in vitro and support bone formation in vivo. Tissue engineering Part A. 2009;15:2571-9.

[35] Wang Y, Shi H, Qiao J, Tian Y, Wu M, Zhang W, et al. Electrospun Tubular Scaffold with Circumferentially Aligned Nanofibers for Regulating Smooth Muscle Cell Growth. ACS Applied Materials & Interfaces. 2014;6:2958-62.

[36] Thapa A, Webster TJ, Haberstroh KM. Polymers with nano-dimensional surface features enhance bladder smooth muscle cell adhesion. Journal of biomedical materials research Part A. 2003;67:1374-83.

[37] Dalby MJ, Riehle MO, Sutherland DS, Agheli H, Curtis AS. Changes in fibroblast morphology in response to nano-columns produced by colloidal lithography. Biomaterials. 2004;25:5415-22.

[38] Leszczak V, Smith BS, Popat KC. Hemocompatibility of polymeric nanostructured surfaces. Journal of biomaterials science Polymer edition. 2013;24:1529-48.

[39] Smith BS, Yoriya S, Grissom L, Grimes CA, Popat KC. Hemocompatibility of titania nanotube arrays. Journal of biomedical materials research Part A. 2010;95:350-60.

[40] Duling RR, Lannutti J, Dupaix RB, Katsube N. Mechanical Characterization of Electrospun Polycaprolactone (PCL): A Potential Scaffold for Tissue Engineering. Journal of Biomechanical Engineering. 2008;130:011006-.

[41] Pektok E, Nottelet B, Tille JC, Gurny R, Kalangos A, Moeller M, et al. Degradation and healing characteristics of small-diameter poly(epsilon-caprolactone) vascular grafts in the rat systemic arterial circulation. Circulation. 2008;118:2563-70.

[42] Woodruff MA, Hutmacher DW. The return of a forgotten polymer—Polycaprolactone in the 21st century. Progress in Polymer Science. 2010;35:1217-56.

[43] Siegismund D, Schroeter A, Schuster S, Rettenmayr M. Quantitative Modeling of Fibrinogen Adsorption on Different Biomaterials. Cel Mol Bioeng. 2013;6:210-9.

[44] Nygren H, Alaeddin S, Lundström I, Magnusson K-E. Effect of surface wettability on protein adsorption and lateral diffusion. Analysis of data and a statistical model. Biophysical Chemistry. 1994;49:263-72.

[45] Raffaini G, Ganazzoli F. Understanding the performance of biomaterials through molecular modeling: crossing the bridge between their intrinsic properties and the surface adsorption of proteins. Macromolecular bioscience. 2007;7:552-66.

[46] Lindon JN, McManama G, Kushner L, Merrill EW, Salzman EW. Does the conformation of adsorbed fibrinogen dictate platelet interactions with artificial surfaces? Blood. 1986;68:355-62.

[47] Ogedegbe HO. An overview of hemostasis. Lab Medicine. 2002;33:948-53.

[48] Cerletti C, Tamburrelli C, Izzi B, Gianfagna F, de Gaetano G. Platelet-leukocyte interactions in thrombosis. Thrombosis research. 2012;129:263-6.

[49] Elstad MR, McIntyre TM, Prescott SM, Zimmerman GA. The interaction of leukocytes with platelets in blood coagulation. Current opinion in hematology. 1995;2:47-54.

[50] Cerletti C, Tamburrelli C, Izzi B, Gianfagna F, de Gaetano G. Platelet-leukocyte interactions in thrombosis. Thrombosis research. 2012;129:263-6.

[51] Blezer R, Willems GM, Cahalan PT, Lindhout T. Initiation and Propagation of Blood Coagulation at Artificial Surfaces Studied in a Capillary Flow Reactor*. Thrombosis and Haemostasis. 1998;79:296-301.

[52] Colman RW, Schmaier AH. Contact system: a vascular biology modulator with anticoagulant, profibrinolytic, antiadhesive, and proinflammatory attributes. Blood. 1997;90:3819-43.

[53] Boon GD. An overview of hemostasis. Toxicologic pathology. 1993;21:170-9.

[54] Sacks SH, Chowdhury P, Zhou W. Role of the complement system in rejection. Current Opinion in Immunology. 2003;15:487-92.

[55] Vijayanand K, Pattanayak DK, Mohan TR, Banerjee R. Interpreting blood-biomaterial interactions from surface free energy and work of adhesion. Trends Biomater Artif Organs. 2005;18:73-83.

CHAPTER 7

CO-CULTURE OF ENDOTHELIAL AND SMOOTH MUSCLE CELLS ON POLYCAPROLACTONE NANOWIRE SURFACES

7.1. Introduction

Stents and vascular grafts have been used routinely for treatment of cardiovascular diseases. Unfortunately, re-endothelialization of biomaterials used for these cardiovascular implants is still a major concern [1]. The communication between cells is essential for the normal maintenance of tissue and a number of pathophysiological responses [2]. In particular, cardiovascular tissue requires interactions between the endothelium with the underlying smooth muscle cells (SMCs), which is vital for cardiovascular health and is considered to be important in the functions of blood vessels [3, 4]. Maintenance of arterial structure relies on this interaction. ECs and SMCs act as a linked system for the communication of signals from receptors confined on the endothelium surface to the arterial wall and vice versa. It has been shown that bidirectional electrical signals flow in response to kinins between ECs and SMCs [5]. ECs and SMCs in the vascular wall can also communicate through the release of signals into the surrounding medium, or via direct cell-cell contact through junctions formed between the cells [6]. For example, during vasculogenesis, growth factors released from ECs promote migration of undifferentiated mesenchymal cells towards ECs and upon contact with ECs the mesenchymal cells differentiate into SMCs [7].

Further, in order to prevent thrombosis, restenosis and ultimate failure of the implant, an intact endothelium at the vessel-biomaterial interface is fundamental, in turn also preventing over-proliferation of the smooth muscle cells. ECs produce both growth inhibitors and

stimulators of SMCs. In particular nitric oxide (NO), released by ECs, is responsible for inhibiting the proliferation of SMCs via the extracellular signal-regulated kinase (ERK) pathway [8]. Studies have also shown that the rate of proliferation of SMCs is directly dependent on the state of endothelium [9]. When the endothelium is in a confluent state, the normal growth rate of SMCs is completely inhibited. Further, ECs cultured with synthetic state SMCs separated by a porous membrane demonstrated increased EC adhesion molecule expression, suggesting that synthetic SMCs activate the endothelium [10].

In this study we attempted to improve endothelialization while limiting over-proliferation of smooth muscle cells on poly(ε-caprolactone), a polymer often used in artificial vessel development [11-13]. This surface was immobilized with collagen, a key component of vascular tissue. In order to provide insights into the material surfaces' feasibility for use as an interface in cardiovascular applications, we are using human microvascular endothelial cells and human aortic smooth muscle cells to test surface-functionalized poly(ε-caprolactone) for its cell stimulatory potential.

7.2. Materials and Methods

7.2.1. Fabrication and characterization of PCL and NW surfaces.

Surfaces were fabricated and characterized as described in detail in section 2.2.1 and 2.2.2. The nanowire surface architecture was examined for uniformity and repeatability using SEM imaging.

7.2.2. Human Aortic Smooth Muscle Cell and Human Microvascular Endothelial Cell Culture

Both human aortic SMCs (Life Technologies) and human microvascular ECs were suspended in MCDB 131 media (Life Technologies) enhanced with SMC growth supplement or microvascular growth supplement, respectively (both supplemented with 2 mmol/l glutamine, 100 ug/ml penicillin, and 100 ug/ml streptomycin) and added to 75 cm^2 culture flasks and incubated at standard culture conditions. This study was performed using SMCs that were passage 4 and ECs at passage 5.

First, SMCs were cultured on PCL, NW, cPCL and cNW surfaces in a 48-well plate. Prior to seeding, all surfaces were subjected to 30 min UV exposure and conditioned for 5 min in 400 µl of culture medium. The SMCs were seeded at a high density of 5×10^6 cells/well. The surfaces were incubated in standard culture conditions in 400 µl of cell rich medium and allowed to adhere for 24 hrs. After 24 hrs in culture, the ECs were seeded at a high density of 5×10^6 cells/well on top of the adhered SMCs. After 24 hrs of co-culture, media changes were done with MCDB 131 media enhanced with with SMC differentiation supplement (supplemented with 2 mmol/l glutamine, 100 ug/ml penicillin, and 100 ug/ml streptomycin). Cellular adhesion and morphology was investigated after 7 days in culture. Cellular differentiation was investigated after 7 and 14 days in culture.

7.2.3. Adhesion and proliferation of co-cultured cells on different surfaces

Cell adhesion and proliferation was investigated by staining cells with rhodamine phalloidin (Cytoskeleton) and 4′,6-diamidino-2-phenylindole dihydrochloride (DAPI) (Invitrogen) nucleus stain by fluorescence microscope imaging after 7 days in culture.

Prior to staining non-adherent cells were removed by aspirating the cell rich medium from the surfaces followed by two gentle rinses with PBS. The surfaces were then transferred to a new 48-well plate and fixed with 3.7% formaldehyde 15 mins at room temperature. This was followed by incubating the surfaces in 1 % Triton-X 100 for 3 mins in order to permeabilize the cells. The surfaces were transferred to a new 48-well plate, then incubated in rhodamine-phalloidin at a concentration of 5 μL/mL for 30 mins. DAPI was added at a concentration of 1 μL/mL after 25 mins. All the surfaces were rinsed with PBS and imaged with a fluorescence microscope (Zeiss).

7.2.4. Morphology of co-cultured cells on different surfaces

The cell morphology was investigated using SEM imaging to visualize the cellular interaction with the surface nanoarchitecture. The non-adherent cells were removed by aspirating the cell rich media from the surfaces followed by two gentle rinses with PBS. The surfaces were then transferred to a clean petri dish where the cells were fixed and dehydrated. The cells were fixed by incubating the surfaces in a solution of primary fixative (3 % glutaraldehyde (Sigma), 0.1 M sodium cacodylate (Polysciences), and 0.1 M sucrose (Sigma)) for 45 min. They were then incubated in a solution of secondary fixative (primary fixative without gluteraldehyde) for 10 min. Subsequently, the surfaces were dehydrated by incubation in consecutive solutions of increasing ethanol concentrations (35 %, 50 %, 70 %, 95 %, and 100 %) for 10 min each. Further dehydration of the cells was accomplished by incubating the surfaces in hexamethyldisilazane (HMDS, Sigma) for 10 min. They were then air dried and stored in a desiccator until further imaging by SEM. The surfaces were coated with a 10 nm layer of gold and imaged at 5-7 kV.

7.2.5. Differentiation of co-cultured cells on different surfaces

Western blotting was performed to identify the expression of EC and SMC specific differentiation proteins, VE-cadherin and heavy chain myosin (MYH) respectively. Further, non-muscle specific myosin IIB (SMemb), a marker of undifferentiated SMCs was blotted for. Briefly, cells on surfaces after 7 and 14 days in culture were homogenized in RIPA lysis buffer (10.0 mM Tris pH 7.4, 100.0 mM NaCl, 5.0 mM EDTA, 5.0 mM EGTA, 1.0% Deoxycholate, 0.1% SDS, 1.0% Triton X-100) containing protease inhibitor cocktail. The lysate protein content was determined by micro-BCA assay. The lysate was heated to 65 °C for 20 mins in sample buffer (62.5 mM Tris-HCl pH 6.8, 10.0 % glycerol, 5.0 % β-mercaptoethanol, 2.0% SDS, 0.025 % Bromophenol blue) in order to denature the proteins prior to gel loading. Approximately 20 μg of total extract protein was electrophoresed through 8 % Tris-SDS gels and transferred to PVDF membranes in 7.5% methanol. Blots were blocked for 1 hr at room temperature. Primary monoclonal antibodies for VE-cadherin, MYH or SMemb were diluted 1:500 in 3% BSA in PBS-tween solution and incubated overnight at 4 °C. The blots were then washed three times with PBS-tween solution (5 mins per wash) before they were incubated with goat anti-mouse or donkey anti-rabbit horseradish peroxidase (HRP) conjugated secondary antibodies (Santa Cruz Biotechnology) at a dilution of 1:5000 for 1 hr at room temperature. The blots were then washed three times with PBS-tween solution (5 mins per wash) followed by protein detection using chemiluminescence (WestPico Chemiluminescent Substrate; Pierce). The blots were imaged using an Alpha Innotech Fluorchem gel documentation system, and band intensities were analyzed using ImageJ software.

7.3. Results and Discussion

7.3.1. Characterization of Surfaces

The surface architecture of the different surfaces before and after the collagen immobilization process was characterized using SEM. Results reveal that surface architecture remains consistent before and after collagen immobilization (**Figure 7.1.**).

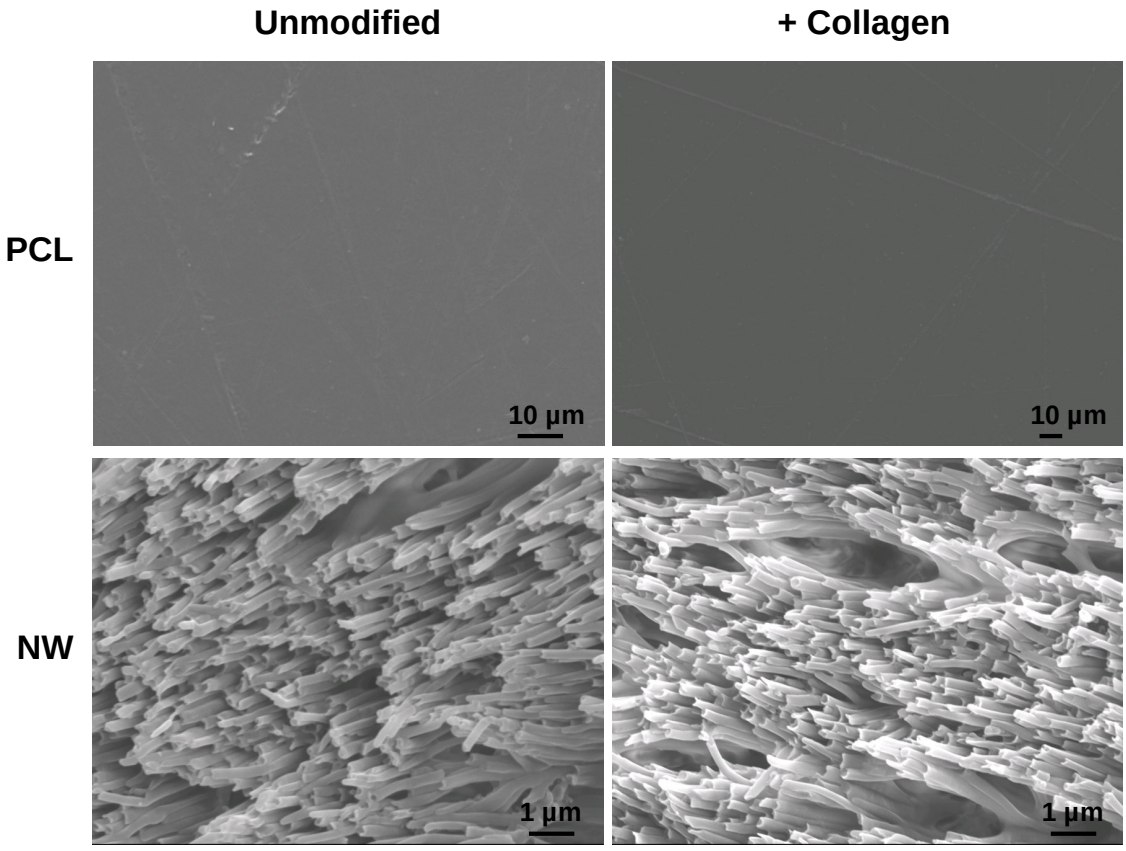

Figure 7.1. Representative SEM images of PCL and NW surfaces before and after collagen immobilization.

7.3.2. Adhesion of co-cultured cells on different surfaces

The adhesion of EC and SMC co-cultures on different surfaces was investigated after 7 days in culture by using Rhodamine Phalloidin (Cytoskeleton) and 4′,6-diamidino-2-phenylindole dihydrochloride (DAPI) (Invitrogen) nucleus stain, followed by imaging with a fluorescence microscope (**Figure 7.2.**). Results indicate that NW, cPCL and cNW surfaces are confluent with cells, unlike PCL surfaces. It is well known that both SMCs and ECs adhere better to either nanotopography or a bioactive surface, which PCL surfaces lack [14-17]. Further, it seems as if cells on all surfaces are aligning. High magnification images show cellular filopodia interactions with surrounding cells on all surfaces.

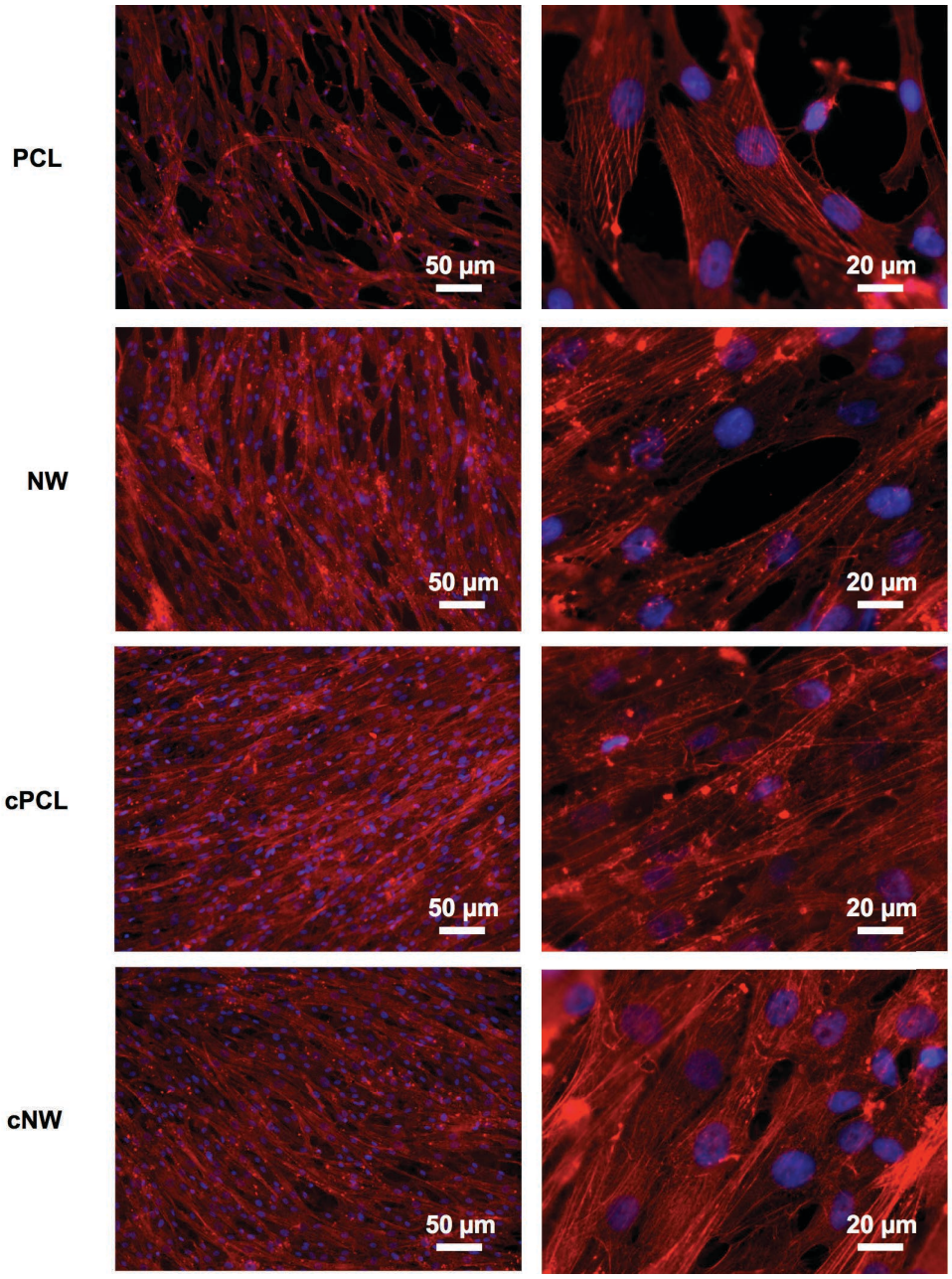

Figure 7.2. Representative fluorescence microscopy images of EC and SMC co-cultures stained with Rhodamine Phalloidin (red) and DAPI (blue) on PCL, NW, colPCL and colNW surfaces. Experiments were replicated on at least three different samples with at least three different cell populations ($n_{min} = 9$).

7.2.4. Morphology of co-cultured cells on different surfaces

The cell morphology was investigated using SEM imaging to visualize the cellular interaction with the surface nanoarchitecture. The results indicate that NW, cPCL and cNW surfaces are confluent with cells (**Figure 7.3.)** Similar to fluorescence imaging results, high magnification images show cellular filopodia interactions with surrounding cells on all surfaces. Further, co-cultures on NW, cPCL and cNW surfaces appear more spindle-shaped (contractile-appearing phenotype), with more evenly distributed cells.

7.3.4. Differentiation of SMC and EC co-cultures on different surfaces

The differentiation of ECs and SMCs in co-culture on surfaces was investigated by detecting VE-cadherin, MYH and SMemb expression through blotting techniques after 7 and 14 days in culture. Both VE-cadherin and MYH are specific to a differentiated EC or SMC phenotype, respectively. VE-cadherin expression is important in cellular contacts, which will eventually regulate the permeability of the blood vessel therefore an increase in VE-cadherin expression is necessary for healthy vasculature.

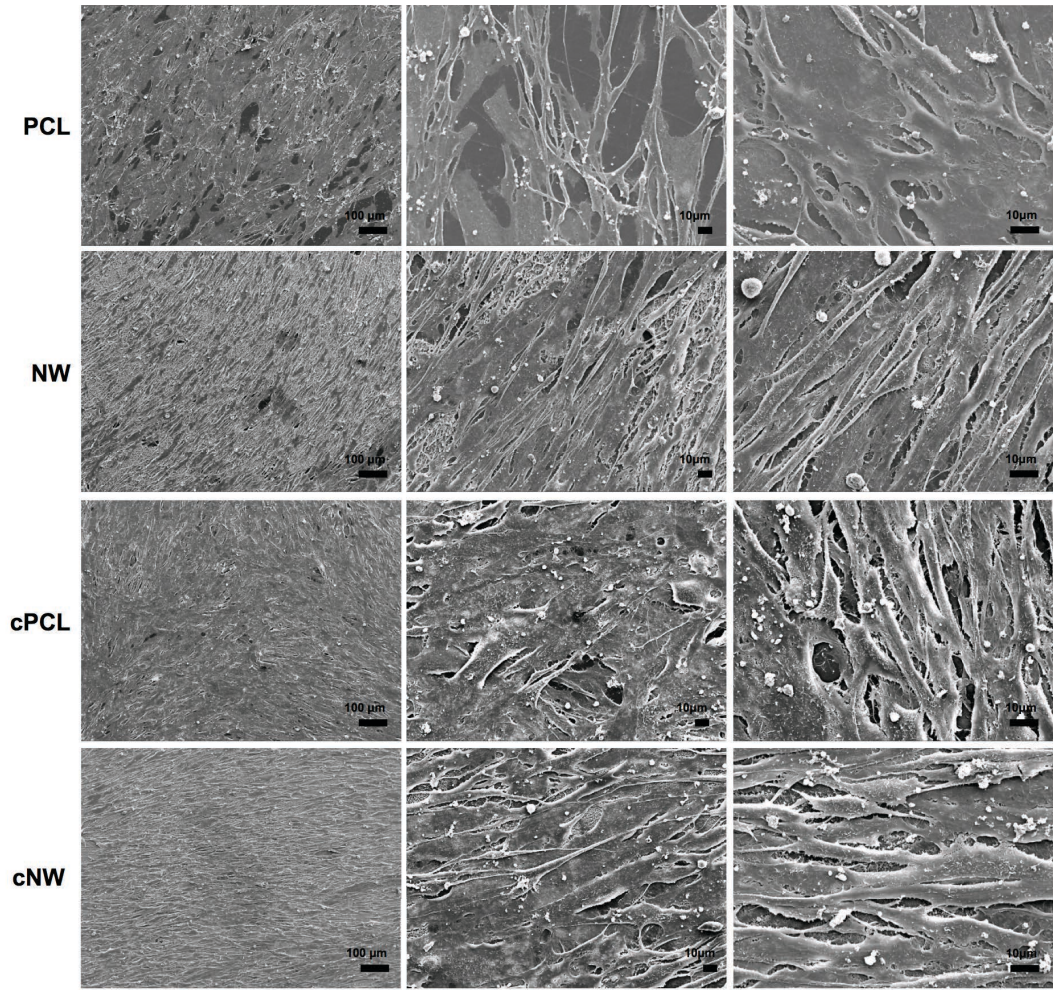

Figure 7.3. Representative SEM images of SMC and EC co-cultures after 7 days of culture on different surfaces. Note: the surfaces were coated with a 10 nm layer of gold and imaged at 7 keV. Experiments were replicated on at least three different samples with at least three different cell populations ($n_{min} = 9$).

MYH expression is an end-state differentiation marker specific to SMCs while SMemb expression is an undifferentiated SMC marker. Down-regulation of SMC lineage markers has been shown to be associated with calcification [18]. Results indicate that normalized VE-cadherin expression is statistically higher on PCL and NW surfaces after 7 days in culture (**Figure 7.4.b)**). However, the normalized expression of VE-cadherin after 14 days in culture

decreases on both PCL and NW surfaces. Normalized VE-cadherin expression on NW, cPCL and cNW surfaces increases significantly from 7 days in culture to 14 days in culture. Further normalized MYH expression significantly decreases on NW, cPCL and cNW surfaces (**Figure 7.4.c)**), while no significant difference was seen in MYH expression on PCL surfaces from day 7 to day 14. The combined results suggest that ECs are developing more cell-cell junctions via VE-cadherin, and perhaps are still proliferating on NW, cPCL and cNW surfaces. Once SMCs are in a differentiated state, their proliferation rates are significantly lower which would account for the decrease in MYH expression compared to total cell number on NW, cPCL and cNW surfaces. This is further verified by the significant decrease in SMemb expression on all surfaces (**Figure 7.4.d**). Studies have shown that SMCs and ECs exhibit favorable interactions when co-cultured [19-21]. By incorporating nanotopography or a cell binding motif, more ECs and SMCs are able to attach, thus explaining the increased expression of differentiation proteins specific to ECs and SMCs on NW, cPCL and cNW surfaces compared to PCL surfaces.

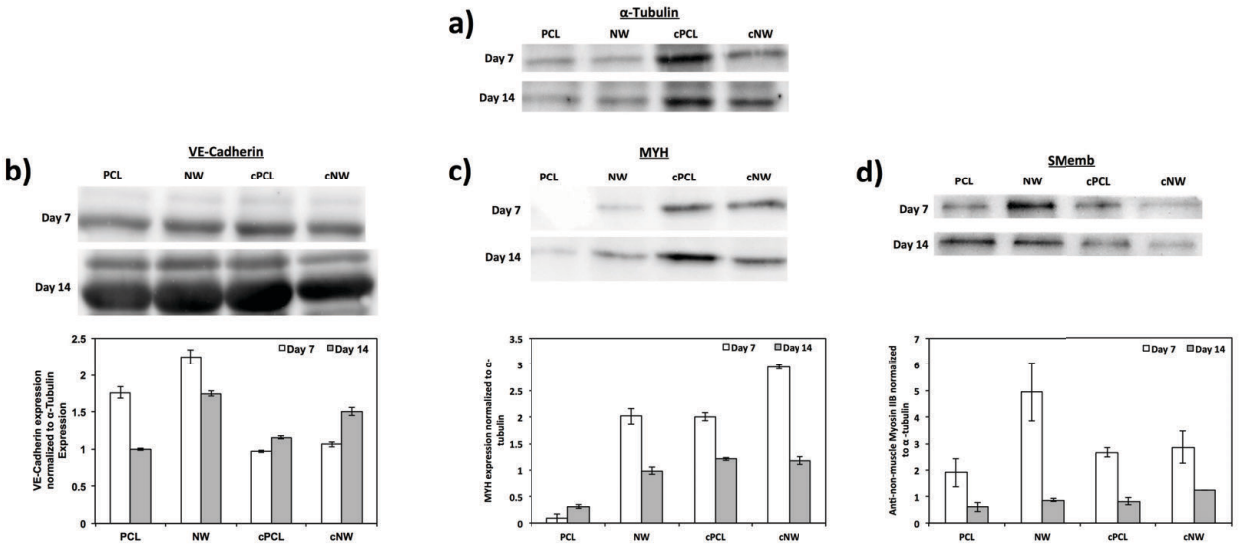

Figure 7.4. Western blot analysis of the expression of (A) α-tubulin, (B) VE-cadherin, (C) MYH and (D) SMemb on different surfaces after 7 and 14 days in culture. Experiments were replicated with western blots with at least three different cell populations (n_{min} = 9). (B) After 7 days in culture PCL and NW surfaces express significantly higher amounts of VE-cadherin compared to cPCL and cNW surfaces. After 14 days in culture VE-cadherin expression is significantly higher on NW and cNW surfaces compared to PCL and cPCL surfaces. (C) After 7 days in culture MYH expression is significantly higher on cNW surfaces compared to PCL, NW and cPCL surfaces, while PCL surfaces express significantly less MYH than NW, cPCL and cNW surfaces. After 14 days in culture, MYH expression significantly decreases on NW, cPCL and cNW surfaces. (D) After 7 days in culture SMemb expression is significantly higher on NW surfaces compared to PCL, cPCL and cNW surfaces. After 14 days in culture there is a significant decrease in SMemb expression on all surfaces, with no significant difference in expression between all surfaces.

7.3. Conclusions

Cardiovascular tissue requires interactions between the endothelium with the underlying SMCs, which is vital for cardiovascular health and is considered to be important in the functions of blood vessels. In this study, we have investigated EC and SMC co-cultures on functionalized poly(ε-caprolactone) surfaces. In order to provide insights into the material surfaces' feasibility for use as an interface in cardiovascular applications, EC and SMC co-culture adhesion, morphology and differentiation on different surfaces was investigated. Fluorescence imaging and SEM results reveal that NW, cPCL and cNW surfaces are confluent with cells. Further, ECs and SMCs on these surfaces seem to be more aligned and more spindle-shaped (contractile-appearing phenotype), with more evenly distributed cells. Western blotting results reveal that there is a significant increase in VE-cadherin expression after 14 days in culture on NW and cNW surfaces. MYH expression decreases on all surfaces from day 7 to day 14 in culture. The decrease in MYH expression can be attributed to the decrease in proliferation of differentiated SMCs. This is confirmed by the significant decrease in SMemb, an undifferentiated SMC marker from day 7 to day 14 in culture. However after 14 days in culture MYH expression is significantly higher on NW, cPCL and cNW surfaces compared to PCL surfaces. These combined results indicate that NW and cNW surfaces may be good surfaces for use in cardiovascular applications and warrants further investigation.

REFERENCES

[1] de Mel A, Jell G, Stevens MM, Seifalian AM. Biofunctionalization of Biomaterials for Accelerated in Situ Endothelialization: A Review. Biomacromolecules. 2008;9:2969-79.

[2] Rossello RA, Kohn DH. Cell communication and tissue engineering. Commun Integr Biol. 2010;3:53-6.

[3] Jones PA. Construction of an artificial blood vessel wall from cultured endothelial and smooth muscle cells. Proceedings of the National Academy of Sciences of the United States of America. 1979;76:1882-6.

[4] Vernon SM, Campos MJ, Haystead T, Thompson MM, DiCorleto PE, Owens GK. Endothelial cell-conditioned medium downregulates smooth muscle contractile protein expression. The American journal of physiology. 1997;272:C582-91.

[5] Bidirectional electrical communication between smooth muscle and endothelial cells in the pig coronary artery1994.

[6] Fillinger MF, Sampson LN, Cronenwett JL, Powell RJ, Wagner RJ. Coculture of Endothelial Cells and Smooth Muscle Cells in Bilayer and Conditioned Media Models. Journal of Surgical Research. 1997;67:169-78.

[7] Hirschi KK, Rohovsky SA, D'Amore PA. PDGF, TGF-beta, and heterotypic cell-cell interactions mediate endothelial cell-induced recruitment of 10T1/2 cells and their differentiation to a smooth muscle fate. The Journal of cell biology. 1998;141:805-14.

[8] Förstermann U. Nitric oxide and oxidative stress in vascular disease. Pflugers Arch - Eur J Physiol. 2010;459:923-39.

[9] Zuckerbraun BS, Stoyanovsky DA, Sengupta R, Shapiro RA, Ozanich BA, Rao J, et al. Nitric oxide-induced inhibition of smooth muscle cell proliferation involves S-nitrosation and inactivation of RhoA. Am J Physiol Cell Physiol. 2007;292:C824-31. Epub 2006 Aug 16.

[10] Chiu JJ, Chen LJ, Lee CI, Lee PL, Lee DY, Tsai MC, et al. Mechanisms of induction of endothelial cell E-selectin expression by smooth muscle cells and its inhibition by shear stress. Blood. 2007;110:519-28.

[11] Wulf K, Teske M, Lobler M, Luderer F, Schmitz KP, Sternberg K. Surface functionalization of poly(epsilon-caprolactone) improves its biocompatibility as scaffold material for bioartificial vessel prostheses. Journal of biomedical materials research Part B, Applied biomaterials. 2011;98:89-100.

[12] Williamson MR, Woollard KJ, Griffiths HR, Coombes AG. Gravity spun polycaprolactone fibers for applications in vascular tissue engineering: proliferation and function of human vascular endothelial cells. Tissue engineering. 2006;12:45-51.

[13] de Valence S, Tille J-C, Mugnai D, Mrowczynski W, Gurny R, Möller M, et al. Long term performance of polycaprolactone vascular grafts in a rat abdominal aorta replacement model. Biomaterials. 2012;33:38-47.

[14] In Jeong S, Kim SY, Cho SK, Chong MS, Kim KS, Kim H, et al. Tissue-engineered vascular grafts composed of marine collagen and PLGA fibers using pulsatile perfusion bioreactors. Biomaterials. 2007;28:1115-22.

[15] Bettinger CJ, Zhang Z, Gerecht S, Borenstein JT, Langer R. Enhancement of In Vitro Capillary Tube Formation by Substrate Nanotopography. Advanced Materials. 2008;20:99-103.

[16] Wenger A, Stahl A, Weber H, Finkenzeller G, Augustin HG, Stark GB, et al. Modulation of in vitro angiogenesis in a three-dimensional spheroidal coculture model for bone tissue engineering. Tissue engineering. 2004;10:1536-47.

[17] Jack GS, Zhang R, Lee M, Xu Y, Wu BM, Rodríguez LV. Urinary bladder smooth muscle engineered from adipose stem cells and a three dimensional synthetic composite. Biomaterials. 2009;30:3259-70.

[18] Steitz SA, Speer MY, Curinga G, Yang HY, Haynes P, Aebersold R, et al. Smooth muscle cell phenotypic transition associated with calcification: upregulation of Cbfa1 and downregulation of smooth muscle lineage markers. Circulation research. 2001;89:1147-54.

[19] Wu H-C, Wang T-W, Kang P-L, Tsuang Y-H, Sun J-S, Lin F-H. Coculture of endothelial and smooth muscle cells on a collagen membrane in the development of a small-diameter vascular graft. Biomaterials. 2007;28:1385-92.

[20] Ziegler T, Alexander RW, Nerem RM. An endothelial cell-smooth muscle cell co-culture model for use in the investigation of flow effects on vascular biology. Ann Biomed Eng. 1995;23:216-25.

[21] Orlidge A, D'Amore PA. Inhibition of capillary endothelial cell growth by pericytes and smooth muscle cells. The Journal of Cell Biology. 1987;105:1455-62.

CHAPTER 8

CONCLUSIONS AND FUTURE WORK

8.1. Conclusions

Cardiovascular disease is the leading killer of people worldwide. Synthetic implants are promising treatments, yet rejection of cardiovascular implants continues to be a problem, eliciting a need for understanding the mechanisms behind tissue-material interaction. An ideal cardiovascular implant surface must be capable of adhering cells and providing appropriate physiological responses while the surrounding tissue integrates with the scaffold. However, tissue integration will not occur if the surface of the implant is not hemocompatible. A thorough understanding of the interaction of cardiovascular cells and whole blood and its components with the material surface is essential in order to have a successful application which promotes healing as well as native tissue integration and regeneration. In this study, the suitability of nanostructured polymeric surfaces as interfaces for cardiovascular applications was investigated by evaluating cellular response as well as hemocompatibility.

The surface properties of implantable cardiovascular devices are critical for long-term success. This research has investigated the characteristics of similar sized features that are aligned differently; NWs are aligned perpendicular to the surface while NFs are aligned parallel to the surface. Further characteristics of collagen immobilized surfaces were also elucidated. These characteristics were evaluated using SEM, contact angle and XPS. Polycaprolactone NFs were fabricated with an electrospinning technique and a novel solvent-free template synthesis technique was used to fabricating controlled arrays of high aspect ratio, substrate-bound NWs. Surfaces were immobilized with collagen utilizing an aminolysis method. The resulting SEM images show the production of either horizontally oriented, uniform NFs or vertically oriented,

high aspect ratio and uniform NWs. Immobilizing collagen to the surfaces did not significantly alter the surface topography. Further, results identify a highly hydrophobic NF surface, while NW surfaces exhibit a more hydrophilic surface. The immobilization of collagen on the surfaces further decreases the contact angle. The simple fabrication, physiologically relevant architecture, low contact angle and large surface area identify nanowire surfaces as promising interfaces for implantable biomedical devices.

The hemocompatibility of nanostructured polycaprolactone surfaces (NW and NF) was investigated through the adsorption of key blood serum proteins (albumin, fibrinogen and immunoglobulin-g), platelet adhesion and activation and the clotting kinetics of whole human blood. Protein adsorption was evaluated using micro-BCA and XPS. The adhesion and activation of human platelets, isolated from whole human blood, were investigated using live-cell staining, MTT assay and SEM imaging. The clotting kinetics of whole human blood was evaluated by measuring the free hemoglobin concentration and further imaging by SEM to visualize the clot formation. The results indicate no significant differences in ALB adsorption on all surfaces. However, NW surfaces had higher total FIB and IgG adsorption compared to NF and PCL surfaces. In contrast, NW surfaces had lower surface FIB and IgG adsorption compared to NF and PCL surfaces. This can be explained based on the structure of FIB and IgG as well as the ability of the surfaces to allow protein infiltration. Platelet adhesion and viability studies show a large amount of adhesion and clustering of platelets on the NF surfaces as compared to PCL and NW surfaces. Platelet activation studies reveal that NW surfaces have the highest percentage of unactivated platelets, whereas NF surfaces have the highest percentage of fully activated platelets. Whole blood clotting results indicate that NW surfaces maintain an increased amount of free hemoglobin during the clotting process compared to PCL and NF surface, indicating less

clotting and slower rate of clotting on their surfaces. The results presented here indicate that the surface nanoarchitecture and how it is presented to the biological environment can modulate the hemocompatibility. Further, NW surfaces were identified as a more favorable template for blood-contacting surfaces.

EC interaction with functionalized NW surfaces was investigated in terms of adhesion, proliferation, viability, morphology and differentiation. A thorough understanding of the interaction between ECs and the biomaterial surface is essential in order to promote healing and regeneration through integration with native tissue. One major obstacle to overcome is adhesion of the anchorage-dependent and slowly renewing ECs on material surfaces. The level of cell growth is also correlated to the characteristics of the material surface and its ability to mimic properties similar to extracellular matrix. Therefore, providing ECs with nanotopography and cell-binding motifs such as collagen may affect the cell adhesion, viability, morphology and differentiation. In this study, ECs exhibited increased adhesion and viability on NW, cPCL and cNW surfaces. ECs have a more elongated body and low shape factor on nanostructured surfaces (NW and cNW) compared to smooth surfaces (PCL and cPCL). The differentiation potential of collagen immobilized nanowire surfaces was also evaluated by immunostaining and western blotting for key endothelial cell markers, vWF and VE-cadherin. The expression of VE-cadherin is increased on nanostructured surfaces after 14 days in cuture, indicating more cell-cell contacts. The expression of vWF is statistically similar on all surfaces after 14 days in culture with no significant increase from 7 to 14 days in culture, indicating that increased perturbation of the endothelial layer on any surface is not occurring. The results presented here indicate that ECs adhesion and differentiation can be modulated by providing surfaces with nanotopography and cell binding motifs such as collagen.

SMC interaction with functionalized NW surfaces was investigated in terms of adhesion, proliferation, viability, morphology and differentiation. Inhibition of unnecessary vascular SMC proliferation and preservation of a differentiated state in SMCs are important aspects in the management and avoidance of vascular diseases. The level of cell functionality on biomaterial surfaces is also correlated to the characteristics of the surface and its ability to mimic properties similar to that of extracellular matrix. Therefore, providing SMCs with nanotopography and cell-binding motifs such as collagen may affect the cell adhesion, viability, morphology and differentiation. In this study, SMCs exhibited increased adhesion on NW, cPCL and cNW surfaces, however SMCs on nanostructured surfaces seemed to be more elongated than those on PCL surfaces. SEM results also revealed considerable amounts of filopodia interacting with surfaces and neighboring cells on NW, cPCL and cNW surfaces, but this interaction is lacking on PCL surfaces. The reduction of MTT was higher on flat surfaces (PCL and cPCL), indicating a higher rate of proliferation. This suggests that SMCs on nanostructured surfaces (NW and cNW) may be in a more differentiated state and slowly dividing. This was confirmed by a significant increase in differentiation markers (CAL and MYH) on these surfaces after 7 days in culture without providing cells with differentiation cues. After giving the cells differentiation media, SMCs on all surfaces become spindle shaped. However the expression of endogenous proteins, CAL and MYH, specific to a contractile SMC phenotype is up-regulated on collagen immobilized surfaces (cPCL and cNW). These results suggest that nanotopography affects cell proliferation as well as cell elongation, while collagen immobilized surfaces greatly affect cell differentiation with proper differentiation cues.

The thrombogenic effects of functionalized NW surfaces were investigated for their use as interfaces for blood-contacting implants. This study sheds light on the intricate relationship of

blood-biomaterial interactions. The clotting cascade consists of many pathways that eventually converge to a common pathway and lead to the formation of a blood clot. It is important to understand how components of the clotting cascade will interact with a biomaterial surface in order to be able to produce a truly biocompatible implant surface. The results presented her indicate a decrease in thrombogenic effects on NW surfaces compared to PCL, cPCL and cNW surfaces. Proteins found in plasma, such as thrombin and fibrinogen, molecules released from platelets and leukocytes and collagen are known to be potent platelet activators [16]. Findings from this study show that even surfaces coated with collagen did not produce fully activated platelets alone, but did produce more platelet aggregation, which is a very interesting finding. Although there were no significant differences in leukocyte adhesion, there was a decrease in platelet adhesion on NW surfaces. SEM images showed a decrease in platelet/leukocyte complexes on cNW surfaces and no apparent complexes were formed on NW surfaces compared to PCL and cPCL surfaces. The increase in these complexes likely contributed to a higher expression of specific markers for platelet and leukocyte activation on PCL and cPCL surfaces. No significant differences were found in contact and complement activation. Further, thrombin anti-thrombin complexes were significantly reduced on NW surfaces. A significant increase in hemolysis and fibrinogen adsorption was identified on PCL surfaces likely caused by its hydrophobic surface. Further studies are now directed towards utilizing other coatings to further enhance the biocompatibility of NW surfaces.

EC and SMC co-cultures on functionalized NW surfaces were investigated in terms of adhesion, morphology and differentiation. Cardiovascular tissue requires interactions between the endothelium with the underlying SMCs, which is vital for cardiovascular health and is considered to be important in the functions of blood vessels. In order to provide insights into the

material surfaces' feasibility for use in cardiovascular applications, we looked at EC and SMC co-culture adhesion, morphology and differentiation on different surfaces. Fluorescence imaging and SEM results reveal that NW, cPCL and cNW surfaces are confluent with cells. Further, ECs and SMCs on these surfaces seem to be more aligned and more spindle-shaped (contractile-appearing phenotype), with more evenly distributed cells. Western blotting results reveal that there is a significant increase in VE-cadherin expression and a significant decrease in MYH expression, both normalized to α-tubulin, on NW, cPCL and cNW surfaces. These results suggest that NW, cPCL and cNW surfaces may be good surfaces for use in cardiovascular applications and warrants further investigation.

The results of this work suggest the improved biocompatibility of polycaprolactone NW surfaces. The findings indicate altered hemocompatibility and improved EC and SMC functionality. This research has promising implications with respect to the use of NW surfaces arrays as interfaces for cardiovascular implants.

8.2. Future Work

The simple solvent free nano-templating fabrication, physiologically appropriate topography, ease of biomolecular modification and appropriate interactions with both cardiovascular cells and whole blood and its components, identify polycaprolactone nanowire surfaces as promising interfaces for cardiovascular implants. There is a correlation between cellular response and nanotopography and this interaction can be optimized. Extruding the nanowires through membranes of varying pore sizes at different temperatures and periods of time can alter the diameters and lengths of the nanowires. Future studies will investigate the effects of varying nanowire characteristics on both cellular response and mechanical properties.

A more in depth study evaluating co-culture of ECs with SMCs, quantifying undifferentiated ECs and SMCs, is necessary to confirm results in Chapter 7. Further, studies aimed at elucidating the molecular mechanisms responsible for differentiation triggered by mechanical cues versus biochemical cues are necessary. In addition, a continuous flow set-up will be required in order to determine the success of these cardiovascular implant surfaces in a more physiologically relevant setting prior to *in vivo* studies. *In vivo* studies will investigate the long-term effect of polycaprolactone nanowire surfaces on healthy tissue development. This future research will provide answers to fundamental questions regarding the long-term functionality of polycaprolactone in highly representative scenarios. Future research will help direct the use of these interfaces for cardiovascular applications.